Proceedings

SAMO 2001

Third International Symposium on Sensitivity Analysis of Model Output

Madrid, June 18-20 2001

Edited by:
Pedro Prado and Ricardo Bolado

MINISTERIO DE CIENCIA Y TECNOLOGÍA
Ciemat Centro de Investigaciones Energéticas, Medioambientales y Tecnológicas
CSN CONSEJO DE SEGURIDAD NUCLEAR
enresa

ORAL SESSION

MODEL-FREE IMPORTANCE INDICATORS FOR DEPENDENT INPUT

Andrea Saltelli, Marco Ratto and Stefano Tarantola

Joint Research Centre of the European Commission,
Institute for Systems, Informatics and Safety, TP 361, 21020 Ispra (VA), Italy
E-mail: stefano.tarantola@jrc.it

1. INTRODUCTION

A number of methods are available to assess uncertainty importance in the predictions of a simulation model for orthogonal sets of uncertain input factors. However, in many practical cases input factors are correlated. Even for these cases it is still possible to compute the *correlation ratio* and the *partial* (or *incrementa*l) importance measure, two popular sensitivity measures proposed in the recent literature on the subject. Unfortunately, the existing indicators of importance have limitations in terms of their use in sensitivity analysis of model output. Correlation ratios are indeed effective for priority setting (i.e., to find out what input factor needs better determination) but not, for instance, for the identification of the subset of the most important input factors, or for model simplification. In such cases other types of indicators are required that can cope with the simultaneous occurrence of correlation and interaction (a property of the model) among the input factors.

In [1] the limitations of current measures of importance were discussed and a general approach was identified to quantify uncertainty importance for correlated inputs in terms of different betting contexts. This work was later submitted to the Journal of the American Statistical Association. However, the computational cost of such approach is still high, as it happens when dealing with correlated input factors. In this paper we explore how suitable designs could reduce the numerical load of the analysis.

2. THE METHOD

A thorough description of sensitivity analysis methods, including linear regression, correlation analysis, importance measures, variance-based and screening methods, can be found in [2]. In the present paper, variance-based importance measures are considered. This approach is a quantitative and model independent and is based on estimating the fractional contribution of each input factor X_i to the variance of the model output, also accounting for interaction terms. In variance-based methods the output variance $V(Y)$ can be decomposed in the sum of a top marginal variance and a bottom marginal variance [3]. Specifically,

$$V(Y) = V[E(Y|U)] + E[V(Y|U)] \qquad (1)$$

where U is a group of one or more factors X_i. The top marginal variance from U is the expected reduction of the variance of Y in case U becomes fully known (it is fixed at some nominal value), whereas the other inputs remain variable as before. The bottom marginal variance from U is the expected value of the variance of Y that would remain in case all inputs but U become fully known, U remaining as variable as before. The main effect, or first order sensitivity index S_i,

representing the sensitivity of Y to the factor X_i, is defined as the top marginal variance for X_i divided by the total variance, where the subset U reduces to the single factor X_i:

$$S_i = V[E(Y|X_i)]/V(Y) \quad (2)$$

Many estimation procedures for S_i are available in the case of independent inputs: the Fourier Amplitude Sensitivity Test, FAST [4], the method of Sobol' [5], and others [6]. In the case of dependent inputs, the S_i can be evaluated, though the procedure can be very demanding in terms of size of the input sample (and hence of number of model runs). The estimation of S_i is done by a sequence of integrals and, given that the factors are correlated, specific sampling strategies are employed to generate the correlated samples.

2.1. Estimator

Let (x_i, i=1,…n) be a random sample of size n from the input factor distribution f_x and let (y_{ik}, k=1, …, r) be a sample of size r from $f_{y|xi}$ for i=1,…n. The sample means are:

$$\bar{y}_i = 1/r \sum_{k=1}^{r} y_{ik} \qquad \bar{y} = 1/n \sum_{i=1}^{n} \bar{y}_i$$

The main effect sensitivity indices are computed by [7] and are called *correlation-ratios*:

$$S_i = \frac{SSB}{SST} \quad SSB = r\sum_{i=1}^{n}(\bar{y}_i - \bar{y})^2 \quad SST = \sum_{i=1}^{n}\sum_{k=1}^{r}(y_{ik} - \bar{y})^2$$

McKay has showed that this kind of sample design introduces a bias for independent inputs (which is discussed briefly below: for details see [7]). McKay does not suggest strategies for correlated input. In this paper we study, through a number of numerical simulations, the statistical properties of the estimator S_i=*SSB/SST* when correlation among factors is present.

2.2. Sampling strategy

The replicated Latin Hypercube Sampling method has been employed in the study (r-LHS: see [8]). In [9], McKay employs a single r-LHS sample in the computation of all the correlation ratios S_i for a set of independent factors. Here we consider correlated input and investigate the possibility to obtain estimates of S_i using one single r-LHS sample.

Pure Monte Carlo (MC) sampling has also been considered in the study as a basis for comparison. A random sample is obtained by fixing n randomly sampled values of the factor of interest (and using them in all the replicates) and by sampling randomly the r replications for the remaining (k-1) factors. To match with a standard typical procedure, a separate MC sample is used for each S_i. The total number of runs is (r x k) for the r-LHS design, while the computational cost must be multiplied by the number of factors in the case of pure random design. In the case of independent input, McKay evaluated the bias of the estimator, which can be written for the limit of high n as

$$\lim_{n\to\infty} \frac{E(SSB)}{E(SST)} = \eta^2 + 1/r(1-\eta^2) \quad (3)$$

where η^2 is the true value of the correlation ratio. There do not seem to be objections in extending this evaluation also to the case of dependent inputs.

2.3. Correlation method

Two methods for inducing correlation in the sample have been considered for the r-LHS: the Iman & Conover rank correlation method [10] and the Stein method [11]. In the case of the pure random sampling strategy, the Cholesky factorisation has been used to correlate the multivariate normal sample. This because, in the test cases, multivariate normal distributions have been considered, in order to obtain analytical solutions for the importance indicators.

3. ANALYTICAL TEST CASES

A few simple test cases have been considered. The factors are assumed to belong to a multi-normal distribution, with zero mean and unit variance. The analyses were repeated several times, to evaluate the properties of the estimator.

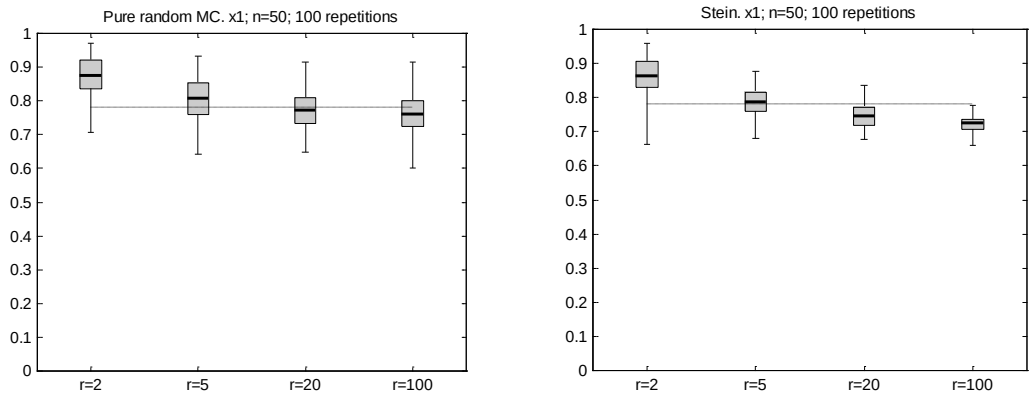

Figure 1. Comparison of importance indicators computed applying pure random sampling and rLHS with Stein method for correlation.

3.1. A two-factor model

In a first test, a two-factor model has been considered. The model is:

$$y = x_1 \cdot x_2 \tag{4}$$

The importance indicators depend on the correlation between the two factors, specifically:

$$S_i = \frac{2\rho^2}{1+\rho^2}$$

Numerical experiments have been performed with ρ=0.8, and they have been repeated for a total of 100 times as to evaluate the distribution of the estimates of S_i. In Figure 1, such distribution is shown, in the form of box plots, when pure MC random sampling or rLHS with Stein method for correlation are employed. Only X_1 is shown due to the symmetry of the problem. As expected from equation (3), for a sufficiently large sample size n, by increasing the number of replicates r, the bias of the estimate tends to vanish. In the case of r-LHS, the estimates of both S_1 and S_2 have been carefully analysed to verify the occurrence of additional bias, due to the fact that one single sample is used. In particular, it has been noticed that:

1) With plain MC and correlation among factors induced by the Cholesky method, the sensitivity indices have a wider distribution and their mean tends to be less biased, while for r-LHS, the distribution is narrower but with a larger bias in the mean.

2) The two estimates of S_1 and S_2 obtained with r-LHS and the method of Stein for correlation are consistent among themselves, i.e. the distributions of the two sensitivity indices are similar to each other and no spurious differentiation between the estimates is induced by the use of the same sample.

3) By applying the Iman and Conover correlation method, however, the mean of the sensitivity index for X_2 is systematically slightly larger than that for X_1. This does not happen with Stein, which can be considered therefore the more consistent correlation method.

4) Using the same sample (i.e. rLHS) the correlation between the estimates of the sensitivity indices can be high: in some cases we computed correlation coefficients of about 0.7.

3.2. Three-factor model

Here, the reference model was:

$$y = x_1 \cdot x_2 \cdot x_3 \tag{5}$$

This model was a quite strong test to analyse the concomitance of interaction and correlation. First, the following simplified covariance structure was considered, $\rho_{12}=\rho_{13}=\rho_{23}=\rho$. The analyses were repeated 50 times, to evaluate the properties of the estimator. A completely analogous behaviour as in the two-factor model was observed. It was confirmed that the Stein method is more consistent. The main difference between pure random design and r-LHS is that with r-LHS the distribution is much narrower. On the other hand, the mean converges more precisely with the random sampling. The augmented order of the interaction structure in the model makes convergence more difficult, implying a larger bias of the estimator at fixed n with respect to the two-factor model.

The properties of the estimator changed by changing the structure of the model and/or the covariance structure: (i) by decreasing the correlation, the bias for the r-LHS design tends to vanish more quickly; (ii) by considering an additive model (i.e. no interaction), $y = x_1 + x_2 + x_3$, complete convergence is attained already with n=50, r=20 for all types of sample design.

4. CONCLUSIONS

The simultaneous occurrence of interaction in the model and of correlation between factors makes the convergence of the estimates to the correct solution more difficult. Advantages of the r-LHS are: the possibility of computing all the sensitivity indices with the same sample, and the fact that the distribution of the estimator is narrower. In spite of this, a residual bias in the mean is more persistent than when pure random sampling is employed: however, such bias tends to vanish for large values of r. Various other tests have been performed by changing the covariance and the model structures: they all confirmed the behaviour of the estimator described above.

5. ACKNOWLEDGEMENTS

The authors gratefully acknowledge support from the *European Statistical Laboratory* project financed by the European Commission.

6. REFERENCES

[1] Tarantola S. (2000) In Proceedings of the Foresight and Precaution Conference (ESREL 2000), Edinburgh.

[2] Saltelli A., Scott M., Chan K., eds., Sensitivity analysis, 2000, John Wiley.

[3] Jansen M. J. W., W. A. H. Rossing and R. A. Daamen. In Predictability and Nonlinear Modelling in Natural Sciences and Economics, Gasman and van Straten (Eds.), 334-343. (1994).

[4] Cukier, R. I., C. M. Fortuin, K. E. Schuler, A. G. Petschek, J. H. Schaibly (1973), The Journal of Chemical Physics, 59 (8), 3873-3878.

[5] Sobol', I. M. (1993), Mathematical Modelling & Computational Experiment, 1, 407-414.

[6] Iman, R. L., and Hora, S. C., (1990). Risk Analysis, 10(3):401-406.

[7] McKay, M. D. (1996), Variance-Based Methods for Assessing Uncertainty Importance in NUREG-1150 Analyses, LA-UR-96-2695, 1-27.

[8] McKay, M. D., Beckman R. J. and Conover W. J. (1979), Technometrics, 21(2), 239-245

[9] McKay, M. D. (1995), Evaluating prediction uncertainty, Los Alamos National Laboratories report NUREG/CR- 6311, LA-12915-MS.

[10] Iman R. L. and Conover W. J . (1982), Comm. Statist. B11(3), 311-334

[11] Stein M. (1987), Technometrics, 29(2), 143-151

TOWARDS A NEW GLOBAL SENSITIVITY ANALYSIS TECHNIQUE BASED ON THE MULTI-DIMENSIONAL FOURIER TRANSFORM.

Stefano Tarantola

Institute for Systems, Informatics and Safety
Joint Research Center of the European Commission
TP. 361 - 21020 Ispra (VA) ITALY
E-mail: stefano.tarantola@jrc.it

The main concern in global sensitivity analysis of model output is to be able to quantify, in an efficient way, the importance of the uncertain input variables in the simultaneous occurrence of generic correlation patterns (a property of the set of input variables) and complex computational models (where the relationships between the output variable and the input variables can be non-additive and non-monotonic).

A general methodology would be appreciated that is capable of estimating the indicators of importance not only for each input variable alone, but also for pairs of input variables, and for any subset of input variables, thus enabling us to answer the different problem settings (e.g., priority setting, identification of subsets of important variables, model simplification, etc.).

In this paper a promising technique is presented, which builds on the multi-dimensional Fourier spectrum of the model output, computed using a set of sample points in the space of the input variables. The Fourier spectrum is obtained using a type of periodogram developed by Lomb (1976) and Scargle (1982), quite powerful to find weak periodic signals in otherwise random, unevenly sampled 1-dimensional data. The Lomb-Scargle approach is extended to a multi-dimensional space to estimate the variance of the model output and the sensitivity indices of any order (and for any group of variables). All these indices can be estimated with a unique (reasonably large) set of sample points. Numerical tests are being performed on different test models. The technique is being tested with crude Monte Carlo and LP-τ sampling design.

1. BACKGROUND

In a review paper, Cukier, Levine and Shuler (1978) give an interpretation of the Fourier spectral components as sensitivity coefficients.

Assume that the computational model under analysis is a function $y = f(x_1, x_2, ..., x_k)$ with *k* input variables $\mathbf{x} = \{x_1, x_2, ..., x_k\}$ and a single output variable y.

Assume that the input variables are defined over the k-dimensional unit hyper-cube, i.e. $\mathbf{x} \in I^k$, where *I* is the unit interval [0,1], and that $\int_{I^k} |f(\mathbf{x})| d\mathbf{x} < +\infty$.

Under these assumptions, a representation formula for $f(\mathbf{x})$ exists (called *Fourier integral*), which is obtained as the extension, for $T \to \infty$, of the Fourier series expansion of a periodic function with period T.

$$f(\mathbf{x}) = \int_{\Re^k} c(r_1, r_2, ..., r_k) \exp\left[i\left(x_1 r_1 + x_2 r_2 + ... x_k r_k\right)\right] dr_1 dr_2 ... dr_k = \\ = \int_{\Re^k} c(r_1, r_2, ..., r_k) \exp\left[i\mathbf{x} \cdot \mathbf{r}\right] d\mathbf{r} \tag{1}$$

The $c(r_1, r_2, ..., r_k)$ are the Fourier coefficients that are defined, over a k-dimensional frequency domain $\Re^k$, as

$$c(r_1, r_2, ..., r_k) = \int_{I^k} f(\mathbf{x}) \exp\left[-i\mathbf{x} \cdot \mathbf{r}\right] dx_1 dx_2 ... dx_k \,. \tag{2}$$

The function $c(\mathbf{r})$ is continuous over $\Re^k$ and $\lim_{|\mathbf{r}| \to \infty} c(\mathbf{r}) = 0$.

2. VARIANCE DECOMPOSITION

Moreover, if $f(\mathbf{x}) \in L^2(I^k)$, ie if $\int_{I^k} |f(\mathbf{x})|^2 d\mathbf{x} < +\infty$ (in this case $f(\mathbf{x})$ is a square-integrable function), the function and its Fourier coefficients are related by

$$\int_{I^k} |f(\mathbf{x})|^2 d\mathbf{x} = \int_{\Re^k} |c(\mathbf{r})|^2 d\mathbf{r} \tag{3}$$

which is called *Parseval* equality. The function $c(\mathbf{r})$ is even over each of its variables, because the function $f(\mathbf{x})$ is real-valued. Due to this symmetry property, the integrals computed over $\Re^k$ can be restricted to $\Re^{+k}$ (ie the subspace of $\Re^k$ where all the frequencies are positive). The total variance *V* of the model output *y* can easily be obtained from (3)

$$V = 2\int_{\Re^{+k}} |c(r_1, r_2, ..., r_k)|^2 dr_1 dr_2 ... dr_k \tag{4}$$

It is easy to prove (see Cukier, Levine and Shuler, 1978) that if we rearrange the integral in (4) into groups of terms where successively larger subgroups of the variables $(r_1, r_2, ..., r_k)$ are nonzero we get the quantities

$$V_i = 2\int_{\Re^+} dr_i |c(0, ..., r_i, ..., 0)|^2 \tag{5}$$

$$V_{ij} = 2\int_{\Re^+} dr_i \int_{\Re^+} dr_j |c(0, ..., r_i, ..., r_j, ..., 0)|^2 \tag{6}$$

$$V_{ijl} = 2\int_{\Re^+} dr_i \int_{\Re^+} dr_j \int_{\Re^+} dr_l |c(0, ..., r_i, ..., r_j, ..., r_l, ..., 0)|^2 \text{ , etc.,} \tag{7}$$

so that each term in the decomposition

$$V = \sum_{i=1}^{k} V_i + \sum_{i=2}^{k} \sum_{j=1}^{i-1} V_{ji} + \sum_{i=3}^{k} \sum_{j=2}^{i-1} \sum_{l=1}^{j-1} V_{lji} + \cdots \tag{8}$$

can be calculated. In summary, once a sample over the space domain has been generated, and the Fourier coefficients have been computed, it is straightforward to calculate all the partial variances at any order as well as the total variance V. The complete set of sensitivity indices is then obtained by simple normalisation

$S_i = V_i / V$ (main effect indices)

$S_{ij} = V_{ij}/V$ (two-way interaction terms), etc.

This procedure is advantageous with respect to the standard evaluation in the space domain whereby each sensitivity index is obtained by

1) integrating $f(\mathbf{x})$ over all but the variables of interest (which are conditioned to some value) and
2) calculating the variance of the resulting function.

For instance, V_{12} would be obtained as $V\left[E\left(f(\mathbf{x}) \mid x_1, x_2\right)\right]$. To compute each partial variance in the decomposition (8) a different sample has indeed to be generated.

3. CALCULATION OF THE FOURIER COEFFICIENTS

The simplest way to calculate Fourier coefficients would be to take a grid of uniformly distributed sample points in the space domain, evaluate $f(\mathbf{x})$ over each of these, and use the multi-dimensional Fast Fourier Transform to obtain the $c(r_1, r_2, ..., r_k)$ over $\Re^{+k}$.

However, this is not practicable for large values of *k*, as a set of evenly spaced points over all the k dimensions would consist of a total of m^k points (*m* is the number of points along each dimension), and as many model evaluations.

Therefore, we have to create a sample of unevenly spaced points over the space domain, (eg a set of 1,024 LP-τ points can be generated whatever the dimension *k* of the space of the input variables is) and compute the Fourier coefficients using such sample.

We take advantage from extensive research made in observational sciences (typically astrophysics), whereby the observer cannot control the time of the observations, but must simply accept a certain dictated set of time points. This concept is a 1-dimensional problem that we have to extend to *k* dimensions for the purpose of sensitivity analysis.

There are some ways to get from unevenly spaced points to evenly spaced ones, such as interpolation. However, multi-dimensional interpolation is a very delicate and costly task (usually also of poor performance) that we prefer to avoid.

A very elegant method of spectral analysis for unevenly sampled data was developed by Lomb (1976), based in part on earlier work by Barning (1963) and Vanicek (1971), and elaborated by Scargle (1982). The Lomb method evaluates the spectral power of $y = f(t)$, a function of time, using the times t_i that are actually measured. Assume that there are *N* data points available: $y_i \equiv f(t_i), i = 1, ..., N$. The Lomb spectral power, as a function of the angular frequency $\omega > 0$, is defined by

$$P_N(\omega) \equiv \frac{1}{2}\left\{\frac{\left[\sum_j (y_i - \bar{y})\cos\omega\,(t_j - \tau)\right]^2}{\sum_j \cos^2\omega\,(t_j - \tau)} + \frac{\left[\sum_j (y_i - \bar{y})\sin\omega\,(t_j - \tau)\right]^2}{\sum_j \sin^2\omega\,(t_j - \tau)}\right\} \tag{9}$$

where $\bar{y}$ is the mean of the data, and τ is a constant (offset) defined by

$$\tan(2\omega\tau) = \frac{\sum_j \sin 2\omega\, t_j}{\sum_j \cos 2\omega\, t_j}, \tag{10}$$

that makes the spectral power independent of shifting all the t_i by any constant. Equations (9) and (10) are a summary of what one would obtain if one estimated the harmonic content of a data set, at a given frequency ω, by linear least-squares fitting to the model $f(t) = A\cos\omega t + B\sin\omega t$. The method can give results superior to Fast Fourier Transform methods, because it weights data on a 'per point' basis instead of on a 'per time interval' basis, when uneven sampling can render the latter seriously in error. The Lomb method has been tested against the classic method, in the special situation of evenly spaced data. In such case the two resulting spectral powers coincide.

In Astrophysics, the Lomb spectral power is used to determine the presence of periodic signals out of background noise. In other words the interest is to determine how significant is a peak in the spectrum. Our interest is different: we need to estimate the total and partial variances. Therefore we have to grasp all the relevant information out of the spectral power. Note that, in the case of unevenly spaced points, the spectral power can be computed using any given frequency sampling step, and up to any desired frequency value. Therefore the relevant information can be redundantly present at different frequencies.

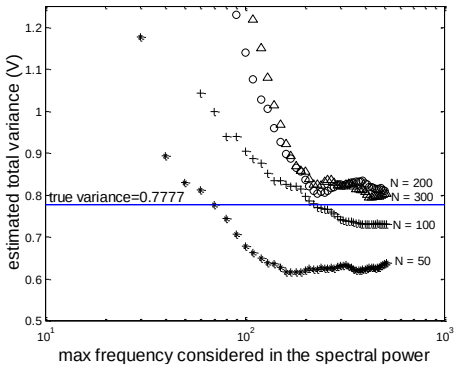

Figure 1: convergency test for V for unevenly spaced points in 2-D. Four different sample sizes are considered: N=50, 100, 200, and 300. The test model is $f(\mathbf{x}) = f(x_1, x_2) = |4x_1 - 2| \cdot |4x_2 - 2| \; \mathbf{x} \in I^2$

Numerical tests (Figure 1) have shown that adding the Lomb spectral power coefficients from low frequencies up to larger and larger frequencies (using equation (4)) provide unbiased estimates of the total output variance. Tests for unevenly spaced points on partial variances (equations (5), (6),…) are in progress.

4. REFERENCES

Lomb, N.R. (1976), *Astrophysics and Space Science*, 39, pp 447-462.
Barning, F.J.M (1963), *Bull. of the Astronomical Institutes of the Netherlands*, 17, 22-28.
Vanicek, P. (1971), *Astrophysics and Space Science*, 12, pp. 10-33.
Scargle, J.D. (1982), *Astrophysical Journal*, 263, pp. 835-853.
Cukier, R. I., Levine H. B. and Shuler K. E. (1978), *J. of Comput. Physics*, 26, pp. 1-42.

THEOREMS AND EXAMPLES ON HIGH DIMENSIONAL MODEL REPRESENTATION

I.M.Sobol´

Inst. for Math. Modelling of the Russian Acad. of Sciences,
4, Miusskaya Square, Moscow 125047, Russia.
E-mail: sobolhq@imamod.ru

1. INTRODUCTION

This investigation was inspired by the talk of Prof. H.Rabitz at the Second International Symposium on Sensitivity Analysis of Model Output (SAMO'98) in Venice [2]. First, there was a reasonable assumption that quite often in high dimensional models small subsets of input variables have the main impact upon the output. And second, a new family of model representations for approximating such models was introduced. The family included an arbitrary reference point.

In this work, a criterion is set up for testing whether the assumption is true; a class of models is described that can be approximated with arbitrary reference points; and another class of models is investigated where a careless choice of the reference point can spoil the approximation.

The present paper contains formulations of main results.

Let I denote the unit interval [0,1], I^n • the n-dimensional unit hypercube and $x \in I^n$. The integrals below are as a rule from 0 to 1 for each variable and $dx = dx_1 ... dx_n$.

The model function $f(x)$ is supposed to be square integrable in I^n. We shall study its representation in the form

$$f(x) = f_0 + \sum_{s=1}^{n} \sum_{i_1 < ... < i_s}^{n} f_{i_1 ... i_s}(x_{i_1} ... x_{i_s}) \qquad (1)$$

where the interior sum is over all sets of s integers $i_1,...,i_s$, that satisfy $1 \le i_1 < ... < i_s \le n$. Relation (1) means that

$$f(x) = f_0 + \sum_i f_i(x_i) + \sum_{i<j} f_{ij}(x_i, x_j) + ... + f_{12..n}(x_1, x_2 ... x_n)$$

and is often called high dimensional model represetation (HDMR). The total number of summands in (1) is 2^n.

2. ANOVA HDMR.

Representation (1) is called ANOVA HDMR if the following requirements are satisfied:

$$\int_0^1 f_{i_1\ldots i_s}\,dx_k = 0 \quad \text{for} \quad k = i_1,\ldots,i_s .$$

These requirements uniquely define all the $f_{i_1\ldots i_s}$ in (1), in particular, $f_0 = \int f(x)dx$; and all the members in (1) are orthogonal. The term ANOVA comes from Analysis Of Variances [1]. In my early writings [6, 7] representation (1) was called decomposition into summands of different dimensions. Clearly, the dimension of $f_{i_1\ldots i_s}$ is the number of variables s.

3. MODEL APPROXIMATIONS.

Consider the constant $D = \int f^2(x)dx - f_0^2$ that for obvious reasons is called total variance.

If the model function $f(x)$ is approximated by another square integrable function $\tilde{f}(x)$, the approximation error will be measured by the scaled L_2 distance

$$\delta(f,\tilde{f}) = \frac{1}{D}\int\left[f(x) - \tilde{f}(x)\right]^2 dx \qquad (2)$$

The scaling allows to distinguish between good and bad approximations. Indeed, if the crudest approximations $\tilde{f}(x) \equiv \text{const}$ are used, the best choice $\tilde{f}(x) \equiv f_0$ implies $\delta = 1$. Hence, good approximations are the ones with $\delta << 1$. Error estimate (2) proved efficient in problems [8, 9], where the number of variables in $\tilde{f}(x)$ is less than n.

Prof. Rabitz's assumption suggests approximations

$$\tilde{f}(x) = f_0 + \sum_{s=1}^{L}\sum_{i_1<\ldots<i_s}^{n} f_{i_1\ldots i_s}(x_{i_1}\ldots x_{i_s}) \qquad (3)$$

with $L < n$. Here the number of variables is again n, but all the summands in (3) are s-dimensional with $s \le L$.

Theorem 1. If the model function (1) is approximated by (3) then the approximation error (2) is

$$\delta(f,\tilde{f}) = 1 - \sum_{s=1}^{L}\sum_{i_1<\ldots<i_s}^{n} S_{i_1\ldots i_s} . \qquad (4)$$

where $S_{i_1\ldots i_s}$ are global sensitivity indices for $f(x)$ [4, 5, 8].

Formula (4) shows that the validity of Prof. Rabitz's assumption can be verified by estimating the low order sensitivity indices.

4. FINITE DIFFERENCE HDMR.

Let $y = (y_1,\ldots,y_n)$, $h = (h_1,\ldots,h_n)$ and both y and $y + h \in I^n$. According to [7], the increment $f(y+h) - f(y)$ can be decomposed into finite differences. Inserting $h = x - y$ we obtain a relation that includes y as a parameter:

$$f(x) = f(y) + \sum_{s=1}^{n}\sum_{i_1<\ldots<i_s}^{n} \Delta_{x_{i_1}-y_{i_1}}\ldots\Delta_{x_{i_s}-y_{i_s}} f(y) \qquad (5)$$

where $\Delta_{h_i} f(y) = f(y_1,...,y_i + h_i,...,y_n) - f(y)$ is the ordinary finite difference operator.

We shall call (5) a finite difference HDMR. It is identical with the cut-HDMR in [3].

In principle, the summands in (5) can be computed much easier than the summands in (1) because there are no integrations in (5). However, in practice this statement is true for small s only: at higher s the number of model estimations 2^s is large and a loss of accuracy may spoil the results.

Instead of (3) the following approximations were suggested in [3]:

$$\tilde{f}(x \mid y) = f(y) + \sum_{s=1}^{L} \sum_{i_1<...<i_s}^{n} \Delta_{x i_1 - y_{i_1}} .. \Delta_{x i_S - y_{i_S}} f(y) \qquad (6)$$

The authors of [3] stress that identity (5) i s true for all $y \in I^n$ and believe that the choice of y is not important. However, approximation (6) does depend on y and an unlucky choice of y (called reference point) can produce an unacceptable approximation error.

First, here are conditions providing for a good situation.

Theorem 2. Assume that all mixed partial derivatives of $f(x)$ that include not more than one differentiation with respect to each variable are continuous, and denote

$$A = \sup_x \sum_{s=L+1}^{n} \sum_{i_1<...<i_s}^{n} \left| \partial^s f / \partial x_{i_1} .. \partial x_{i_s} \right|$$

Then for an arbitrary choice of $y \in I^n$

$$\delta(f(x), \tilde{f}(x \mid y)) \le A^2 / D .$$

It follows from Theorem 2 that approximation (6) will be good if A is sufficiently small, and the choice of y does not matter.

Second, here is a numerical example showing the bad situation.

Example. Consider a model function

$$f(x) = (1+p)^{-3} \prod_{i=1}^{3} (1 + 3p x_i^2) .$$

For this function $D = (1+\beta)^3 - 1$, where $\beta = 0.8 p^2 (1+p)^{-2}$.

Approximation (6) with $L = 2$ can be written easily:

$$\tilde{f}(x \mid y) = f(x) - (1+p)^{-3} \prod_{i=1}^{3} (1 + 3p x_i^2 - 3p y_i^2) .$$

It can be verified that the reference point $y = (1/\sqrt{3},\ 1/\sqrt{3}, 1/\sqrt{3})$, provides for the best approximation with $\delta_{\min} = \beta^3 / D$, while the point $y = (1,1,1)$ yields the worst approximation $\delta_{\max} = 216 \delta_{\min}$. If p is large, $\beta \approx 0.8$, $\delta_{\min} \approx 0.11$ But $\delta_{\max} \approx 23$ which is clearly unacceptable.

5. ACKNOWLEDGEMENT.

The author is grateful to A.Saltelli and S.Tarantola (Joint Research Centre, Ispra) who supported this investigation.

6. REFERENCES.

1. G.E.B.Archer, A.Saltelli, I.M.Sobol´. Sensitivity measures, ANOVA-like techniques and the use of bootstrap. J.Statist. Comput. Simul. 58(1997), 99-120.
2. K.Chan, S.Tarantola, F.Campolongo, eds. Proc. of SAMO'98, Venice. Official Publ. European Communities, Luxembourg (1998).
3. H.Rabitz, O.F.Alis, J.Shorter, K.Shim. Efficient input-output model representation. Computer Physics Communs, 117, N1-2 (1999), 11-20.
4. A.Saltelli, I.M.Sobol´. Sensitivity analysis for nonlinear mathematical models: numerical experience. Matem. Modelirovanie, 7, N11(1995), 16-28 (in Russian).
5. A.Saltelli, I.M.Sobol´. About the use of rank transformation in sensitivity analysis of model output. Reliab. Engng and System Safety, 50, N3(1995), 225-239.
6. I.M.Sobol´. The use of Haar series in estimating the error in the computation of infinite-dimensional integrals. Dokl. Akad. Nauk SSSR, 175, N1(1967) (in Russian). English Transl.:Soviet Math. Dokl., 8, N4(1967), 810-813.
7. I.M.Sobol´. Multidimensional Quadrature Formulas and Haar Functions. Nauka, Moscow (1969) (in Russian).
8. I.M.Sobol´. Sensitivity estimates for nonlinear mathematical models. Matem. Modelirovanie, 2, N1(1990), 112-118 (in Russian). English Transl.: MMCE, 1, N4(1993), 407-414.
9. I.M.Sobol´. On ,,freezing" unessential variables. Vestnik Mosk. Univ., ser. Matem. 6(1996), 92-94 (in Russian). English Transl.:Moscow Univ. Math. Bull. (Allerton Press, 1996.

ADVANCES IN THE EFFICIENT USE OF FAST

R. Bolado[1], P. Prado[2]

[1]Laboratorio de Estadística, Universidad Politécnica de Madrid
José Gutiérrez Abascal 2,
28006 - Madrid. Spain
Email: rbolado@ingor.etsii.upm.es

[2]Departamento de Medio Ambiente del CIEMAT
Avda. Complutense, 22
28040 - Madrid. Spain
Email: pedro.prado@ciemat.es

1. ABSTRACT

FAST (Fourier Amplitude Sensitivity Test) is a sensitivity technique developed in the early 70's to estimate the fraction of the variance of an output model variable due to each input uncertain parameter. In its early versions only the contribution of main effects to the total variance could be computed. This technique is based in two key underlying ideas. The first key idea is to apply the ergodic theorem as demonstrated by Weyl, that allows the computation of an integral in an n-dimensional space through a mono-dimensional integral, in such a way that the integral

$$\langle Y \rangle = \int ..n.. \int Y(x) \cdot f(x) \cdot dx_1 ... dx_n \qquad (1)$$

may be assumed to be equal to the integral

$$\hat{Y} = lim_{T \to \infty} \frac{1}{2T} \int_{-T}^{T} Y\big(X(S)\big) \cdot dS \qquad . \qquad (2)$$

The second key idea is to scan the multidimensional input parameter space through a search curve obtained varying simultaneously all the input parameters according to some specific frequencies (variable *S* in integral (2) is a real variable defined on that search curve).

Recent research activities have extended the use of FAST to estimate global sensitivity indices. In this case not only first order effects contribution of each parameter to the output variable variance are computed, but also the contribution of all its interactions of any order. Anyway, though useful, the new technique does not provide a full error analysis that could provide the user a measure of the error in his estimates of the contribution of each parameter to the total variance. In this work we use bootstrap techniques conditioned by the Nyquist criterion on the sample in order to provide error estimates. Additionally, we study the problem of the incrementalism of this technique. In this case the possibility of merging several FAST samples to provide common estimates is studied.

SENSITIVITY ISSUES IN THE BAYESIAN ANALYSIS OF FAILURES IN REPAIRABLE SYSTEMS

F. Ruggeri

CNR--IAMI
Via Ampere 56, 20131 Milano (Italy)
Email: fabrizio@iami.mi.cnr.it

1. INTRODUCTION

The paper arises from a consulting project in which failures (gas escapes) are considered in the steel pipelines of an urban gas distribution network. The available data are the 33 failure times from 1978 to 1997 over a network of 275 kilometres. More details on the data can be found in [1]. Steel pipelines are subject to ageing and the global system reliability is barely affected by one failure. Thus, we consider the network as a repairable system, since it keeps the same reliability when minimal repairs immediately follow failures. Failures of such systems are often described by non-homogeneous Poisson processes (NHPP), which take in account the degradation of the components; see, e.g., [2].

In the paper we model the failures pattern with a NHPP with logarithmic intensity and present different sensitivity analyses when relaxing the assumption on the parametric model. We operate in a robust Bayesian framework; see [3] for a thoroughly illustration of the approach. In the paper we do not focus on the commonly addressed issue of sensitivity to the prior, but we are interested in model sensitivity and consider two ways to build classes of models around the NHPP. In the first approach, we consider the NHPP as an element of a class of processes, defined through differential equations whose solutions are mean value functions of NHPPs. In the second, nonparametric approach, we consider processes whose mean value functions are distribution functions of random measures. In both cases, we compare the models with the baseline, logarithmic NHPP.

In Section 2 we analyse the logarithmic NHPP and the class of parametric models, whereas comparison between parametric and nonparametric models is performed in Section 3. Some concluding remarks are presented in Section 4.

2. PARAMETRIC MODEL

We consider the NHPP N_t with intensity $\lambda_\theta(t)=a\ log\ (1+bt)+c$, $\theta=(a, b, c) \in R_+^3$. Its choice is well justified since the engineers in the project are confident the intensity function is increasing and concave. The mean value function (m.v.f.) of N_t, $E\ N_t=\Lambda_\theta(t)$, is given by

$$\Lambda_\theta(t)=\int_0^t \lambda_\theta(s)ds = [a\ (1+bt)log(1+bt)]\ /\ b+(c-a)t.$$

Suppose N_T failures, $y=(y_1, ..., y_{N_T})$, are observed in $[0, T]$, then the likelihood is given by

$$L(\theta \mid \underline{y}, N_T) = (1+bT)^{-a(1+bT)/b} e^{(a-c)T} \prod_{j=1}^{N_T} (a \log(1+by_j)+c).$$

Following a Bayesian approach, we choose independent Gamma priors on the parameters because of their mathematical tractability and flexibility. Namely, the Gamma priors are $G(\mu_a,\rho_a)$, $G(\mu_b,\rho_b)$ and $G(\mu_c,\rho_c)$ for a, b and c, respectively. Combining the prior with the likelihood, we have that the posterior distribution $\pi(\theta|\underline{y}, N_T)$ is proportional to

$$(1+bT)^{-a(1+bT)/b} a^{\mu_a-1} b^{\mu_b-1} c^{\mu_c-1} \prod_{j=1}^{N_T} (a\log(1+by_j)+c) e^{-[(1/\rho_a - T)a + b/\rho_b + (1/\rho_c + T)c]}$$

Choice of hyperparameters, parameters estimation, HPD intervals, predictive distributions, estimation of reliability (i.e. probability of no failures in a subset) and m.v.f., Kolmogorov-Smirnov (K-S) test to check if the data are coming from the estimated logarithmic NHPP are illustrated in [4] and [5]. Prior sensitivity analyses are well justified in this context since the choice of hyperparameters was only remotely related to the experts' opinions, which were collected and used for different purposes, as shown in [1]. Here we report that, according to the K-S test, there is not enough evidence to reject the model but visual inspection of the optimal m.v.f. is quite unsatisfactory. Therefore, we consider a recently proposed ([6]) class of other NHPPs containing the logarithmic one.

In [6] it is observed that the m.v.f. and the intensity function of many commonly used NHPPs are functionally related. Using the well-known fact that the latter is the derivative of the former, the m.v.f.'s of those NHPPs can be seen as the solutions of a differential equation. Therefore, we define a class of NHPPs whose m.v.f.'s satisfy $M(0)=0$ and are the solutions of

$$M' = \frac{\alpha M + \beta t}{\gamma + \delta t}.$$

The (general) solutions are given by

$$M = e^{\int \alpha/(\gamma+\delta x)\,dx} \{ \int \frac{\beta x}{\gamma+\delta x} e^{-\int a/(\gamma+\delta z)\,dz} dx + c \}.$$

Very different NHPPs can be found and we are currently investigating the meaning of the parameters and their role in determining features of the processes. In particular, we are interested in considering neighbourhoods of models, defined by intervals on the parameters, and finding the model leading to the smallest Bayes factor. In a preliminary study, we consider what happens when taking a couple of processes from the class, namely the Homogeneous Poisson Process (HPP) with intensity function $\lambda(t)= \lambda$ and the Power Law Process (PLP) with $\lambda(t)=\beta\gamma t^{\gamma-1}$. The Bayes factor shows the HPP is slightly better than the logarithmic NHPP, whereas both are better than the PLP (see [5]). We observe that the estimators of the intensity function under both the HPP and the logarithmic NHPP are very close in the considered interval. Thus, there is the need for a different model, which is not too far from the trusted, logarithmic NHPP.

3. NONPARAMETRIC MODEL

We now embed the parametric logarithmic NHPP in a class of models given by a weighted Gamma process, stemming from results in [7]. We compare the parametric NHPP with the nonparametric models through the Bayes factor, like other authors did in different contexts. The novel comparison for weighted Gamma processes is thoroughly presented in [4] and [5], where we apply results from the theory of random measures: more details on them can be found in [8].

Given a measure μ and a measurable subset B, we define $\mu B := \mu(B)$.

Definition 1. *Let α be a finite, σ-additive measure on ($\mathbf{S}$, S). The random measure μ follows a **Standard Gamma** distribution with shape α (denoted by $\mu \sim \mathbf{GG}(\alpha, 1)$) if, for any family $\{S_j, j=1, ..., k\}$ of disjoint, measurable subsets of $\mathbf{S}$, the random variables μS_j are independent and such that $\mu S_j \sim \mathbf{G}(\alpha S_j, 1)$, for $j = 1, ..., k$.*

Definition 2. *Let β be an α-integrable function and $\mu \sim \mathbf{GG}(\alpha, 1)$. The random measure $\nu = \beta\mu$ follows a **Generalised Gamma** distribution, with shape α and scale β (denoted by $\nu \sim \mathbf{GG}(\alpha, \beta)$).*

The Generalised Gamma distributions are conjugate for the Poisson processes as shown by the next result (see [7] for more details).

Theorem 1. *Let $\underline{\xi} = (\xi_1, ... \xi_n)$ be n Poisson processes with intensity measure M. If $M \sim \mathbf{GG}(\alpha, \beta)$ a priori, then $M \sim \mathbf{GG}(\alpha + \sum_{i=1,n}\xi_i, \beta / (1+\beta))$ a posteriori.*

Under a squared loss function, Bayesian estimators of the intensity measure and the reliability are found in [7] and [5], respectively. Here we focus on the nonparametric model as a neighbourhood of the logarithmic NHPP and we search in a class of *parameters* of the nonparametric model for the best ones. We start with the logarithmic NHPP with m.v.f. Λ_θ and embed it in a nonparametric model with intensity measure M whose expected value coincides with Λ_θ. We consider the same prior $\pi(\theta)$ for both models and compare the two alternatives via Bayes factor. Interest in comparisons between parametric (H_P) and nonparametric (H_N) alternatives is rapidly growing; see, e.g., [9], [10] and [11]. Weighted Gamma processes have been considered in [4] and [5] and we refer to them for further details.

We consider the case in which the interval $[0, T]$ is split into n disjoint intervals $I_j = (t_{j-1}, t_j]$, $j=1, ...,n$ and we record the failures in each of them. The sample will be $\underline{k} = (k_1,..., k_n)$ from the random vector $\underline{N} = (NI_1,...,NI_n)$. Since each NI_j has a Poisson distribution, then the likelihood is given by

$$f(\underline{k} \mid \Lambda) = e^{-\Lambda(T)} \prod_{j=1}^{n} \frac{(\Lambda I_j)^{k_j}}{k_j!}$$

We consider the following hierarchical structure to centre the model around the NHPP: $\underline{k} \mid M, \theta \sim f(\underline{k} \mid M_\theta)$, $M \mid \theta \sim GG(\Lambda_\theta/\sigma, \sigma)$ and $\theta \sim \pi$, where f is the above likelihood and π is the same prior used for the NHPP. As σ varies, we get a class of nonparametric processes. Looking at the Bayesian estimator of the m.v.f. in [5], the role of σ is evident: the weight of the prior decreases with respect to the observed processes when σ increases and vice versa. The Bayes factor becomes (see [5])

$$\frac{\int_{R_+^3} e^{-\Lambda_\vartheta(T)} \prod_{j=1}^{n} (\Lambda_\vartheta I_j)^{k_j} \pi(\theta) d\vartheta}{\int_{R_+^3} \prod_{j=1}^{n} [(1+\sigma)^{-(\Lambda_\vartheta I_j/\sigma + k_j)} \prod_{i=0}^{k_j-1} (\Lambda_\vartheta I_j + i\sigma)] \pi(\vartheta) d\vartheta}$$

The Bayes factor of H_P vs. H_N is a concave function of σ, which is smaller than *1* for $\sigma <$ *1.7* and smaller than *1/3* (mild evidence in favour of H_N) for *0.2* $< \sigma <$*1.1*, with a minimum at *0.509*. The best value of σ, that is the one leading to the smallest Bayes factor, has been

considered in [5], where the nonparametric Bayesian estimators of intensity function and reliability have been compared with the optimal ones under the logarithmic NHPP. The new model definitely improves upon the previous ones. Wider classes, with general $\beta(x)$, are currently under investigation.

4. CONCLUSIONS

We have illustrated some of the sensitivity issues we have addressed in analysing gas escapes in the steel pipelines: more details and plots will be presented in the talk. Our main interest has been devoted to model sensitivity and we have illustrated two approaches based on recent results. In the paper we have discussed current directions of research, as well. In the last few years we have been working a lot with gas failures data. We have found that modelling these data is a difficult but stimulating task: we have been pursuing different strategies and sensitivity analysis has always played a relevant role in it; see [12] as an example.

5. ACKNOWLEDGEMENTS

The speaker gratefully acknowledges the contribution of his former B.Sc. student, Davide Cavallo, co-author of some of the results mentioned in the paper.

6. REFERENCES

[1] Cagno, E., Caron, F., Mancini, M., Pievatolo, A. and Ruggeri, F. (1999), Bayesian assessment of corrosion-related failures in steel pipelines, *Submitted*.

[2] Thompson, W.A. (1988), Point Process Models with Applications to Safety and Reliability, Chapman and Hall, London.

[3] Rios Insua,D.and Ruggeri, F.eds.(2000),Robust Bayesian Analysis, Springer, NewYork.

[4] Cavallo, D. (1999), Nuovi modelli bayesiani nell'analisi dell'affidabilità dei sistemi riparabili, B.Sc. Dissertation, Dip. Matematica, Università degli Studi di Milano.

[5] Cavallo, D. and Ruggeri, F. (2001), Bayesian models for failures in a gas network, to appear in Proceedings of ESREL 2001, Torino.

[6] Ruggeri, F. (2000), Sensitivity issues in the Bayesian analysis of the reliability of repairable systems, in Proceedings of MMR'2000 (Mathematical Methods in Reliability), Bordeaux.

[7] Lo, A.Y. (1982), Bayesian nonparametric statistical inference for Poisson point processes, Zeitschrift für Wahrscheinlichkeitstheorie und verwandte Gebiete, 59, 55-56.

[8] Kallenberg, O. (1983), Random measures, Academic Press, London.

[9] Verdinelli, I. and Wasserman, L. (1998), Bayesian goodness-of-fit testing using infinite-dimensional exponential families, Annals of Statistics, 26, 1215-1241.

[10] Carota, C. and Parmigiani, G. (1996), On Bayes factors for nonparametric alternatives, in Bayesian Statistics 5 (J.M.Bernardo, J.O.Berger, A.P.Dawid and A.F.M. Smith eds), 507-511.

[11] Berger, J.O. and Guglielmi, A. (1999), Bayesian testing of a parametric model versus nonparametric alternatives, Quaderno IAMI, 99.3, CNR-IAMI, Milano.

[12] Cagno, E., Caron, F., Mancini, M. and Ruggeri, F. (2000), Sensitivity of replacement priorities for gas pipeline maintenance, in Robust Bayesian Analysis (D. Rios Insua and F. Ruggeri, eds.), Springer, New York.

USING NEURAL NETWORKS AS NONLINEAR MODEL INTERPOLATORS IN VARIANCE DECOMPOSITION-BASED SENSITIVITY ANALYSIS

[1]Marzio Marseguerra, [1]Riccardo Masini, [1]Enrico Zio and [2]Giacomo Cojazzi

[1] Department of Nuclear Engineering,
Polytechnic of Milan
Via Ponzio 34/3, 20133 Milan, Italy,
E-mail: enrico.zio@polimi.it

[2] Institute for Systems, Informatics and Safety,
Industrial Hazards Unit
Joint Research Centre, JRC-Ispra TP 723 ,
I-21020 ISPRA (VA), Italy

ABSTRACT

In this paper, we investigate the possibility of embedding neural networks, appropriately trained on the results of a Monte Carlo plant reliability evaluation, within a classical decomposition scheme for efficiently performing multiparametric sensitivity analyses of a reliability model. These analyses are of great importance for the identification of critical systems, structures and components of hazardous plants, such as nuclear or chemical ones, thus providing significant insights for their risk-based design and management.

1. INTRODUCTION

Sensitivity analysis provides an important tool to the risk-based design and management of risky plants such as the nuclear and chemical ones, aiding the identification of the critical systems, structures and components. Several approaches have been developed for performing sensitivity studies, ranging from differential to Monte Carlo analysis, response surface methodology, and Fourier amplitude sensitivity test (FAST) [1]. Typically, these approaches entail to compute the model output (a reliability or risk measure in our case of interest) several times for different input values (system, structures or components reliability characteristics in our case of interest) sampled from appropriate ranges. Often, the computation times required by the numerical solution of the model render these analyses prohibitive, so that one has to resort to simplified but fast models or empirical response surfaces.

The objective of this work is to devise a method for performing a multiparametric uncertainty and sensitivity analysis of the reliability model of a properly selected system. The technique used is based on the variance decomposition method [2]. It consists in considering several evaluations of the system unreliability characteristics in correspondence of different values of the uncertain parameters (e.g. components failure rates) and computing a variance-based *index of importance* that measures how much a set of these parameters influences the uncertainty in the system unreliability. When the model of the plant is realistically complicated, its analytical evaluation is at least impractical and one has to resort to Monte Carlo simulation which, however, could be computationally burdensome [3]. Therefore, since the variance decomposition method requires a large number of system evaluations, each one to be performed by Monte Carlo, the need arises for substituting the Monte Carlo simulation model with a fast, approximated, algorithm. In our work, we employ an empirical model built

by training artificial neural networks on the results of Monte Carlo simulations. The type of neural network here employed is the classical multi-layered, feed-forward one trained by the error back-propagation method [4]. The networks used have been generated with a user-friendly software NEST (NEural Simulation Tool) developed at the Department of nuclear engineering of the Polytechnic of Milan (www.cesnef.polimi.it/nest.htm). The training patterns for the ANNs have been generated using a user-friendly Monte Carlo simulation code, MARA (Montecarlo Availability Reliability Analysis), also developed at the Department of nuclear engineering of the Polytechnic of Milan (www.cesnef.polimi.it/mara.htm).

2. THE PLANT MODEL

The plant logic is given in Figure 1. There are 3 macro-components (called "block") made of a redundancy configuration of components with different failure and repair characteristics.

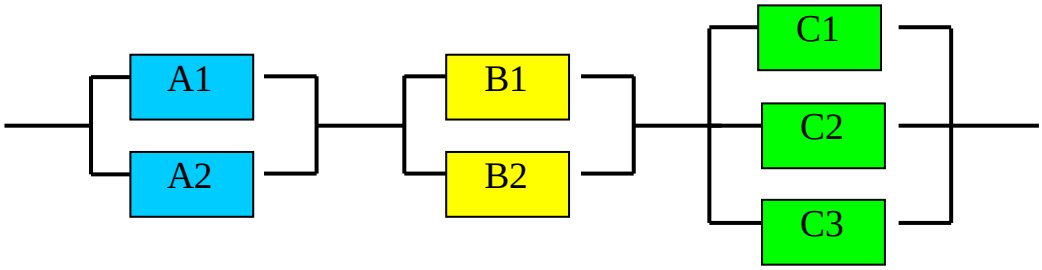

Figure 1: Plant layout

We consider the following assumptions: i) components B2, C2, C3 are in cold stand-by; ii) the components age linearly: failure rate $\lambda_i = \lambda_i^0 + a \cdot t$, where λ_i^0 is the nominal value and a is set to 10^{-4}; iii) imperfect repairs are possible according to the Brown-Proschan model with a probability p=0.1. Such imperfect repairs have a deteriorating effect in that they determine an increase by a factor of $1+\pi$ of the failure rate of the repairing component and a corresponding reduction of the repair rate of the same factor, where π =0.1; iv) the components are subject to maintenance at variable periods τ as determined from the model in [5]. The devised model is complicated enough so as to entail a Monte Carlo simulation evaluation. Embedding such simulation procedure within a variance decomposition scheme of multiparametric sensitivity analysis can lead to impractically large computing times.

3. THE ARTIFICIAL NEURAL NETWORK

Here we focus our attention on the importance of the components' failure rates which are assumed to vary within the ranges specified in Table 1, whereas the repair rates are kept constant at their nominal values. The plant model output we refer to in the analysis is the unreliability at mission time, Tm=30 years. The training set is composed of 500 different input(failure rates)/output(unreliability at T_m) patterns created by the MARA code, with failure rates values sampled from uniform distributions over the ranges of Table 1. Note that the components of blocks A and B have been purposely chosen to have nominally the same failure rates so as to allow us to highlight the effects of different logic configurations.

Table 1: range of variability of failure and repair rates.

Comp.	Nominal State	Failure rate $\lambda_i[y^{-1}]$				Repair rate $\mu_i[y^{-1}]$
		Nominal	Lower	Upper	Mean	Nominal
A1	Working	6.00E-03	1.90E-03	1.90E-02	1.04E-02	1.70E-01
A2	Working	6.00E-03	1.90E-03	1.90E-02	1.04E-02	1.00E-01
B1	Working	6.00E-03	1.90E-03	1.90E-02	1.04E-02	3.00E-01
B2	Stand-by	1.50E-02	4.75E-03	4.74E-02	2.61E-02	1.00E-01
C1	Working	8.10E-03	2.56E-03	2.56E-02	1.41E-02	5.00E-01
C2	Stand-by	2.50E-02	7.91E-03	7.90E-02	4.35E-02	3.00E-01
C3	Stand-by	5.00E-02	1.58E-02	1.58E-01	8.69E-02	5.00E-01

The optimal network architecture contains 7 input nodes receiving the 7 failure rates values, 7 hidden nodes performing intermediate processing and the single output node providing an ANN estimate of the plant unreliability at mission time.

Figure 2 shows the comparison of the estimates of the plant unreliability at mission time by the MARA code with 10^6 trials (ordinates) and the predictions of the ANN (abscissas) for different values of the 7 input failure rates of the components sampled within their respective ranges. The top picture regards the predictions on the 500 examples of the training set whereas the bottom one regards the predictions on other 500 examples never processed by the ANN during the training. The approximation made by the ANN is certainly satisfactory, considering the fact that the space spanned by the 7 input parameters is rather large.

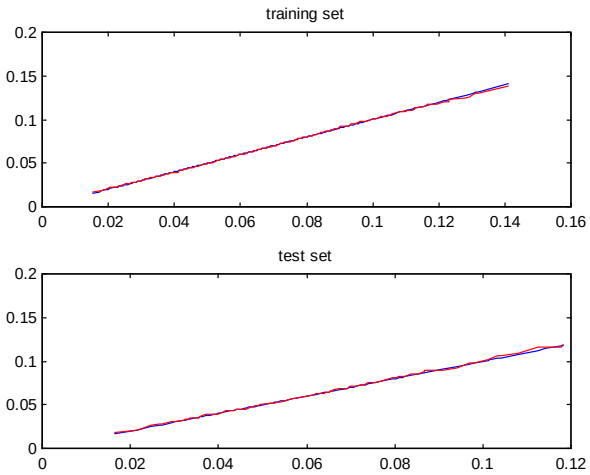

Figure 2: plant unreliability at mission time computed by the Monte Carlo code with 10^6 trials (ordinates) and predicted by ANN (abscissas): top, in the training set; bottom, in the test set

4. RESULTS

In order to study the sensitivity of the plant unreliability *y* to the uncertainty in the components failure rates X, we consider the decomposition of the variance of y [2]. This method leads to the definition of the correlation ratio $\eta_X^2 = V\left[E\left(y|X\right)\right]/V\left[y\right]$ which is taken as the importance measure of a given subset of input variables X. With the ANNs trained over the ranges of Table 1, it is possible to perform a variance decomposition sensitivity analysis

of the plant model in various situations characterized by different nominal values of the input parameters. Indeed, the trained Artificial Neural Network (ANN) can efficiently substitute the Monte Carlo code: on the same machine 100,000 runs of the ANN take about 2 minutes, so that in terms of computation speed there is a ratio of 1/50,000 with respect to the Monte Carlo evaluation.

Figure 3 shows the results of the calculation of the index of importance η_X^2 for the 3 blocks A, B, C: the vector X thus contains, in turn, the failure rates of all the components in each block. The results reflect the logic of the plant configuration so that uncertainties in the failure rates values pertaining to the least reliable block A have a greater impact on the uncertainty in the plant unreliability than those pertaining to the more reliable blocks B (identical to A except that B2 is in stand-by and not in a critical parallel) and C (with two stand-bys).

Index of importance of each block on plant unreliability at mission time	
Block	η^2
A1 –A2	0.610
B1 – B2	0.356
C1 – C2 – C3	4.862e-2

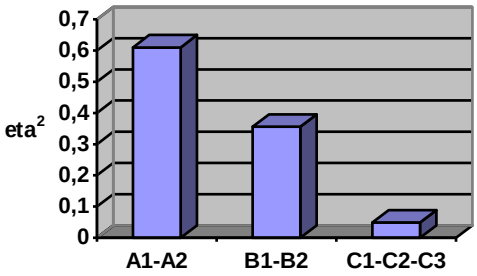

Figure 3: index of importance of the parameters of a block of components with respect to the plant unreliability at the mission time

5. CONCLUSIONS

This paper concerns the feasibility of using neural networks to build empirical models for use in variance decomposition-based sensitivity analysis. The idea behind the approach stands on the possibility of exploiting the speed of neural computing in the numerous model evaluations typically required to perform a thorough sensitivity analysis. Being a methodological feasibility study, the investigation was carried out on a suitable reference plant model, structured so as to easily show the influence of the different parameters involved.

The approach followed has led to satisfactory results in both the training of neural networks to provide reasonably accurate model outputs and in the savings of computing time. Thus, we conclude that it is feasible to employ the approximate mapping provided by neural networks for the repetitive model evaluations required by thorough multiparametric sensitivity analysis.

6. REFERENCES

1. A. Saltelli, K. Chan, E. M. Scott eds., Sensitivity Analysis, John Wiley & Sons, 2000.
2. M. D. McKay,Variance-Based Methods for Assessing Uncertainty Importance in NUREG-1150 Analyses,LA-UR-96-2695,Los Alamos National Laboratory,1996,pp. 7-11.
3. A. Dubi, Monte Carlo Applications in Systems Engineering, Wiley, 1999.
4. D. E. Rummelart, J. L. McClelland, Parallel distributed processing, vol. 1, MIT Press, Cambridge, MA, 1986.
5. M. Cantoni, M. Marseguerra, E. Zio, Genetic Algorithms and Monte Carlo Simulation for Optimal Plant Design, Reliab. Engng. And Sys. Safety, 68, 2000, pp. 29-38.

APPROXIMATING EXTREME PROBABILITIES IN RELIABILITY ANALYSES USING POLYTOPES

Enrique Castillo[(1)], *Alfonso Fernández-Canteli*[(2)] *and Roberto Mínguez*[(1)]

[(1)] Department of Applied Mathematics and Computational Sciences
University of Cantabria, 39005 Santander, SPAIN.
Email: castie@unican.es

[(2)] Department of Construction and Fabrication Engineering, University of Oviedo
SPAIN

1. ABSTRACT

In this paper a new method for calculating the probability of failure is introduced. The method is based on transforming the initial set of variables into a n-dimensional uniform random variable in the unit hypercube, together with the failure region. In this way, the joint probability density reduces to unity and then, the probability of failure simply becomes the hypervolume of the failure region. Next, the probability of failure is calculated by approximating the corresponding hypervolume by two polytopes, one interior and one exterior to the region of interest, that give upper and lower bounds of the desired probability. If the desired bounds are not satisfactory, the user can increase the number of polytopes and improve the approximations. Two are the main advantages of the proposed method with respect to the classical methods: a simpler transformation of the initial set of variables is required, and two bounds, allowing a measure of the error, are obtained. Finally, an example of application is used to ilustrate the new procedure.

2. INTRODUCTION

Since the pioneering works of Freudenthal[5] in the fifties, safety analyses have been based on probabilistic concepts and the computation of the probability of failure, in a more or less direct fashion. Consequently, the classical methods, based on partial safety coefficients, are in the process of being abandoned.

In the reliability of a system, there are many variables $(X_1,X_2,\ldots,X_n)$ involved. They belong to an n-dimensional space, which can be divided in two regions: the safe, $g(x_1,\ldots,x_2)>0$, and the failure, $g(x_1,\ldots,x_2)\le 0$, regions, where $W=g(X_1,X_2,\ldots,X_n)$ is a random variable.

In general the function $g(.)$ is not unique and can be written in many different, though equivalent, forms, with the only condition being that the region $g(x)<=0$ be associated with the system failure. The boundary of such a regions is defined by the system limit states.

The probability of failure of the system can be calculated by

$$P_f = P(W \le 0) = F_W(0) = \int_{g(x_1,x_2,\ldots,x_n)\le 0} f(x_1,x_2,\ldots,x_n)dx_n dx_{n-1}\ldots dx_1,$$

where $f(X_1, X_2,\ldots, X_n)$ is the pdf of $(X_1, X_2,\ldots, X_n)$. The main problem is that the integral is usually difficult to calculate, due to the complicated forms of $f(\mathbf{x})$ and $g(\mathbf{x})$. Thus, approximate

methods are used to obtain the failure probability (see Galambos[6], Castillo[1] and Castillo, Solares and Gómez[2,3,4]).

3. PROPOSED METHOD

The proposed method for calculating the probability of failure of a given system is as follows:

Step 1. Transforming to uniform variables

The initial set of variables is transformed into a set of variables in the unit hypercube with standard uniform marginals *U(0,1)*, using the Rosenblatt[7] transformation:

$$U_1 = F_1(X_1);\ \ U_2 = F_1(X_2 \mid X_1);\ \ \ldots\ \ U_n = F_1(X_n \mid X_1, X_2, \ldots, X_n),$$

where $F_1(X_1)$, $F_2(X_2|X_1)$, ... , $F_n(X_n|X_1,X_2,\ldots,X_n)$ are the cdf of the X_1 marginal and the cdfs of the indicated conditional random variables.

Step 2. Forcing the origin to belong to the failure region

This makes the failure region to be a neighbourhood of the origin and simplifies the identification of the failure region. We assume that the random variables involved are such that any change in its value has a monotone influence on the safety of the system being studied. This assumption implies that either the end point value *0* or the end point value *1* for such variable is the worst possible value with respect to the safety of the system. Then, it is clear that if we transform the variables U_k with 1 as their worst possible values, to $1\text{-}U_k$, we get new variables such that the origin is the worst possible combination of values for all variables, and then, the origin belongs to the failure region.

Step 3. Approximating the failure region by unions of disjoint polytopes

To this end we present two options:

- **Option 1:** Partition the failure region in polytopes as similars as possible, in terms of volume. To this end, we minimize the volume variance $\frac{1}{n}\sum_{i=1}^{n}\left(v(i)-\bar{v}\right)^2$, where *v(i)* is the volume of the polytope *i*, and *v* is its mean. In other words, we minimize the polytopes volume variance with respect to the positions of the triangle vertices subject to the boundary constraints, i.e. the corner nodes are fixed, the boundary nodes are restricted to move in the boundary, and the interior nodes are free to move in any direction, as illustrated in Figure 1. An illustrative example is shown in Figure 2, where it is assumed that we look for the volume associated with the region $0 < z < sin(x)sin(y)$, that is shown in the upper part of the figure, together with the corresponding triangularization, obtained from an initial regular projected triangular mesh (lower part of the figure) that evolves, during the optimization process, to the final projected mesh in the figure.

- **Option 2:** An spherical regular mesh is used to intersect the failure region and the intersection points are selected as the polytope vertices (see Figure 3).

Step 4. Calculating the probability of failure

- **Option 1:** We calculate two estimates of P_f : $v_{1i} = \frac{1}{3} a_i \left(3z_{gi} + 2(z_{i1} + z_{i2} + z_{i3})\right)$ and $v_{2i} = \frac{1}{3} a_i z_{gi}$, where a_i is the area of the polytope triangular basis and z_{i1},, z_{i2},, z_{i3} and z_{gi} are the z-values associated with the three vertices x_{i1} , x_{i2} ,x_{i3} , and its center of gravity respectively. These two formulas give the lower and the upper bounds for the polytope volumes. Determination of which one is the lower and which is the upper bound can be done by a simple comparison.

- **Option 2:** The polytopes are decomposed in simplices and the corresponding determinant formula is used to calculate their volumes.

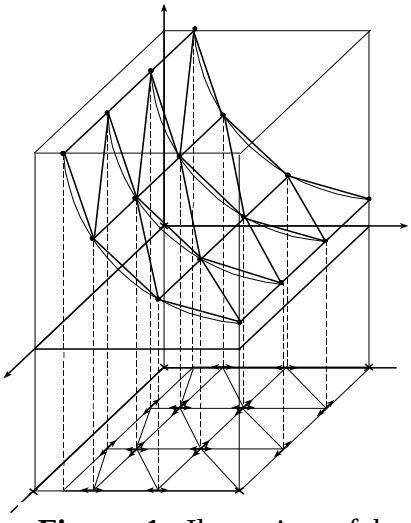

Figura 1: Ilustration of how the net is generated.

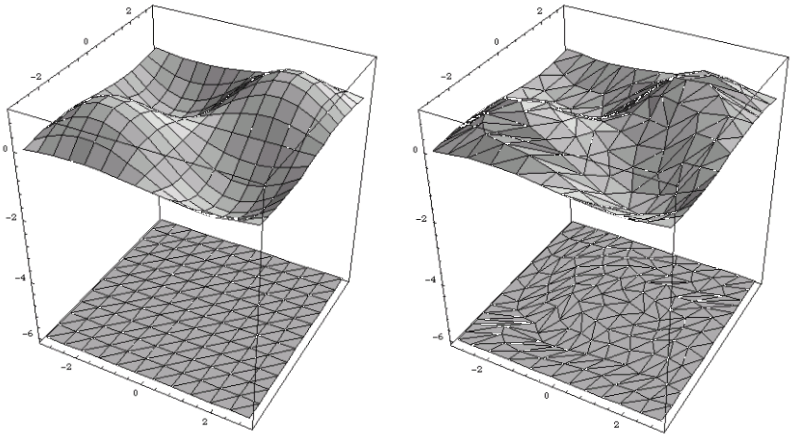

Figure 2: Surface to be triangulated, initial and final meshes, and resulting triangulated surface.

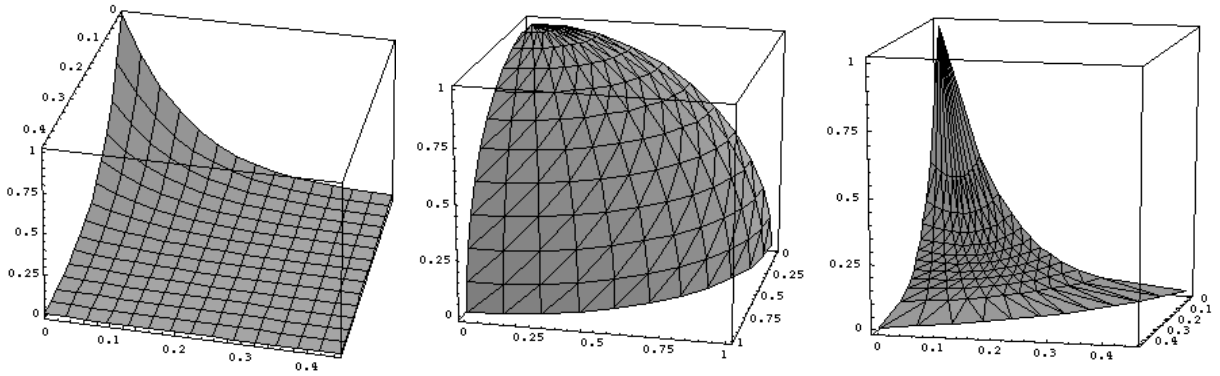

Figure 3: Initial surface to be triangulated, spherical regular mesh and resulting triangulated surface.

4. PERFORMANCE OF THE METHOD

To test the goodness of the method, it has been applied to the following example. Let X_1, X_2 and X_3 be independent and identically distributed (iid) random variables with exponential distribution, $E(\lambda)$.

Consider the random variable, $Z = (X_1 + X_2)/(X_1 + X_2 + X_3)$, which is known to have a cumulative distribution function $F_Z(z) = z^2; 0 \le z \le 1$. Since in this case we know the exact cdf of *Z*, we can compare the exact and the approximated results. Suppose that we want to calculate $F_Z(0.1)$, which exact value is *0.01*. Table 1 shows the obtained results for differents number of polytopes in which we divide the failure region, for Options 1 and 2.

Option 1			**Option 2**		
Size	Lower bound	Upper bound	Size	Lower bound	Upper bound
25 (32)	0.00841	0.01599	25 (28)	0.00822	0.01167
36 (50)	0.00803	0.01497	36 (45)	0.00850	0.01115
49 (72)	0.00825	0.01393	49 (66)	0.00870	0.01080
64 (98)	0.00866	0.01271	64 (91)	0.00884	0.01057
81 (128)	0.00886	0.01217	81 (120)	0.00894	0.01038
100 (162)	0.00899	0.01190	100 (153)	0.00903	0.01023
121 (200)	0.00920	0.01143	121 (190)	0,00909	0.01014
144 (242)	0.00935	0.01205	144 (231)	0.00914	0.01003
Infinity	0.01000	0.01000	*Infinity*	0.01000	0.01000

Table 1: Estimations of the failure probability for an increasing number of polytopes. The size column gives the number of nodes and polytopes (in parenthesis)

5. CONCLUSIONS

The Rosenblatt transformation together with a partition of the failure region in polytopes seems to be a useful way of calculating failure probabilities associated with complicated regions. Upper and lower bounds are easily obtainable. Option 2 is better than Option 1 because it requires much less computational power.

6. REFERENCES

[1] E. Castillo. *Extreme Value Theory in Engineering*. Academic Press, New York, 1988.

[2] E. Castillo, C. Solares, and P. Gómez. Tail sensitivity analysis in Bayesian networks. In Proceedings of the Twelfth Conference on Uncertainty in Artificial Intelligence (UAI'96), Portland (Oregon), Morgan Kaufmann Publishers, San Francisco, California, 133-140, 1996.

[3] E. Castillo, C. Solares, and P. Gómez. Estimating Extreme Probabilities Using Tail Simulated Data. *International Journal of Approximate Reasoning*, 1996.

[4] E. Castillo, C. Solares and P. Gómez. High Probability One-sided Confidence Intervals in Reliability Models. *Nuclear Science and Engineering*, Vol. 126, 158-167, 1997.

[5] A. N. Freudenthal. Safety and the probability of structural failure. *Transactions, ASCE 121*, 1337-1397, 1956.

[6] J. Galambos. *The Asymptotic Theory of Extreme Order Statistics*. Robert E. Krieger Publishing Company. Malabar, Florida, 1987.

[7] M. Rosenblatt. Remarks on a multivariate transformation. *Ann. Math. Stat. 23(3)*, 470-472, 1952.

EPISTEMIC SENSITIVITY ANALYSIS BASED ON THE CONCEPT OF ENTROPY

Bernard Krzykacz-Hausmann

Gesellschaft für Anlagen- und Reaktorsicherheit (GRS)
D 85748 Garching
E-mail: krb@grs.de

1. INTRODUCTION

Applications of computational models to complex real situations are often subject to uncertainty. In many cases this uncertainty is of "epistemic" type, i.e. it is due to the imprecise knowledge of deterministic parameter values, phenomena, model assumptions [IAEA, 1989]. The aim of sensitivity analysis in such cases is to quantitatively express the degree of impact of the uncertainty from the specific sources on the resulting uncertainty of final model output. This information helps the analyst to identify the most important contributors to output uncertainty and, hence, to find the most effective ways of reducing that uncertainty.

Various indices of sensitivity are currently used for this purpose. The best known among them are the traditional correlation/regression-related sensitivity and their rank counterparts [Helton 1993]. However, it is well known that sometimes these indices may not be appropriate, e.g. in models with highly non linear or non monotonic relationships between input and output. Therefore, more recently, a new class of sensitivity indices has been introduced which result from the principle of "expected reduction in variance". The main characteristic of this principle is that it considers the variance of a probability distribution as an overall scalar measure of uncertainty which expresses by a single number the total amount of uncertainty represented by this distribution. This principle leads to the well-known expressions like

$$\mathrm{varY} - \mathrm{EvarY}|\, X_i \quad \text{or} \quad \mathrm{E\ varY}|X_1,...,X_{i-1},X_{i+1},...,X_n$$

which may be interpreted as "the amount of variance of output Y that is expected to be removed if the true value of parameter X_i will become known" respectively as "the amount of variance of output Y that is expected to remain if the true values of all parameters except X_i will become known". Expressions of this kind and their sample versions have been considered by several authors [Iman & Hora 1990, McKay 1995, Homma & Saltelli 1996].

However, when considering the variance and its basic properties more closely, one may easily find some inconsistencies with the properties intuitively expected from an overall scalar measure of "epistemic" uncertainty. E.g. many people would agree that, over a bounded interval, the highest possible degree of "epistemic" uncertainty is expressed by the uniform distribution. Consequently, a scalar overall uncertainty measure should attain its maximum possible value for the uniform distribution over that interval. However, as simple examples may show, this is not the case if variance is used as a scalar "epistemic" uncertainty measure.

An overall scalar uncertainty measure that is maximized by the uniform distribution is *entropy* [Kapur 1989, Kullback 1959, Reza 1961, Johnson & Kotz 1982]. It is defined by

$$H(Y) = - \sum p_i \ln p_i$$

for a discrete distribution of Y with the probability function $(p_1,..., p_n)$, respectively by

$$H(Y) = - \int f(y) \ln f(y) \, dy$$

for a continuous distribution of Y with the probability density f(y).

It may be interpreted as "a measure of the extent to which the distribution of Y is concentrated over a small range of values or dispersed over a wide range of values", or, in other words, as a measure of the degree of *indeterminacy* of Y represented by its distribution. In contrast to the variance, it possesses the desirable property (for "epistemic" uncertainty) that among all distributions over a bounded interval the uniform distribution has the maximum possible entropy value. From this and other properties it appears that the notion of entropy may be appropriate to represent the uncertainty of "epistemic" type while the notion of variance seems to be more appropriate to represent the uncertainty of "aleatory" type [IAEA, 1989].

2. BASIC APPROACH

The most basic form of an entropy-based index may be obtained analogously to the variance based index varY–EvarY|X. One therefore considers the following expressions:

$$H(Y) = - \int f(y) \ln f(y) \, dy ,$$

i.e. the (unconditional) entropy of output Y interpreted as a 'measure of the total (unconditional) uncertainty of Y, i.e. uncertainty coming from all parameters',

$$H(Y|x) = - \int f(y|x) \ln f(y|x) \, dy$$

i.e. the conditional entropy of Y given X=x, i.e. the entropy of the conditional distribution of Y given X=x, interpreted as 'measure of uncertainty of Y coming from the other parameters if the value of the parameter X is known to be x',

$$H(Y|X) = \int H(Y|x) f(x) \, dx = - \int \int f(y|x) \ln f(y|x) f(x) \, dy \, dx$$

i.e. the expectation of the conditional entropy of Y given X, interpreted as the 'expected uncertainty of Y if the true value of parameter X will become known', and finally

$$H(Y) - H(Y|X)$$

i.e. the difference between the unconditional entropy of Y and the expected conditional entropy of Y given X. It may, analogously to varY–EvarY|X , be interpreted as

"the amount of entropy of output Y that is expected to be removed if the true value of parameter X will become known" .

Comments:

1. Properties of H(Y) – H(Y|X) as sensitivity index are: it is not negative, it is 0 if X and Y are independent, it is symmetric in X and Y, it is invariant under bijective transformations of X and Y. Note that its variance-based counterpart varY–EvarY|X is not symmetric and invariant solely under bijective transformations of X alone. Both H(Y) – H(Y|X) and varY–EvarY|X can easily be extended to vector-valued X thus providing sensitivity indices with respect to parameter subsets. However, only H(Y) – H(Y|X) can be extended to vector-valued Y providing sensitivity indices for multidimensional model output Y.

2. By elementary manipulations the following alternative expression

$$H(Y) - H(Y|X) = \int\int f(x,y) \ln \frac{f(x,y)}{f(x)f(y)} \, dx \, dy$$

may easily be derived. Therefore, with the concept of the *Kullback-Leibler measure of discrepancy* between two probability densities g and h [Kullback 1959, Kapur 1989] defined by

$$I[g/h] = \int g(u) \ln \frac{g(u)}{h(u)} \, du ,$$

the following useful interpretation can be formulated:

H(Y) – H(Y|X) = "discrepancy between the joint density of parameter X and output Y and the product of the marginal densities of X and Y"

which indicates that H(Y) – H(Y|X) may also be regarded as a kind of degree of departure of output Y from being independent of parameter X (somehow like the covariance).

3. A normalized version of H(Y) – H(Y|X) that ranges between 0 and 1 is given by

$$\eta = \frac{H(Y) - H(Y \mid X)}{H(Y)}$$

for discrete variables Y and by

$$\rho_H^2 = \frac{\exp(2H(Y)) - \exp(2H(Y \mid X))}{\exp(2H(Y))} = 1 - \exp[-2(H(Y) - H(Y|X))]$$

for continuous variables Y. It is also called 'coefficient of entropic or informational correlation' [Linfoot 1957, Kent 1983]. In the bivariate Normal case it coincides with $\rho 2$.

4. Extending the above considerations to vector valued X one can consider the expression

$$H(Y \mid X_1,...,X_{i-1},X_{i+1},...,X_n)$$

$$= \int...\int H(Y| x_1,...,x_{i-1},x_{i+1},...,x_n) \, f(x_1,...,x_{i-1},x_{i+1},...,x_n) \, dx_1...dx_{i-1}dx_{i+1}...dx_n$$

$$= \int...\int [-\int f(y|x_1,...,x_{i-1},x_{i+1},...,x_n) \ln f(y|x_1,...,x_{i-1},x_{i+1},...,x_n) dy] \, f(x_1,...,x_{i-1},x_{i+1},...,x_n)$$

$$dx_1...dx_{i-1}dx_{i+1}...dx_n$$

which is the expectation of the entropy of the conditional distribution of Y given parameters X1,...,Xi-1,Xi+1,...,Xn. It can be interpreted as "the amount of entropy/uncertainty of Y that is expected to remain if the values of all parameters except Xi will become known" and can therefore be viewed as an global sensitivity index accounting for the 'total effect of parameter X i' analogously to its variance-based counterpart E varY| X1,...,Xi-1,Xi+1,...,Xn mentioned before and discussed e.g. in [Homma & Saltelli 1996] for independent parameters.

3. A SIMPLE ANALYTICAL EXAMPLE

To illustrate the preceding results a simple example is presented where both variance-based and entropy-based sensitivity indices can be determined analytically and compared.

Let the model output Y be a linear function

$$\mathbf{Y = a_1X_1 + a_2X_2 + ... + a_nX_n}$$

of the n parameters $X_1,....,X_n$ having a joint multivariate Normal distribution $N_n(\boldsymbol{\mu},\boldsymbol{\sigma},\mathbf{R})$, $\boldsymbol{\mu}/\boldsymbol{\sigma}$ = vectors of means/variances, $\mathbf{R} = (\rho_{ij})$ = correlation matrix.

Then it is not very difficult to verify that for any parameter X_i

$$\text{varY} - \text{EvarY}|X_i = (\sum a_k \sigma_k \rho_{ik})^2 .$$

$$H(Y) - H(Y|X_i) = -1/2 \ln [1 - (\sum a_k \sigma_k \rho_{ik})^2 / \mathbf{a}^t \mathbf{C}\, \mathbf{a}]$$

with $\mathbf{a}^t = (a_1 ,..., a_n)$ and $\mathbf{C} = (\sigma_i \sigma_j \rho_{ij})$ the variance-covariance matrix of the parameters. In the simpler case with independent parameters (i.e. $\mathbf{R} = \mathbf{I}_n$) the corresponding expressions are

$$\text{varY} - \text{EvarY}|X_i = a_i^2 \sigma_i^2 \quad \text{and} \quad H(Y) - H(Y|X_i) = -1/2 \ln [\, 1 - a_i^2 \sigma_i^2 / \sum a_k^2 \sigma_k^2 \,]$$

Obviously, the two methods provide different values of the corresponding measures but the same parameter importance ranking, since one measure is a monotone function of the other. Moreover, their normalized versions $(\text{varY} - \text{E varY}|X_i)/\text{var}(Y)$ and $1 - \exp(-2[H(Y) - H(Y|X_i)])$ are identical.

Furthermore, in this example both versions of the 'global sensitivity index for parameter X_i' $\text{E varY}| X_1,...,X_{i-1},X_{i+1},...,X_n$ and $H(Y \mid X_1,...,X_{i-1},X_{i+1},...,X_n)$ can be determined. For i=1:

$$\text{E varY}|(X_2 ,..., X_n) = a_1^2\sigma_1^2[\, 1 - (\rho_{12} ,...,\rho_{1n})\, \mathbf{R_{22}^{-1}}\, (\rho_{12} ,...,\rho_{1n})^t \,]$$

$$H(Y| X_2 ,..., X_n) = 1/2 \ln (2\pi\, e\, a_1^2\, \sigma_1^2 [1 - (\rho_{12} ,...,\rho_{1n})\, \mathbf{R_{22}^{-1}}\, (\rho_{12} ,...,\rho_{1n})^t \,])$$

where $\mathbf{R_{22}^{-1}}$ is the inverse of the correlation sub-matrix $\mathbf{R_{22}}$ of $\mathbf{R}$ for parameters $X_2,...,X_n$. In the simpler case with independent parameters the corresponding expressions are

$$\text{E varY}|(X_2 ,..., X_n) = a_i^2 \sigma_i^2 \quad , \quad H(Y| X_2 ,..., X_n) = 1/2 \ln [\, 2\pi\, e\, a_i^2 \sigma_i^2].$$

Again, the expressions are different but their normalized versions $\text{E varY}|(X_2 ,..., X_n)/\text{varY}$ and $\exp(2\, H(Y| X_2 ,..., X_n))/\exp(2H(Y))$ and the parameter importance ranking are the same.

4. ESTIMATES FROM SAMPLES

In practical applications all the quantities considered above cannot be determined analytically but must rather be estimated from appropriately generated sample values. Moreover, many computational models are extremely time-consuming to run such that only a relatively small number of model runs can be afforded for sample generation. The so-called 'simple random sampling (SRS)' may be appropriate in such cases. An estimate of $H(Y) - H(Y|X)$ using the sample values (x_j, y_j), j=1,...,N of the fixed parameter X and output Y is derived as follows:

The three probability density functions f(x) = marginal density of parameter X,

f(y) = marginal density of outcome Y, f(x,y) = joint density of parameter X and outcome Y appearing in the above expression for $H(Y) - H(Y|X)$ may be estimated by the following simple empirical density functions:

$$f^*(x) = \sum n_{i.}/n.. \, (a_i - a_{i-1})^{-1} \, \mathbf{1}[a_{i-1},a_i)(x) \,, \qquad f^*(y) = \sum n_{.j}/n.. \, (b_j - b_{j-1})^{-1} \, \mathbf{1}[b_{j-1},b_j)(y)$$

$$f^*(x,y) = \sum\sum n_{ij}/n.. \, (a_i - a_{i-1})^{-1} \, (b_j - b_{j-1})^{-1} \mathbf{1}[a_{i-1},a_i)(x) \, \mathbf{1}[b_{j-1},b_j)(y)$$

where, $a_0<a_1<...<a_k$ and $b_0<b_1<...<b_m$ are partitions of the ranges of X and Y into k respectively m disjoint subintervals to be provided by the user; n_{ij} = number of sample points (x_k,y_k) falling into the rectangle $[a_{i-1},a_i)x[b_{j-1},b_j)$; $n_i.$ = number of x_k values falling into the interval $[a_{i-1},a_i)$; $n._j$ = number of y_k values falling into the interval $[b_{j-1},b_j)$; n.. = total number of sample points (= N) , and $\mathbf{1}[a_{i-1},a_i)$, $\mathbf{1}[b_{j-1},b_j)$ are the indicator functions of the intervals $[a_{i-1},a_i)$, $[b_{j-1},b_j)$.

Inserting these empirical density functions into the above expression for H(Y) – H(Y|X) one obtains the estimate

$$H^*(Y)–H^*(Y|X) = \int\int f^*(x,y) \ln \frac{f^*(x,y)}{f^*(x) f^*(y)}\, dx\, dy = ... = \sum_j \sum_i \frac{n_{ij}}{n_{..}} \ln\left[\frac{n_{ij}/n_{..}}{(n_{i.}/n_{..})(n_{.j}/n_{..})}\right]$$

The above mentioned discrete normalized version of this estimate ranging between 0 and 1 is

$$\eta^* = \frac{H^*(Y) - H^*(Y \mid X)}{H^*(Y)} = \sum_j \sum_i \frac{n_{ij}}{n_{..}} \ln\left[\frac{n_{ij}/n_{..}}{(n_{i.}/n_{..})(n_{.j}/n_{..})}\right] / - \sum \frac{n_{.j}}{n_{..}} \ln\left[\frac{n_{.j}}{n_{..}}\right]$$

This expression can also be identified as a measure of association in contingency tables, the so-called (asymmetric) *uncertainty coefficient U* [Brown 1975], or *Theil's coefficient* η [Theil 1970, Johnson & Kotz 1982]. Its asymptotic sampling distribution may be used to construct approximate confidence intervals for η.

5. REFERENCES

IAEA, 1989. Evaluating the Reliability of Predictions Made Using Environmental Transfere Models. Safety Series Report No. 100, Vienna, International Atomic Energy Agency

Helton, J.C., 1993. Uncertainty and sensitivity analysis techniques for use in performance assessment for radioactive waste disposal. *Reliability Engineering and System Safety* Vol. 42, no. 2-3, 327-367

Iman, R.L., Hora, S.C., 1990. A robust measure of uncertainty importance for use in fault tree system analysis. *Risk Analysis,* 10, 401-406

McKay M.D., 1995. Evaluating prediction Uncertainty. Tech. Rep. NUREG/CR-6311. U.S. Nuclear Regulatory Commission and Los Alamos National Laboratory.

Homma, T., Saltelli A., 1996. Importance measures in global sensitivity analysis of nonlinear models. *Reliability Engineering and System Safety* Vol. 52, 1-17

Kapur J.N., 1989. Maximum entropy models in science and engineering. John Wiley & Sons

Reza F.M., 1961. Introduction to Information Theory. McGraw-Hill, New York.

Kullback, S., 1959. Information Theory and Statistics. John Wiley, New York.

Kotz S., Johnson N.L., 1982. Encyclopedia of statistical sciences. John Wiley & Sons Inc.,

Linfoot E.H., 1957. An Informational Measure of Correlation. *Information and Control,* 1, 85-89

Kent J.T., 1983. Information gain and a general measure of correlation. *Biometrika* 70, 1, 163-73

Brown M.B., 1975. The asymptotic standard errors of some estimates of uncertainty in the two-way contingency table, *Psychometrika*, Vol. 40, no. 3, 291-296.

Theil H., 1970. On the estimation of relationships involving qualitative variables. *American Journal of Sociology* 76, 103-154.

SAMPLING IN THE FREQUENCY DOMAIN TO IDENTIFY A METAMODEL

Thierry Alex MARA, Philippe LAURET

University of La Réunion Island, Laboratoire de Génie Industriel,
BP 7151, 15 avenue René Cassin, 97 715 Saint-Denis, France.
Email : mara@univ-reunion.fr.

1. SUMMARY

The paper deals with regression analysis. We propose a special sampling that consists in oscillating each factor in its uncertainty range to identify the regression polynomial. We illustrate the method identifying the fifth order metamodel of eleven factors model.

2. REGRESSION ANALYSIS

Regression analysis consists in approaching the model by a polynomial also called a metamodel. Let's suppose that the model is not linear as regard to its *p*-factors but contains non negligible second order interactions. Then, the metamodel is a second degree polynomial of the form :

$$y = \beta_0 + \sum_{h=1}^{p} \beta_h x_h + \sum_{h} \sum_{h'} \beta_{hh'} x_h x_{h'} + \varepsilon \qquad (1)$$

The relative importance of each factor is measured by the absolute value of β_h, provided that the factors are *standardized* (mean 0 and variance 1). Moreover, verification of the numerical model can be partially achieved by analysing whether the metamodel has main effects with the *correct signs* (*what-if analysis*) [1].

Classically, design of experiments (DOE) is used to build the previous polynomial. DOE consists in simulating the appropriate combination of factors (for instance, fractional factorial design, the Plackett & Burman design,…) to estimate the regression coefficients of the presumed metamodel.

3. THE PROPOSED DESIGN

The proposed approach is based upon a special sampling of the factors in the frequency domain. Indeed, each continuous factor *X* is sampled as follow :

$$X_i^k = X_i^0 + \theta_i \sin(2\pi f_i k/n) \qquad (2)$$

where

X_i	is the i^{th} factor (X_i^0 its nominal value)
θ_i	is the oscillation amplitude, range over which the level settings are changed
f_i	is the *driving frequency* of factor *i*
n	is the number of simulation runs
k	*is the simulation number*

This particular design is similar to the Fourier amplitude sensitivity technique (FAST, see [2]). To understand the interest of such an approach, one must notice that *standardization* brings to:

$$x_i = sin(2\pi f_i u) \text{ with } u = k/n \text{ and } u \in \{0, 1/n, 2/n, \ldots,(n\text{-}1)/n\}$$

Hence, the number of simulation runs n is equal to the sampling frequency (f_s) of the factors' value. Substituting the latter relationship in eq. (1) and neglecting the error term gives:

$$\Delta y \approx \sum_{h=1}^{p} \beta_h \, sin\left(2\pi f_h u\right) + \sum_{h} \sum_{h'} \frac{\beta_{hh'}}{2} \left(-cos\left(2\pi \left(f_h + f_{h'} \right) u\right) + cos\left(2\pi \left(f_h - f_{h'} \right) u\right)\right) \qquad (3)$$

$\Delta y = y - \beta_0$ is the variation of the output due to the oscillation of the factors around their nominal value according eq. (2).

Qualitative inferences about the relative importance of a factor is possible analysing the spectrum of the Fourier transform of Δy :

$$TF_{\Delta y}(f) \approx \sum_{h=1}^{p} \frac{\beta_h}{2} . \delta(f - f_h) + \sum_{h} \sum_{h'} \frac{\beta_{hh'}}{4} . \left[\delta\left(f - \left(\left| f_h - f_{h'} \right| \right) \right) - \delta\left(f - \left(f_h + f_{h'} \right) \right) \right] \quad \forall f \geq 0 \qquad (4)$$

δ is the distribution of Dirac.

Several inferences can be drawn analysing Eq. (4) :

1) the more a factor is influential on the output, the higher the amplitude at its assigned *frequency*.
2) interaction between two factors induces two other *frequencies* which are the sum and the difference of the interacting factors' *driving frequencies*.
3) the induced frequencies may interfere with the original factors' *driving frequencies*. The latter must be incommensurate to avoid such an interference or aliasing.
4) Nyquist criterion requires that the frequency sampling of the factor's value (in other words, the number of simulations) must be at least greater than $2 \times \max_{i \in [1,p]} \left(f_i \right)$.

Because *sinus* and *cosinus* are orthogonal functions, regression coefficients of the metamodel can be easily estimated. Indeed, according eq. (3), this property implies that :

$$\beta_h = \frac{2}{n} \sum_{k=0}^{n-1} \Delta y \, sin\left(2\pi f_h k / n\right)$$

and $$\beta_{hh'} = -\frac{4}{n} \sum_{k=0}^{n-1} \Delta y \, cos\left(2\pi \left(f_h + f_{h'} \right) k / n\right) = \frac{4}{n} \sum_{k=0}^{n-1} \Delta y \, cos\left(2\pi \left(f_h - f_{h'} \right) k / n\right)$$

The proposed method based upon a special sampling in the frequency domain allows the estimation of the factors' effects on the model's output. This estimation is unbiased if aliasing is avoided. It is important to note that the advantage of the proposed design is to put forward the interactions between factors.

4. APPLICATION TO A MODEL OF INDOOR SOLAR ABSORTANCE

To illustrate the method, let's consider the 11-factor model of indoor solar radiation absorptance. In the present study, to ensure a highly order polynomial, a large range of variation are assigned to the factors (Table 1).

Table 1. **The eleven factors and their assigned frequency.**

Factors	Nominal value	Range	f	**Standardized factors**
Direct incident solar radiation (X_D)	500 W	[0 ; 1000] W	179	$x_D = X_D /500 - 1$
Diffuse solar radiation (X_d)	500 W	[0 ; 1000] W	209	$x_d = X_d /500 - 1$
Indoor absorptance of the floor ($X_{a,sol}$)	0.5	[0.05 ; 0.95]	293	$x_{a,sol} = (X_{a,sol} - 0.5)/0.45$
Average absorptance of envelope walls ($X_{a,par}$)	0.5	[0.05 ; 0.95]	301	$x_{a,par} = (X_{a,par} - 0.5)/0.45$
Average absorptance of internal walls ($X_{a,int}$)	0.5	[0.05 ; 0.95]	168	$x_{a,int} = (X_{a,int} - 0.5)/0.45$
Average absorptance of windows ($X_{a,vit}$)	0.075	[0.05 ; 0.1]	137	$x_{a,vit} = (X_{a,vit} - 0.075)/0.025$
Area of the floor ($X_{S,sol}$)	30 m²	[10 ; 50] m²	233	$x_{S,sol} = (X_{S,sol} - 30)/20$
Area of envelope walls ($X_{S,par}$)	80 m²	[50 ; 110] m²	251	$x_{S,par} = (X_{S,par} - 80)/30$
Area of internal walls ($X_{S,int}$)	7 m²	[0 ; 14] m²	270	$x_{S,int} = (X_{S,int} - 7)/7$
Area of windows ($X_{S,vit}$)	10 m²	[1 ; 19] m²	154	$x_{S,vit} = (X_{S,vit} - 10)/9$
Average transmittance of windows (X_t)	0.7	[0.5 ; 0.9]	219	$x_t = (X_t - 0.7)/0.2$

We perform 4096 (f_s) simulation runs as described previously with the frequencies mentioned in Table 1. For each run, variation of total solar radiation absorbed by the room (Δy) is calculated (y_0 = 920 W). Then, we estimate the Fourier transform of Δy. Analysis of the spectrum of Δy (Fig. 1) allows to identify the most important spectral component of the signal. For instance, according Fig. 1, we identify a first order polynomial of the form :

$$P_1 = y_0 + \beta_1 x_D + \beta_2 x_d + \beta_3 x_{a,sol} + \beta_4 x_{a,par} + \beta_5 x_{S,vit}\ sin(2\pi f_i u)$$

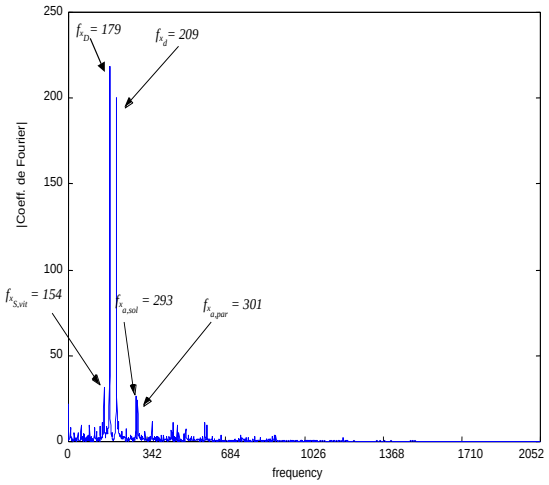

Fig. 1: Spectrum of Δy . Identification of *driving frequencies.*

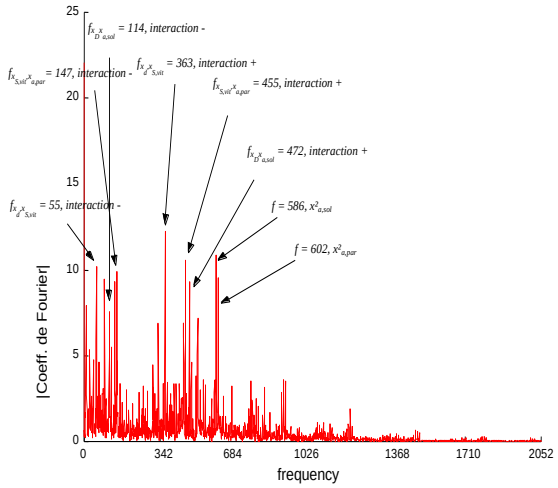

Fig. 2: Spectrum of (Δy - P_1). Frequencies induced by first order interactions.

Because of the non linearity, we use a fitting algorithm to identify the regression coefficients β_i. Then, we analyse the spectrum of (Δy - P_1) shown on Fig. 2. The latter puts forward the interactions (first order) between factors. According Fig. 2, it is possible to increase the degree of the previous polynomial to a second order one of the form :

$$P_2 = y_0 + \beta_1 x_D + \beta_2 x_d + \beta_3 x_{a,sol} + \beta_4 x_{a,par} + \beta_5 x_{S,vit} + \beta_6 x_d x_{S,vit} + \beta_7 x_{a,par} x_{S,vit} + \beta_8 x_{a,sol} x_D + \beta_9 (x_{a,par})^2 + \beta_{10} (x_{a,sol})^2 + \ldots$$

In the same way, a third order polynomial can be determined analysing the spectrum of ($\Delta y - P_2$). The procedure is kept on until a *satisfying* metamodel is obtained. As far as we are concerned, we stop the procedure when the regression coefficients fall under 20W. The identified metamodel is the following 5th order polynomial :

$$\phi_{tot,abs} = 920 + \mathbf{449} x_d + \mathbf{473} x_D + \mathbf{29} x_{a,par} + \mathbf{38} x_{a,sol} - \mathbf{66} x_{S,vit} - \mathbf{22} x_t + 27 x_{a,sol} x_D - 49 x_d x_{S,vit} + 41 x_{a,par} x_{S,vit} - 25 x_{a,par} x_{a,sol} + 38 x_{a,par} x_d + 31 x_{a,sol} x_{S,vit} - 27 x_D x_{S,vit} - 25 (x_{a,par})^2 + 26 x_{a,par} x_d x_{S,vit} - 28 x_{a,sol} x_{a,par} x_{S,vit} - 24 (x_{a,par})^2 x_d + 22 (x_{a,sol})^2 x_{a,par} - 28 x_{a,sol} x_{a,par} x_D + 28 x_{a,sol} x_D x_{S,vit} - 20 x_{a,sol} x_{a,par} x_d - 22 (x_{a,par})^2 x_{S,vit} + 26 (x_{a,par})^3 - 34 (x_{a,sol})^2 (x_{a,par})^2 - 35 (x_{a,par})^4 + 29 (x_{a,par})^2 x_d x_{a,sol} + 20 (x_{a,par})^2 x_D x_{a,sol} + 19 (x_{a,par})^2 x_{S,vit} x_{a,sol} + 19 (x_{a,par})^2 (x_{S,vit})^2 + 30 (x_{a,sol}) (x_{a,par})^3 + 23 (x_{a,par})^4 x_{a,sol}$$

5. DISCUSSION

Analysing the previous response surface, one may notice that main effects (bold) are preponderant and that the sign of the latter are in agreement with physical sense. Indeed, concerning window's properties ($x_{S,vit}$, x_t), the higher they are the less the amount of solar radiation absorbed by the room (or the more the amount of solar radiation leaving by the window). A comparison between the original model and the metamodel is carried out using a pseudo-random sampling. Fig. 3 shows that the metamodel gives very satisfying results. The coefficient of determination is about $R^2 = 0.96$.

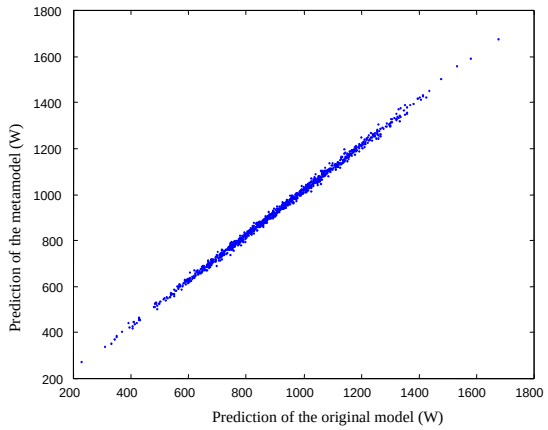

Fig. 3
Comparison between the regression polynomial and the original model.

6. REFERENCES

[1] Kleijnen J.P.C. : *Experimental design for sensitivity analysis, optimization, and validation of simulation models*, Chapter 6 in : Handbook of Simulation, edited by J. Banks, Wiley, New York, pp. 173-223, August 1998.

[2] Cukier R. I., Fortuin C. M., Schuler K. E. & al. : *Study of the Sensitivity of Coupled Reaction Systems to Uncertainties in Rate Coefficients, Part I Theory*, Journal of Chemical Physics Vol. 59, pp. 3873-3878, 1973.

SENSITIVITY ANALYSIS AND ROBUST DESIGN USING CELLULAR EVOLUTIONARY STRATEGIES AND INTERVAL ARITHMETIC TECHNIQUES

Claudio M. Rocco S., José Alí Moreno, Néstor Carrasquero

Universidad Central Venezuela Facultad de Ingeniería
Apartado 47937, Caracas 1040ª
Email: crocco@reacciun.ve

SUMMARY

Sensitivity analysis is a technique by which one can determine, with good approximation, whether a system will work within the specification limits when the part parameters vary between their limits. This paper shows the use of Interval Arithmetic as an alternative and valid technique to calculate how system accuracy varies as parameters vary.

Although this type of analysis, from input to output, can provide useful information to the decision-maker, we present an approach based on the use of Cellular Evolutionary Strategies (CES) and Interval Arithmetic (IA) in which the inverse problem can be solved especially when there are specifications for the outputs.

1. SENSITIVITY, UNCERTAINTY ANALYSIS AND ROBUST DESIGN

For examining the effects of uncertain inputs within a model, various analytic and computational techniques exist. These include methods for sensitivity analysis, uncertainty propagation, and uncertainty analysis [1]. Although this type of analysis, from input to output, can provide useful information to the decision-maker, we present an approach in which the inverse problem can be solved especially when there are specifications for the outputs.

The robustness of a design is defined as the maximum size of component deviations from a design that can be made in such a way that the system still meets all defined specifications. This paper proposes an innovative approach based on optimisation instead of mapping from the output into the input space.

2. INTERVAL ARITHMETIC

Interval arithmetic originates from the recognition that frequently there is uncertainty associated with the parameters used in a computation [2-4]. This form of mathematics uses interval "numbers", which are actually an ordered pair of real numbers representing the lower and upper bound of the parameter range [4]. Interval arithmetic is built upon a basic set of axioms. If we have two interval numbers **T** = [a, b] and **W** = [c, d] ($a \le b$, $c \le d$ then [6-10]:

T+W=[a,b]+[c,d] = [a+c, b+d]; **T-W** = [a,b] +(- [c,d]) = [a-d,b-c];

1/T = [1/b , 1/a], $0 \notin$[a,b]; **T*W** =[min{ac,ad,bc,bd}, max{ac,ad,bc,bd}];

T/W =[a,b]/[c,d] = [a,b]*[1/d,1/c], $0 \notin$ [c,d]

Only some of the algebraic laws valid for real numbers remain valid for intervals. For example, the distributive law does not always hold for interval arithmetic [2]. But the subdistributivity law does hold: $T(W+Z) \subseteq TW+TZ$. The failure of the distributive law often causes overestimation (dependency problem [3]). In general, when a given variable occurs more than once in an interval computation, it is treated as a different variable in each occurrence and overestimation could occur.

The interval function F is an interval extension of f, if: $F(t_1..t_n)=f(t_1..t_n)$. Moore [3] states that the range of a function f of real variables over an interval can be calculated from the interval extension F, changing t_i by T_i. In this case, $f(t_1..t_n) \subseteq F(T_1..T_n)$, $\forall\ t_i \in T_i$ (i =1.. n). In many practical problems, it could be difficult to obtain an expression in which each variable occurs not more than once. In these cases, a single computation of the interval extension of $f(t_1..t_n)$ only yields an interval $F(T_1..T_n)$, that is wider than the exact range for $f(t_1,..,t_n)$. Several techniques have been developed to avoid the dependence problem [5].

Sensitivity analysis is performed using Interval Arithmetic by assigning bounds (interval) to some or all the input parameters and determining the output interval, that will contain all possible solutions due to the variations in input parameters [4]. These intervals can be interpreted as worst cases values and are obtained with only *one calculation*.

3. EVOLUTIONARY APPROACH

During the last years, (global) optimisation algorithms imitating certain principles of nature have proved their usefulness in various domains of applications. A population of individuals each of which representing one point of the solution space collectively evolves towards better solutions by means of a parent's selection process, a reproduction strategy and a substitution strategy. Parent selection determines which individuals participate in the reproduction strategy [6-8].

Evolutionary Strategies (ES) (or Evolution Strategies [8]) were developed as a powerful tool for parameter optimisation tasks [6,9]. Three basic types of ES have been developed. In a two-member or (1+1) evolution strategy (ES(1+1)), one 'parent' produces one offspring per generation by applying a normally distributed perturbation, until a 'child' performs better than its ancestor and take its place [6]. In this technique, each individual (proposed solution) is represented by a couple $(\mathbf{y},\boldsymbol{\sigma})$, where $\mathbf{y}$ is a vector that identifies a point in the search space and $\boldsymbol{\sigma}$ is a vector of perturbation. In the next iteration an offspring is generated by the expression: $\mathbf{y}^{t+1} = \mathbf{y}^t + N(0,\boldsymbol{\sigma})$. The term $N(0,\boldsymbol{\sigma})$ represents a vector of independent random numbers normally distributed with mean 0 and standard deviation in the vector $\boldsymbol{\sigma}$ [7]. Schwefel and Bäck [9] and Bäck and Schwefel [10] generalized these strategies to the multimember evolution strategy now denoted by $ES(\mu + \lambda)$ and $ES(\mu,\lambda)$. In these strategies, the standard deviation for mutation becomes part of the individual and evolves by means of mutation and recombination, a process called self-adaptation of strategy parameters [10]. The (μ,λ) strategy is more realistic and tends to emphasize on global search properties.

Cellular Evolutionary Strategies (CES) [7] are an approach that combines the $ES(\mu,\lambda)$ techniques with concepts from Cellular Automata. In the CES approach, each individual is located in a cell of a two-dimension array and update looking only at determined cells (its neighbourhood). While the ES were originally designed with the parameter optimisation

problem in mind, the CES were designed to find the global optimum or "near" optimum for complex multi-modal functions.

4. ROBUST DESIGN METHODOLOGY

The designer formulates target values on the quality of a product by setting lower and upper bounds on the property $y_i(\mathbf{x})$. Suppose the area shown in figure 1a is the Feasible Solution Set (FSS) [11]. An exact description of the FSS (figure 1a) is in general not simple and could be limited by non-linear functions. For this reason, approximate descriptions are often looked for, using simply shaped sets like boxes or ellipsoids containing (outer bounding, figure 1b) or contained in (inner bounding, figure 1c and 1d) the set of interest [24]. In particular **M**aximum volume **I**nner **B**ox (MIB) (figure 1c and 1d) are of interest. The maximum ranges of possible variations of the feasible values define the so-called Tolerance Region . We define the following slack function $g_i(\mathbf{x})$: $g_i(\mathbf{x})=UB_i - y_i(\mathbf{x})$ when there is an upper bound requirement or $g_i(\mathbf{x})= y_i(\mathbf{x})-LB_i$ when there is an lower bound requirement (i=1..m) [12].

To obtain the MIB it is required that all the points inside the generated box satisfy the constraints. The mathematical formulation is: Let $B:=\{\mathbf{x},\mathbf{C}\in\Re^n \mid x_i\in[x_{i,lower},x_{i,upper}]$, $C_i=(x_{i,upper}+x_{i,lower})/2\}$ and $F:=\{g_i(\mathbf{x})\geq 0\}$, (i=1....m). Then

Center Specified	**Center Unspecified**
$\max_{\mathbf{x}} \prod_{i=1}^{n} abs((x_i - C_i))$	$\max_{\mathbf{x,C}} \prod_{i=1}^{n} abs((x_i - C_i))$
s.t. $\mathbf{x}\in F\cap B$	s.t. $\mathbf{x, C} \in F\cap B$

5. GENERAL APPROACH

We generate an initial random point $x_{1o},.,x_{n0}$ (initial vertex) and check if this point is a feasible point. If the point is infeasible, then we generate a new point and check it for feasibility. If the generated point is feasible, we generate a symmetrical "box" (hyper rectangle) using **C** as symmetry centre. To check the feasibility of the generated box, we can evaluate g_i at each vertex of the box. If each vertex is feasible, then we calculate the associated volume. The goal is then to maximize the inner volume. If at least one vertex is not feasible, then we discard the generated box, and generate a new point. In the case of centre unspecified, we also generate along with the initial random point $x_{1o},.,x_{n0}$ (initial vertex), the initial random centre co-ordinate $\mathbf{C}= \{C_{1o},..,C_{n0}\}$.

To avoid the function evaluation at 2^n vertices and the fact that extreme values are not necessarily at vertices of the tolerance region, constraint functions are evaluated using IA. Note that in the case that the FSS is non-convex, feasibility check using IA will consider this.

6. EXAMPLE: A TEMPERATURE CONTROLLER [13]

Consider the following example related to a temperature controller. The performance function is: $R_{T-on} = \frac{R_1R_2(E_2R_4 + E_1R_3)}{R_3(E_2R_4 + E_2R_2 - E_1R_2)}$. We will use the proposed robust design approach in order to define the MIB to guarantee that $R_{T\text{-}on}$ belongs to the interval [2.9,3.1] kΩ. Because of the stochastic nature of CES, 20 trials were performed and the best solution from among the 20 trials was used as the final solution. All CES runs were performed using 30

generations, 49 individuals in a 7x7 grid, $\sigma = 0.01$, Von Neumann neighbourhood with radius =1 and asynchronous substitution. Table 2. shows the result obtained using the hybrid approach CES and IA, with a MIB volume of 930296.40. The final intervals produce an output $R_{T\text{-}on}$ belonging to [2905.73,3099.99] Ω. The MIB volume obtained using a non-linear optimisation program, was 931811.45, that is 0.163 % greater than the obtained with the CES-IA approach. The average relative error obtained in 20 runs was only 0.272 %.

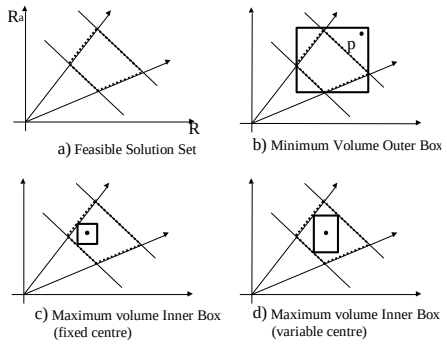

Figure 1: Feasible Solution Set and approximate descriptions

Table 2: Robust design using CES and IA approach

VARIABLE	Starting INTERVAL	Final Interval
$\mathbf{R_1}$	[0.5,1.5] kΩ	[0.994,1.005]] kΩ
$\mathbf{R_2}$	[6,12] kΩ	[8.956,9.044]] kΩ
$\mathbf{R_3}$	[2,6] kΩ	[3.973,4.027]] kΩ
$\mathbf{R_4}$	[16,48] kΩ	[31.428,32.572]] kΩ
$\mathbf{E_1}$	[7.5,9.5] V	[8.427,8.573] V
$\mathbf{E_2}$	[4.5,7.5] V	[5.946,6.0535] V

REFERENCES

1. Granger M., Henrion M.:. *Uncertainty: A Guide to Dealing with Uncertainty in Quantitative Risk and Policy Analysis*. Cambridge University Press. 1993.
2. Hansen E.: *Global Optimization Using Interval Analysis*, M. Dekker, New York, 1992
3. Moore R. *Methods and Applications of interval analysis*. SIAM. 1979. Philadelphia.
4. Kolev L.V.: *Interval Methods for Circuit Analysis*, World Scientific, 1994, Singapore.
5. Rocco C.: Techniques to Analyse System Performance Under Uncertainty, PhD Thesis, The Robert Gordon University, Aberdeen, Scotland
6. Kursawe F.: Towards Self-Adapting Evolution Strategies, Proc. Of the Tenth International Conference on Multiple Criteria Decision Making, G Tzeng and P. Yu (Eds), Taipei 1992
7. Medina M., Carrasquero N., Moreno J.: Estratégias Evolutivas Celulares para la Optimización de Funciones, IBERAMIA'98, Lisboa, Portugal, 1998
8. Michalewicz Z.: Genetic Algorithms+Data Structure=Evolution Programs, Springer-Verlag, 1992
9. Schwefel H., Back Th.:Evolution Strategies:Variants and their computational implementation,in J. Periaux and G. Winter, *Genetic Algorithm in Engineering and Computer Science*, J.Wiley&Sons,1995.
10. Bäck Th., Schwefel H.P.: Evolutionary Computation: An overview, Proc. Of the 1996 IEEE Int'l Conf. On Evolutionary Computation (IECC'96), Nagoya, Japan, 20-29, IEEE Press, NY, 1996
11. Milanese M. et al (Ed.): *Bounding Approaches to system Identification*, 1996, Plenum Press, New York
12. Hendrix E.M.T.: Global Optimization at Work, Landbouwuniversiteit Wageningen, 1998
13. Hadjihassan S., Walter E., Pronzato L., Quality Improvement via Optimisation of Tolerance Intervals During the Design Stage, *in Applications of Interval Computations*, Ed. Kearfott R.B., Kreinovich V., Kluwer Academic Publishers, Dordrecht, 1996

MODELLING, MAKING INFERENCES AND MAKING DECISIONS: THE ROLES OF SENSITIVITY ANALYSIS

Simon French

Manchester Business School,
The University of Manchester,
Booth Street West,
Manchester, M15 6PB, UK.
Email: simon.french@mbs.ac.uk

1. INTRODUCTION

The common theme that unites members of SAMO is that we all use techniques of sensitivity analysis. We are here at this conference to discuss advances in these techniques and how we may make use of them in applications. But do we notice that just as our use of the techniques unites us, the context of that use may distinguish us? We use sensitivity analyses for many different purposes: e.g.

A. to build and explore of models;
B. to support the elicitation of judgemental inputs to an analysis;
C. to develop efficient computational algorithms;
D. to design experiments;
E. to guide us in making inferences, forecasts and decisions;
F. to explore and build consensus;
G. to build understanding.

The manner in which we use sensitivity analysis to serve one of these purposes may be inappropriate to serving another. A further complication is that, because of their complexity models are often evaluated by Monte Carlo and other simulation methods, which are key techniques used in (global) sensitivity analysis, thus creating potential for further confusion of purpose. In this paper, I categorise and explore the use of sensitivity analysis throughout a full Bayesian analysis, and in doing so I hope to provide a guide to a bludgeoning literature.

2. BAYESIAN ANALYSIS

It will come as little surprise that I write this paper as a Bayesian [1], [2], [3]: no other framework is able to structure statistical and decision analyses coherently. The Bayesian approach has two simple mathematical formulae at its heart: the *subjective expected utility* model (SEU) and *Bayes Theorem*. The former ranks alternative actions $a \in A$ according to:

$$\max_{a \in A} E_\theta\left[u\left(c\left(a,\theta\right)\right)\middle| x\right] = \max_{a \in A} \int_\Theta u\left(c\left(a,\theta\right)\right) p_\theta\left(\theta \middle| x\right) d\theta \qquad (1)$$

where $p_\theta(\cdot \mid x)$ is a probability distribution encoding the decision maker's (DM's) *current* beliefs, i.e. *posterior* beliefs after observing data x, about the state of the world θ and $u(.)$ is a (multi-attribute) utility function encoding her preferences for possible consequences, $c(a, \theta)$,

which arise when action a is taken in the face of state θ. Bayes Theorem determines how her prior beliefs $p_\theta(\cdot)$ are updated in the light of data x to her posterior beliefs $p_\theta(\cdot \mid x)$:

$$p_\theta(\theta|x) \underset{\theta}{\propto} p_X(x|\theta)p_\theta(\theta)$$

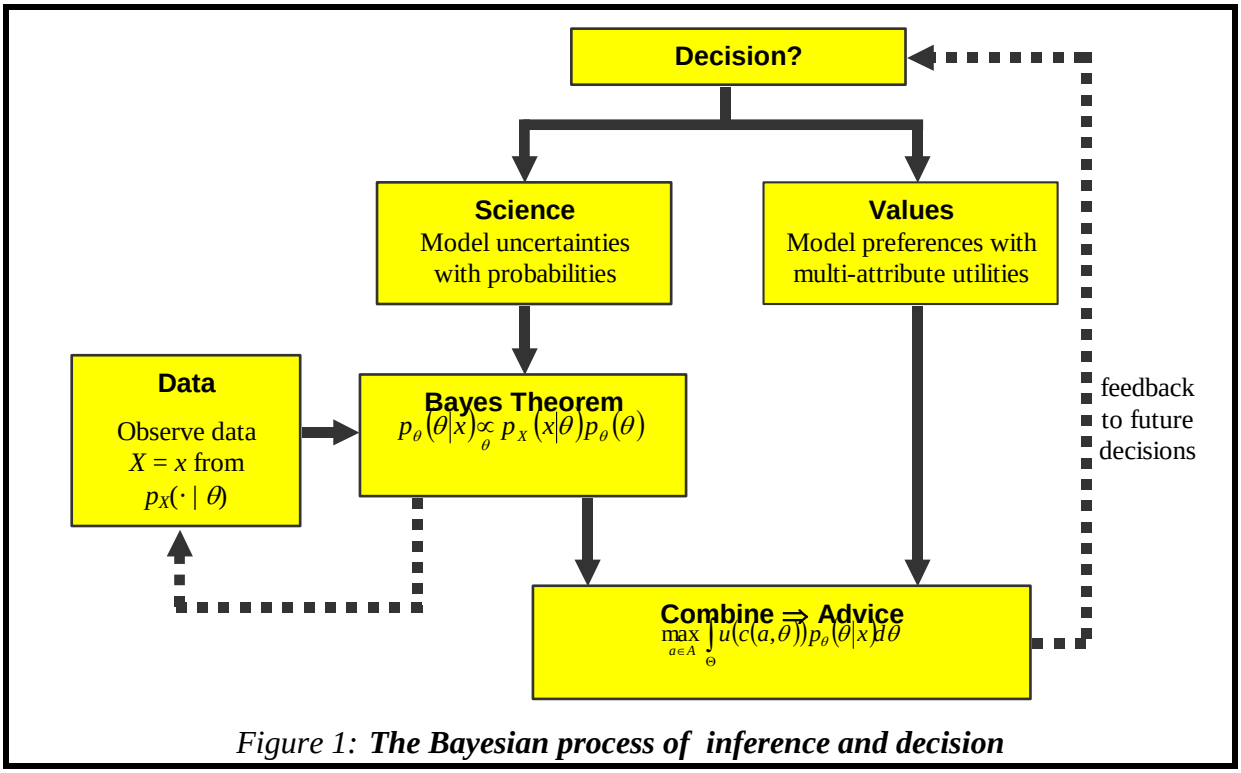

Figure 1: ***The Bayesian process of inference and decision***

See, e.g., [2], [3] for details. Within the Bayesian paradigm, consequences are modelled by $c(a, \theta)$, a function which predicts the consequence of taking action a when the state of the world is θ. The development and structuring of $c(\cdot,\cdot)$ is precisely the scientific modelling process that lies at the heart of much work within the SAMO community: $c(\cdot,\cdot)$ will be built upon the basis of our biological, economic, environmental and similar understandings of the world. It will help if we restructure and define the arguments of the consequence model so that $c(a, \theta) = M(a, \theta, \alpha)$, such that a represents parameters defined by the choice of action, θ are the parameters representing the state of the world and α are modelling parameters, although the distinctions, particularly between θ and α, are somewhat arbitrary [3].

These two formulae fit into the process whereby Bayesian analysis supports inference and decision as shown in Figure 1. Note how the process separates the science and modelling of what might happen from the valuation of its impact if it does. Also note how this separation corresponds to separation of roles between experts advising the DMs and the stakeholders in the decision. The DMs may, of course, be themselves experts and/or stakeholders. Analysts support the process as indicated in Figure 1.

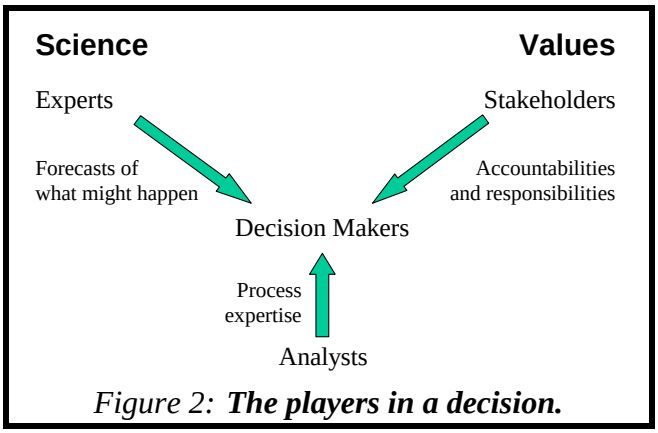

Figure 2: ***The players in a decision.***

3. SENSITIVITY ANALYSIS

Sensitivity analysis simply seeks to learn how the output of a model changes with variations in the input [4]. The output needs to be interpreted with great care whenever it varies significantly for input variations that are 'within the bounds of possible error'. I have used scare quotes here because the what is meant by 'bounds of possible error' will require some exploration in interpreting the value and purpose of sensitivity calculations in different contexts. Broadly, there are two classes of sensitivity analysis: *local* and *global*. In local analyses, parameters are varied over a neighbourhood around what is believed to be their 'correct' or 'appropriate' values. In global analyses the variation is over their whole domain space, usually according to some probability distribution representing the uncertainty in their values.

Bayesian analysis involves the following input parameters:

Consequences model: $M(a, \theta, \alpha)$ – this involves parameters a, representing the action, θ, the state, and α, the modelling parameters noted above.

Prior distribution: $p_\theta(\theta)$ – Firstly, in eliciting the distribution the DM or the experts will be asked for judgements to which the distribution will be fitted. These judgements are input parameters in our meaning of the term. Secondly, in the fitting process the distribution may be constrained to fit some general property such as symmetry or a simple correlation structure, again introducing input parameters in a general sense. Let these parameters be denoted β_θ. We may also note that θ may be partitioned into parameters of direct interest and nuisance, ancillary and other modelling parameters.

Likelihood: $p_X(x \mid \theta)$ – Again, there will be parameters, call them β_X, related to the elicitation. We may also think of the observation x as a parameter.

Utility functions: $u(c)$ – Utilities are elicited from the DMs and stakeholders so again there are parameters representing input judgements: call them γ. Some of these will be values on individual attributes; some will be weights bringing the attribute scales together, and some will relate to the structure of the multi-attribute utility function.

To these must be added, convergence and accuracy parameters set within the numerical processes of optimisation and integration in the SEU model (1). Call these parameters δ.

Thus to explore the purpose and interpretation of sensitivity analysis, we need to consider what we can learn by varying locally or globally each of a, θ, α, β_θ, β_X, γ and δ, either singly or in combination, in relation to each of the following purposes:

A. to build and explore of models;
B. to support the elicitation of judgemental inputs to an analysis;
C. to develop efficient computational algorithms;
D. to design experiments;
E. to guide us in making inferences, forecasts and decisions;

F. to explore and build consensus;
G. to build understanding.

See Figure 3 for an indication at where these fit into the Bayesian process of inference and decision.

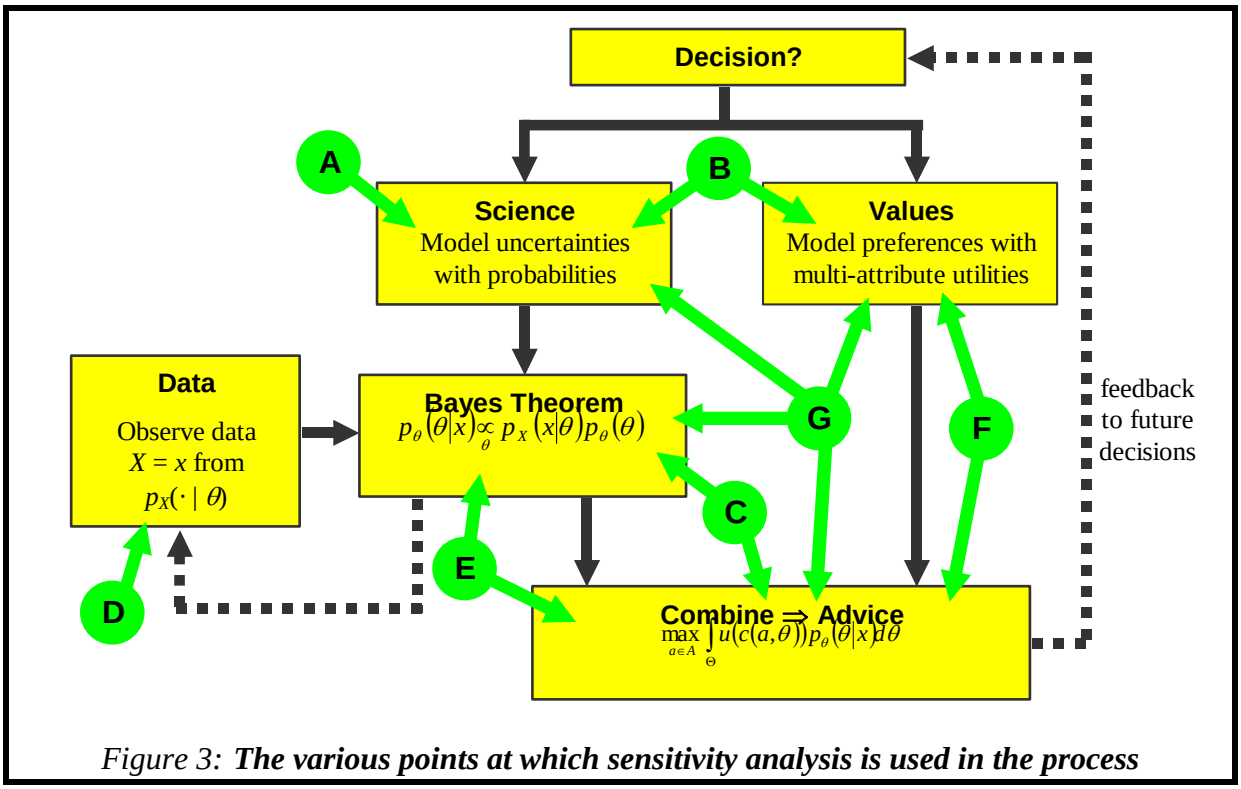

Figure 3: ***The various points at which sensitivity analysis is used in the process***

4. DISCUSSION

A full paper discussing these and related issues will be available at the time of the conference. (Email: simon.french@mbs.ac.uk)

5. REFERENCES

[1] S. French (1998) 'Sensitivity analysis and uncertainty modelling in decision support systems'. In K. Chan, S. Tarantola and F. Campolongo, Eds, *SAMO: Second International Symposium on Sensitivity Analysis in Model Output.* EU Joint research Centre, European Commission, Luxembourg, EUR 17758 EN. 117-120.

[2] S. French and J.Q. Smith, Eds (1997) *The Practice of Bayesian Analysis*. Edward Arnold, London

[3] S. French annd D. Rios Insua (2000) *Statistical Decision Analysis*. Edward Arnold, London.

[4] A. Saltelli, K. Chan and E.M. Scott, Eds. (2000) *Sensitivity Analysis*. John Wiley and Sons, Chichester.

SENSITIVITY ANALYSIS IN A MULTIATTRIBUTE ADDITIVE UTILITY DECISION SUPPORT SYSTEM

S. Ríos-Insua[(1)], A. Mateos[(1)], A. Jiménez[(1)], M. A. Henares[(1)]and E. Gallego[(2)]

[1] Dept. of Artificial Intelligence
Madrid Technical University (Spain)
Email: srios, amateos, ajimenez@fi.upm.es

[2] Dept. of Nuclear Engineering, Madrid Technical University (Spain)
Email: gallego@ctn.din.upm.es

1. INTRODUCTION

Many complex decision problems have multiple objectives which may be conflicting in the sense that, once dominated strategies or alternatives have been discarded, further achievement in terms of one objective can occur only at the expense of some achievement of another objective. Therefore, preference trade-offs between differing degrees of achievement of one and other objectives must be taken into account by the decision maker (DM). Also, real problems are usually plagued by uncertainty and one can not predict with certainty the consequences of each strategy under consideration. Formal analysis is required because it is very difficult to consider the above complexities informally in the mind.

This paper describes a decision support system based on multiattribute additive utility model to identify the optimal strategy, which is intended to allay many of the operational difficulties involved in assessing and using multiattribute utility functions.

The usual or traditional approach to Decision Analysis (DA) demands for unique or precise values for the different inputs of the model, i.e., for the weight and utility assessments as well as for the multiattributed consequences of the generated alternatives. However, we shall develop here a system based on a less demanding approach for the DM, because it will possible to provide instead of unique values, ranges or value intervals, that will be later used in different sensitivity analyses (SA). The system allows for imprecise assignments in weights and utilities and uncertainty in the multiattribute strategies, which can be defined in terms of ranges for each attribute instead of unique values. Different sensitivity analyses are possible over the inputs permitting the users to test the robustness of the ranking of the strategies to gain insight and confidence on the final solution. The system that we shall describe has been implemented as the evaluation module of the MOIRA system (Model based computerised system for management support to Identify Optimal strategies for restoring Radionuclide contaminated Aquatic Ecosystems and drainage areas), see [1] and [7].

2. METHODOLOGY

The system follows the DA methodology beginning the definition of an objectives hierarchy with a maximum of 100 nodes and with the necessary objective levels to be considered. Due to the flexibility of the system, it will be possible at any moment to add or to drop a node if the DM considers convenient. An attribute will be next introduced for each one lowest-level objective and used as a measure of the effectiveness of each strategy. Next, feasible strategies must be identified and to establish how such strategies are measured in

terms of attributes. Thus, the consequences of a decision strategy S_j can be described under certainty by the vector $\mathbf{x}^j=(x_1{}^j,...,x_n{}^j)$, where $x_i{}^j$ is a level of attribute X_i and under uncertainty by a vector of ranges $[\mathbf{x}^{Lj}, \mathbf{x}^{Uj}]=([x_1{}^{Lj}, x_1{}^{Uj}] ,\ldots, [x_n{}^{Lj}, x_n{}^{Uj}])$, where $x_i{}^{Lj}$ and $x_i{}^{Uj}$ are the lower (L) and upper (U) levels of attribute X_i for S_j. In the first case, when there are no uncertainties surrounding the problem, the meaning is that the impact for each strategy is known and thus the task of selecting the best strategy is reduced to selecting the best $\mathbf{x}^j$. In case under uncertainty the systems ranks the strategies taking the midvalue of the utility intervals obtained from the extremes $x_i{}^{Lj}$ and $x_i{}^{Uj}$, being the best strategy that with the best midpoint, although additional information from the ranges $[x_i{}^{Lj}, x_i{}^{Uj}]$ will be provided for the DM.

Quantifying preferences involves assessing the DM single attribute utility functions and the relative importance of each one. Both will be used later to evaluate the strategies through a multiattribute utility function. First, we shall consider the utility assessment and then it will be provided the weight elicitation.

The utility functions assessment is possible to be conducted by three different procedures depending on level of knowledge and characteristics of the attribute under consideration. The first procedure should be applied in the case of a natural attribute and when there is scarce knowledge or experience about the topic. Such procedure is based on the combination of two slightly modified standard procedures for utility assessment, the probability equivalent method and the certainty equivalent method, to mitigate some problems like biases and inconsistencies. Moreover, instead of obtaining only one precise number in each probability question, as these methods demand, we allow DMs to provide a range of responses, allowing DMs to provide incomplete preference statements by means of intervals rather than unique numbers. As a consequence, we obtain a class of utility functions rather than a single one for each method. As the evaluation process demands precise utility functions for the evaluation of the strategies, the system provides fitted utility functions by taking mid-points of the utility intervals of the intersection area for each u_i and then fitting natural cubic splines to these data points. Consistency checks are run to verify the bounds assessed for the specific certainty equivalence and probability equivalence methods. If the DM is not consistent in the above sense, the system suggests possible changes until he/she reaches the consistency.

The second procedure consist of constructing a class of piecewise linear utility functions. This will be useful when there also is a natural attribute but with a deep and precise knowledge about it. The user is asked to provide up to three intermediate intervals so the utility function will be constructed in this case by joining up to four linear segments between the best and the worst values.

Finally, the third procedure is referred to the case in which the DM decides not to use a utility function but a subjective scale which consists of a thermometer scale, suitable for subjective attributes. Thus, in the case of subjective scales, the DM will enter utilities or utility intervals by hand using scrollbars.

The very essence of multicriteria problems means that it is usually necessary to use some means to account for the relative importance of criteria. In the case of our system we have provided two procedures for assessing weights. The first procedure is based on trade-offs, see [4], among the respective attributes of the lowest-level objectives stemming from the same objective. As in the case of utility elicitations, we assume imprecision allowing the DM to provide an interval, rather than a unique value, and the system normalize the corresponding precise weights w_i. The second procedure, perhaps more suitable for upper level objectives that could have a more political character, is based on a direct assessment. Here the DM is

demanded to provide as before, weight intervals, that in the case of degenerated intervals assessment a precise value is provided.

Note that when the system is opened, the starting point is equally weighted objectives, but any interval weight or precise weight may be changed and the system automatically cares for how these changes must be propagated in the objectives hierarchy and recalculates the overall utility for each strategy. The weight intervals together with the value intervals will be used in SA, on the one hand to gain insight and confidence in the ranking of the strategies and, on the other, on aid in reducing if possible the set of alternatives.

3. EVALUATING ALTERNATIVES

This step involves evaluating each of the alternatives by means of the multiattribute additive

$$u(S_q) = \sum_{i=1}^{n} w_i \cdot u_i(x_i^q)$$

if the utility independence is fulfilled, see [4], where u_i are the component utility functions for each evaluation measure and w_i are the weights or scaling constants for each component utility function obtained by multiplying the respective weights of the objectives of each path from the root (global objective) until each leaf (attribute).

The evaluation of the set of strategies and their ranking is automatically done and can be displayed directly. The system provides a graphical representation with bars and including their overall utilities and the minimum and maximum utilities which are obtained from the minimum and the maximum strategy values, respectively. Some other displays are possible presenting useful information to the DM. Thus, it will be possible to watch by selecting a strategy, the objectives hierarchy with the assigned weights on each objective and the strategy values or subjective values. There is another display which shows the interval weights and the normalised weights that are associated to each attribute, obtained from the weights of the upper level objectives. The global weights (for the attributes) are represented both numerically (the normalised ones) and through a graphic. Note that such global weights will sum 1. Finally, it is possible to compare selected pairs of attributes for all the strategies by means of a graphical representation of the utility values resulting for these chosen attributes for the different strategies under analysis. This would help the DM to compare the performance of the strategies for each pair of selected attributes looking what are more relevants.

4. SENSITIVITY ANALYSIS

Sensitivity analysis (SA), which essentially involves examining changes in the ranking as input parameters (weights and or utilities) varying within a reasonable range, can give further insight into the quantitative analysis. Some types of sensitivity analysis are described in [5] and [6], which introduces a framework for sensitivity analysis in multiobjective decision-making, see [7], which gives an introduction to sensitivity analysis in the MOIRA project.

SA is usually performed by changing the weights or utilities and observing their impact on the ranking of alternatives. Hence, if the DM makes a change to a weight or the weight range, the system takes cares of how these changes should be propagated in the objective hierarchy and automatically recalculates the overall utility for each strategy and the resulting ranking.

Another way of performing SA involves assessing the interval in which weights can vary without affecting the overall strategy ranking. Suppose that there is now a ranking of the given strategies and the DM chooses a node or leaf of the tree, which has an associated weight. The system then calculates the weight interval for this node/leaf so that the ranking does not change, i.e., if the weight is changed and the new value is within the range, then the ranking will not change. However, if the new value is not within the range, the new ranking will be different to the previous one.

The system also performs simulation techniques for SA. This kind of sensitivity analysis, see [2], allows for simultaneous changes of the weights and generates results that can easily statistically analysed to provide more insights into the multiattribute model recommendations. We propose selecting the weights at random using a computer simulation program so that the results of many combinations of weights, including a complete ranking, can be explored in an efficient manner. Three general classes of simulation will be presented: random weights, rank order weights and response distribution weights. We shall describe them briefly.

- *Random weights*. As an extreme case, weights for the attributes are generated completely at random. This approach implies no knowledge whatsoever of the relative importance of the attributes. Once the simulation is conducted in this case, the system computes several statistics about the rankings of each strategy.
- *Rank order weights*. Randomly generating the weights while preserving their attributes rank order places substantial restrictions on the domain of possible weights that are consistents with the DM's judgement of attribute importance. Therefore, the results from the rank order simulation may provide more meaningful results.
- *Response distribution weights*. The third type of sensitivity analysis using simulation recognizes that the weight assessment procedure is subject to variation. For a single DM, this variation may be in the form of response error associated with the weight assessment. Now attributes weights are randomly assigned values taken into account the interval weights provided by the DM in the weights assignment methods.

All this information may be useful to discard some strategies and as an aid, the system displays for each above case a multiple boxplot for the strategies.

Finally, the system also obtains the sets of nondominated solutions, potentially optimal and adjacent potentially optimal to the optimal one. The calculation of these sets supposes from a theoretical point of view, to solve different nonlinear optimization problems. However, due to the concrete characteristics of the problems and the use of natural cubic splines instead of exponential functions as utility functions, we can transform this nonlinear problem into equivalent linear problems, making possible to exploit the many advantages of the linearity.

ACKNOWLEDGEMENTS

This paper was supported by CAM project 07T/0027/2000, CICYT project HID98-0379-C02-2 and the European Commission projects FIP-CT96-0036 and ERBIC15-CT98-0203-COMETES.

REFERENCES

[1] A. Appelgren *et al.* (1996), "An Outline of a Model-based Expert System to Identify Optimal Remedial Strategies for Restoring Contaminated Aquatic Ecosystem: the Project MOIRA", Report RT/AMB/96/17 ENEA.

[2] J. Butler, J. Jia and J. Dyer (1997), "Simulation Techniques for the Sensitivity Analysis of Multicriteria Decision Models", *EJOR* 103, 531-546.

[3] P.H. Farquhar (1984), "Utility Assessment Methods", *Man. Sci.* 30, 1283-1300.

[4] R.L. Keeney and H. Raiffa (1976), *Decision with Multiple Objectives: Preferences and Value-Tradeoffs*, Wiley, New York.

[5] D. Ríos Insua (1990), *Sensitivity Analysis in Multiobjective Decision Making*, LNEMS 347, Springer, Berlin.

[6] D. Ríos Insua and S. French (1991), "A Framework for Sensitivity Analysis in Discrete Multi-Objective Decision-Making", EJOR 54, 176-190.

[7] D. Ríos Insua, E. Gallego, A. Mateos and S. Ríos-Insua (2000), "MOIRA: A Decision Support System for Decision Making on Aquatic Ecosystem Contaminated by Radioactive Fallout", Annals of Operations Research 95, 341-364.

SENSITIVITY ANALYSIS AS A TOOL FOR THE IMPLEMENTATION OF A WATER QUALITY REGULATION BASED ON THE MAXIMUM PERMISSIBLE LOADS POLICY.

Pastres [(1)] R., S. Ciavatta [(1)], G. Cossarini [(2)], C. Solidoro[(2)]

[1] Dip. di Chimica Fisica, Univ.of Venice
Dorsoduro 2137, 30123 Venezia

[2] Osservatorio Geofisico Sperimentale
P.O.Box 2011, 34016 Opicina, Trieste

The Italian government recently issued a new law for the regulation of pollutant loads in water-bodies, which is based on the so-called Maximum-Permissible-Loads (MPLs) policy. Within this framework, Local Authorities should make an inventory of the sources of pollution and then fix the level of emission of each of these activities, in order not to overstep a set of given concentration thresholds within the system, called "quality targets", QT. The implementation of this new policy may clearly benefit from the use of mathematical models, which can be used as a tool for both estimating the MPLs by solving the so-called "inverse problem" and exploring the consequences of different input scenarios. In fact, in mathematical terms, the loads are specified by a set of boundary conditions: numerical models can then be used for determining a functional relationship between the set of boundary conditions and the output variables which one decides to compare with the Quality Targets. Once this task has been accomplished, one can invert this function in order to estimate the MPLs which are compatible with the targets.

These problems are investigated in this paper using the lagoon of Venice as a case-study and the sensitivity analysis in respect of each source of pollution as a tool. Because of its peculiarity, this system has been thoroughly investigated and a 3D reaction-diffusion water quality model is already available (Pastres et al., 1995). The reaction-diffusion equation (1), is solved using a finite-difference scheme.

$$\partial \boldsymbol{c}(x,y,z,t)/\partial t = \nabla (\boldsymbol{K}(x,y,z) \nabla \boldsymbol{c}(x,y,z,t)) + \boldsymbol{f}(\mathbf{c}(x,y,z), \boldsymbol{\beta}, t) \quad (1)$$

In eq. (1), $\boldsymbol{c}$ is the state vector, $\boldsymbol{K}$ the tensor of eddy diffusivities, $\boldsymbol{f}$ is the reaction term and $\boldsymbol{\beta}$ the set of site-specific parameters. The model simulates the dynamic of the ecosystem up to the second trophic level by using twelve state variables, among which the concentration of the two main forms of inorganic nitrogen, ammonium and nitrate, and inorganic reactive phosphorous one: these chemicals are considered to be the main cause of the eutrophication and, therefore, the current legislation fixes their quality target for the lagoon of Venice. In this paper, we have applied the method outlined below to the estimation of the MPL's of ammonium and nitrate: the sum of their concentration gives the Total Inorganic Nitrogen (TIN), as the concentration of nitrite is very low. At present, the concentration of TIN is above the target, while the concentration of phosphorous is already low, as its use in detergents was prohibited in 1989.

The dependence of the state of the system on the set of boundary conditions, which specifies the yearly evolution of the loads of ammonium and nitrate, has been investigated using a local sensitivity analysis with respect to each source. Ammonium, NH4, and nitrate, NO3, are carried into the lagoon by the rivers, and are directly released from the Industrial area of Porto Marghera, on the edge of the lagoon, and from the city of Venice and the nearby islands. The yearly evolutions of these inputs are modelled using Von Neumann-type time-dependent boundary conditions: the fluxes Φ_i are specified using a set of trigonometric polinomia:

$$\Phi_i{}^{NH4}(t) = \alpha_{i,0}{}^{NH4} + \Sigma_{j=1}{}^{3} [\alpha_{i,2j-1}{}^{NH4}\cos(2\pi jt/365) + \alpha_{i,,2j}{}^{NH4}\mathrm{sen}(2\pi jt/365)] \quad (3a)$$

$$\Phi_i{}^{NO3}(t) = \alpha_{i,0}{}^{NO3} + \Sigma_{j=1}{}^{3} [\alpha_{i,,2j-1}{}^{NO3}\cos(2\pi jt/365) + \alpha_{i,,2j}{}^{NO3}\mathrm{sen}(2\pi jt/365)] \quad (3b)$$

where $\Phi_i{}^{NH4}(t)$ and $\Phi_i{}^{NO3}(t)$ are the daily fluxes of ammonium of nitrate released by the i-th source at time t, expressed in days.

The parameters $\alpha_{i,0}{}^{NH4},..\alpha_{i,6}{}^{NH4}, \alpha_{i,0}{}^{NO3},..\alpha_{i,6}{}^{NO3},$ were estimated for each source by means of a least squares regression of monthly data. The exchanges with the Adriatic sea at the three inlets are described by means of Dirichlet-type boundary conditions: the concentrations of ammonia and nitrate at the boundaries are estimated by using the trigonometric polinomia (3) to interpolate a time series of field observations. On the basis of the available data, it was possible to define sixteen sources, which, plus the three inlets, lead to a total of 7x19 parameters, to be considered as potential input factors.

The dimension of the problem and the time required by a single run, about 5400 seconds to simulate one year on a 2-CPU Digital AU533Mhz WS, do not allow one to use MonteCarlo techniques to explore the dependence of the state of the system on the variation of the set of $\boldsymbol{\alpha}$ parameters. We therefore decided to use local sensitivity analysis with respect to each parameter α in order to:

- estimate the role of each source in determining the concentration of TIN in a given cell of the spatial domain
- estimate the MPL for TIN, MPL^{TIN}, given the water quality target, QT^{TIN};
- obtaine an initial idea of the evolution of the system within the MPL^{TIN} input scenario.

In order to simplify the problem, we supposed that the QT^{TIN} had to be respected for the yearly average concentration of the system: this interpretation of the law was arbitrary, but, at the moment, no precise statement exists about the type of average to be compared with the quality target. In this case, one has to take into consideration only the first parameters $\alpha_{1,0}{}^{NH4},\ldots\ \alpha_{i,0}{}^{NH4}$, $\alpha_{ns,0}{}^{NH4}$, $\alpha_{1,0}{}^{NO3},\ldots\ \alpha_{i,0}{}^{NO3}$, $\alpha_{ns,0}{}^{NO3}$, for the *ns* manageable sources (*ns*=16). For the sake of conciseness, in the following development the second subscript index is dropped and the parameters are regrouped in a single vector, by setting $\alpha_i{}^{NO3} = \alpha_{ns+i}$.

The sensitivity equation for a generic parameter α_i reads as:

$$\partial \mathbf{S}_{\alpha i}(x,y,z,t)/\partial t = \nabla (\underline{\mathbf{K}}(x,y,z)\ \nabla \mathbf{S}_{\alpha i}(x,y,z,t)) + \underline{\mathbf{J}}\mathbf{S}_{\alpha i} \quad (4)$$

where **S** is the sensitivity vector and $\mathbf{J} = \partial \mathbf{f}/\partial c$ is the Jacobian matrix of the vector function **f**. The set of 2xns vector equations (4) is solved by means of the direct method, (Koda et al., 1979). The partial derivatives which form the Jacobian matrix are calculated using symbolic

calculus: this may appear to be a limit, with regard to extending this approach to other problems, but such calculations are now performed automatically by a number of software packages, which also give the corresponding piece of Fortran code as an output.

The estimation of the MPL^{TIN} is based on the linearization of the state equation (1): this hypothesis could be critical, but it allows one to obtain a quick first guess. Under this assumption, the effect of the simultaneous variation of all the parameters α_i^{NH4}, α_i^{NO3} , on the state vector can be expressed as:

$$\mathbf{\Delta c(x,y,z,t) \approx \Sigma_{i=1}^{2xns} S_{\alpha i}(x,y,z,t)\, \Delta\alpha_i} \qquad \mathbf{(5)}$$

In physical terms, equation (5) is an estimate of the effect of the variation of the yearly load of TIN, which is given by the sum $\Sigma_{i=1}^{2xns} \Delta\alpha_i$, on each state variable. In accordance with eq. 5, the variation of TIN = NH4 + NO3, can be estimated as:

$$\Delta c^{TIN}(x,y,z,t) \approx \Sigma_{i=1}^{2xns}[S_{\alpha i}^{NH4}(x,y,z,t) + S_{\alpha i}^{NO3}(x,y,z,t)]\, \Delta\alpha_i \qquad (6)$$

The effect on the average yearly concentration, c_{av}^{TIN} is obtained by integration over the spatial and time domains:

$$\Delta c_{av}^{TIN} \approx (1/V)(1/T)\, \Sigma_{i=1}^{2xns} \Delta\alpha_i \int_T\int_V [S_{\alpha i}^{NH4}(x,y,z,t) + S_{\alpha i}^{NO3}(x,y,z,t)]\, dVdt \qquad (7)$$

which can be related to our problems and rewritten in a more compact form:

$$\Delta c_{av}^{TIN} \approx QT^{TIN} - c_{av}^{TIN}(\boldsymbol{\alpha}) \approx \Sigma_{i=1}^{2xns} [S_{av,\alpha i}^{NH4} + S_{av,\alpha i}^{NO3}]\, \Delta\alpha_i \qquad (8)$$

where $S_{av,\alpha i}^{iv} = (1/V)(1/T) \int_T\int_V [S_{\alpha i}^{iv}(x,y,z,t)dvdt$, iv=NH4, NO3 and $c_{av}^{TIN}(\boldsymbol{\alpha})$ is the average concentration obtained using the current estimates of the loads $\boldsymbol{\alpha}$.

Eq. 8, can then be used to assess the MPL^{TIN}, together with the equation:

$$L^{TIN} = \Sigma_{i=1}^{2xns} \alpha_i \qquad (9)$$

which gives the total daily load of TIN. Eq. (8) and (9) form a set of two constraints for the 2xns unknowns: in order to obtain a unique solution, one has to state in mathematical form the other 2xns-2 constraints: this could be done, for example, by taking into consideration the costs of reducing the load of each source, in order to optimize the interventions required to respect the QT. In this modelling exercise, we chose a very simple hypothesis, that is, to reduce all the loads in the same proportion, thus setting $\Delta\alpha_i = -\delta\alpha_i$.

By substituting the above expression in eq. (9) and (8) one gets:

$$\delta \approx -[QT^{TIN} - c_{av}^{TIN}(\boldsymbol{\alpha})] \,/\, \{\, \Sigma_{i=1}^{2xns} [S_{av,\alpha i}^{NH4} + S_{av,\alpha i}^{NO3}]\, \alpha_i \,\} \qquad (10)$$

$$MPL^{TIN} = \Sigma_{i=1}^{2xns} (1-\delta)\alpha_i \qquad (11)$$

It should be noted that the estimate (11) can be obtained from a single run of the program which solves eq. (1) and (4) and that, once the sensitivity vectors $\boldsymbol{S}_{\alpha i}$ are computed and stored, one can easily compare the water quality targets with other linear functions of the state vector and take into account other external constraints.

The new input scenario, given by eq. (11), has been used in a second simulation, in order to assess the validity of the linear hypothesis in this case study and to evaluate the carrying capacity of the ecosystem. The results show that the linear assumption leads to a slight

overestimation of the reduction, around 5%, and that the productivity of the ecosystem could be strongly affected by the reduction of inputs required to meet the quality target: this may suggest a revision of this threshold, if one wishes to maintain the activities of sustainable fishery and acquaculture in the lagoon of Venice.

REFERENCES

Koda, M., Drogu, A.H., Seinfeld, J.H., 1979. Sensitivity analysis of partial differential equations with applications to reaction and diffusion processes. J of Computational Physics, Vol. 30: 259-282

Pastres, R., Franco D., Pecenik, G., Solidoro, C., Dejak, C., 1995. Using parallel computers in environmental modelling: a working example. Ecological Modelling, Vol. 80: 69-85.

THE ANALYSIS OF DELTA HEDGING ERRORS FOR INTEREST RATE DERIVATIVES VIA SENSITIVITY ANALYSIS

F. Campolongo, A. Rossi

European Commission, Joint Research Centre
Institute for Systems Informatics and Safety, Ispra (VA), Italy
Email: francesca.campolongo@jrc.it; alessandro.rossi@jrc.it

SUMMARY

Banks trade every day a number of different financial instruments. Some of those, such as *derivatives*, are more difficult to be dealt with as their values depend, sometime complexly, on the behaviour of more basic financial instruments. Complex mathematical models are developed to evaluate derivatives (*pricing*), to quantify the maximum risk that a bank is facing trading these instruments, and to suggest an effective strategy to manage the risk (*hedging*). The construction of a hedging strategy involves the assessment of the risk deriving from a given contract and the search for one or more contracts to offset such risk. The final objective is that of building a portfolio that has minimum risk (ideally risk-less). A number of different hedging strategies can be thought. These depend on the type of risk that one is willing to offset (the risk associated with changes in the underlying, in volatility, and so on). In this paper it is shown how uncertainty and sensitivity analysis can be valuable tools to analyse the error made when hedging a certain financial instrument via a *delta hedging* strategy, which is a strategy offsetting the risk associated with changes in the underlying.

1. INTRODUCTION

Assume the financial instrument to be hedged is a caplet, which is an interest rate sensitive derivative. A natural candidate to offset the delta risk incurred when trading caplets is a forward rate agreement (FRA), which is a contract where two parties agree that a certain interest rate will apply to a certain amount of money (principal) for a certain period in the future. At time zero the investor sells a caplet and decides to buy a certain amount of FRA's in order to offset the (delta) risk associated with the caplet. The amount of FRA's is chosen such that the resulting portfolio (made by the caplet and FRA's) is, at time zero, delta neutral i.e. insensitive to certain movements of the yield curve (the curve relating interest rates to bond with different maturity). Delta neutrality is a local property. As time passes the portfolio tends to lose it. In principle, only revising the portfolio continuously it would be possible to maintain the delta neutrality. In practice a hedging error is generated as the portfolio is updated only at discrete times.

The hedging error is defined as the discrepancy between the value of the portfolio at maturity and what it would have been gained investing the initial value of the portfolio at the risk free rate till maturity. Several studies have dealt with hedging error analysis in different contexts. Valuable examples are [1,2,3].

In our case study we consider the delta hedging error as a random variable with a certain distribution centred on zero. Our purpose is that of focusing on the 5^{th} percentile of this distribution. This value can be interpreted as the maximum loss that the portfolio's owner is facing with a probability of 95%. In the literature it is referred as *value at risk* [4].

A Monte Carlo experiment is performed in order to obtain the hedging error empirical distribution and to estimate its 5^{th} percentile. Uncertainty analysis is then used to quantify the uncertainty in the variable of interest, while sensitivity analysis is used to identify where this uncertainty is coming from, which is what factors are causing the value of the maximum loss to be uncertain. The method adopted is the Fourier Amplitude Sensitivity Test (FAST) in its extended version proposed by Saltelli et al. [5].

Section 2 describes the financial framework assumptions and the hedging strategy adopted. Section 3 describes the uncertainty and sensitivity analysis settings, while section 4 recalls the FAST method. Section 5 reports the results of the analysis and conclusions.

2. THE FINANCIAL FRAMEWORK

To quantify the hedging error, the value of the portfolio has to be known at time zero and at each time at which the portfolio composition is updated. This requires knowledge of the yield curve at any time, as well as the prices of FRA's and caplet. Therefore to perform our analysis we first need to recover the yield curve dynamic.

Let assume movements in the yield curve to be driven by only one factor, namely the short-term interest rate (spot rate). This is assumed to evolve according to the Hull and White one-factor model (HW, hereafter) [6]. HW describes the spot rate dynamic as:

$$dr_t = \mu(t, r_t)dt + \sigma(t, r_t)dW_t \tag{2.1}$$

with

$$\mu(t, r_t) = \Theta(t) - ar_t \text{ and } \sigma(t, r_t) = \sigma . \tag{2.2}$$

The terms $\mu(t, r_t)$ and $\sigma(t, r_t)$ are respectively the drift and the standard deviation (volatility) of the spot rate, while $\{W_t : t \geq 0\}$ is a (standard) Wiener process. The model is mean reverting (with *a* the constant mean-reverting parameter) and the choice of the time dependent function $\Theta(t)$ can be directly recovered from the initial yield curve.

It can be shown that the whole yield curve at any time *t*, can be recovered from the knowledge of: the model parameters (σ and *a*), today's pure discount bond (PDB) prices, and the level of the spot rate at time *t*. Therefore simulating a path for the spot rate dynamic from (2.1)-(2.2) is sufficient to derive the yield curve at any time.

Let now consider a European put option, which in general is a contract giving the owner the right to sell the underlying *S* for a certain price *K* (*strike*) at a certain date *t* in the future (*maturity*). At maturity the contract pays off the amount $\max(0, K - S_t)$.

The financial instrument of interest here is a *caplet*, which is an option that provides a payoff when a specified interest rate is above a certain level. Consider two times t_1 (*resetting time*) and t_2. Let Δ (*tenor*) denotes the difference between t_2 and t_1, R the interest rate prevailing in the time interval (t_1, t_2), X the interest rate fixed at the outset of

the contract, and L the principal. A caplet is a contract paying at time t_2 the amount $L\max(0, R - X)\Delta$.

It is easy to show that the caplet is equivalent to a put option on a PDB with principal L and maturity t_2, with strike $K = 1/(1 + X\Delta)$, and expiry t_1.

In the HW framework, the actual price of a European put option can be recovered analytically. Hence, the same applies to a caplet.

The problem of hedging involves the search of one (or more) financial instrument which sensitivity to movements in the yield curve is of opposite sign. The idea is to build a portfolio with zero sensitivity to changes in the yield curve. However, since there are many ways in which the yield curve can move, many different strategies can be thought. In this paper we consider *delta hedging*, which aims at offsetting the risk associated with shifts in the yield curve. As stated above, the instrument chosen to hedge the caplet is a FRA. A common market practice (non arbitrage arguments) makes the present value of the contract equal to

$$F(0,t,T) = PDB(0,t) - PDB(0,T) - R_{FRA}PDT(0,T)(T-t) \qquad (2.3)$$

where PDB(0,τ) indicates the today' s value of a PDB with maturity τ, and RFRA designs the interest rate earned for the period of time between t and T on a certain principal. It is worth noting that the caplet and FRA have an opposite behaviour with respect to movements in the yield curve.

The amount of FRA's to be purchased in order to hedge the caplet depend on the underlying assumption about the type of movement followed by the yield curve. Three different scenarios are considered: a parallel shift up, a parallel shift down, and a curve inversion. In each scenario, changes in the FRA and caplet values are computed as the difference between the observed values and the ones given respectively by formula (2.3) and the HW analytical formula when applied in the new scenario. The ratio of these changes equals the amount of FRA's to be purchased. By construction, such amount is such that the resulting portfolio is insensitive to such movements.

The portfolio is updated a finite number of times (no updating it is also possible). Transaction costs are included in our analysis and are assumed to be a fixed proportion of the amount exchanged. These costs partially offset the benefit deriving from increasing the number of portfolio adjustments.

3. THE ANALYSIS

Our analysis focuses on the maximum loss that the portfolio's owner is facing, at least with 95% confidence level. This translates into the 5th percentile of the distribution of the hedging error. There are several factors contributing to the uncertainty in this value. These include: the features of the caplet (resetting time, interest rate agreed at the outset of the contract, tenor), the parameters of the model (the mean reverting parameter a and the spot rate volatility σ), the strategy used to build the hedging portfolio (represented as a trigger factor describing the type of movements in the yield curve with respect to which the portfolio is immunised), and the number of times at which the portfolio is updated.

Uncertainty and sensitivity analysis are used respectively to quantify the uncertainty in the objective function and to apportion it to sources (factors).

From a computational point of view, every single figure for the objective function is obtained via Monte Carlo. One hundred paths for the spot rate r are simulated from the discrete version (2.1)-(2.2) using the Eulero scheme for a period of time covering 3 years with weekly frequency. From the spot rates the PDB prices are computed by the HW model and the corresponding yield curve structure is then recovered (note that a one to one simple relationship holds between the yield curve and the PDB prices for different maturities). Given a yield curve, the prices of the caplet and FRA's are computed in closed form. Knowledge of those prices allows the construction and the evaluation of the hedging portfolio at any time. In particular, it allows to establishing the final value of the portfolio and the hedging error.

4. THE FAST METHOD

The method used to perform SA on our case study is the Fourier Amplitude Sensitivity Test (FAST). FAST was proposed in the 70's and was successfully employed in investigating the sensitivity of large sets of coupled reaction systems to uncertainties in rate coefficients. Later on, the method was reviewed and re-interpreted as to fit into an ANOVA setting. In an ANOVA setting the total output variance D is decomposed into orthogonal terms of increasing dimensionality, e.g. for a model with three factors:

$$D = D_1 + D_2 + D_{12} + D_{13} + D_{23} + D_{123} \tag{4.1}$$

The first order term D_i captures the effect on the output uncertainty due to variations in factor *i*, while all the other factors are averaged over their range of uncertainty. The second order term D_{ij} is a two-way interaction between factors *i* and *j* not including the individual effects due to *i* and *j*, which are already taken into account by D_i and D_j. Higher order partial variances express the influence on the output uncertainty due to higher order interactions among factors, and are defined in a similar way. The FAST sensitivity indices $\mathrm{S}_{i_1,i_2,\ldots}$ are obtained by dividing equation (4.1) by D.

In FAST, the input factors of a model are assumed to be non-correlated and all of them are varied simultaneously over their ranges of uncertainty, so that a global appreciation of the sensitivities can be achieved.

The FAST method was extended by Saltelli et al. [5] in order to allow for the estimation of total effects, S_{T_i}, $\forall i = 1,2,\ldots,k$. A total effect index S_{T_i} is defined as the sum of the indices $\mathrm{S}_{i_1,i_2,\ldots}$, which include the index *i*. For instance, in a model with three factors the total index for factor 1 looks like: $\mathrm{S}_{T_1} = \mathrm{S}_1 + \mathrm{S}_{12} + \mathrm{S}_{13} + \mathrm{S}_{123}$. The total index S_{T_i} is a more accurate measure of the effect of a factor on the model output since it takes into account all interaction effects involving that factor. In the version proposed by Saltelli et al. the computation of the total indices comes at no extra cost: the same set of model evaluations used to estimate the S_i's can be used also to obtain the S_{T_i}'s.

Here the method has been employed for a 7-factor model with a total computational cost of 959 model evaluations. The selected input factor distributions are specified in Table 1.

Table 1. Input factor distributions

Factor	Distribution
a	N(0.03; 0.01)
σ	U(0.05;0.055)
r cap (1.2X, 1.1X, X, 0.9X, 0.8X)[1]	Discrete Uniform
tenor (12, 24,48)	Discrete Uniform
resetting time (72,78,82,86,90,94,98)	Discrete Uniform
number of portfolio revisions (n rev) (0,1,…,72)	Discrete Uniform
hedging (1,2,3)	Discrete Uniform

5. RESULTS AND CONCLUSIONS

The main statistics computed on the objective function distribution, after it has been normalised by the principal, are: mean -0.43%; standard deviation 0.41%; 5th percentile -1.27%, skewness –2.91%. These allow to drawing a number of conclusions. The mean value stresses that the average maximum loss faced by the portfolio's owner is 0.43% of the amount invested (principal). In the worst case, this maximum loss reaches the value of 1.27%.

While these figures may seem to be relatively low, it is worth noting that in our framework the yield curve dynamic is quite simple and it has been simulated using the same model used for hedging. Taking into account a more realistic evolution of the yield curve independent of the model used for hedging, would imply a lower ability of the model in hedging the caplet and hence a higher maximum loss.

The sensitivity indices computed for the 7 input factors are illustrated in the pie charts in Figures 1 and 2. The sum of the first order indices (Figure 1) indicates that nearly 55% of the output variance is due to interaction effects among factors. For models with such a high non-additivity, the total indices represent a more meaningful measure to look at.

The symmetry in Figure 2 indicates a model where almost all input factors are similarly important on the output, which is a well-balanced model. This is not surprising as the number of factors included in the analysis is limited. Furthermore, a factor such the number of portfolio revisions, which a priori might be thought as a leading factor, it is likely to lose its role when transaction costs are included. The gain due to an increase in the number of revisions is offset by higher costs incurred updating the portfolio.

The hedging trigger factor is the most important one. In our feelings its relevance could further increase when widening the number of possible hedging strategies.

As expected, the caplet resetting time is the less important factor. We suspect that the main effect due to this factor is its interaction with the number of portfolio revisions. Further analysis may focus on an investigation of the importance of this effect.

[1] X is the forward rate (as seen from zero) prevailing in the interval starting at resetting time and with length equal to tenor.

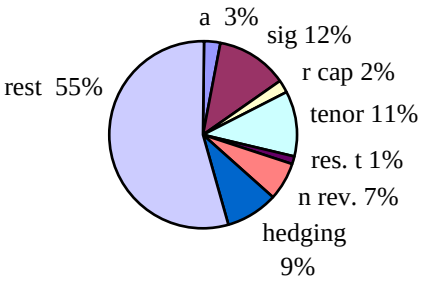

Figure 1 First order sensitivity indices

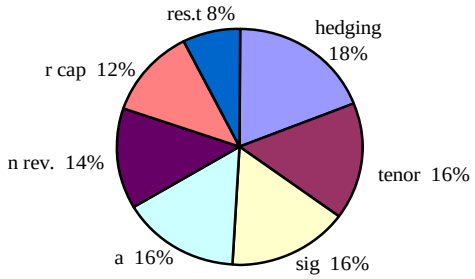

Figure 2 Total order sensitivity indices

6. REFERENCES

[1] R. Bookstaber, 1991. Option pricing and investment strategies. Probus Publishing.

[2] L. Clewlow, S. Hodges, R. Martinez, M Selby C, Strickland and X. Xu, 1993. Hedging Option position risk: an empirical examination. FORC Preprint, University of Warwick.

[3] M. Kamal, 1998. When you cannot hedge continuously: the corrections to Black-Scholes. Quantitative Strategies Research Notes, Goldman, Sachs & Co.

[4] JP Morgan, 1995. Riskmetrics Technical manual. JP Morgan, New York

[5] A. Saltelli, S. Tarantola, and K. Chan, 1999. A quantitative, model independent method for global sensitivity analysis of model output. Technometrics, 41, 39-56.

[6] J. Hull and A. White, 1990. Pricing interest rate derivative securities Review of Financial studies, 3, 4, 573-592

SENSITIVITY ANALYSIS IN GAUSSIAN NETWORKS

Enrique Castillo[(1)], Uffe Kjaerulff[(2)] and Linda C. van der Gaag[(3)]

[(1)] Department of Applied Mathematics and Computational Sciences, University of Cantabria, Avda. Castros s/n, 39005 Santander, Spain. Email: castie@unican.es

[(2)] Department of Computer Science, Aalborg University, Fredrik Bajers Vej 7, DK-9220, Aalborg, Denmark. Email: uk@cs.auc.dk

[(3)] Computer Science Department, Utrecht University, P.O. Box 80.089, 3508 TB Utrecht, The Netherlands Email: linda@cs.uu.nl

1. INTRODUCTION

As computer supported decision making is becoming increasingly important and popular, it is crucial that the underlying mathematical models can be thoroughly validated before deployment of the decision support system. An important element in model validation is sensitivity analysis: how sensitive are the resulting recommendations to changes in the model parameters? In some cases, the choice of parameter values is extremely influential on final results. For example, it is well known distributional assumptions and parameter values are highly influential on tail distributions [8,2]. If this influence is neglected, the consequences can be disastrous.

Bayesian networks play an important role in modelling complex decision problems. In recent years, a number of approaches to sensitivity analysis in Bayesian networks have been suggested. Laskey [11] introduced a method for computing the partial derivative of a posterior marginal probability with respect to a given parameter. Castillo, Gutiérrez and Hadi [4,3] have shown that a posterior probability can be expressed as a quotient of linear functions in the parameters and the evidence; in the case of Gaussian distributed variables, covariances can appear squared. This discovery simplifies sensitivity analysis in Bayesian networks. Computationally efficient methods have been developed for determining the coefficients of such quotients [10,7].

In this paper we address the problem of sensitivity analysis in Gaussian networks (i.e., Bayesian networks with Gaussian distributed variables) and show how changes in the parameter and evidence values influence marginal and conditional probabilities given the evidence.

2. BAYESIAN NETWORKS

In this section we briefly review Bayesian networks and, specifically, Gaussian networks. For details on Bayesian networks and Gaussian networks, see e.g. [14,9,15,12].

Definition 1 (Bayesian network) *A Bayesian network is a pair (D,P), where D is a directed acyclic graph, $P=\{p(x_1|\pi_1),\ldots,p(x_n|\pi_n)\}$ is a set of n conditional probability densities (CPD), one for each variable, and Π_i is the set of parents of node X_i in D. The set P defines the associated joint probability density (JPD) as*

$$p(x) = \prod_{i=1}^{n} p(x_i \mid \pi_i)\,. \qquad (1)$$

The key features of Bayesian networks are the factorisation given by (1) and the fact that conditional independence relations can be inferred directly from the graph *D*.

Definition 1 (Gaussian network) A Bayesian network is said to be a Gaussian network if and only if the joint probability density associated with its variables *X* is a multivariate normal (or Gaussian) distribution, $N(\mu,\Sigma)$, given by

$$f(x) = (2\pi)^{-n/2} \mid \sum \mid^{-1/2} \exp\left\{1/2(x-\mu)^T \sum^{-1}(x-\mu)\right\},$$

where μ is the *n*-dimensional mean vector, Σ is an *nxn* covariance matrix, $|\Sigma|$ is the determinant of Σ, and μ^T denotes the transpose of μ.

The *JPD* of the variables in a Gaussian network can be specified as in (1) with the *CPD* for variable X_i given by

$$f(x_i \mid \pi_i) \sim N\left(\mu_i + \sum_{j=1}^{j=i-1} \beta_{ij}(x_j - \mu_j), \upsilon_i\right),$$

where β_{ij} is the regression coefficient of X_j in the regression of X_i on the parents, Π_i, of X_i and

$$\upsilon_i = \sum_i - \sum_{i\Pi_i} \sum_{\Pi_i}^{-1} \sum_{i\Pi_i}^{T}$$

is the conditional variance of X_i given $\Pi_i = \pi_i$ where Σ_i is the unconditional variance of X_i, $\Sigma_{i\Pi i}$ are the covariances between X_i and the variables in Π_i ,and $\Sigma_{\Pi i}$ is the covariance matrix of Π_i. Note that β_{ij} measures the strength of the relationship between X_i and X_j. If $\beta_{ij}=0$, then X_j is not a parent of X_i.

The following is an illustrative example of a Gaussian network.

Example 1 Consider the Gaussian network indicated in Figure 1. Suppose the random variable

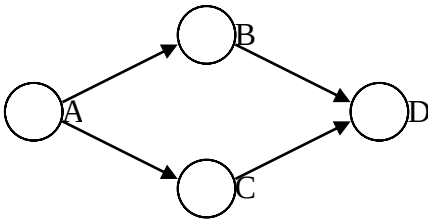

Figure 1: The independence graph of a Gaussian

$X=(A,B,C,D)$ is normally distributed, i.e., $X \sim N(\mu,\sum)$,. A Gaussian network is defined by specifying the set of *CPDs* appearing in the factorisation (1) which gives

$$f(x) = f(a,b,c,d) = f(a)\,f(b \mid c)\,f(c \mid a)\,f(d \mid b,c),$$

where

$$f(a) \sim N(\mu_A, \upsilon_A),$$
$$f(b \mid a) \sim N(\mu_B + \beta_{BA}(a - \mu_A), \upsilon_B),$$
$$f(c \mid a) \sim N(\mu_C + \beta_{CA}(a - \mu_A), \upsilon_C),$$
$$f(d \mid b, c) \sim N(\mu_C + \beta_{DB}(b - \mu_B) + \beta_{DC}(c - \mu_C), \upsilon_D).$$

This set of *CPDs* represents the Gaussian network. Three sets of parameters are involved in this representation, namely $\{\mu_A, \mu_B, \mu_C, \mu_D\}$, $\{\upsilon_A, \upsilon_B, \upsilon_C, \upsilon_D\}$, $\{\beta_{BA}, \beta_{CA}, \beta_{DB}, \beta_{DC}\}$.

Note that so far, all parameters have been considered in symbolic form. Thus, we can specify a Bayesian model by assigning numerical values to the parameters above. For example, for

$$\mu_A = 3,\ \mu_B = 4,\ \mu_C = 9,\ \mu_D = 14,$$
$$\upsilon_A = 4,\ \upsilon_B = 1,\ \upsilon_C = 4,\ \upsilon_D = 1,\ \beta_{BA} = 1,\ \beta_{CA} = 2,\ \beta_{DB} = 1,\ \beta_{DC} = 1$$

we get

$$\mu = \begin{pmatrix} 3 \\ 4 \\ 9 \\ 14 \end{pmatrix} \text{ and } \Sigma = \begin{pmatrix} 4 & 4 & 8 & 12 \\ 4 & 5 & 8 & 13 \\ 8 & 8 & 20 & 28 \\ 12 & 13 & 28 & 42 \end{pmatrix}$$

3. PROPAGATION IN GAUSSIAN NETWORKS

In this section we present a conceptually simple and efficient algorithm for propagating evidence in Gaussian networks. The algorithm is based on the following theorem, which characterises the *CPDs* obtained from a Gaussian *JPD* (see e.g. [1]).

Theorem 1 (Conditionals of a Gaussian distribution) Let Y and Z be two sets of random variables having a joint multivariate Gaussian distribution with mean vector and covariance matrix given by

$$\mu = \begin{pmatrix} \mu^Y \\ \mu^Z \end{pmatrix} \text{ and } \Sigma = \begin{pmatrix} \Sigma^{YY} & \Sigma^{YZ} \\ \Sigma^{ZY} & \Sigma^{ZZ} \end{pmatrix},$$

where μ^Y and Σ^{YX} are the mean vector and covariance matrix of Y, μ^Z and Σ^{ZZ} are the mean vector and covariance matrix of Z, and $\Sigma^{YZ} = \Sigma^{ZY}$ is the covariance matrix of Y and Z. Then the *CPD* of Y given $Z=z$ is multivariate Gaussian with mean vector $\mu^{Y|Z=z}$ and covariance matrix $\Sigma^{Y|Z=z}$ given by

$$\mu^{Y|Z=z} = \mu^Y + \Sigma^{YZ} \Sigma^{ZZ^{-1}} (z - \mu^Z), \qquad (2)$$

$$\Sigma^{Y|Z=z} = \Sigma^{YY} - \Sigma^{YZ} \Sigma^{ZZ^{-1}} \Sigma^{ZY} \qquad (3)$$

Note that the conditional mean (2) depends on z but the conditional variance (3) does not.

Theorem 1 suggests an obvious procedure to obtain means and variances of any subset of variables $Y \subset X$ given a set of evidence variables $E \subset X$ whose values are known to be e. Replacing Z in (2) and (3) by E, we obtain the mean vector and covariance matrix of the conditional distribution of Y given evidence e.

Although there exist more sophisticated methods for evidence propagation [16,6,12,13], in order to simplify the calculations, we shall use an incremental method, updating one evidence variable at a time (taking elements one by one from *E*). In this case we do not need to calculate the inverse of a matrix because Σ^{ZZ} degenerates to a scalar. Moreover, μ^{Y} and Σ^{YX} and are column vectors. Then the number of calculations needed to update the probability distribution of the non-evidence variables given a single piece of evidence is linear in the number of variables in *X*.

Below we illustrate symbolic computation in Gaussian networks using the conceptually simple method outlined above. The computations are performed in *Mathematica*; for details see [5].

Example 2 Consider the mean vector and covariance matrix in Example 1, where some of the parameters are specified in symbolic form:

$$\mu = \begin{pmatrix} p \\ 4 \\ 9 \\ q \end{pmatrix} \text{ and } \Sigma = \begin{pmatrix} a & 4 & d & f \\ 4 & 5 & 8 & c \\ d & 8 & 20 & 28 \\ f & c & 28 & b \end{pmatrix}$$

This gives us

$$\Sigma^{YY} = \begin{pmatrix} 5 & c \\ c & b \end{pmatrix}, \Sigma^{YY} = \begin{pmatrix} a & d \\ d & 20 \end{pmatrix}, \Sigma^{YY} = \begin{pmatrix} 4 & 8 \\ f & 28 \end{pmatrix}.$$

We use *Mathematica* to calculate the conditional means and variances for variables *B* and *D* given evidence $\{A=x_1, C=x_3\}$, and we get

$$\mu_B^{Y|A=x_1,C=x_3} = \frac{4(2a+(9-d)d+(2d-20)p+(20-2d)x_1+(2a-d))x_3}{20a-d^2},$$

$$\sigma_B^{YY|A=x_1,C=x_3} = \frac{36a+64d-5d^2-320}{20a-d^2},$$

$$\mu_D^{Y|A=x_1,C=x_3} = \frac{-252a+9df+(28d-20f)p+(20a-d^2)q+(20f-28d)x_1+(28a-df)x_3}{20a-d^2},$$

$$\sigma_D^{YY|A=x_1,C=x_3} = \frac{20ab-bd^2+56df-20f^2-748a}{20a-d^2}.$$

We see that the conditional means and variances are ratios of polynomials in the parameters. For example, the polynomials are first-degree in *p*, *q*, *a*, *b*, x_1, and x_3 (i.e., in the mean and variance parameters, and in the evidence values), and second-degree in *d* and *f* (i.e., the covariance parameters). Note also the common denominator for these functions.

The observations made in Example 1 are formalised in Theorem 2 (see [4] for a proof).

Theorem 1 (Rational functions of polynomials) The mean and variances of the conditional probability distributions of the variables of a Gaussian network are rational functions of polynomials. Specifically, the polynomials involved are of degree at most one in the evidence variables, the mean parameters, and the variance parameters, and of degree two in the covariance parameters involving at least one evidence variable. Also, the polynomial in the denominator is the same for all variables.

4. SENSITIVITY ANALYSIS

For Gaussian networks, one normally compute probabilities of the form

$$\begin{aligned} P(X_i > a \mid e) &= 1 - F_{X_i|e}(a), \\ P(X_i \le a \mid e) &= F_{X_i|e}(a), \\ P(a < X_i \le b \mid e) &= F_{X_i|e}(b) - F_{X_i|e}(a). \end{aligned} \tag{5}$$

Therefore, in performing sensitivity analyses on these probabilities with respect to a given parameter $\theta \in \Theta$ or evidence value $\varepsilon \in e$, it is important to know the partial derivatives

$$\frac{\partial F_{X_i|e}(a; \mu(\Theta; e), \sigma(\Theta; e))}{\partial \theta} \text{ and } \frac{\partial F_{X_i|e}(a; \mu(\Theta; e), \sigma(\Theta; e))}{\partial \varepsilon}.$$

In what follows we use the compact notation $\Lambda = (\Theta, e)$ and denote by λ a single component of Λ (i.e., $\lambda \in \Theta \cup e$). We can write

$$\frac{\partial F_{X_i|e}(a; \mu(\Lambda), \sigma(\Lambda))}{\partial \lambda} = \frac{\partial F_{X_i|e}(a; \mu(\Lambda), \sigma(\Lambda))}{\partial \mu} \frac{\partial \mu(\Lambda)}{\partial \lambda} + \frac{\partial F_{X_i|e}(a; \mu(\Lambda), \sigma(\Lambda))}{\partial \sigma} \frac{\partial \sigma(\Lambda)}{\partial \lambda} \tag{6}$$

Since

$$F_{X_i|e}(a; \mu(\Lambda), \sigma(\Lambda)) = \Phi\left(\frac{a - \mu(\Lambda)}{\sigma(\Lambda)} \right), \tag{7}$$

we have

$$\frac{\partial F_{X_i|e}(a; \mu(\Lambda), \sigma(\Lambda))}{\partial \mu} = f_{N(0,1)}\left(\frac{a - \mu(\Lambda)}{\sigma(\Lambda)} \right) \left(\frac{-1}{\sigma(\Lambda)} \right)$$

and

$$\frac{\partial F_{X_i|e}(a; \mu(\Lambda), \sigma(\Lambda))}{\partial \sigma} = f_{N(0,1)}\left(\frac{a - \mu(\Lambda)}{\sigma(\Lambda)} \right) \left(\frac{\mu(\Lambda) - a}{\sigma(\Lambda)^2} \right)$$

and then (6) becomes

$$\frac{\partial F_{X_i|e}(a; \mu(\Lambda), \sigma(\Lambda))}{\partial \lambda} = f_{N(0,1)}\left(\frac{a - \mu(\Lambda)}{\sigma(\Lambda)} \right) \left[\left(\frac{-1}{\sigma(\Lambda)} \right) \frac{\partial \mu(\Lambda)}{\partial \lambda} + \left(\frac{\mu(\Lambda) - a}{\sigma(\Lambda)^2} \right) \frac{\partial \sigma(\Lambda)}{\partial \lambda} \right].$$

Thus, the partial derivatives $\partial F_{X_i|e}(a; \mu(\Lambda), \sigma(\Lambda)) / \partial \lambda$ can be obtained by a single evaluation of $\mu(\Lambda)$ and $\sigma(\Lambda)$, and determining the partial derivatives $\partial \mu(\Lambda) / \partial \lambda$ and $\partial \sigma(\Lambda) / \partial \lambda$ with respect to all the parameters or evidence variables being considered. Thus, efficient computation of these partial derivatives is crucial.

They can be calculated either from the algebraic structure of the conditional means and variances or by direct differentiations of the formulas (2) and (3). Below, we shall concentrate on the former approach; see [5] for details on the latter.

To calculate $\partial\mu_N(\Lambda)/\partial\lambda$ and $\partial\sigma_N(\Lambda)/\partial\lambda$ for node *N* we need to know the dependence of $\mu_N(\Lambda)$ and $\sigma_N(\Lambda)$ on the parameter or evidence variable λ. This can be done with the help of Theorem 2. To illustrate we use the previous example.

From Theorem 2 we can write

$$\mu_N^{Y|A=x_1,C=x_3}(a)=\frac{\alpha_1 a+\beta_1}{\gamma a+\delta} \text{ and } \sigma_N^{Y|A=x_1,C=x_3}(a)=\frac{\alpha_2 a+\beta_{21}}{\gamma a+\delta},$$

where *N* is *B* or *D*, and since we have only *6* unknowns, calculation of $\mu_N^{Y|A=x_1,C=x_3}(a)$ and $\sigma_N^{Y|A=x_1,C=x_3}(a)$ for three different values of *a* allows determining the constant coefficients α_1, α_2, β_1, β_2, γ and δ. Then, the partial derivatives with respect to *a* becomes

$$\frac{\partial\mu_N^{Y|A=x_1,C=x_3}(a)}{\partial a}=\frac{\alpha_1\delta-\beta_1\gamma}{(\gamma a+\delta)^2} \text{ and } \frac{\partial\sigma_N^{Y|A=x_1,C=x_3}(a)}{\partial a}=\frac{\alpha_2\delta-\beta_{21}\gamma}{(\gamma a+\delta)^2}.$$

Similarly, from Theorem 2 we have

$$\mu_N^{Y|A=x_1,C=x_3}(f)=\frac{\alpha_3 f-\beta_3}{\gamma_1} \text{ and } \sigma_N^{Y|A=x_1,C=x_3}(f)=\frac{\gamma_4 f^2+\alpha_4 f+\beta_4}{\gamma_1},$$

and, again, we determine the constant coefficients based on different values of $\mu_N^{Y|A=x_1,C=x_3}(f)$ and $\sigma_N^{Y|A=x_1,C=x_3}(f)$. Then, the partial derivatives with respect to *f* are

$$\frac{\partial\mu_N^{Y|A=x_1,C=x_3}(f)}{\partial f}=\frac{\alpha_3}{\gamma_1} \text{ and } \frac{\partial\sigma_N^{Y|A=x_1,C=x_3}(f)}{\partial f}=\frac{2\gamma_4 f+\alpha_4}{\gamma_1}.$$

Note that if *N=B*, then $\alpha_3=\alpha_4=\beta_3=\beta_4=0$, and we need no calculations.

Finally, we can also obtain the partial derivatives with respect to evidence values. From Theorem 2 we have

$$\mu_N^{Y|A=x_1,C=x_3}(x_1)=\alpha_5 x_1+\beta_5 \text{ and } \sigma_N^{Y|A=x_1,C=x_3}(x_1)=\gamma_2.$$

Then, the partial derivatives with respect to x_1 are

$$\frac{\partial\mu_N^{Y|A=x_1,C=x_3}(x_1)}{\partial x_1}=\alpha_5 \text{ and } \frac{\partial\sigma_N^{Y|A=x_1,C=x_3}(x_1)}{\partial x_1}=0.$$

Note that if partial derivatives with respect to several parameters are to be computed, the number of computations reduces even more because some of them are common.

Example 3 We continue with the previous example and calculate now the probabilities of *B* exceeding the critical value *11*, and *D* exceeding the critical value *30*, because they have been determined as those producing important damages in the associated areas *B* and *D*, respectively. Using (5) and (7) we get

$$P(B>11\mid A=7,C=17)=1-F_{B|A=7,C=17}(11)=1-\Phi\left(\frac{11-8}{1}\right)=0.00135$$

$$P(D>30\mid A=7,C=17)=1-F_{D|A=7,C=17}(30)=1-\Phi\left(\frac{30-26}{\sqrt{2}}\right)=0.00234,$$

where the stepwise propagation method outlined in Sec 3 with evidence *A=7* and *C=17* yields

$$\mu^{\{B,D\}|A=7,C=17}=\begin{pmatrix}8\\26\end{pmatrix} \text{ and } \sum^{\{B,D\}|A=7,C=17}=\begin{pmatrix}1 & 1\\1 & 2\end{pmatrix}.$$

In Table 1 we have calculated all the normalised partial derivatives of the failure probabilities. We have used the parameter values for the normalisation.

t	$\frac{t\partial P(B>11\mid A=7,C=17)}{\partial t}$	$\frac{t\partial P(D>30\mid A=7,C=17)}{\partial t}$
p	-0.01330	-0.01550
q	0.00000	0.07233
a	0.00886	0.00000
b	0.00000	0.21700
d	0.00000	0.04134
f	0.00000	-0.06200
x_1	0.03102	0.03617
x_3	0.00000	0.08783

Table 1: Normalised partial derivatives with respect of all parameters.

5. CONCLUSIONS

Sensitivity analysis in Gaussian networks is greatly simplified due to the knowledge of the algebraic structure of the conditional means and variances. The fact that conditional means and variances are quotients of linear or quadratic functions of the parameters and evidence values, which appear as linear or quadratic terms, allows an efficient evaluation. Closed-form expressions for the partial derivatives of probabilities of the form $P(X_i>a\mid e)$, $P(X_i\le a\mid e)$ and $P(a<X_i\le b\mid e)$ with respect to the parameters can be obtained.

6. REFERENCES

[1] Anderson, T. W. (1984), *An introduction to multivariate statistical analysis*, 2nd edition. John Wiley and Sons, New York.

[2] Castillo, E. (1988), Extreme value theory in engineering. Academic Press, New York.

[3] Castillo, E., Gutiérrez, J. M. and Hadi, A. S. (1997), Sensitivity analysis in discrete Bayesian networks. IEEE Transactions on Systems, Man and Cybernetics, Vol 26, No. 7, 412-423.

[4] Castillo, E., Gutiérrez, J. M., Hadi, A. S. and Solares, C. (1997), Symbolic propagation and sensitivity analysis in Gaussian Bayesian networks with application to damage assessment. Artificial Intelligence in Engineering, 11:173-181.

[5] Castillo, E., Kjaerulff, U., and Gaag, L. C. van der (2001), Sensitivity Analysis in Normal Bayesian Networks. Technical Report.

[6] Chang, K. C. and Fung, R. (1991), Symbolic probabilistic inference with continuous variables. In Proceedings of the Seventh Conference on Uncertainty in Artificial Intelligence. Morgan Kaufmann Publishers, San Mateo, CA, 77-85.
[7] Darwiche, A. (2000), A differential approach to inference in Bayesian networks. In Proceedings of the Sixteenth Conference on Uncertainty in Artificial Intelligence. Morgan Kaufmann Publishers, San Mateo, CA, 123-132.
[8] Galambos, J. (1987), The asymptotic theory of extreme order statistics. Robert E. Krieger Publishing Company. Malabar, Florida.
[9] Jensen, F. V. (1996), An Introduction to Bayesian Networks. UCL Press, London.
[10] Kjaerulff, U. and van der Gaag, L. C. (2000), Making sensitivity analysis computationally efficient. In Proceedings of the Sixteenth Conference on Uncertainty in Artificial Intelligence. Morgan Kaufmann Publishers, San Mateo, CA, 317-325.
[11] Laskey, K. B. (1995), Sensitivity analysis for probability assessments in Bayesian networks, IEEE Transactions on Systems, Man, and Cybernetics, 25, 901-909.
[12] Lauritzen, S. L. (1992), Propagation of probabilities, means, and variances in mixed graphical association models. Journal of the American Statistical Association, 87:1098-1108.
[13] Normand, S.-L. and Tritchler, D. (1992), Parameter updating in Bayes network. Journal of the American Statistical Association, 87:1109-1115.
[14] Pearl, J. (1988), Probabilistic Reasoning in Intelligent Systems: Networks of Plausible Inference}. Morgan Kaufmann Publishers, San Mateo, California.
[15] Shachter, R. and Kenley, C. (1989), Gaussian influence diagrams. Management Science, 35(5):527-550.
[16] Xu, L. and Pearl, J. (1989), Structuring causal tree models with continuous variables.In Kanal, L. N., Levitt, T. S., and Lemmer, J. F., editors, Uncertainty in Artificial Intelligence 3. North Holland, Amsterdam, 209-219.

BAYESIAN CALIBRATION OF MODEL PARAMETERS: A CASE STUDY

M.J.W. Jansen and H.F.M. Ten Berge

Plant Research International, P.O. Box 16
6700 AA Wageningen, The Netherlands
Email: m.j.w.jansen@plant.wag-ur.nl ; www.plant.wageningen-ur.nl

SUMMARY

Bayesian model calibration is introduced, and some of its advantages are mentioned. The theory is illustrated by the case of a simple model for a crop's nitrogen uptake.

1. INTRODUCTION

Many studies in uncertainty and sensitivity analysis focus on the analysis stages taking place after the assessment of the uncertainty distribution of the model parameters (e.g. Saltelli, Chan and Scott; 2000). By now, quite a number of reasonably satisfying procedures exits for these latter stages. Thus it may be argued that the assessment of model parameter uncertainty is the bottleneck of uncertainty analysis. Since parameter uncertainty has to be assessed in the form of a probability distribution, it seems very appropriate to perform this assessment by means of Bayesian statistical methods, which supplies such a distribution. We will call this a Bayesian calibration.

Apart from its seamless link to uncertainty analysis, Bayesian calibration has several other advantages – at least in principle. In modelling, one typically uses very heterogeneous information to shed a light on a subject about which direct information is insufficient. The information available comes from observations and experiments at several spatio-temporal scales, from literature, from experts etcetera. Bayesian methods seem more apt to integrate such diverse information than classical frequentist methods. When calibrating a model otherwise, one has to decide which parameters to change and which to keep fixed; what measure of discrepancy between observations and prediction to choose; how to comply with expert knowledge; etcetera. After a non-Bayesian calibration the uncertainty about the parameters is often obscure. In Bayesian calibration the answer is: to consider all parameters; the criterion follows from the stochastic model for the data; and expert knowledge can be used as prior information (see also Kennedy and O'Hagan, 2001).

Thus, the Bayesian approach promises to be very suitable for model calibration. This paper describes a first exercise for a relatively simple case – in order to find out if the promises

come true. We consider a model describing a crop's response to the application of nitrogen. The model is descriptive and contains seven parameters specific to a situation – a field under particular weather conditions. After describing the model, we discuss the Bayesian estimation of parameters of a single data set from some situation. Next we discuss the possibilities of a Bayesian analysis of several data sets stemming from a number of situations. Such an analysis is appropriate when one wishes to make predictions for a new situation. The analysis is based on the assumption that the vector of seven parameters varies randomly from situation to situation.

1.1. The case studied

A single data set records the response of a sugar beet crop to the application of the nutrient nitrogen (N); it consist of the N-applications (A), the corresponding measured N-uptakes (U) and the dry-matter yields (Y). In an experiment of typical size 6, the data consists of three columns with length 6: $A_{1...6}$, $U_{1...6}$ and $Y_{1...6}$ (in Kg per ha).

In this paper we fit the seven-parameter model QUADMOD (Ten Berge et al. 2000) to such data. The model consists of a function u(a) that describes how the uptake depends on the application a, and a function y(u) describing how the yield depends on the uptake u. The response functions u(a) and y(u) share some parameters. Fig. 1 and 2 show data and model fit for a particualar situation: sugar beet, 1988.

The uncertainty about the parameter values that remains after taking into account the information in a data set, is assessed with the – Bayesian – Metropolis algorithm (e.g. Gelman et al., 1995). The result is a sample of parameter vectors expressing the remaining uncertainty.

The seven parameters describing the two crop response curves will be denoted by $\theta_1...\theta_7$. Apart from these, there are two stochastic parameters σ^2 and τ^2. As model for the measurements we took

$$U_i = u(A_i, \theta_1...\theta_4) + \varepsilon_i$$
$$Y_i = y(U_i, \theta_1...\theta_7) + \eta_i$$

in which the ε's are mutually independent normal$(0,\sigma^2)$, while the η's are mutually independent normal$(0,\tau^2)$, independent of the ε's. These random components account for measurement errors and for variation between the plots in the field. Note that the two response functions u() and y() share some parameters, which is an argument to fit the two responses simultaneously.

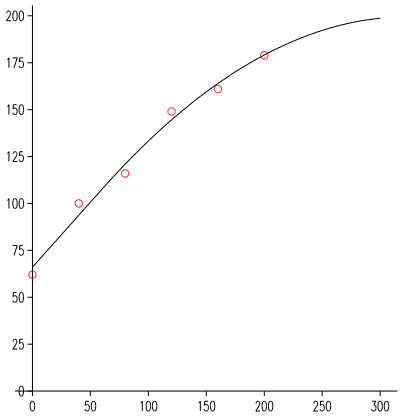

Figure 1. Uptake vs. application

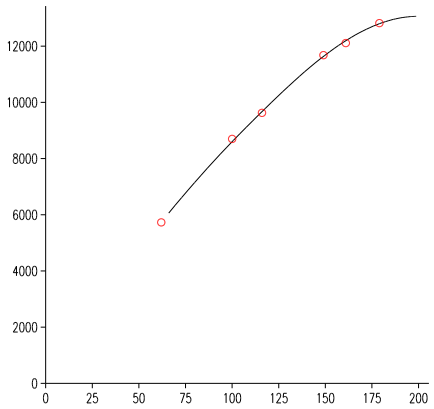

Figure 2. Yield vs. uptake

2. METHODS AND RESULTS

In a Bayesian analysis the uncertainty about the parameters before and after the analysis of a data set is represented by probability distributions: the prior and the posterior distribution. The prior distribution contains the information already present before the experiment. In our case there is not much prior information and the priors for parameters $\theta_1...\theta_7$, $\ln(\sigma)$ and $\ln(\tau)$ are assumed to be homogeneously distributed between liberal minima and maxima, which mainly exclude theoretically impossible values, like efficiencies greater than 1.

The data come in through the likelihood, say ℓ. According to the stochastic model assumed, we have

$$\ell = c \prod_i \{\sigma^{-1} \exp-(U_i - u(A_i, \theta_1...\theta_4))^2 / (2\sigma^2)\} \prod_i \{\tau^{-1} \exp-(Y_i - y(U_i, \theta_1...\theta_7))^2 / (2\tau^2)\}$$

in which c is a constant of no importance. According to Bayes' rule, the posterior density, say q, is proportional to the product of the prior, say p, and the likelihood ℓ, i.e. $q(\theta) \propto p(\theta)\ \ell(\theta)$, in which θ stands for the parameter vector $(\theta_1...\theta_7, \sigma, \tau)$.

A sample from the posterior distribution, expressing the remaining uncertainty about the parameters, is obtained with the Metropolis algorithm (e.g. Gelman et al., 1995). At each iteration, a new value θ^* is proposed by some random mechanism. The proposal is accepted by lot, namely when $\ell(\theta^*)\ p(\theta^*) > \mathbf{u}\ \ell(\theta)\ p(\theta)$, in which **u** is uniform(0,1). The next value in the sequence will be set to θ^* if the proposal is accepted, otherwise the next value will be set to the old θ again. The sequence thus obtained converges to a non-independent sample from the posterior distribution.

Fig. 3 illustrates an aspect of a posterior sample: a scatterplot graph of parameters θ_3 and θ_6 for the 1988 sugar beet data set (sample of size 1000). Note the strong dependence, probably caused by the relatively large number of parameters. The range plot Fig. 4 summarises a feature of the analysis of 11 similar experiments with sugar beet done at one site in 1985-1995. It shows the means and standard deviations of the uncertainty distribution of a derived parameter, namely the uptake at application 100 kg/ha.

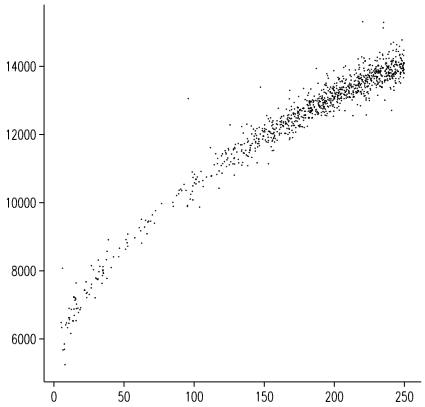

Figure 3. Posterior sample: θ_6 vs. θ_3

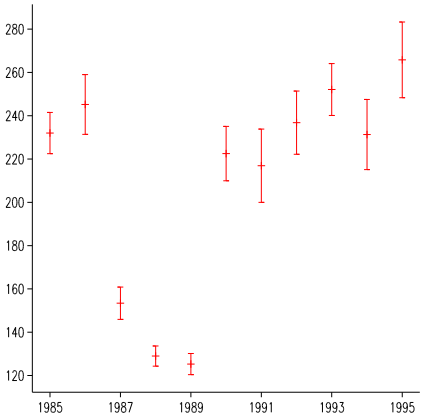

Figure 4. Uptake range plot for 11 years

Subsequently, we tried to combine the results of the analysis of several data sets, which were considered as sample from a population of situations about which one wants to make predictions. The combined analysis can be used to provide the parameter uncertainty for a *new* situation from the same population of experiments. It is assumed that the 7-vector θ of parameters varies randomly from case to case, because of the variation that can been observed in Fig. 4 – presumably due to differences in weather conditions and field plots. We could easily answer this question for individual parameters, but we have not succeeded to answer it for the complete parameter vector, due to theoretical as well as practical problems (familiarity with Bayesian methods, software and computer-time). The major problem was that the stochastic model for several data sets comprises a 7-by-7 covariance matrix for variation of θ from case to case, which implies many additional parameters, for which one should fabricate a suitable non-informative prior.

3. DISCUSSION

In the case studied, the number of observations in individual data sets was often hardly greater than the number of parameters. Although it takes more computer time than usual, a Bayesian analysis per data set appeared to be quite feasible. It often leads to strong correlations in the posterior distribution, and to large uncertainties in some of the response function parameters; but seldom to large uncertainties in the values of the response functions in the observed range.

For the purpose of a subsequent uncertainty analysis, a Bayesian analysis of all parameters simultaneously over several similar data sets would be the most relevant. Unfortunately, we were not able to perform such an analysis, due to theoretical as well as practical problems. In contrast, a Bayesian analysis of individual parameters over several data sets posed no problems.

In summary, although Bayesian calibration is a promising area, there is still much to do to make the promises come true – even in relatively simple situations.

4. ACKNOWLEDGEMENTS

We would like to thank prof. dr. Mariusz Fotyma, Institute of Soil Science and Plant Cultivation, Pulawy, Poland, for providing the field data of the case discussed.

5. REFERENCES

Gelman, A., Carlin, J.B., Stern, H.S. and Rubin, D.B., 1995. Bayesian data analysis, London: Chapman & Hall.

Kennedy, M.C. and O'Hagan, A., 2001, Bayesian calibration of computer models. J.Roy.Statist.Soc, B (to appear).

Saltelli, A., Chan, K. and Scott, E.M. (eds.), 2000, Sensitivity analysis. Chichester: Wiley.

Ten Berge, H.F.M., Withagen, J.C.M., De Ruiter, F.J., Jansen, M.J.W. and Van Der Meer, H.G., 2002, Nitrogen responses in grass and selected field crops: QUADMOD parameterisation and extensions for STONE application. Wageningen: Plant Research International, Report 24.

BAYESIAN VARIANCE-BASED UNCERTAINTY ANALYSIS

J.E. Oakley, A. O'Hagan

Department of Probability and Statistics, University of Sheffield,
Hicks Building, Houndsfield Road, Sheffield, S3 7RH, UK
Email: j.oakley@sheffield.ac.uk , a.ohagan@sheffield.ac.uk

SUMMARY

We consider the problem of measuring uncertainty induced in model outputs by model inputs with uncertain values. Specifically, we address the problem of ascertaining which uncertain inputs contribute most to the uncertainty in the output. In variance-based sensitivity analysis this is achieved by partitioning the variance of the output into components relating to each input and their interactions. Monte Carlo methods are usually employed to estimate this partition. However, this may be impractical when the model is computationally expensive, so that inferences must be made using a small number of model runs. We propose a Bayesian alternative to conventional Monte Carlo variance-based sensitivity analysis. The Bayesian method allows accurate estimation of variance and components of variance from a much smaller number of runs of the code.

1. INTRODUCTION

A deterministic computer model returns an output y when provided with a set of input values $\boldsymbol{x}$. We represent the code by a function $y = \eta(\boldsymbol{x})$. Though the output will often be a vector, we only consider a scalar output y. It is further supposed that the function $\eta(.)$ is computationally expensive, so that the user of the model will be restricted to a relatively small number of runs of the code. We are interested in the case when there is uncertainty regarding some or all of the input values relevant to a particular situation. The true, unknown input values are denoted by $\boldsymbol{X}$, and our uncertainty about $\boldsymbol{X}$ is represented by the distribution G. We then wish to know the distribution of the corresponding unknown output, denoted by $Y = \eta(\boldsymbol{X})$, which we call the uncertainty distribution. In principle, the uncertainty distribution can be determined using Monte Carlo methods; a large sample of inputs is drawn from G, the code is run at each set of inputs, and a sample from the distribution of Y is obtained. This approach is not practical in the case when $\eta(.)$ is computationally expensive, due to the number of runs of the code required.

A method for dealing with this problem is to model the code $\eta(.)$ itself as a random variable, simply in the sense that the output of $\eta(\boldsymbol{x})$ will be unknown until the code is run. We can then consider the distribution of $\eta(\boldsymbol{x})$ given a small number of runs of the code. Providing the function $\eta(.)$ is fairly smooth, knowing the value of $\eta(\boldsymbol{x})$ should give us good information about $\eta(\boldsymbol{x}')$ for $\boldsymbol{x}$ close to $\boldsymbol{x}'$. Whereas the conventional Monte Carlo approach uses sampling to learn about how much $\eta(\boldsymbol{x})$ varies with $\boldsymbol{x}$, the Bayesian method uses a

small number of code runs to estimate $\eta(\boldsymbol{x})$ for all $\boldsymbol{x}$. This leads to quite different and potentially more efficient ways to estimate the output uncertainty.

Since we are modelling the function $\eta(.)$ as a random variable, the distribution of Y is now also a random variable, and we must make inferences about the uncertainty distribution. Haylock and O'Hagan [1] derived the distribution of the expectation of Y, and the posterior mean and variance of the variance of Y, given a small number of runs of the code. Oakley and O'Hagan [2] considered inference about the distribution and density functions of Y. Here, we address the problem of assessing which elements in the vector $\boldsymbol{X}$ are most responsible for inducing the uncertainty in Y. In particular, we follow the variance-based methods described in Chan et al [3], and give analogous techniques within the Bayesian framework. Some technical details of our method are presented in the next section, where we describe inference about the unknown function $\eta(.)$ and give details of the computation of a partition of the variance of Y in the case of independent inputs. A simple illustration is given in section three.

2. METHODOLOGY

We now review the Gaussian process model for the function $\eta(.)$ used in Haylock and O'Hagan [1] and Oakley and O'Hagan [2]. We suppose that for any collection of inputs $\mathrm{x}_1,\ldots,\mathrm{x}_n$, the corresponding set of outputs $\mathrm{y}_1,\ldots,\mathrm{y}_n$, have a multivariate normal distribution. A priori we state that

$$E\{\eta(\boldsymbol{x}) \mid \boldsymbol{\beta}\} = \boldsymbol{h}^T(\boldsymbol{x})\boldsymbol{\beta},$$

for some vector of known functions $\boldsymbol{h}$, and that

$$Cov\{\eta(\boldsymbol{x}), \eta(\boldsymbol{x}') \mid \boldsymbol{\beta}, \sigma^2\} = \sigma^2 c(\| \boldsymbol{x} - \boldsymbol{x}' \|),$$

where $c(d)$ decreases as d increases, and $c(0) = 1.$ Weak prior distributions for $\boldsymbol{\beta}$ and σ^2 are commonly used, although the designers of the computer code may have proper prior knowledge about the function $\eta(.)$. Incorporating this knowledge into the analysis is the subject of Oakley [4]. We now observe data $\boldsymbol{d} = \{\eta(\boldsymbol{x_1}),\ldots,\eta(\boldsymbol{x_n})\}^T$, and using standard results for multivariate normal distributions, outputs at any untested inputs also have normal distributions, with

$$E\{\eta(\boldsymbol{x}) \mid \boldsymbol{\beta}, \boldsymbol{d}\} = \boldsymbol{h}^T(\boldsymbol{x})\boldsymbol{\beta} + \boldsymbol{t}(\boldsymbol{x})^T A^{-1}(\boldsymbol{d} - H\boldsymbol{\beta}),$$
$$Cov\{\eta(\boldsymbol{x}), \eta(\boldsymbol{x}') \mid \boldsymbol{\beta}, \sigma^2\} = \sigma^2\{c(\| \boldsymbol{x} - \boldsymbol{x}' \|) - \boldsymbol{t}(\boldsymbol{x})^T A^{-1}\boldsymbol{t}(\boldsymbol{x})\},$$

where

$$\sigma^2\boldsymbol{t}(\boldsymbol{x}) = Cov\{\eta(\boldsymbol{x}), \boldsymbol{d} \mid \boldsymbol{\beta}, \sigma^2\},$$
$$\sigma^2 A = Var(\boldsymbol{d} \mid \boldsymbol{\beta}, \sigma^2),$$
$$H = \{\boldsymbol{h}(\boldsymbol{x_1}),\ldots,\boldsymbol{h}(\boldsymbol{x_n})\}^T.$$

Using the conjugate prior for $\boldsymbol{\beta}$ and σ^2, the normal inverse gamma distribution, it is then straightforward to remove the conditioning on $\boldsymbol{\beta}$ and σ^2 to show that $\eta(\boldsymbol{x}) \mid \mathrm{d}$ has a Student-t distribution.

2.1. Variance decomposition

A variance decomposition of Y for an input $\boldsymbol{X} = (X_1, \ldots, X_r)$ given in Cox [5] is

$$Var(Y) = \sum_{i=1}^{r} V_i + \sum_{i<j} V_{ij} + \ldots + V_{ij\ldots k}, \qquad \textbf{(1)}$$

where

$$\begin{aligned} V_{ijk\ldots} &= Var(Z_{ijk\ldots}), \\ Z_i &= E(Y \mid X_i), \\ Z_{ij} &= E(Y - \textstyle\sum_{k=1}^{r} Z_k \mid X_{i,} X_j), \\ Z_{ijk} &= E(Y - \textstyle\sum_{l=1}^{r} Z_l - \sum_{l<m} Z_{lm} \mid X_i X_j X_k), \end{aligned}$$

and so on. The elements $X_1, \ldots, X_r$ must be independent. We can think of V_i as a main effect term giving the contribution to the variance of Y from X_i acting individually, and V_{ij} as describing the variance due to the interaction of X_i and X_j. In Chan et al [3], a total sensitivity index for a particular input is considered, which takes into account all interactions involving that input. Correspondingly, we can compute the total contribution of X_i to *Var(Y)* by calculating $Var(Y) - Var\{E(Y \mid \boldsymbol{X}_{-i})\}$, where $\boldsymbol{X}_{-i}$ denotes all the inputs in $\boldsymbol{X}$ except X_i.

Since the code $\eta(.)$ is also treated as a random variable, the terms in (1) are also random variables, and so each term must be approximated by its posterior mean given the data d. In particular, we have

$$Var\{E(Y \mid \boldsymbol{X}_{-i})\} = E_{-i}\{E(Y \mid \boldsymbol{X}_{-i})^2\} - E(Y)^2,$$

and the posterior mean of this with respect to $\eta(.)$ is

$$\int_{X_{-i}} \int_{X_i} \int_{X_i'} E_\eta\{\eta(x_i, x_{-i})\eta(x_i', x_{-i})\} dG(x_i) dG(x_i') dG(\boldsymbol{x}_{-i}) - \int_{X} \int_{X'} E_\eta\{\eta(\boldsymbol{x})\eta(\boldsymbol{x}')\} dG(\boldsymbol{x}) dG(\boldsymbol{x}')$$

3. EXAMPLE

We now give a synthetic example to demonstrate the methodology described previously. A simple eight dimensional function is used:

$$\eta(\mathbf{x}) = \sum_{i=1}^{8} w_{1_i} x_i + \sum_{i=1}^{8} w_{2_i} x_i x_{j_i} + \textstyle\sum_{i=1}^{8} w_{3_i} x_i x_{k_i} x_{l_i},$$

where $\mathrm{x} = (x_1, \ldots, x_8)$, and weights $w_{1_i}, w_{2_i}, w_{3_i}$ and indices j_i, k_i, l_i all chosen randomly. Input X_i is assumed to have distribution $N(i,1)$. Based on one hundred runs of the code, we estimate relative first order effects $\dfrac{V_i}{Var(Y)}$, and relative total effects $\dfrac{Var(Y) - Var\{E(Y \mid \boldsymbol{X}_{-i})\}}{Var(Y)}$. (Estimating $Var(Y)$ based on a small number of runs of the code is described in Haylock and O'Hagan [1]). The estimates along with the correct values for

comparison are plotted in figure 1. We can see that in this example, fairly accurate estimates have been obtained using one hundred function evaluations only.

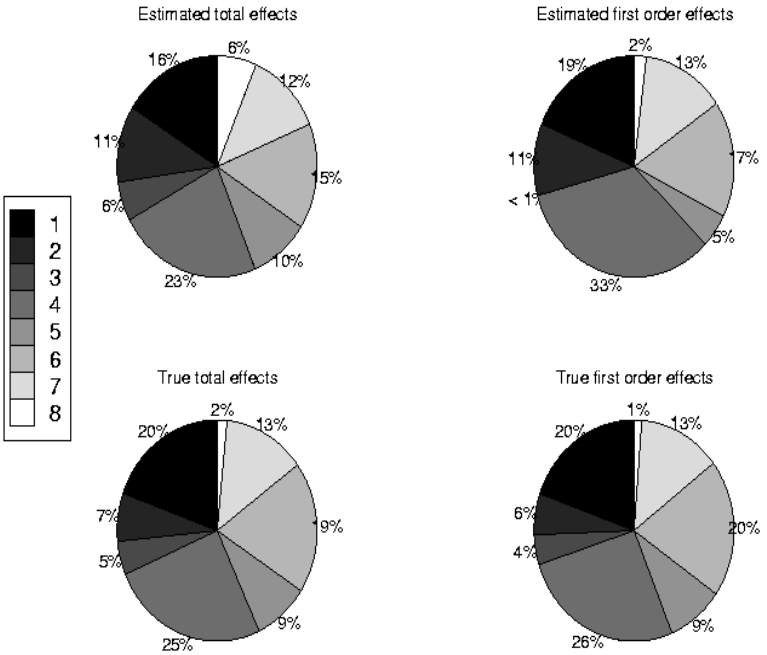

Figure 1: Relative first order and total effects of each model input.

4. DISCUSSION

We have considered a partition of the variance of the uncertain model output, and shown that it is possible to estimate terms in this sum accurately using a relatively small number of runs of the code. The plots in figure 1 then provide a graphical summary of the contribution of each input to the uncertainty in the output. Other summaries can also be produced from the Bayesian model for $\eta(.)$, such as plots of $E(Y \mid X_i)$ against X_i, and contour plots of $E(Y \mid X_i, X_j) - E(Y \mid X_i) - E(Y \mid X_j)$ against X_i and X_j to illustrate interactions. Such outputs require very large numbers of runs using Monte Carlo methods, and provide a detailed analysis of the sensitivity of the output to one or more inputs.

REFERENCES

[1] Haylock, R. G. and O'Hagan, A. (1996). On inference for outputs of computationally expensive algorithms with uncertainty on the inputs. In: *Bayesian Statistics 5* (ed J. M. Bernado, J. O. Berger, A. P. Dawid and A. F. M. Smith). Oxford: University Press.

[2] Oakley, J. E. and O'Hagan, A. (2000). Bayesian inference for the uncertainty distribution, *Technical report,* University of Sheffield.

[3] Chan, K., Tarantola, S., Saltelli, A. and Sobol', I. (2000). Variance-based methods. In: *Sensitivity Analysis* (ed A. Saltelli, K.Chan and E. M. Scott). Wiley, New York.

[4] Oakley, J. E. (2000). Eliciting Gaussian process priors for complex computer codes. *Technical report,* University of Sheffield.

[5] Cox, D. C. (1982). An analytical method for uncertainty analysis of nonlinear output functions, with application to fault-tree analysis. *IEEE Trans. Reliab.* R-31, 265-268.

A MODULAR APPROACH TO SIMULATION WITH AUTOMATIC SENSITITVTY CALCULATION

Kenneth M. Hanson and Gregory S. Cunningham

Los Alamos National Laboratory, MS P940, Los Alamos, NM 87545 (USA)
Email: kmh@lanl.gov, WWW: http://public.lanl.gov/kmh/

1. INTRODUCTION

When using simulation codes, one often has the task of minimising a scalar objective function with respect to numerous parameters. This situation occurs when trying to fit (assimilate) data or trying to optimise an engineering design. For simulations in which the objective function to be minimised is reasonably well behaved, that is, is differentiable and does not contain too many multiple minima, gradient-based optimisation methods can reduce the number of function evaluations required to determine the minimising parameters. However, gradient-based methods are only advantageous if one can efficiently evaluate the gradients of the objective function. Adjoint differentiation efficiently provides these sensitivities [1]. One way to obtain code for calculating adjoint sensitivities is to use special compilers to process the simulation code [2]. However, this approach is not always so 'automatic'. We will describe a modular approach to constructing simulation codes, which permits adjoint differentiation to be incorporated with relative ease.

2. ADJOINT DIFFERENTIATION

Figure 1 schematically shows a data-flow diagram for a sequence of calculations. The goal is to determine the derivatives of the scalar output φ from this sequence with respect to the input data vector **x**. Since φ is a function of **z**, **z** is a function of **y**, and **y** is a function of **x**, the chain rule of differentiation applies:

$$\frac{\partial \varphi}{\partial x_i} = \sum_{j,k} \frac{\partial \varphi}{\partial z_k} \frac{\partial z_k}{\partial y_j} \frac{\partial y_j}{\partial x_i} \tag{1}$$

Theoretically, the order of the summation doesn't matter. However, in computations it is better to sum over *k* before *j*, to avoid propagating large derivative matrices in the forward direction. This reverse flow for the derivative calculation, shown in Fig. 1 as the dashed arrows, is called the adjoint differentiation calculation.

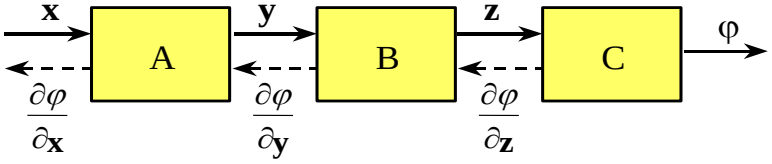

Figure 1. A data-flow diagram describing a sequence of transforms of an input data vector **x** into a scalar output functional φ. The data structures **x**, **y** and **z** may be large.

Derivatives of φ with respect to **x** are most efficiently evaluated by propagating derivatives of φ with respect to the intermediate variables in the reverse (adjoint) direction (dashed lines).

In the modular approach implied by Fig. 1, each box represents a software module that performs a particular transformation of the input data to produce output data. In this approach adjoint differentiation can be achieved relatively easily. The only requirement is that each module not only be able to perform its forward transformation, but also be able to calculate the derivative of its outputs with respect to its inputs. The forward simulation process is achieved by linking together the necessary modules. The output of the simulation is the objective function to be minimised, for example, the measure of mismatch to some given measurements. The data-flow diagram (network or graph) that describes the forward calculation automatically provides the path for the reverse or adjoint calculation needed to accumulate the sensitivities of the objective function to any parameters in the simulation model. In this framework, the sensitivities of the output objective function with respect to all the simulation parameters can be automatically calculated in a time that is comparable to the forward simulation calculation

3. BAYES INFERENCE ENGINE

The Bayes Inference Engine (BIE) provides a superb example of the modular approach to modelling and sensitivity analysis. The BIE is a computer application for analysing radiographs and making inferences about an object being radiographed [3]. The BIE is a graphical programming tool that automatically implements adjoint differentiation, which facilitates advanced model building and allows hundreds or thousands of parameters to be determined by matching a radiograph in a reasonable time.

The BIE represents a computational approach to Bayesian inference, as opposed to the traditional analytical approach. The computational approach affords great flexibility in modelling, which facilitates the construction of complex models. The BIE easily deals with data that are nonlinearly dependent on the model parameters. Furthermore, the computational approach allows one to use nonGaussian probability distributions, such as likelihood functions based on Poisson distributions. Figure 2 shows the canvas of the BIE for a tomographic reconstruction problem in which three projections of a 2D object are used to determine the shape of the object. The reconstructed object is modelled as a uniform (known) density inside a flexible boundary, specified in terms of a 60-sided polygon. A smoothness prior is placed on the boundary. The BIE's automatic adjoint differentiation permits the 120 variables to be determined in 20 optimiser iterations, or in a time corresponding to around 50 forward-model evaluations.

The BIE is designed and programmed within an object-oriented framework in which it id easy to make connections work in the reverse direction. An interesting aspect of the BIE is that there is no supervisory code. The modules act autonomously by responding to requests from other modules that are connected to their output for updated results. Each module asks its inputs for current information and then does its own calculation. It is the module at the end of the calculation, the optimiser in Fig. 2, that initiates the requests and finally gets the results of the calculation. The parameter modules (boxes labelled as P) terminate requests for forward calculations. This modular approach greatly simplifies adjoint calculations. The reverse flow of the derivatives proceeds in much the same manner.

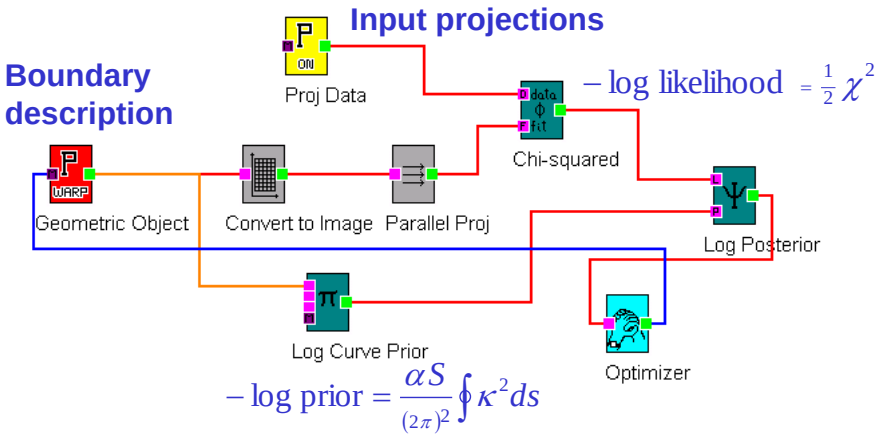

Figure 2. A canvas from the BIE showing a data-flow diagram composed to simulate a radiographic measurement of an object that is defined in terms of a geometric description of its boundary. The minus-log-likelihood is added to a minus-log-prior to obtain a minus-log-posterior, which is to be minimised with respect to the geometry. Derivatives of the minus-log-posterior with respect to the geometric parameters are automatically calculated in the BIE in a computational time that is comparable to the forward simulation calculation.

Figure 3. An optimisation achieved with the BIE with the diagram shown in Fig. 2. Three noisy projections of the original object (left) are available, making this a very difficult reconstruction problem. The image on the right represents the shape that minimises the minus-log-posterior on the right in Fig. 2, obtained by varying the 120 parameters that describe its geometric boundary.

4. DISCUSSION

The modular approach to adjoint sensitivity calculation incorporated in the BIE can readily be applied to other simulation applications. References [4] and [5] demonstrate the use of adjoint differentiation to solve a complex inversion problem involving the diffusion of infrared light in tissue. Figure 4 shows the data-flow diagram, which could be used as a basis for creating the modular design described above.

Adjoint sensitivities are only not useful for optimisation, but also for drawing inferences about the uncertainties in model parameters. For example, the Hamiltonian method of Markov Chain Monte Carlo [6] uses the gradient of the minus-log-posterior function. MCMC is implemented in the BIE by replacing the optimiser by an MCMC module.

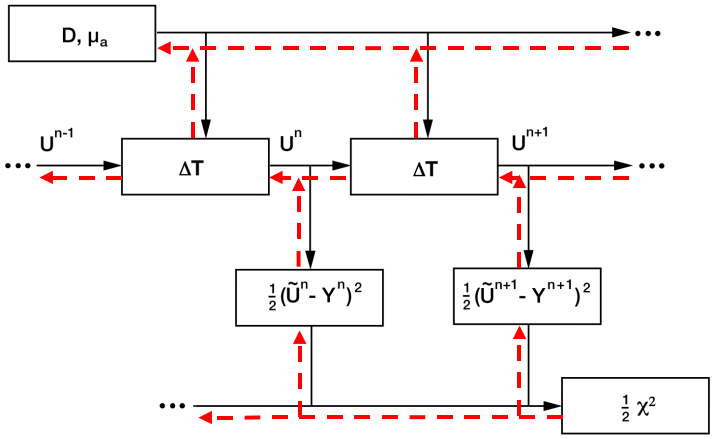

Figure 4. A data-flow diagram for the simulation of a time-dependent diffusion process. The parameters in the upper-left hand box, the position-dependent diffusion constant and absorption coefficient, control the diffusion. The ΔT boxes provide the time-step calculation for the light-intensity field U, which is sampled to compare to time-dependent measurements. The output of the calculation is the scalar $\chi^2/2$, which is to be minimised to obtain the best match to the measurements. The minimisation is efficiently accomplished through use of the gradients calculated by the adjoint method, which follows the direction of the dashed arrows.

5. ACKOWLEDGEMENTS

For many valuable interactions and collaborations, we would like to thank Rudy Henninger, Maria Rightley, Xavier Battle, Suhail Saquib, Andreas Hielscher, and Alex Klose. This work was supported by US-DOE under contract W-7405-ENG-36.

6. REFERENCES

[1] Hanson, KM, Cunningham (1998), Inversion based on computational simulations, *Maximum Entropy and Bayesian Methods*, pp. 121-135, Kluwer Academic, Dordrecht.

[2] Giering, R (1997), *Tangent-linear and Adjoint Model Compiler, Tech. Report TAMC 4.7, Max-Planck-Institut für Meterologie.*

[3] Hanson, KM, Cunningham (1999), Operation of the Bayes Inference Engine, *Maximum Entropy and Bayesian Methods*, pp. 309-318, Kluwer Academic, Dordrecht.

[4] Saquib, SS, Hanson, KM, Cunningham, GS (1997), Model-based image reconstruction from time-resolved diffusion data, *Medical Imaging: Image Processing, Proc. SPIE* **3338**, pp. 369-380.

[5] Hielscher, AH, Klose, AD, Hanson, KM (1999), Gradient-based iterative image reconstruction scheme for time-resolved optical tomography, *IEEE Trans. Med. Imag.* **18**, pp. 262-271.

[6] Hanson, KM (2001), Markov Chain Monte Carlo posterior sampling with the Hamiltonian method, *Proc. Sensitivity Analysis of Model Output*, P. Prado, ed..

LINEARIZATION OF LOCAL PROBABILISTIC SENSITIVITY VIA SAMPLE RE-WEIGHTING

R.M.Cooke[(1)], D. Kurowicka[(1)], I. Meilijson [(2)]

[(1)] Dep. of Math.,Delft University of Technology, Delft, The Netherlands
Email: R.M.Cooke@its.tudelft.nl , D.Kurowicka@its.tudelft.nl

[(2)] School of Mathematical Sciences, Tel Aviv University, Tel Aviv, Israel,
Email: isaco@math.tau.ac.il

ABSTRACT

Local probabilistic sensitivity of input variable *X* with respect to output variable *Z* is proportional to the derivative of the conditional expectation *E*(*X*|*z*). This paper reports on experience in computing this conditional expectation. Linearized estimates are found to give acceptable performance, but are not generally applicable. A new method of linearization based on re-weighting a Monte Carlo sample is introduced. Results are comparable to the linearized estimates, but this method is more widely applicable. Results generally improve by conditioning on a small window around *z*.

1. INTRODUCTION

Local probabilistic probability measures (LPSM) were introduced in [3] to describe the importance of an input variable *X* to a given contour of an output variable *Z*:

$$LPSM(X) = \frac{\sigma_Z}{\sigma_X}\frac{\partial E(X|Z=z)}{\partial z}\Big|_{z=z_0} = \frac{\sigma_Z \partial E(X|z_0)}{\sigma_X \partial z_0} \qquad (1)$$

This measure is indicated when we are particularly interested certain values of the output variable. Thus when *Z* represents the 'strength - load' of a structure, we are particularly interested in the value *Z = 0* corresponding to failure of the structure. It was shown that if the regression *E*(*X*|*Z*) is linear, then *LPSM(X)* = ρ*(Z,X)* (see section (5)). In special cases, including the independent normal linear model, *LPSM*(*X*) can be computed analytically [3].

Problems in computing *LPSM* have motivated further study of its properties. It can be shown that in the case of independent linear normal models, the *LPSM* and the standard global measures are dual in a straightforward sense. The generalization of the standard global measure to non-linear models makes use of the correlation ratio. A similar generalization is conjectured for the *LPSM*. The duality relation suggests alternative ways of calculating the *LPSM* which appear to give acceptable performance.

Section (2) illustrates problems that can arise in computing the LPSM in Monte Carlo simulation. Section (3) reviews sensitivity measures in the linear model. Section (4) explores properties of the correlation ratio. Section (5) establishes the duality relationship for the independent linear normal case. This relationship suggests new ways of calculating the derivative of the conditional expectation. Analytical methods and linear approximations are

discussed. Though not always applicable in practice, these nonetheless provide a benchmark for the method introduced in section (6). This method `linearizes by re-weighting' a Monte Carlo sample, and can always be applied in Monte Carlo simulation. In section (7) the performance of these methods is compared. A final section gathers conclusions.

2. AN EXAMPLE

The obvious way to approximate *LPSM(X)* in Monte Carlo simulations is to compute

$$\frac{E(X\,|\,Z \in (z_0, z_0+\varepsilon)) - E(X\,|\,Z \in (z_0-\varepsilon, z_0))}{2\varepsilon} \tag{2}$$

In some cases this is very unstable. Consider the following example, which was proposed by Ton Vrouwenvelder, where X and Y are independent standard normal:

$$Z = min(3-X, 3-Y)$$

One can calculate that (see appendix):

$$\frac{\partial E(X\,|\,Z=z)}{\partial z}\;\Big|_{z=0} = -0.507\,.$$

On a Monte Carlo simulation with 5,000,000 samples and ε = 0.1 the above method yields the estimates

$$\frac{\partial}{\partial z}E(X\,|\,z=0)_{simulation} = -0.517,$$
$$\frac{\partial}{\partial z}E(Y\,|\,z=0)_{simulation} = -0.807.$$

Of course, by symmetry these two derivatives must be equal. The number of samples used is unrealistically large, and still performance is poor. This is explained by a number of factors. First if high accuracy is desired, ε must be chosen small in (2). On the other hand the difference in conditional expectations must be large enough to be statistically significant. In the above example this difference was barely significant at the 5% level for *Y* and was not significant for *X*. In this case, the difference in conditional expectations in (2) is small, because, roughly speaking, *X* feels the effect of conditionalizing on *Z = 0* on only one half of the samples. Finally, conditionalizing on extreme values of *Z*, as in this case, can introduce strong correlations between the input variables. In this case the conditional correlations are negative. This means that sampling fluctuations in the estimates of the conditional expectations in (2) will be correlated. Indeed, it required an unrealistically large number simply to obtain estimates whose signs were both negative (see also the results in Table 4).

It is clear that alternative methods of calculating the LPSM are needed.

3. THE LINEAR MODEL

Let $Z = Z(X)$ be a function of vector $X=(X_1,...,X_n)$. Assuming that Z is analytic, it can be expanded in the neighbourhood of some point $x^* = (x_1^*,...,x_n^*)$ and neglecting higher order terms (HOT's):

$$Z(X) \sim Z(x^*) + \sum_{i=1}^{n} \partial_i Z(x^*)(X_i - x_i^*) \tag{3}$$

where ∂_i denotes $\partial / \partial_{X_i}$.

Let μ_i and σ_i denote mean and standard deviation of X_i respectively. We obtain

$$E(Z) \sim Z(x^*) + \sum_{i=1}^{n} (\mu_i - x_i^*)\partial_i Z(x^*),$$

$$Var(Z) \sim + \sum_{i,j=1}^{n} Cov(X_i, X_j)\partial_i Z(x^*)\partial_j Z(x^*).$$

If X_i are all uncorrelated then

$$Cov(Z, X_i) = \sigma_i^2 \partial_i Z = \rho(Z, X_i)\sigma_Z \sigma_{X_i}.$$

Hence, in the linear uncorrelated model, the rate of change of Z with respect to X_i may be expressed as

$$\partial_i Z = Cov(Z, X_i) / \sigma_i^2. \tag{4}$$

We note that the left hand side depends on the point x^* whereas the right hand side does not. This of course reflects the assumption of non-correlation and the neglect of HOT's. A familiar sensitivity measure involves a "sum square normalization":

$$\alpha_i = \rho(Z, X_i) = \frac{\partial_i Z(x^*)\sigma_i}{\sigma_Z}.$$

The factor α_i gives the influence of variable X_i on the standard deviation of Z. It depends on the slope of the tangent line of Z in the point z^*. For the linear model and when X_i's are uncorrelated,

$$R^2 = \sum_{i=1}^{n} \alpha_i^2 = 1. \tag{5}$$

This can be considered as a measure of the variance of Z explained by the linear model. If R^2 is less then one, this may be caused either by dependencies among X_i's or by the contribution of higher order terms neglected in (3).

When employing the Taylor expansion as above, it is common to introduce a transformation of the variable Z which enables us to capture as much of the behaviour of the transformed variable as possible in low order terms. Alternatively, one could transform the variables X_i toward the same end. These considerations lead to the correlation ratio, whose properties we study in the next section.

4. CORRELATION RATIO

The correlation ratio is one of the most important non-directional measures of uncertainty contribution [2].

Definition 4.1 *(Correlation ratio) Let G be a random variable, and X a random vector. The quantity* $\frac{\sigma^2_{E(G|X)}}{\sigma^2_G}$ *is called the correlation ratio of X to G and denoted CR(X,G).*

We consider a function $G = G(X,Y)$ of random vectors X and Y with $\sigma^2_G < \infty$. In analogy with non-linear regression methods, we may ask for which function $f(X)$ with $\sigma^2_{f(X)} < \infty$ is $\rho^2(G, f(X))$ maximal? The answer given in the following

Proposition 4.2 Let G = G(X,Y) with $\sigma^2_G < \infty$ then

(i) $Cov(G, E(G|X)) = \sigma^2_{E(G|X)}$

(ii) $max_{f;\sigma^2_{f(x)}<\infty}\rho^2(G, f(X)) = \rho^2(G, E(G|X)) = \frac{\sigma^2_{E(G|X)}}{\sigma^2_G} = CR(X, G)$

Proof:

(i) $Cov(G, E(G \mid X)) = E(E(GE(G \mid X)|X)) - EGE(E(G \mid X)) = E(E^2(G \mid X)) - E^2(E(G \mid X))$

(ii): Let δ(X) be any function with finite variance.

Put, $A = \sigma^2_{E(G|X)}$; $B = Cov(E(G|X), \delta(X))$, $C = \sigma^2_G$; $D = \sigma^2_\delta$, Then

$$\rho^2(G, E(G|X) + \delta(X)) = \frac{(A+B)^2}{C(A+D+2B)}, \tag{6}$$

$$\frac{\sigma^2_{E(G|X)}}{\sigma^2_G} = \frac{A}{C}, \tag{7}$$

$$\frac{(A+B)^2}{C(A+D+2B)} \le \frac{A}{C} \Leftrightarrow B^2 \le AD\,. \tag{8}$$

The latter inequality follows from the Cauchy Schwarz inequality. This is similar to a result in [5].

The correlation ratio of X to G may be taken as the general global, variance based sensitivity measure of G to X. This may be understood by recalling the simple relation:

$$Var(G) = Var(E(G|X)) + E(Var(G|X))\,.$$

Dividing both sides by Var(G), we may interpret *CR(X,G)* as the percentage of the variance of G which is explained by X.

Note that the correlation ratio is always positive, and hence gives no information regarding the direction of the influence. Note also that in general *CR(G,X)≠CR(X,G)*

The following propositions explore some properties of the correlation ratio.

Proposition 4.3 *Let G(X, Y) = f(X) + h(Y) where f and g are invertible functions with* $\sigma_f^2 < \infty, \sigma_h^2 < \infty$, *and X,Y are not both simultaneously constant* ($\sigma_G^2 > 0$). *If X and Y are independent then*

$$\rho^2(G, E(G|X)) + \rho^2(G, E(G|Y)) = 1.$$

Proof:

We have $E(G|X) = E(G|f(X))$, and $h(Y) \perp E(G|f(X))$, $f(X) \perp E(G|h(Y))$; therefore,

$$\begin{aligned}
\sigma_G^2 &= Cov(G,G) = Cov((G, f(X) + h(Y)) \\
&= Cov(G, f(X)) + Cov(G, h(Y)) \\
&= Cov(E(G|f(X)), f(X) + Cov(E(G|h(Y)), h(Y)) \\
&= Cov(E(G|f(X)) + E(G|h(Y)), f(X) + h(Y)) \\
&= Cov(E(G|f(X)) + E(G|h(Y))), G) \\
&= Cov(E(G|X) + E(G|Y), G) = \sigma^2_{E(G|X)} + \sigma^2_{E(G|Y)}.
\end{aligned}$$

The result now follows with Proposition (4.2). □

Proposition 4.4 *Let G=G(X,Y), with Cov(E(G|X), E(G|Y)) = 0* then

$$\rho^2(G, E(G|X)) + \rho^2(G, E(G|Y)) \le 1.$$

Proof:

$$\rho(E(G|X), G - E(G|Y)) = \frac{Cov(E(G|X), G - E(G|Y)}{\sigma_{E(G|X)}\sqrt{\sigma_G^2 - \sigma^2_{E(G|Y)}}} = \frac{\sigma_{E(G|X)}}{\sqrt{\sigma_G^2 - \sigma^2_{E(G|Y)}}} \le 1,$$

$$\sigma^2_{E(G|X)} + \sigma^2_{E(G|Y)} \le \sigma_G^2.$$

4.1. Computing the correlation ratio

The computations frequently use Monte Carlo methods. Efficiency in this context usually means on-the-fly. That is, we would like to perform all necessary calculations on a sample, then discard the sample and proceed to the next sample. A computation which involves retaining the entire sample is not efficient.

Computing the correlation ratio may be difficult in some cases. However, if we can sample *Y'* from the conditional distribution *(Y|X)* independently of *Y*, and if the evaluation of G is not too expensive, then the following simple algorithm may be applied (Ishigami and Homma [4]):

1. Sample *(x,y)* from *(X,Y),*
2. Compute *G(x,y),*
3. Sample *y'* from *(Y|X = x)* independent of *Y = y,*
4. Compute *G' = G(x, y')*
5. Store *Z = G * G'*

6. Repeat

The average value of Z will approximate $E(E^2(G|X))$, from which the correlation ratio may be computed as

$$\frac{E(E^2(G|X)) - E^2(G)}{\sigma_G^2}.$$

Of course, if *Y* and *X* are independent, then this algorithm poses no problems. If *Y* and *X* are not independent, then it may be difficult to sample from *(Y|X).* In this case there is no alternative to the "pedestrian" method: save a large sample, compute $E(G \mid X = x_i \pm \varepsilon)$ for suitable $x_{1,\ldots,}\ x_n$, and compute the variance of these conditional expectations. To do this for a large number of variables can be slow.

The notion of the correlation ratio can be generalized by introducing the following definition

Definition 4.5 [Generalized correlation ratio] *Correlation ratio G with* $X_{i_1},\ldots,X_{i_s}$ *is*

$$CR\left(G,\left\{X_{i_1},\ldots,X_{i_s}\right\}\right) = \frac{Var\left(E\left(G\middle|\left\{X_{i_1},\ldots,X_{i_s}\right\}\right)\right)}{Var(G)}.$$

5. LOCAL PROBABILISTIC SENSITIVITY MEASURES

The local sensitivity measure (1) is intended to measure the rate of change with respect to *Z* of "some function" of *X|Z* at a given point. For the uncorrelated linear model, "global" and "local" are equivalent, hence the global and local measures should coincide. This motivates choosing "some function" as a normalized conditional expectation in (1). In fact, local probabilistic and global sensitivity measures may be be seen as dual, in the following sense. Apply the Taylor expansion to *E(X|Z)*:

$$\begin{aligned} Cov(Z,X) &= Cov(Z - E(Z), E(X|Z)) \\ &\sim Cov\left(Z - E(Z), E(X|z_0) + (Z - z_0)\frac{\partial E(X|z_0)}{\partial z_0}\right) = \sigma_Z^2 \frac{\partial E(X|z_0)}{\partial z_0}. \end{aligned}$$

Thus, if the regression of *X* on *Z* is linear, then higher order terms vanish and

$$\frac{\partial E(X|z_0)}{\partial z_0} = \frac{Cov(Z,X)}{\sigma_Z^2}. \qquad (9)$$

which may be compared with (4). If the roles of *Z* and *X* were reversed in the linear uncorrelated model, then (9) would express the rate of change of *X* with respect to *Z*. Of course, these roles cannot be reversed, as *Z* is correlated with $X_{1,\ldots,}X_n$. However, the regression *E(X|Z)* can be linear, indeed this arises for linear normal, mixed normal and elliptical models (correlated as well as uncorrelated) ([1]). Hence in the uncorrelated linear models with linear regression of *X* on *Z*, we have

$$\frac{\partial Z}{\partial x_0} = \frac{Cov(Z,X)}{\sigma_X^2}, \qquad (10)$$

$$\frac{\partial E(X|z_0)}{\partial z_0} = \frac{Cov(Z,X)}{\sigma_Z^2}. \tag{11}$$

Note that the quantities on the right hand side are global, whereas those on the left are local. As seen above, the correlation ratio of *X* to *Z* is the maximal squared correlation attainable between *Z* and some function of *f(X)* of *X* with finite variance. In the same vein, we could ask, `which function *f(X)* of *X* maximizes

$$\left(\frac{\sigma_Z}{\sigma_{f(X)}}\frac{\partial E(f(X)|z_0)}{\partial_{Z_0}}\right)^2 ?$$

We conjecture that the maximum is attained for *f(X) = E(Z|X).*

We first discuss methods of computing and approximating $\frac{\partial E(X|z_0)}{\partial z_0}$. These methods cannot always be applied in practice, but serve as a benchmark. In the following section we develop a method based on the above duality.

5.1. Computing $\frac{\partial E(X|z_0)}{\partial z_0}$

We discuss methods for computing the derivative of a conditional expectation. In general, if the rightmost integral converges absolutely for all z_o;

$$\frac{\partial E(X|z_0)}{\partial z_0} = \frac{\partial}{\partial z_0}\int x f(x|z_0)dx = \int\left(\frac{\partial x}{\partial z_0} f(x|z_0) + x\frac{\partial f(x|z_0)}{\partial z_0}\right)dx.$$

Alternatively, we could compute the conditional expectation *E(X|Z)* directly and take its derivative. Assume for example that *X,Y* are independent and uniformly distributed on [0, 1], and let *Z=Z(X,Y)* be sufficiently differentiable in both arguments. To compute the expectation of X given $Z=z_o$, we define a density along the contour $Z=z_o$ which is proportional to arc length. If the contour is simple we may parametrize arc length in terms of *x* and write $z_o=Z(x,y(x))$ The arc length element, *ds* and conditional expectation are given by

$$ds = \sqrt{dx^2 + dy^2} = dx\sqrt{1+(dy/dx)^2}$$

$$E(X|z_0) = \int x f(X|z_0)dx = \frac{\int x\sqrt{1+(dy/dx)^2}\,dx}{\int\sqrt{1+(dy/dx)^2}\,dx}$$

The reader may verify the following examples:

Example 5.1

$$Z = 2X + Y;\ f(x|z) = 2/z;\ 0 < x < z/2,$$

$$Z = XY;\ f(x|z) = \frac{\sqrt{1+z^2/x^4}}{\int_z^1\sqrt{1+z^2/x^4}\,dx};\ 0 \le z \le 1,\ z < x < 1,$$

$$Z = X^2 Y;\ f(x|z) = \frac{\sqrt{1+4z^2/x^6}}{\int_{\sqrt{z}}^{1}\sqrt{1+z^2/x^6}\,dx};\ 0 \le z \le 1,\ \sqrt{z} < x < 1,$$

$$Z = X^2 + Y^2;\ f(x|z) = \frac{\sqrt{1+x^2/(z^2+y^2)}}{\int_{0}^{\sqrt{z}}\sqrt{1+x^2/(z^2+y^2)}\,dx};\ 0 \le z \le 1,\ 0 < x < \sqrt{z}.$$

5.2. Linear approximations

Since (9) does not depend on z_o, it does not provide a good basis for linear approximations. For random variables *X, Y* let *Z=Z(X,Y)* and suppose for some analytic function G we can write *X=G(Z,Y).* The Taylor expansion gives:

$$X = G(z_0, y_0) + (Z - z_0)\partial_{z_0} G + (Y - y_o)\partial_{y_0} G + (Z - z_0)(Y - y_o)\partial_{z_0}\partial_{y_0} G + \frac{(Y - y_o)^2}{2}\partial_{y_0}^2 G + \frac{(Z - z_o)^2}{2}\partial_{z_0}^2 G + HOT$$

Take $y_o = E(Y|z_o)$ and take conditional expectations on both sides with respect to z_o. The first order terms, the cross term and the second order term in *Z* all vanish. We find

$$E(X \mid z_0) \sim G(z_0, E(Y \mid z_0)) + \tfrac{1}{2}\partial_{y_0}^2 (GVar(Y \mid z_0)). \tag{12}$$

We now take derivatives on both sides with respect to zo. Retaining only the first term yields *estimate 1*:

$$\frac{\partial E(X \mid z_0)}{\partial z_0} \sim \frac{\partial}{\partial z_0} G(z_0, E(Y \mid z_0)) \tag{13}$$

Retaining both terms yields *estimate 2*:

$$\frac{\partial E(X \mid z_0)}{\partial z_0} \sim \frac{\partial}{\partial z_0}\left(G(z_0, y_0) + \tfrac{1}{2}\partial_{y_0}^2 (GVar(Y \mid z_0))\right). \tag{14}$$

Note that both these estimates depend on z_o.

6. LINEARIZATION VIA RE-WEIGHTED MONTE CARLO SIMULATION

The methods of the previous section are not generally useful in practice. Indeed, *estimate 1* will typically require $\frac{\partial}{\partial z_0} E(Y \mid X)$ to estimate $\frac{\partial}{\partial z_0} E(X|Z)$ which is just as hard to calculate as quantity being estimated. *Estimate 2* requires $\frac{\partial}{\partial z_0} Var(Y|z_0)$ which is more difficult to estimate than $\frac{\partial}{\partial z_0} E(X|z_0)$.

A new method of calculating $\frac{\partial E(X|z_0)}{\partial z_0}$ suggested by Meilijson is currently being developed. The idea is the to make the duality relation (9) approximately true by re-weighting the sample emerging from a Monte Carlo simulation. Since *E(X|Z)* can be expanded around z_o as

$$E(X \mid Z) = E(X \mid Z = z_0) + (Z - z_0)\frac{\partial E(X|z_0)}{\partial z_0} + \frac{1}{2}(Z - z_0)^2 \frac{\partial^2 E(X|z_0)}{\partial z_0^2} + HOT$$

then

$$Cov(X, Z) = Cov(E(X \mid Z(, Z) =$$

$$\sim \frac{\partial E(X|z_0)}{\partial z_0} VarZ + \frac{1}{2}\frac{\partial^2 E(X|z_0)}{\partial z_0^2}\left\{E(Z - z_0)^3 + (z_0 - EZ)(E(Z - z_0)^2)\right\}.$$

So if we assign a "local distribution" to *Z* such that the terms between curly brackets are equal to zero then

$$\frac{\partial \overline{E}(X|z_0)}{\partial z} = \frac{\overline{Cov}(X, Z)}{\overline{Var}(Z)}.$$

To achieve this the local distribution should be chosen so that

$$\overline{E}Z = z_o$$

and

$$\overline{E}(Z - z_o)^3 = z_o$$

where $\overline{Z}$ means *Z* with a local distribution. We want this distribution to be as close as possible to the distribution of *Z*. In our case we take the distribution which minimizes the relative information with respect to the original distribution of *Z*.

7. RESULTS

Z	z_o	$\frac{\partial E(X\|z_0)}{\partial z_0}$	*est1*	*est2*
2X+Y	0.25	0.25	0.25	0.25
	0.5	0.25	0.25	0.25
	1.5	0.5	0.5	0.5
	2.5	0.25	0.25	0.25
X^2+Y^2	0.1	1.0066	1.2189	1.2024
	0.5	0.4488	0.5451	0.5063
	0.9	0.3355	0.4056	0.3538
XY	0.1	1.0724	1.8046	1.7764
	0.5	0.6342	0.7768	0.7095
	0.9	0.5180	0.5361	0.5271
X^2Y	0.1	1.2698	1.8013	1.5733
	0.5	0.4454	0.5099	0.4501
	0.9	0.2746	0.2816	0.2746

The first table presents the theoretical results for the functions given in example (5.1). *X,Y* are independent and uniform on [0, 1]. The theoretical values have been computed with MAPLE. Note that for *Z=2X+Y* the estimates are exact, as the regression is piece-wise linear: *E(X|z)*=z/4; $0 < z < 1$; $2 < z < 3$; but *E(X|z)* = z/2 ; $1<z<2$.

Table 1: Comparison of theoretical values and linearized estimates.

Table 2 shows the re-weighted estimates for the same models as in Table 1. To show the sampling fluctuations, the results have been computed on five runs, each run using 10,000 samples. The weights defining the local distribution for *Z* have been computed with MOSEK. We see that the results are reasonably stable and are generally between those of *estimate 1* and *estimate 2* in Table 1. An exception occurs for $Z = 2X + Y$; in this case the second derivative of the regression function $E(X|z)$ does not exist for $z=1$. This suggests that better results could be obtained by first defining a window around the value z_o and applying the re-weighting method within this window.

Z	*zo*	$\frac{\partial E(X\|z_0)}{\partial z_0}$	*1*	*2*	*3*	*4*	*5*
$2X+Y$	0.25	0.25	0.2577	0.2387	0.2447	0.2500	0.2436
	0.5	0.25	0.2646	0.2496	0.2603	0.2514	0.2560
	1.5	0.5	0.4021	0.4007	0.3966	0.4022	0.4002
	2.5	0.25	0.2484	0.2440	0.2475	0.2540	0.2602
X^2+Y^2	0.1	1.0066	1.1626	1.2117	1.1473	1.1391	1.1568
	0.5	0.4502	0.5309	0.5163	0.5428	0.5238	0.5317
	0.9	0.3355	0.4388	0.4441	0.4440	0.4411	0.4475
XY	0.1	1.0020	1.4854	1.5025	1.5200	1.4916	1.6087
	0.5	0.6342	0.6939	0.7018	0.7031	0.6955	0.6860
	0.9	0.5180	0.4666	0.5908	0.4641	0.5108	0.5182
X^2Y	0.1	1.2698	2.3313	2.3890	2.3878	2.3453	2.3634
	0.5	0.4454	0.5784	0.5839	0.5822	0.5808	0.5782
	0.9	0.2746	0.2706	0.2974	0.2498	0.2636	0.2717

Table 2: Comparison of theoretical values and re-weighting method, five runs of 10,000 samples.

The results in Table 3 are obtained by drawing 100,000 samples, and conditionalizing on the window $Z \in (z_o - 0.2, z_o + 0.2)$. Two runs are shown; Ñ indicates number of samples in the conditional distribution on each run. We note that for $Z = X^2Y = 0.1$ the results are poor, despite the fairly large number of samples falling in the window. The function $Y(x) = 0.1/x^2$; $x \in [0.1,1]$ is highly non-linear; the derivative ranges over 4 orders of magnitude. Reducing the window size to 0.05 returns results comparable to estimate 2.

Z	*zo*	$\frac{\partial E(X\|z_0)}{\partial z_0}$	*1*	*Ñ1*	*2*	*Ñ2*
2X+Y	0.25	0.25	0.2530	5021	0.2464	4832
	0.5	0.25	0.2573	10079	0.2608	9874
	1.5	0.5	0.4943	19867	0.4894	20015
	2.5	0.25	0.2570	10047	0.2501	9949
X^2+Y^2	0.1	1.0066	1.1564	23774	1.1655	23593
	0.5	0.4502	0.4610	31320	0.4509	31300
	0.9	0.3355	0.4141	29323	0.4180	29347
XY	0.1	1.0724	1.5140	66131	1.5260	66072
	0.5	0.6342	0.6438	28813	0.6464	28713
	0.9	0.5180	0.5167	5020	0.5363	5038
X^2Y	0.1	1.2698	2.3759	79690	2.3580	79403
	0.5	0.4454	0.4564	17792	0.4469	17855
	0.9	0.2746	0.2689	2638	0.2871	2658

Table 3: Comparison of theoretical values with re-weighting method results with window.

Table 4 shows results for *X, Y* independent standard normal. There are five runs with 10,000 samples per run and no window (the use of a window did not improve results). The results for *Z = min(3-X,3-Y)=0* are quite bad and quite unstable. This presumably reflects the small number of samples in the region *z = 0*. The other values are quite acceptable.

Z	*zo*	$\frac{\partial E(X\|z_0)}{\partial z_0}$	*1*	*2*	*3*	*4*	*5*
X+Y	0	0.5	0.5058	0.4964	0.5000	0.4921	0.4965
	2	0.5	0.5387	0.4831	0.4983	0.5030	0.5086
	3	0.5	0.4292	0.4415	0.4840	0.4681	0.5826
2X+Y	0	0.4	0.4005	0.4037	0.4012	0.3967	0.3939
	1	0.4	0.4006	0.3992	0.3497	0.3996	0.3967
	3	0.4	0.4033	0.3996	0.3927	0.4027	0.4027
Min{3-X,3-Y}	0	-0.5067	-0.8779	0.7641	0.3178	1.1178	-0.6585
	1	-0.5568	-0.6478	-0.5839	-0.5445	-0.7650	-0.4516
	2	-0.6852	-0.6925	-0.6686	-0.7204	-0.6676	-0.6792
	3	-0.8183	-0.8061	-0.8031	-0.8002	-0.7979	-0.8048

Table 4: Comparison of theoretical and re-weighting method results for normals.

With regard to the example *Z=min{3-X,3-Y}* the results are better than those given in section (2), but not overwhelming. With 5,000,000 samples and window $z \in [-0.1,0.1]$ we find

$$\frac{\partial E(X \mid Z = z)}{\partial z}\Big|_{z=0} = -0.5029,$$

$$\frac{\partial E(Y \mid Z = z)}{\partial z}\Big|_{z=0} = -0.5038.$$

Needless to say, this number of samples is not realistic in practice. With only 10,000 samples the results were not acceptable. Note that in this case the linearized estimates are not defined, as the function G satisfying $X = G(Z,Y)$ does not exist.

8. CONCLUSIONS

In the linear model (3), with $X_1,\ldots,X_n$ independent normal, we have observed following relations:

$$\frac{\partial Z}{\partial X} = \frac{Cov(X_i, Z)}{\sigma^2_{X_i}} = \frac{\rho(Z, X_i)\sigma_Z}{\sigma_{X_i}},$$

$$\frac{\partial E(X / Z = z)}{\partial z} = \frac{Cov(X_i, Z)}{\sigma^2_Z} = \frac{\rho(Z, X_i)\sigma_{X_i}}{\sigma_Z}.$$

When these assumptions do not apply, one can still use these relations by way of crude estimation. Thus one can estimate the rate of change of Z with respect to X_i as, $\frac{\rho(Z, X_i)\sigma_Z}{\sigma_{X_i}}$ and one can estimate the rate of change of $E(X|z)$ with respect to z as $\frac{\rho(Z, X_i)\sigma_{X_i}}{\sigma_Z}$. Better estimates can be obtained by the linearization techniques introduced in sections (5.2, 6). In particular the re-weighting approach to linearization gives acceptable results in most of the benchmark problems and is applicable quite generally. None the less, there is room for improvement. We have tried adding additional constraints to the re-weighting algorithm, but did not find any constraints which produced better results for all of the benchmark functions. Reducing the window size generally leads to better results, but of course this drives up the number of samples required. For difficult problems, such as that discussed in section (2) the re-weighting method returns good results only after using a small window with a very large number of samples. It seems likely that the re-weighting method of linearization can still be further improved.

Acknowledgements. We gratefully acknowledge assistance of M. Kallen, M. Poelman.

9. APPENDIX

Let *Z=min(3-X,3-Y)* with *X,Y* independent standard normal.

$$\begin{aligned} E(X \mid Z = z) = & \quad E(X \mid Z = z, X < Y)P(X < Y) + E(X \mid Z = z, Y \le X)P(Y \le X) \\ = & \quad (E(X \mid Y = 3 - z, X < Y) + E(X \mid X = 3 - z, X \ge Y))/2 \\ = & \quad (E(X \mid X < 3 - z) + E(X \mid X = 3 - z, Y < 3 - z))/2 \\ = & \quad E(X \mid X = 3 - z) + 3 - z)/2 \end{aligned}$$

where

$$E(X \mid X < 3 - z) = \frac{\int_{-\infty}^{3-z} x\phi(x)dx}{\int_{-\infty}^{3-z} \phi(x)dx}$$

and ϕ is the standard normal density, with cumulative distribution function Φ. The partial derivative of the right hand side at *z = 0* is

$$\frac{-3\phi(3)\Phi(3) + \phi(3)\int_{-\infty}^{3} x\phi(x)dx}{2\Phi(3)^2} - 0.5 = -0.507 .$$

10. REFERENCES

[1] R.M. Cooke D.Kurowicka. Conditional, partial and rank correlation for elliptical copula; dependence modeling in uncertainty analysis. Proc. of ESREL 2001, 2001.

[2] M.G. Kendall and A. Stuart. The Advanced Theory of Statistics, vol. 2. Griffin, London, 1967.

[3] J. van Noortwijk R.M. Cooke. Local probabilistic sensitivity measures for comparing form and monte carlo calculations illustrated with dike ring reliability calculations. Computer Physics Communications, 117:86-98, 1998.

[4] T. Homma T. Ishigami. An importance quanti_cation technique in uncertainty analysis for computer models. In Proceedings of the ISUMA '90 First International Symposium on Uncertainty Modeling and Analysis, University of Maryland, pages 398-403, 1990.

[5] Whittle. Probability via Expectation. Springer Verlag, New York, 1992.

ON LOCAL IMPORTANCE MEASURES

E. Borgonovo and G.E. Apostolakis

Department of Nuclear Engineering, Room 24-221
Massachusetts Institute of Technology
Cambridge, MA 02139-4307 USA
Email: eborgonovo@aol.com, apostola@mit.edu

1. INTRODUCTION

In this paper, we propose a formal definition of local and global importance measures (Section 2). This definition is, then, the basis for the definition of additivity property for importance measures (Section 3). In Section 4 we introduce the Differntial Importance Measure (DIM) and other local measures based on partial derivatives. In Section 5 we deal with the problem of finding the local importance of multiple parameters. We show that it is not possible to compute the importance of parameter groups through normalized partial derivatives. This is however possible using DIM, since the importance of a set of parameters is the sum of the individual parameter DIMs.

2. DEFINITION OF LOCAL AND GLOBAL IMPORTANCE MEASURES

In the literature several IMs are available that act on the point estimate of the output, with the parameters fixed at a nominal value (Borgonovo and Apostolakis, 2000; Saltelli, 1999; Cheok, Parry and Sherry, 1998; Turany and Rabitz, 2000). These measures are generlly referred to as "local". However, a formal definition of Local Importance has not been given yet. We propose the following definition of local importance measure. Let s be the set of input parameters($x_1, x_2, \ldots, x_n$), in general a subset of $\Re$ or C.

Definition of local importance measure: {I: s$\rightarrow\Re$} is a Local Importance Measure if it is an operator $I(x_i)\hat{}[F]$ on the function F(x_1,x_2,…,x_n), $\{F(\underline{x}): \Re^n \rightarrow \Re^n\}$, such that it associates to the set s (the parameters x_I) a set of real numbers I(x_i) (the importance of the parameters with respect to F).

This definition can be generalized to lead to the definition of global importancemeasures as follows. If the parameters are characterized by uncertainty, each parameter is described by a distribution. Thus the parameter itself is a subset of $\Re$. We now indicate this subset as X_i. Let us denote with S the collection of these sets, that is the collection of all the parameter distributions. The following follows:

Definition of Global Importance Measure: {I: s$\rightarrow\Re$} is a Global Importance Measure, if it is an operator on the function F(x_1,x_2,…,x_n), $\{F(\underline{x}): \Re^n \rightarrow \Re^n\}$, such that it associates to the set S (the set of the parameter distributions) a set of real numbers I(X_i).

3. IMPORTANCE OF PARAMETER GROUPS: ADDITIVITY PROPERTY

In many applications, the analyst is interested in the importance of a group of parameters, that we denote as: $I(x_1 \cup x_2, \ldots, \cup x_n)$. We say that an importance measure is additive if:

$$I(x_1 \cup x_2, \ldots, \cup x_n) = \sum_{j=1}^{n} I(x_j) \tag{1}$$

This property is useful from a computational point of view, since no further evaluation of the model is necessary to get the importance of any combination of model parameters, once the individual importance has been found.

4. DIM AND NORMALIZED PARTIAL DERIVATIVE (NPD) MEASURES

The definition of DIM is as follows:

$$\mathrm{DIM}(x_i) \equiv \frac{dF_{x_i}}{dF} = \lim_{\delta x \to 0} \frac{\delta F_{x_i}}{\delta F} = \frac{\frac{\partial F}{\partial x_i} \cdot dx_i}{\sum_{j=1}^{n} \frac{\partial F}{\partial x_j} \cdot dx_j} \tag{2}$$

where: dF_{xi} is the contribution to the F total differential of parameter x_i, dF: total differential of F.

It easy to see that DIM is additive (Borgonovo and Apostolakis, 2000), i.e.:

$$DIM(x_1 \cup x_2 \cup \ldots \cup x_n) = DIM(x_i) + DIM(x_j) + \ldots + DIM(x_k) \tag{3}$$

Local Importance Measures based on partial derivatives are defined as follows (Saltelli, 1999; Helton, 1993):

$$\mathrm{PDI}(x_i) = \frac{\partial F}{\partial x_i} \cdot \frac{x_i}{F_0} \tag{4}$$

where: $PDI(x_i)$= partial derivative importance of parameter x_i, F_0 = F base case value, x_i = base case value of parameter x_i. The rationale behing PDI is the following normalization of the differntial (Helton, 1993):

$$\frac{F - F_0}{F_0} \cong \sum_j \frac{\partial F}{\partial x_j} \cdot \frac{x_0}{F_0} \frac{(x - x_0)}{x_0} = \sum_j PDI(x_0) \cdot \frac{(x - x_0)}{x_0} \tag{5}$$

The right hand side represents the percentage of variation of the output due to a small change in the input, while the terms in the summation in the left hand side contains the percentage of variation of the input $(x\text{-}x_0 / x_0)$ multiplied by a weighting factor. For each individual parameter, solving the following equations:

$$\frac{F_{x_i} - F_0}{F_0} = \frac{\partial F}{\partial x_i} \cdot \frac{x_{i0}}{F_0} \cdot \frac{(x - x_{i0})}{x_{i0}} = \alpha_{x_i} \frac{(x_i - x_{i0})}{x_{i0}} \tag{6}$$

the coefficients or weighting factors can be defined and taken as the importance of the contribution of parameter x_i to the total variation of y, as stated in (5).

It is possible to see (Borgonovo and Apostolakis, 2000), that for individual parameters, under the hypothesis: $\frac{dx_k}{x_k} = \frac{dx_j}{x_j} = const$, DIM($x_i$) and PDI($x_i$) are related as follows (Borgonovo and Apostolakis, 2000):

$$DIM(x_i) = \frac{PDI(x_i)}{\sum_j PDI(x_j)} \tag{7}$$

In the next Section, we show that this relation cannot hold for multipe parameters, since NPDs cannot be defined for multiple parameters.

5. GROUP IMPORTANCE THROUGH NPD MEASURES

We now show that it is not possible to use NPD measures to compute the importance of parameter groups. In fact, as we have seen in eqs. (4),(5) and (6), the logic for the definition of PDI(x_i) is a normalisation of the partial derivatives and leads to coefficients independent of the parameter variations. Suppose we want the local importance of a group of parameters, x_I, x_j and x_k. Using the partial derivatives logic, we have to extract the coefficient from the following equation:

$$\frac{F_{x_i} - F_0}{F_0} = \frac{\partial F}{\partial x_j} \cdot \frac{x_{j0}}{F_0} \cdot (x_i - x_{i0}) + ... + \frac{\partial F}{\partial x_j} \cdot \frac{x_{j0}}{F_0} \cdot (x_j - x_{j0}) + \frac{\partial F}{\partial x_k} \cdot \frac{x_{k0}}{F_0} \cdot (x_k - x_{k0})$$

$$= PDI(x_j \cup x_k \cup ... \cup x_k) \cdot [(x_i - x_{i0}) + (x_j - x_{j0}) + \cdot (x_k - x_{k0})] \tag{8}$$

It is easy to see that this and anlogous multiple parameter equations canot be solved for coefficients independent of the parameter variations, as in eq. (5). Thus eq. (5) cannot be generalized to the importance of parameter groups. Furthermore, eq. (7) cannot hold for multiple parameters.

6. CONCLUSIONS

In this paper, we have presented a general defintion of local and global importance measures, that sets importance measures as operators among abstract spaces and enables to formally define the additivity property for importance measures. We have, then, focused on local importance measures, and we have seen that the importance of multiple parameters cannot be found using a the normalization of partial derivatives. The underlying reason is that, when considering the output variation, the relative way parameters are varied is relevant. Normalized partial derivatives alone are not able to take this into account. If we shift the focus from the partial derivatives to the differential as in eq.(2), the way parameters are varied will be automatically accounted for. Furthremore, since the differential is linear in the terms of the individual parameters, the importance of a set of parameters will always be the sum of the importance of the individual parameters, computed under any assumption on the parameter variations, as eq.(3) states.

7. REFERENCES

Borgonovo E. and Apostolakis G.E.: “A New Importance Measure for Risk-Informed Decision Making,” Reliability Engineering and System Safety, accepted for publication, November 2000.

Cheok M.C., Parry G.W., and Sherry, R.R., 1998: “Use of Importance Measures in Risk-Informed Regulatory Applications,” Reliability Engineering and System Safety, 60, 213-226.

Helton J.C., 1993: “Uncertainty and Sensitivity Analysis Techniques for Use in Performance Assessment for Radioactive Waste Disposal”, Reliability Engineering and System Safety, 42, 327-367.

Saltelli A., 1999: "Sensitivity Analysis: Could Better Methods be Used?," Journal of Geophysical Research, 104, 3789-3793.

Turanyi T. and Rabitz H., 2000: “Local Methods,” in: Sensitivity Analysis, Editors: Saltelli A., Chan K., and Scott E.M., John Wiley&Sons, Chichester, United Kingdom.

SENSITIVITY ANALYSIS AND IDENTIFIABILITY FOR DIFFERENTIAL EQUATION MODELS

H P Wynn and N Parkin

Department of Statistics, University of Warwick,
Coventry, CV4 7AL, England
Email: Hpw@stats.warwick.ac.uk, N.Parkin@warwick.ac.uk

1. INTRODUCTION

When using classical optimization techniques to estimate the parameters of dynamic models, the sensitivities of the model, namely the rates of change of the model responses with respect to parameters, play a central role. They are often used at each step of the parameter estimation process to compute the gradient of the objective function in Newton type optimizers. At the final stage of the estimation process they can be used to calculate the Fisher information matrix, and then, for example, to construct confidence regions for the parameters.

We give a brief summary of one method for calculating sensitivities. The method discussed is an efficient and reliable procedure for calculating model sensitivities together with the model solution. In the remainder of the paper we are concerned with system identifiability - in particular with local identifiability [8]. A minimum requirement for successful estimation of the parameters of a model is that the model be identifiable. Differential algebra methods can be used to check the identifiability of linear and non-linear dynamic models [6]. We consider statistical identifiability and the connection with differential algebra methods, via the model sensitivities and information matrix. In section three we present a theorem stating the equivalence of these two versions of identifiability.

2. DEFINITIONS AND DISCUSSION

2.1. Model and Sensitivities

2.1.1. Definition

For a system of ordinary differential equations,

$$\frac{\partial x}{\partial t} = g(x,\theta,t), \quad x(t_0) = x_0(\theta), \tag{2.1}$$

where , $x = (x_1,...,x_n)^T$ *and* $\theta = (\theta_1,...,\theta_p)^T$, *the* sensitivity, z_{ij} , *of the response* x_i *with respect to* θ_j *is,*

$$z_{ij} = \frac{\partial x_i}{\partial \theta_j}, \quad z_{ij}(t_0) = \frac{\partial x_{0i}}{\partial \theta_j}, \quad i = 1,...,n \quad j = 1,...,p$$

and the sensitivity matrix , Z , *is* (z_{ij}).

2.1.2. Computing Sensitivities

When equation (2.1) is not integrable we must resort to numerical methods to calculate the sensitivities. One class of such numerical procedures are known as direct methods, and are outlined below.

First differentiate the i^{th} equation from (2.1) with respect to θ_j, to give,

$$\frac{\partial}{\partial \theta_j}\frac{\partial x_i}{\partial t} = \sum_{k=1}^{n}\frac{\partial g_i}{\partial x_k}\frac{\partial x_k}{\partial \theta_j} + \frac{\partial g_i}{\partial \theta_j}, \tag{2.2}$$

then write $J_x = \left(\partial g_i \big/ \partial x_k\right)$, and $J_\theta = \left(\partial g_i \big/ \partial \theta_k\right)$ for the Jacobian matrices. Assuming the order of differentiation can be reversed, collecting together the n equations (2.2) gives,

$$\frac{\partial Z}{\partial t} = J_x Z + J_\theta, \quad Z(t_0) = \frac{\partial x_0}{\partial \theta}. \tag{2.3}$$

These equations are called the sensitivity equations. Note that they are linear whatever form g takes. All versions of the direct method bring together systems (2.1) with (2.3) and solve the combined equations numerically. The linearity of (2.3) and its close relationship to (2.1) means that very efficient numerical methods can be developed for the joint system. See [1], [2], [3], [5].

2.2. Local and Statistical Identifiability

2.2.1. Statistical Model

If we are observing a physical process for which we assume a model of the kind given in (2.1), then of course the model predictions will not agree perfectly with our observations. The deviations can be incorporated in a number of ways, one method is to regard the deviations as measurement errors, in the simplest case these would be distributed normally, independent, and added to the model solution. Thus, our model is,

$$x = G(\theta, t) + \varepsilon(t), \tag{2.4}$$

where $\varepsilon(t)$ are independent random variables $\varepsilon(t) \sim N(0, \sigma^2 I)$, and G represents the time integral of g in (2.1).

2.2.2. Fisher Information and Statistical Identifiability

For the model (2.4) the Fisher information matrix, I_f, for the parameters θ is calculated using the sensitivity matrices at each time point, t_i ,

$$I_f = \Sigma_m^T \Sigma_m,$$

where

$$\Sigma_m = \left(Z(t_1)^T \quad Z(t_2)^T \quad ... \quad Z(t_m)^T\right)^T.$$

We say that the model is statistically identifiable at θ if $\left|I_f\right| \neq 0$ for some $m = 1,2,....$

Of course, it may happen by accident that for our chosen $t_1,...,t_m$, the information matrix is singular. A more precise statement of our meaning is this :

if we are able to find a set of q time points $t, t+\delta t, ..., t+(q-1)\delta t$ 'close' to some time $t \in (t_0, \infty)$ such that the square matrix

$$\Sigma = \begin{pmatrix} Z(t) \\ Z(t+\delta t) \\ \vdots \\ Z(t+(q-1)\delta t \end{pmatrix}$$

is non-singular then the model is statistically identifiable at θ. Note that we have assumed for the sake of simplicity that $p = qn$ for $q \in N$.

2.2.3. Local Identifiability and Differential Information

Alternatively we may say, roughly speaking, that the model is locally identifiable at θ if and only if, when we are able to observe without error the process x, and its time derivatives d_i where $d_i = \partial^i x / \partial t^i$ the transformation

$$X = G(t, \theta), \tag{2.5}$$

is invertable for some $t \in (t_0, \infty)$, where

$$X = \left(x^T \quad d_1^T \quad ... \quad d_{q-1}^T\right)^T,$$

so that $\theta = H(t, X)$. That (2.5) is invertable implies that the Jacobian

$$G_\theta = \frac{\partial X}{\partial \theta}$$

is non-singular. This is the matrix of differential sensitivities,

$$G_\theta(t) = \begin{pmatrix} Z(t) \\ Z'(t) \\ \vdots \\ Z^{(q-1)}(t) \end{pmatrix},$$

and $G_\theta^T(t) G_\theta(t)$, the differential information, measures the amount of information in the model output at time t. In the next section we present a theorem which states that these two types of identifiability are equivalent.

3. EQUIVALENCE THEOREM

For the system defined by,

$$\frac{\partial x}{\partial t} = g(x,\theta,t), \quad x(t_0) = x_0(\theta),$$

where , $x = (x_1,...,x_n)^T$, $\theta = (\theta_1,...,\theta_p)^T$, and $p = qn$ for $q \in N$. Let

$$I_f = \Sigma^T\Sigma, \text{ where } \Sigma = \begin{pmatrix} Z(t) \\ Z(t+\delta t) \\ \vdots \\ Z(t+(q-1)\delta t) \end{pmatrix},$$

for some $\delta t > 0$ and $t \in (t_0,\infty)$. Furthermore let the terms

$$\frac{\partial g_i}{\partial \theta_j}(t,\theta),$$

be q times continuously differentiable in $[t, t+(q-1)\delta t]$. Then the model is locally identifiable at θ if and only if

$$\frac{|\Sigma(t)|}{\delta t^{nq(q-1)/2}} \to d > 0 \text{ as } \delta t \to 0 .$$

A sketch proof of theorem will be presented.

The proof of this theorem is easily modified for the case when the number of parameters is not a multiple of the number of equations.

4. REFERENCES

[1] M Caracotsios and W E Stewart. Sensitivity Analysis of Initial Value Problems With Mixed ODEs and Algebraic Equations. *Computers and Chemical Engineering*, 9(4):359-365, 1985.

[2] R P Dickinson and R J Gelinas. Sensitivity Analysis of Ordinary Differential Equation Systems – a Direct Method. *Journal of Computational Physics*, 21:123-143, 1976.

[3] W F Feehery, J E Tolsma, and P I Barton. Efficient Sensitivity Analysis of Large Scale Differential Algebraic Systems. *Applied Numerical Mathematics*, 25:41-54, 1997.

[4] K R Godfrey. *Compartmental Models and their Applications.* Academic Press, New York and London, 1983.

[5] T Maly and L R Petzold. Numerical Methods and Software for Sensitivity Analysis of Differential Algebraic Equations. *Applied Numerical Mathematics*, 20:57-79, 1996.

[6] G Margaria. *Applications of Differential Algebra to Structural Identifiability of Non-Linear Systems.* PhD Thesis, Politecnico di Torino, 2000.

[7] H Pohjanpalo. System Identifiability Based on the Power Series Expansion of the Solution. *Mathematical Bioscience*, 41:21-33, 1978.

[8] E Walter and L Pronzato. *Identification of Parametric Models from Experimental Data.* Communications and Control Engineering. Springer, 1997.

HYDROCODE SENSITIVITIES BY MEANS OF AUTOMATIC DIFFERENTIATION

Rudy Henninger[(1)], Paul Maudlin[(1)] and Alan Carle[(2)]

[1] Los Alamos National Laboratory
Los Alamos, NM 87545 (USA)
Email: rjh@lanl.gov

[2] Rice University
Houston, TX 77005 (USA)

1. INTRODUCTION

The purpose of this project has been to provide sensitivities of results from an Eulerian hydrodynamics computer code (hydrocode) [1] for use in design-optimization and uncertainty analyses. We began [2] by applying an equation-based sensitivity technique used successfully in the early eighties that was applied to reactor-safety thermal-hydraulics problems [3,4], which is called Differential Sensitivity Theory (DST) [5,6]. The methodology is as follows: the system of partial differential equations (the forward or physical PDEs) is assembled, and differentiated with respect to the model parameters of interest; the adjoint equations are then determined using the inner-product rules of Hilbert spaces [5]; and finally, the resulting adjoint PDEs are solved using straightforward numerical operators. The forward-variable solutions when needed for the adjoint solutions are provided by the original computer code that solves the physical (or forward) problem. In the present hydrocode application, acceptable results were obtained for one-material, one-dimensional problems. The DST results were then improved by means of "compatible" finite difference operators [6,7]. We have seen, however, that DST techniques do not produce accurate values for sensitivities to all of the parameters of interest and for problems with discontinuities such as a multi-material problem [8]. To obtain accurate sensitivities for arbitrary numerical resolution a more code-based approach was then tried. We attempted to apply automatic differentiation (AD) in the forward mode using Automatic DIfferentiation of FORtran (ADIFOR, version 2.0) [9] and the Tangent-linear and Adjoint Model Compiler (TAMC) [10] in the forward and adjoint modes. We were successful for one-dimensional problems in both modes but failed to obtain accurate sensitivities in the adjoint mode for two-dimensional problems [11].

Here we present the successful results for two-dimensional problems in both the forward and adjoint modes using ADIFOR, version 3.0 [12]. In what follows, we describe AD methods in the context of their use for a hydrocode. We then examine setup time, results, accuracy, and computer run times for three test problems obtained by ADIFOR. Finally, we outline our plans for future work.

2. AUTOMATIC DIFFERENTIATION METHODS FOR A HYDROCODE

Both code- and equation-based methods can be implemented in either the forward or adjoint mode. By forward and adjoint, we mean the direction through the solution and in time and space in which the derivative values are obtained. The forward mode is more efficient for determining the sensitivity of many responses to one or a few parameters,

while the adjoint mode is better suited for sensitivities of one or a few responses with respect to many parameters. The most recent version of ADIFOR [12] that is used here is applied in both the forward and adjoint modes.

AD tools require several steps to get from the original code to an executable code with derivative coding included. A precompiler first analyzes the code and modifies it to include code that calculates the derivatives of interest. For a non-linear hydrocode, information from the forward calculation is needed in the adjoint calculation. Independent storage or recalculation can provide this information. The second step in the process is to determine and set up the required storage. For a large problem a technique called checkpointing is required. This technique consists of dumping the solution at checkpoints as the forward solution is generated. The forward solution is stored from the final checkpoint to the final time of the forward calculation. One then calculates the adjoint solution backward from the final state. The forward solution is then calculated from the second to the last checkpoint. This process is repeated until the starting time of the forward calculation is reached. The last step is to compile the enhanced code, auxiliary storage code, and the adjoint code, including run-time libraries that satisfy the external subroutine calls.

3. PROBLEM DESCRIPTIONS AND RESULTS

Setup time, accuracy, and run times are described for three problems. The problem test set consists of a one-dimensional shock-propagation problem, a two-dimensional metal-jet-formation problem, and a two-dimensional shell-collapse problem. The physical situations for the problems are depicted in Figure 1.

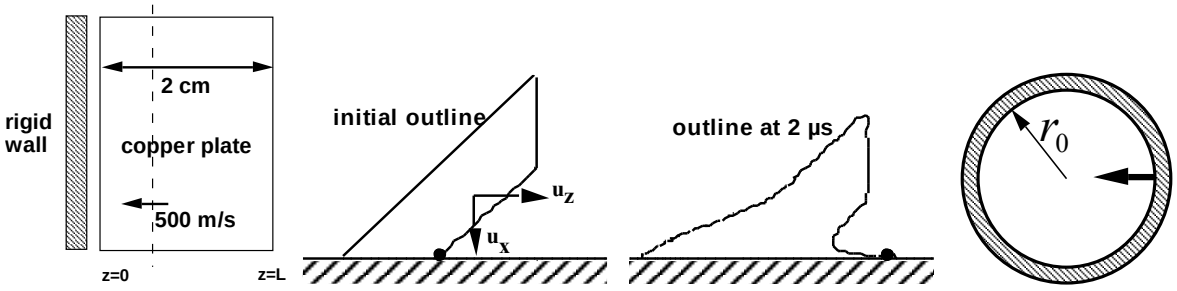

1a. 1b. 1c.

Figure 1. Test problems: 1D shock; jet-formation; and shell collapse.

To compare the computational times on an equal footing all of the problems had 17 parameters and one response. The model parameters were 4 initial conditions, 3 equation-of-state parameters, 2 artificial-viscosity parameters, 5 boundary conditions, and 2 material-strength parameters. Setup time for ADIFOR was approximately two man-months starting from a simplified fixed-dimension version of the original code. Creation of the simplified code and getting it running on an SGI platform represents several months of work. Run times for the problems are compared below in Table 1.

3.1. One-Dimensional Shock Problem

The first test problem is the one-dimensional impact of a copper plate with a rigid boundary where the plate has an initial velocity 500 m/s as indicated in Fig. 1a. Upon impact the plate experiences a right-going shock. The impact problem was simulated to a

final time of 2.0 μs. The response for the problem was arbitrarily chosen to be the time-averaged density a distance of 0.6 cm from the rigid wall.

3.2. Jet-Formation Problem

The second test problem is a two-dimensional jet-formation problem in which a copper bar impacts a rigid boundary as is shown in Figure 1b. The bar has an initial axial velocity ($u_z(t=0)$) of 100 m/s and was run with three transverse velocities ($u_x(t=0)$): 0.0; 100; and 700 m/s, respectively. For the non-zero transverse velocities a jet is formed that flows along the axis as in Figure 1b. The response of interest is the final speed of a marker particle that is placed on axis at the right side of the copper bar (shown as a black dot in Figure 1b). The problem was run to a final time of 1 μs. The sensitivity of the final speed to the initial axial velocity is 1.000 for the zero transverse-velocity case. This seemingly trivial result provided an excellent test of the advection-scheme adjoint code. When 1.000 was obtained for the adjoint initial-velocity sensitivity, the other sensitivities agreed well with the forward results obtained by ADIFOR (which is viewed as the "correct" solution) and by finite differences. The sensitivities produced by the adjoint code for 100 m/s also agreed well with those of the forward code and finite differences. It was not possible to produce reasonable sensitivities for times greater than 0.8 μs by any method for the 700 m/s transverse velocity case. Examination of the computed results for this case showed that the sensitivity was proportional to the marker particle acceleration, which became unstable after 0.8 μs. A different response choice (other than following a marker particle) will be necessary to obtain a numerically smoother characterization of the jet tip speed and stable sensitivities. We intend to explore this issue in future work.

3.3. Shell-Collapse Problem

The third test problem is a free-running shell collapse. In this problem, a spherical shell of elasto-plastic material is given an initial velocity toward its center (Figure 1c). During the collapse, the shell thickens, and the kinetic energy is irreversibly converted to internal energy. Under the appropriate initial conditions, the shell will stop at a finite inner radius r_0' when all of its kinetic energy has been dissipated. We chose r_0' as the response. Verney [13] has provided the analytical solution for the plastic work done during the collapse of the shell from r_0 to r_0'. By equating the plastic work to the initial kinetic energy, an initial velocity distribution may be determined that is consistent with a specified final inner radius. The initial shell radius is 8 cm and its thickness is 2 cm. For a final inner radius r_0' of 3 cm, the initial inner-radius velocity is 670 m/s. Using this velocity, the fully collapsed (>99 % kinetic energy converted) inner radius was calculated to be approximately 3 cm, which is in good agreement with the analytical result. For the analytical solution the only parameter that matters is the yield strength. The yield strength is also the parameter with the largest sensitivity.

3.4. Accuracy and Timing Comparisons

ADIFOR-processed code provided accurate (as compared to finite difference) parameter sensitivities in both the forward and adjoint modes for all of the problems. The run times for the various methods used to obtain the test problem sensitivities are listed in Table 1. These test problems had 17 model parameters and one response. We find that the ADIFOR forward mode is up to 39% slower and the ADIFOR adjoint mode is at least 11% faster

than finding the gradient by means of finite differences. Problems of real interest will certainly have more parameters. The adjoint mode is thus favored since the computational time increases only slightly for additional parameters.

Table 1. Comparison of computational times on an SGI Origin 2000 for test problems with 17 model parameters and one response.

Problem	**1D Shock**	**Jet**	**Shell**
Problem Information			
Cells in 2D	3 X 40	60 X 100	42 X 42
Time steps	400	100	1000
Run Times CPU seconds			
Finite Difference	36	126	347
ADIFOR-Forward	15	146	484
ADIFOR-Adjoint	12	63	309

4. SUMMARY AND FUTURE WORK

We have applied the automatic differentiation tool ADIFOR (version 3.0) to MESA2D (a Fortran77 code) and have obtained accurate sensitivities for three test problems in both the forward and adjoint modes. We will apply this capability to experimental data assimilation and result uncertainty analysis with this code. We will then extend the capability to parallel hydrocodes written in languages other than Fortan77.

5. REFERENCES

1. D. J. Cagliostro, D. A. Mandell, L. A. Schwalbe, T. F. Adams, and E. J. Chapyak, "MESA 3-D Calculations of Armor Penetration by Projectiles with Combined Obliquity and Yaw," *Int. J. Impact Engineering*, **10**, (1990).

2. P. J. Maudlin, R. J. Henninger, and E. N. Harstad, "Application of Differential Sensitivity Theory to Continuum Mechanics," Proc. ASME Winter Annual Meeting, 93, New Orleans, Louisiana (November 28-December 3, 1993).

3. P. J. Maudlin, C. V. Parks and C. F. Weber, "Thermal-Hydraulic Differential Sensitivity Theory," ASME paper No. 80-WA/HT-56, Proc. ASME Annual Winter Conference (1980).

4. C. V. Parks and P. J. Maudlin, "Application of Differential Sensitivity Theory to a Neutronic/Thermal Hydraulic Reactor Safety Code," *Nucl. Technol*., **54**, 38 (1981).

5. D. G. Cacuci, C. F. Weber, E. M. Oblow and J. H. Marable, "Sensitivity Theory for General Systems of Nonlinear Equations," *Nucl. Sci. Eng.*, **75**, 88 (1980).

6. R. Henninger, P. Maudlin, and M. L. Rightley, "Accuracy of Differential Sensitivity for One-Dimensional Shock Problems," LA-UR-97-596, 1997 APS Shock Compression of Condensed Matter Conference, pages 187-190, Amherst, MA (27 July -1 August 1997).

7. M. Shashkov, *Conservative Finite Difference Methods on General Grids*, CRC Press, Boca Raton (1996).

8. R. J. Henninger, P. J. Maudlin, and E. N. Harstad, "Differential Sensitivity Theory Applied to the MESA2D Code for Multi-Material Problems," Proceedings of the APS Meeting on Shock Compression of Condensed Matter, pages 283-286, Seattle, WA, (August 1995).

9. C. Bischof, A. Carle, P. Khademi, and A. Mauer, "The ADIFOR 2.0 System for the Automatic Differentiation of Fortran 77 Programs,"Argonne National Laboratory Report ANL-MCS-P481-1194 (1995).

10. R. Giering, "Tangent Linear and Adjoint Model Compiler Users Manual," Manual Version 1.1, TAMC Version 4.76, 1997.

11. R. J. Henninger, M. L. Rightley, and P. J. Maudlin, "Code Differentiation for Hydrodynamic Model Optimization," Shock Compression of Condensed Matter – 1999, Proceedings of the Conference of the American Physical Society, Topical Group on Shock Compression of Condensed Matter, LA-UR-99-3075, pages 359-362, Snowbird, UT (27 June – 2 July 1999).

12. – "ADIFOR 3.0 Overview", Rice University Technical Report CAAM-TR-00-02 (February 2000).

13. D. Verney, “Evaluation de la Limite Elastique et Cuivre et de l’Uranium par des Experiences d’Implosion «Lente»,” *Behavior of Dense Media under Dynamic Pressures*, Symposium H. D. P., International Union of Theoretical and Applied Mechanics, page 293, Gordon and Breach, New York (1968).

A FRAMEWORK FOR COMPUTER MODEL VALIDATION WITH A STOCHASTIC TRAFFIC MICROSIMULATOR AS TEST-BED

Jerome Sacks[(1)] *, Nagui M. Rouphail*[(2)] *B. Brian Park*[(3)]

[(1)]National Institute of Statistical Sciences
Research Triangle Park, NC
Email: sacks@niss.org

[(2)]North Carolina State University
Raleigh, NC
Email: rouphail@eos.ncsu.edu

[(3)]University of Virginia
Charlottesville, VA
Email: bpark@virginia.edu

1. INTRODUCTION

The validation of computer (simulation) models is a crucial element in assessing their utility for science and for policy-making. Often discussed and sometimes practiced informally, the process is straightforward conceptually: data are collected that represent both the inputs and the outputs of the model, the model is run at those inputs, and the output is compared to field data. In reality, complications abound: field data may be expensive, scarce or noisy, the model may be so complex that only a few runs are possible, and uncertainty enters the process at every turn. Even though it is inherently a statistical issue, model validation lacks a unifying statistical framework.

The need to develop such a framework is compelling, even urgent. The use of computer models by scientists and planners is growing; costs of poor decisions are escalating; and increasing computing power, for both computation and data collection, is magnifying the scale of the issues.

Building a framework for validation of computer models requires an assortment of procedures and considerations and recognition of the multiple stages in the development and use of the models. *Verification*, which encompasses procedures to assure that the computer code is bug-free, is often seen as a predecessor of validation whereas, in fact, it may be enmeshed with validation. *Feedback* from outcomes of steps in the validation process can impact model development through detection of flaws or gaps – the result is an intertwining of validation with development.

We will focus on (the) five essential characteristics of a validation*: context, data, uncertainty, feedback, and prediction* and use a traffic microsimulator model applied to the planning of traffic signal timing as a test-bed. Our goal is to draw attention to the many complexities that need to be considered in order to achieve a successful validation.

Figure 1: Network (Chicago, IL)

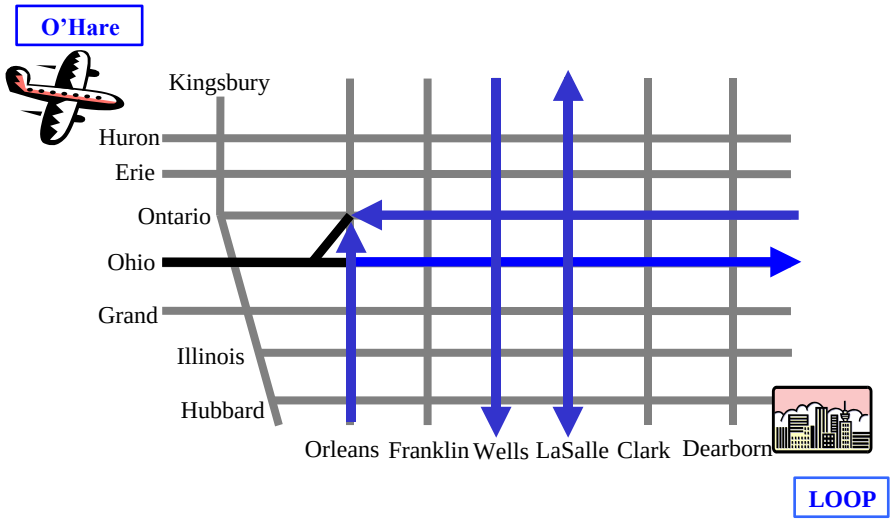

2. THE TEST-BED

The test-bed is the traffic simulation model, CORSIM ([3]); a model in prominent use by transportation engineers in the United States, especially for traffic operations. CORSIM is a stochastic simulator that moves vehicles second by second through a network. The urban street network in Figure 1 is an important one adjacent to the central business district in the city of Chicago.

Specification of the network includes a set of fixed inputs describing the geometry (e.g., distance between intersections, number of traffic lanes, length of turn pockets), the placement of stop signs, bus stops and routes, and parking conditions. At each entry node of the network vehicles (autos, trucks, and buses) are generated through the sampling of interarrival time distributions. The interarrival time distributions are assumed to be independent (vehicle-to-vehicle, node-to-node), different for each entry node. CORSIM allows gamma densities

$$p(t \mid \lambda, k) = \frac{(\lambda k)^k}{(k-1)!} t^{k-1} \exp(-k\lambda t)$$

we take k=1 for all nodes. The parameter λ (different at each node) must be estimated. The designation of vehicle type—auto or truck—is made through independent Bernoulli trials with a fixed probability. Buses are treated according to their schedule and routes, with random dwell times at bus stops and random interarrival times at entry nodes.

Behaviour of the traffic is affected by other random factors such as turn probabilities, p, which will differ from link to link. Driver characteristics (car-following parameters, left-turn "jumpers", acceptable gaps between vehicles, lane-changing maneuvers) are a set of random factors with discrete distributions on 10 points. These distributions are very difficult to measure in the field but can be specified by use of defaults provided in CORSIM or used as tuning parameters.

Signal settings must also be specified. They consist of

- cycle length
- green times at each intersection—how long the signal is green for straight through movement and how long for protected left turns, where present
- offsets—the difference in time between the start of the "green" through-movement at a signal and the time of the start of the green through-movement at a reference signal.

The approach to improve existing signal-timing plans on the network of Figure 1 begins with collection of data to provide the necessary inputs to run CORSIM. The computer model is then to be used to find an optimum (or, at least, an improved) signal timing plan which could be implemented in the field. To convince the Chicago Department of Transportation to put the new plan in effect, three questions must be answered:

- Does CORSIM reliably reflect reality under existing conditions?
- Can the current signal plan be improved (as measured in CORSIM)?
- Can CORSIM be trusted to reflect reality under untried conditions?

The first and third questions are at the heart of the validation process. The second question, of course, must be answered affirmatively before signal settings are changed.

3. VALIDATION ACTIVITIES

The validation framework includes a list of activities, dynamic because some may be repeated as conditions are updated. Explicit carrying out of the activities may be very complicated and require substantial subject-matter knowledge and development of methodology.

The activities are readily categorized as

- Specification of inputs and related uncertainties
- Specification of evaluation criteria
- Data collection
- Parameter estimation, calibration and tuning
- Analysis
- Prediction
- Interpretation

3.1. Specification of Input/Uncertainties

Table 1 lists, for the test-bed, inputs and some comments on the (initial) uncertainties to be attached to them. The geometry of the street network (lanes of traffic, left-turn lanes, signals, stop signs, bus stops, etc.) is a critical detail. Detecting errors in transcription or identification of specific elements of the geometry may not always be obvious. For example, entering a stop sign where one is absent may go undetected unless doing so causes extreme conditions such as "spillback" or gridlock which may be detected during runs of the model.

INPUT		UNCERTAINTY	COMMENT
GEOMETRY		Adjusted to reality after observation	dependence on data
SIGNALS	cycle	fixed at 75 seconds	
	green time	----------	to be optimized
	offsets	----------	to be optimized
DEMAND – arrival rates		independent exponentials	Estimates from counts; Bayes estimates
TURNING MOVEMENTS		independent multinomials	" " " "
DRIVER BEHAVIOR aggressiveness, etc		10 pt distributions	default; tunable
FREE FLOW SPEED		speed limit	tunable

Table 1. Inputs

3.2. Evaluation Criteria

Evaluation criteria require

- Specification of an evaluation function (or functions) defined on model output.
- Specification of the domain of input variables over which evaluation is sought.

These specifications are context-driven. The need to compare model output with real data constrains the choices of evaluation functions to ones that have both model and field counterparts that can be feasibly calculated. Evaluation quantities that are feasibly calculated from field data and available as model output are *throughput*, *stop time*, *queue length* for individual links for each signal cycle. Stop-time per stopped vehicle (STVS) on specified links over a one-hour period was selected as the evaluation function. The definition: Fix the link; fix the cycle. Compute the stop-time for each vehicle in the link during the cycle. Aggregate the stop-time for all such vehicles and count the number of such vehicles with positive stop-time. Accumulate both quantities over all 48 cycles (3600/75) in the one-hour period and divide to get STVS for the link

3.3. Data Collection

For our test-bed example field data were collected initially on a single day (Thursday, May 25, 2000). Processing of the data and analyses were limited to the rush-hour periods, 8am-9am and 5pm-6pm. Traffic volume data were collected manually (by observers counting vehicles) and, on an interior twelve intersections, by video (camera) recording of traffic. The video data are highly reliable and costly; the manual data are notoriously unreliable.

These data were used to estimate key parameters for the inputs to CORSIM (see 3.4 below). With such inputs and other specifications CORSIM runs were made and output examined. CORSIM has an animation module that exhibits the motion of vehicles through the network. Visual comparison of the CORSIM animation with the video data turned out to be an essential tool in detecting anomalies of the model that ultimately fed back to adjustments of the inputs (see 3.5).

The data were used to answer the first two questions, leading to a new signal plan that was put into effect on September 26, 2000. New data, only from cameras, were collected on September 27, 2000 to assess the predictions made by the computer model (see 3.6).

3.4. Parameter Estimation, Calibration and Tuning

The parameters λ and p, as well as the vehicle mix, were directly estimated from the field data for each of the one-hour periods. λ, at an entry link, was estimated by the total number of vehicles entering the link/3600. At each intersection, the turn (left-turn, right-turn) probabilities, p, were estimated by proportions of vehicles making those turns. Vehicle mix was similarly estimated from counts at each entry link.

Some λ's were later (ad hoc) adjusted to reduce discrepancies between downstream counts generated by CORSIM and those observed by video – the discrepancies are believed to be due to inaccuracy of manual counts. The effect on uncertainty of these modifications and manual measurement errors is addressed in [1].

With these inputs CORSIM was run a number of times (different random seeds), output was collected and compared to field data. Several anomalies were observed. In particular, a key corridor (LaSalle Street in Figure 1) had far less STVS in CORSIM than in the field. This led to a visual examination and comparison of CORSIM animation with the video data, revealing the presence of illegally parked vehicles that had the effect of removing an entire traffic lane. The resulting revision to the geometry of the network was, of course, data dependent and affects uncertainty calculations, but in non-obvious ways. This calibration "fix" did not completely solve the problem: traffic in CORSIM still moved too smoothly and swiftly compared to the video data. By experimenting with the free-flow speed parameter and changing it to reflect the speed at which traffic did move on the LaSalle corridor we were able to better tune[2] the model. The feedback process was not simple – it required familiarity with the particular network and careful detective work to go from suspect numerical output to visualization and detection of the discrepancies.

3.5. Analysis

A first level comparison of CORSIM with reality is visual: comparing CORSIM animation with video. Defects, other than those noted in 3.4, were revealed that stemmed from CORSIM's difficulty in recovering from congestion created by a temporary spillback.

A more data analytic approach is to construct histograms of throughput and STVS (see 3.2) from a battery of 100 CORSIM runs. This reveals the inherent variability in CORSIM and allows a "test" of whether observed field values are consistent with the CORSIM distribution. In general there was reasonably close agreement. Additional comparisons were made between a time-series of a CORSIM run (selected as a median run among 100 independent runs) and the corresponding time-series from the field (Figure 2).

[2] Tuning is a phrase commonly associated with adjusting input parameters to match model output. In this instance, free-flow speed is a somewhat artificial parameter affecting the movement of vehicles in the model.

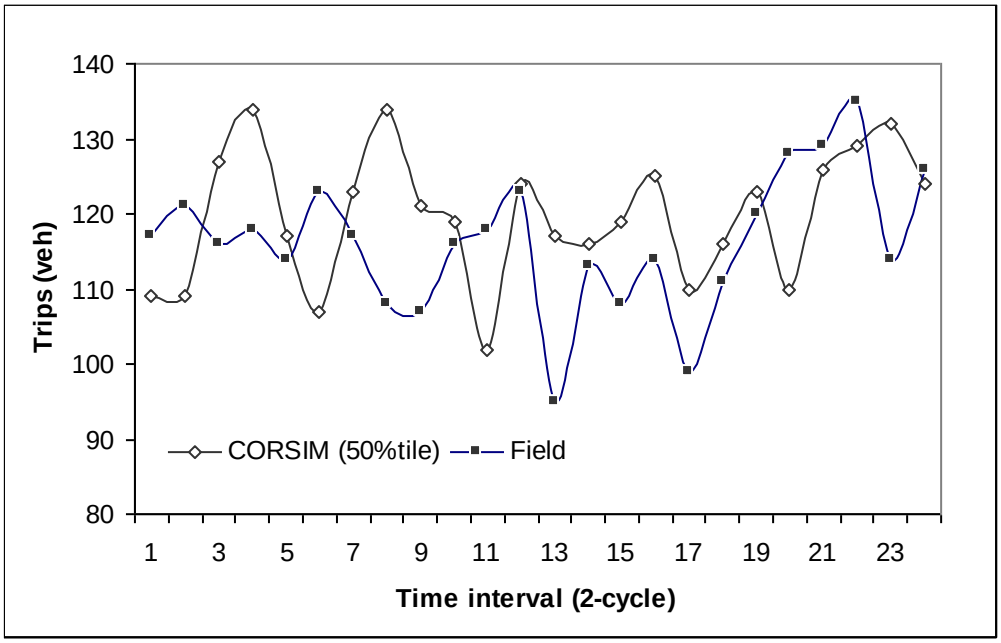

Figure 2. Comparison of CORSIM and Field Time Series

All of these comparisons are, of course, coloured by the use and reuse of the same data collected in May, 2000. Steps towards a more coherent analysis are in [1]. An indication of the effect of incorporating parameter uncertainty was observed by producing a ("Bayes") histogram from 200 runs of CORSIM with each run including a selection of λ and p from a prior distribution. This histogram was compared with that obtained from 200 runs with λ and p fixed at their estimates given in 3.4. The Bayes histogram showed greater variability and a 10% probability of extreme values, compared to a 2% "tail" in the second histogram. These extreme values correspond to serious congestion and even gridlock, conditions that do not occur on the network. The interpretation of this result and its effect on validity is unclear.

Optimization of the parameters of the signal plan is difficult because the number of parameters is large (over 50), the computer model is stochastic, and the dependence on the signal parameters, especially the offsets, is not smooth. A genetic algorithm was used but limited to optimizing over a corridor at a time. The objective function (not an evaluation function) was the system queue time (total amount of time vehicles spend either stopped or moving at very low speed). The current plan's queue time could be improved by about 8%, with enough improvement on key links to warrant implementation.

3.6. Prediction

The most compelling form of validation is through confirmation by predictions in new circumstances. In the test-bed example the new plan was put in place four months after the initial field data were collected. The predictions made for the new plan in September assumed that the conditions in the field in September were the same as in May, except for the signal settings. The predictions were then compared to the data collected in September by camera.

Only one discrepancy was large enough to cause further investigation. On one link (an entrance to a freeway at Orleans and Ohio) inspection of the video revealed that drivers were

effectively using 20 seconds of green time instead of the displayed 16 seconds. Implementing this change reduced the large discrepancy to a minor one.

An informative evaluation function of CORSIM is the change in CORSIM predictions, ΔCORSIM (September STVS - May STVS) compared to the corresponding change in the field values, ΔField. Even though the CORSIM predictions were not always accurate, the Δ's are close and of the same sign (Table 2). On one link there was degradation in performance both in the field and in CORSIM, a reflection of the failure to implement the proposed improved signal plan on all parts of the network – the new plan is the implemented one.

Table 2. Δ CORSIM vs. Δ Field

Link	ΔCORSIM	ΔReality
EB Ohio at LaSalle	0	3
SB LaSalle at Ohio	-11	-10
NB LaSalle at Ontario	-9	-5
NB Orleans to Freeway	13	15
NB Orleans at Ontario	1	-2

Δ = STVS[September] – STVS[May]

3.7. Interpretation and Conclusions

The details encountered in carrying out the validation activities are the essence of the validation process. The criticality of context cannot be overstated: it drives the formulation of evaluation, the collection of data and affects interpretations of uncertainty. Thus, in the test-bed some of the observed discrepancies between model and field are statistically significant (albeit, overstated by not taking account of estimation, measurement errors and tuning) but are of no practical significance. Engineering/scientific expertise is essential in detecting, circumventing and correcting flaws in the model. There are no convenient recipes for such "forensic" activity - suspicions may be aroused by numerical discrepancies but tracking the sources is typically through informal, ad hoc investigations assisted by expertise and, as in the test-bed, by visualization.

The model has flaws that cannot be fixed. It may have been possible to "hide" the flaws by tuning the model (especially through driver characteristics) but we refrained from that except for treating the free-flow speed parameter on one corridor. Despite the flaws, predictions for the new signal plan were reasonably close to reality and, strikingly, as seen in Table 2, changes were predicted correctly.

CORSIM predicts gridlock uncomfortably often. Levels of uncertainty must be assessed to determine how often (but see [1]). Our conclusion at this time is that CORSIM can be used for signal planning and the frequency of gridlock is unlikely to be large enough to be troublesome. This does imply, however, that the distribution of CORSIM outputs must be examined, lest a single run of CORSIM be misleading.

Open Questions

Collecting data for validation is most conveniently done simultaneously with data collection for inputs. The use of the same or closely related data for both input and validation is an issue that is rarely confronted. The conventional wisdom is that such dual-use of the data is "forbidden". In fact, it can be done but how to attach computable uncertainties, essential to producing fully reliable results, is not straightforward. An approach based on [2] holds promise for producing methodology to treat the issue.

The impact of data of inferior quality on the model has barely been studied. The problem is complicated by the need to specify the "brunt of the impact"; quantify scenarios of alternative collections of data; measure the consequences, or sensitivities, of model output to wrong data inputs including incorrect signal settings or drifts in signal timing.

4. REFERENCES

[1]. Berger, J., Bayarri, M.J., and Molina, G. (2001). Fast Simulators for Assessment and Propagation of Model Uncertainty (In these Proceedings).

[2] Bayarri, M. J., and J. O. Berger (1999). Quantifying surprise in the data and model verification. In Bayesian Statistics 6, 53-82. (J. M. Bernardo, J. O. Berger, A. P. Dawid and A. F. M. Smith, etds.). Oxford University Press, London.

[3] FHWA (1997). CORSIM User's Manual, U.S. Department of Transportation

APPLYING DIMENSIONAL AND SIMILARITY ANALYSES TO THE PROPAGATION OF UNCERTAINTIES: A PHYSICAL EXAMPLE

José Mira, Ricardo Bolado and Pablo Solana

E. T. S. de Ingenieros Industriales
c/ José Gutierrez Abascal, 2, 28006 Madrid (Spain)
E-mail: jmira@etsii.upm.es

ABSTRACT

Dimensional and similarity analyses are used in Physics and Engineering, specially in Fluid Mechanics, to reduce the dimension of the input variable space. Here, we apply these techniques to the Propagation of Uncertainties for Computer Codes in order to reduce the variance of the estimators of the parameters of the output variable distribution. We illustrate it with an application to a physical problem.

Keywords: Dimensional Analysis, Similarity Analysis, Propagation of Uncertainties, Simulation Codes.

1. INTRODUCTION

Since real experimentation is very expensive, with the introduction of faster and cheaper computers, computer code simulation has become an essential research tool of science and engineering. The relationship between input and output is very frequently expressed through functional equations (differential equations or finite difference equations).

Let us consider a system of functional equations where $Z_1,...,\ Z_n$ are the dependent or output variables and $X_1\ ,...,X_m$ are the independent variables (e.g., space coordinates and time). Let $Y_1\ ,...,\ Y_p$ be the parameters of the system, i.e., coefficients of the differential equations and of the initial and boundary conditions. The solutions to the system are $Z_j = I_j(X_1,...,\ X_m;\ Y_1,...,\ Y_p)$. Let us assume that some of the values of $Y_1,...,\ Y_p,\ X_1,...,\ X_m$ are not known precisely, i.e., there is uncertainty about their values, this uncertainty is described through a known probability distribution. This implies that $Z_1,...,\ Z_n$ become stochastic, and the problem arises of calculating their joint distribution for given values of the non-stochastic subset of $X_1,...,\ X_m$. In computer code simulation literature, this problem of transformation of variables in probability theory is often called *propagation of uncertainties or uncertainty analysis*. In general, the problem can not be solved analytically, so approximate methods are applied, preferably Monte Carlo, where variance reduction methods are applied to reduce computational costs. The most frequently used variance reduction methods are stratified sampling, importance sampling and Latin Hypercube Sampling (McKay, Conover and Beckman 1979).

In physics, one speaks of similarity between two problems when one can transform one problem into the other by a change of scale in the variables. It is shown that this is possible when a set of dimensionless numbers (in mathematical terms, we shall speak instead of invariant functions) which are functions of the parameters $Y_1,...,\ Y_p$ coincide in both problems.

A classical example is the Reynolds number in fluid mechanics. The dimension of the parameter space, originally *p*, can thus be reduced to the number of dimensionless quantities which define the system of functional equations as far as the parameters are concerned. This problem is referred to in the literature as dimensional analysis, and though in many physics and engineering works it is formulated in terms of physical magnitudes and dimensions, the authors prefer to deal with it using a more abstract, mathematical and hence physics independent language, such as in Moran (1971).

An a priori different problem is the reduction of the number of independent variables $X_1,...,$ X_m. For example, a partial differential equation can be thus reduced to an ordinary differential equation.

In this paper, we see how one can use the two dimension reduction problems mentioned above to increase the efficiency of variance reduction techniques in uncertainty analysis and we illustrate it with an example.

2. USING GENERALISED DIMENSIONAL ANALYSIS IN UNCERTAINTY ANALYSIS

Moran and Marshek (1972) have shown that the two problems of the reduction in the number of parameters through dimensional analysis and the reduction of the number of independent variables, can be formulated in terms of a more general framework called generalised dimensional analysis which includes both.

Moran and Marshek's generalised dimensional analysis consists in finding a set of linear transformations:

$$\begin{aligned} \overline{Z_j} &= A_1^{a_{j1}} ... A_r^{a_{jr}} Z_j \ (j = 1,..., n \geq 1) \\ \overline{X_k} &= A_1^{b_{k1}} ... A_r^{b_{kr}} X_k \ (k = 1,..., m \geq 1) \\ \overline{Y_e} &= A_1^{c_{e1}} ... A_r^{c_{er}} Y_e \ (e = 1,..., p \geq 1) \end{aligned} \tag{1}$$

where the a_{ji}, b_{kl} and c_{et} are exponents such that the system of functional equations is invariant under the transformations i.e., $Z_j = I_j(X_1,..., X_m; Y_1,..., Y_p)$ transforms to $\overline{Z_j} = I_j(\overline{X_1},..., \overline{X_m}; \overline{Y_1},..., \overline{Y_p})$. The system of functional equations can then be expressed in terms of $q=n+m+p-r$ invariant ("dimensionless" in the physics terminology) functions Π_j and π_k of the type $\pi = Z_1^{\alpha 1} ... Z_n^{\alpha n} X_1^{\beta 1} ... X_m^{\beta m} Y_1^{\gamma 1} ... Y_p^{\gamma p}$ instead of in terms of the original and larger set formed by $Z_1,..., Z_n; X_1,..., X_m; Y_1,..., Y_p$.

$$\Pi_j(Z_j; X_1,..., X_m; Y_1,..., Y_p) = F_j(\pi_1(X_1,..., X_m; Y_1,..., Y_p),..., \pi_\delta(...)) \tag{2}$$

where $\delta = m+p-r$, so, since there are now $m+p-r$ independent variables and parameters instead of the original $m+p$, there is a dimension reduction which can be used for a better analysis of the system of functional equations. The invariants π_i which are in general a function of the independent variables $X_1,..., X_m$ and the parameters $Y_1,..., Y_p$ can be built in such way that there is a reduction in either the number of parameters or in both the number of parameters and independent variables. The reduction of dimensionality can be of use for the problem of propagation of uncertainties formulated above because we avoid redundant sampling.

3. APPLICATION

We apply the ideas above to the problem of the release and transport of a radioactive contaminant in a porous medium. We shall use the results provided by Moran and Marshek (1972).

We assume that there is a nuclear waste repository with an initial mass of contaminant M_0. The quantity of contaminant in the repository decreases due to radioactive decay (at constant fractional rate λ) and release (at constant fractional rate k). The contaminant released from the repository gets into a porous medium through which it is transported to the biosphere. We assume that there is uncertainty about the actual pathway that the contaminant may follow to reach the biosphere, and the pathway is characterised by its length x, the fluid velocity v, the retardation coefficient R and the dispersivity length d. The transport in the pathway is simulated as an advective diffusive process in a 1-D medium with radioactive decay. We are interested in the flux F of contaminant in x, the junction of the porous medium and the biosphere, as a function of time. This physical problem is formulated through the following differential equation:

$$\frac{\partial F}{\partial t} + \alpha \frac{\partial F}{\partial x} - \beta \frac{\partial^2 F}{\partial x^2} + \lambda F = 0 \, , 0 \le x \le \infty \quad , \tag{3}$$

with the following boundary and initial conditions

$$\begin{aligned} & F(0,t) = kM_0 e^{-t(\lambda+k)}, t > 0 \\ & \lim_{x \to \infty} F(x,t) = 0, t \ge 0 \\ & F(x,0) = 0, x \ge 0 \end{aligned} \quad .$$

There is thus one dependent variable F, two independent variables x and t, and five parameters α, β, λ, k, M_0. In the notation defined above, $m=2$, $n=1$ and $p=5$. If α, β and x are given random nature, then the response F becomes a random function with index t and, given the distribution of x, α and β, it is of interest to calculate the distribution of F.

Applying Moran and Marschek's generalised's dimensional analysis, we obtain the following invariants: $\Pi = F/\lambda M_0 ; \pi_1' = \lambda t ; \pi_2' = \lambda x/\alpha ; \pi_4'' = \beta\lambda/\alpha^2 ; \pi_5'' = k/\lambda$, so that we have reduced the variables and parameters from the initial set formed by F, x, t, α, β, λ, k, M_0 to the new one formed by $\Pi, \pi_1', \pi_2', \pi_4''$ and π_5''. As mentioned above, the reduction is concentrated entirely on the parameters: the original response or dependent variable F is replaced by the "mixed " invariant Π (mixed in that it is a function of both the original dependent variable and the original parameters); x, t, the initial set of two independent variables, is replaced by also two "mixed " invariants π_1' and π_2' (functions of both the original independent variables and the original parameters); the original set of five parameters α, β, λ, k and M_0 is replaced by the two invariants π_4'' and π_5''. However, since only α, β and x are considered random, as far as uncertainty analysis is concerned, we only profit from the reduction of dimensionality in replacing the subset formed by α, β and x by that formed by π_4'' and π_5''. This means a reduction from 3 to 2 in the dimension of the stochastic input space for the uncertainty analysis.

4. RESULTS

Calculating the full distribution of the random function F would imply obtaining the joint distribution of any set $(F(t_1),...,F(t_u))$ for all possible vectors $(t_1,...,t_u)$. In this paper, to illustrate the use of dimensional analysis we have taken 100 equally spaced time points between 0 and 100,000 years and estimated a) the mean, variance and distribution function for each of the corresponding marginal distributions, b) the correlation coefficients between the response at t=30,000 years and the responses at each of the remaining 99 time points. We have drawn 60 samples of size 64 of the random input. The four following sampling techniques have been applied when drawing each sample:

1. Stratified sampling in an input space of dimension 3: we sample on the joint distribution of α, β, x;
2. Latin hypercube sampling (LHS) in the same input space and with the same sample size as in point 1;
3. Stratified sampling in the input space of size two of α^2/β and x/α, thus profiting from the results of dimensional and similarity analysis;
4. Conventional Monte Carlo (random sampling) in the same input space and with the same sample size as in points 1 and 2.

An example of the results is shown on figures 1 and 2: In figure 1 we show, for each of the four sampling techniques and for each of the 100 time points, the values of the mean of the 60 sample means; in figure 2 we show the standard deviation of the 60 sample means.

We see how the standard deviations (figure 2) are significantly smaller for the third sampling technique (stratified sampling in the two dimensional input space), while the differences between the remaining sampling techniques are less important. This result was to be expected, because we avoid a certain degree of redundant sampling from regions of the three dimensional space which turn out to be the same, as far as the response is concerned, in the two dimensional input space. However, the results for the LHS samples are rather disappointing and should be studied more deeply in future research.

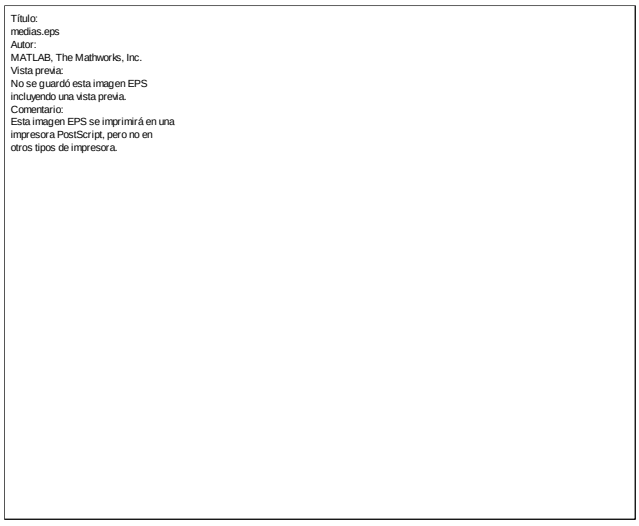

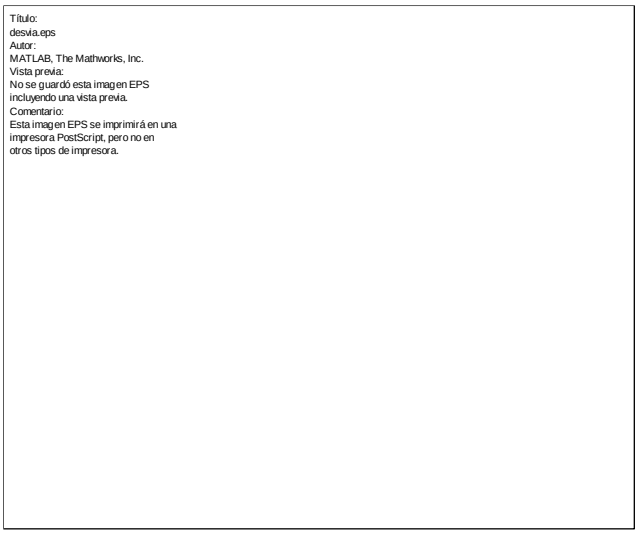

5. REFERENCES

McKay, M.D., Beckman, R.J., Conover, W.J., (1979). A Comparison of Three Methods for selecting Values of Input Variables in the Analysis of Output from a Computer Code. **Technometrics**, Vol.21,No.2, pp 239-245.

Moran, M.J., Marshek, K.M., (1972). Some Matrix Aspects of Generalised Dimensional Analysis. **J. Engr. Math.** Vol. 6, No. 3, pp. 291-303.

VALIDATION OF TRANSIENT STRUCTURAL DYNAMICS SIMULATIONS: AN EXAMPLE

Scott W. Doebling[(1)], Thomas A. Butler[(2)], John F. Schultze[(3)], Francois M. Hemez[(2)]
Leslie M. Moore[(4)], Michael D. McKay[(4)]

[(1)] Technical Staff Member, Engineering Analysis Group (ESA-EA), Email: doebling@lanl.gov
[(2)] Technical Staff Member, Engineering Analysis Group (ESA-EA)
[(3)] Postdoctoral Research Associate, Engineering Analysis Group (ESA-EA)
[(4)] Technical Staff Member, Statistical Sciences Group (D-1)
Los Alamos National Laboratory, Los Alamos, NM, 87 544, USA

1. INTRODUCTION

The field of computational structural dynamics is on the threshold of revolutionary change. The ever-increasing costs of physical experiments coupled with advances in massively parallel computer architecture are steering the engineering analyst to be more and more reliant on numerical calculations with little to no data available for experimental confirmation.

New areas of research in engineering analysis have come about as a result of the changing roles of computations and experiments. Whereas in the past the primary function of physical experiments has been to confirm or "prove" the accuracy of a computational simulation, the new environment of engineering is forcing engineers to allocate precious experimental resources differently. Rather than trying to "prove" whether a calculation is correct, the focus is on learning how to use experimental data to "improve" the accuracy of computational simulations. This process of improving the accuracy of calculations through the use of experimental data is termed "model validation."

Model validation emphasises the need for quantitative techniques of assessing the accuracy of a computational prediction with respect to experimental measurements, taking into account that both the prediction and the measurement have uncertainties associated with them. The "vugraph norm," where one overlays transparencies of simulated data and experimental data in an attempt to show consistency, is no longer an adequate means of demonstrating validity of predictions.

To approach this problem, a paradigm from the field of statistical pattern recognition has been adopted [1]. This paradigm generalises the extraction of corresponding "features" from the experimental data and the simulated data, and treats the comparison of these sets of features as a statistical test. The parameters that influence the output of the simulation (such as equation parameters, initial and boundary conditions, etc.) can then be adjusted to minimise the distance between the data sets as measured via the statistical test. However, the simple adjustment of parameters to calibrate the simulation to the test data does not fully accomplish the goal of "improving" the ability to model effectively, as there is no indication that the model will maintain accuracy at any other experimental data points.

Effective model validation requires "uncertainty quantification" to ensure that the adequate agreement achieved between the numerical prediction and the experimental measurement is

robust to changes in the experimental conditions. Uncertainty quantification refers to the exploration and understanding of the sources of uncertainty in a simulation:

- Solution uncertainties, such as errors introduced by spatial and temporal discretization, as well as model form errors
- Parametric uncertainties, such as distributions on simulation inputs and the propagation of these distributions to the simulation outputs
- Relationship between simulation inputs and outputs, such as the generation of reduced-order models (response surfaces) using design of experiments sampling techniques

The contents of this paper will illustrate the pursuit of a systematic treatment of this problem via an example. The validation of transmission of shock energy through a complex, jointed structural assembly is the problem of interest, and the solution uncertainty is neglected for the purposes of the example. (This neglecting is legitimate, as the uncertainties introduced via simulation parameters are typically much more significant in structural mechanics applications.)

2. EXAMPLE APPLICATION

Quantifying shock transmission through complex, jointed structures has traditionally been possible only with experimental methods. These experiments are expensive and time-consuming and thus only a few cases can be studied. With the advent of large scale computing capabilities estimation of the shock transmission with numerical models has become a tractable problem. A primary advantage of these models is that, when validated, parametric studies can be efficiently performed to evaluate the effects of different input loads and variations to the structure's design or to load path changes caused by ageing. The U.S. Department of Energy's Accelerated Strategic Computing Initiative (ASCI) is developing massively parallel hardware and software environments for modelling these types of problems.

The ASCI computing environment is being used at Los Alamos to study the transmission of shock through a complex, jointed structure. A three-dimensional explicit finite element model has been developed that includes a detailed representation of the geometry and contact surfaces including preloading effects. A series of full-scale experiments has been performed to provide data for model validation and uncertainty quantification.

Several issues of open research are addressed in this example. First, large computer simulations tend to generate enormous amounts of output that must be synthesised into a small number of indicators for the analysis. This step is referred to as data reduction or feature extraction [1]. These features are typically used to define the test-analysis correlation metrics optimised to improve the predictive accuracy of the model. The main issue in feature extraction is to define indicators that provide meaningful insight regarding the ability of the model to capture the dynamics investigated.

Second, efficient numerical optimisation requires that the correlation between the model's input variables and output features be assessed with adequate accuracy. Statistical response surface models (RSM) must be generated to replace the expensive, large-scale simulations. One difficulty of fitting RSM's is efficient sampling, i.e. the generation of sufficient information in regions where representative variation in the features of interest will be observed.

The test article used for the experiments and subsequent analyses consists of several components fabricated from a variety of materials. A titanium component designated the "mount" to which all other components are attached is shown in Figure 1. Two payload mass simulators and two aluminium shells attach to this mount. For the experiments the test article was suspended using wire rope creating a pendulum with a length of about 1m. An impulse of a few microseconds in duration was delivered to the assembly using an explosive charge. A total of four experiments were performed. SRI International performed these tests at their Menlo Park, California facility.

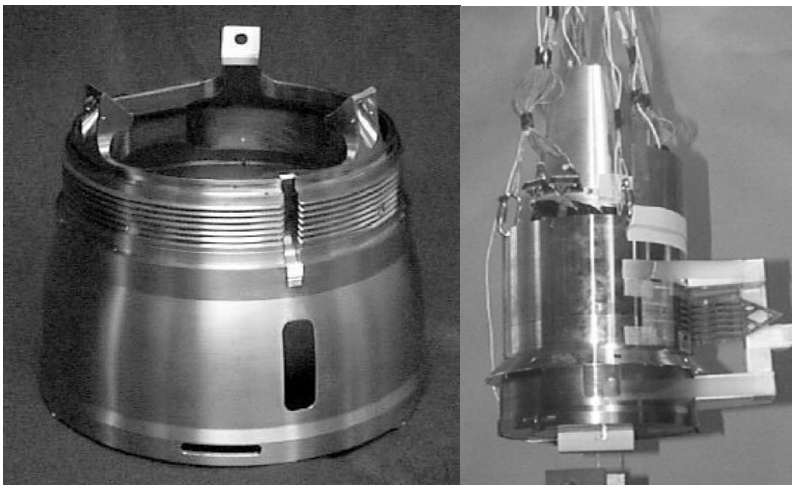

Figure 1: Titanium Mount (left) and Experimental Test Configuration (right)

The explicit finite element model (FEM) of the test article was developed using the ParaDyn finite element code [2]. The resulting model had approximately 1.4 million 8-node hexahedral elements, 56,000 4-node shell elements, and 1.8 million node points. The finite element model was run on 504 processors on the Los Alamos Blue Mountain computer. Using this number of processors resulted in 1.3 CPU hours for each ms of the simulation. A typical response of the model after a short increment of time is shown in Figure 2.

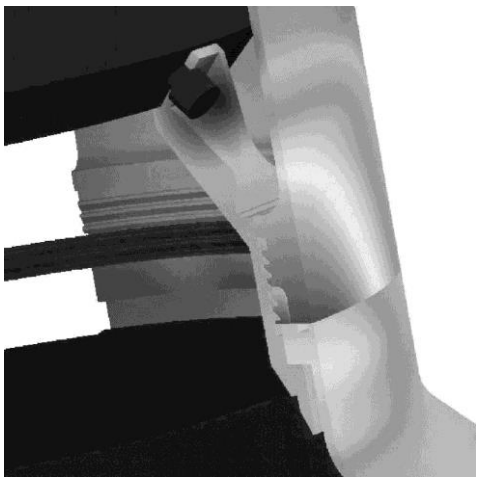

Figure 2: Displacement Contours of the Mount ParaDyn Model

3. PARAMETER SCREENING: FEATURE SELECTION & MAIN EFFECTS ANALYSIS

To quantify and understand the influence of each of the simulation model parameters on the model response, a higher-order RSM must be constructed. Because of the large number of simulation runs required (to cover many levels of each parameter), and the length of time required to run each simulation, the number of parameters must be limited to about 5.

Based on the judgement of the engineering analysts, a total of twelve parameters in the finite element model were selected as being of possible importance to the response and also having a relatively high uncertainty associated with their value. These parameters consist of three component preloads, four static and four kinetic coefficients of friction, and the magnitude of the explosive impulse. So the first step in the model validation/uncertainty quantification process was to build a multidimensional linear RSM of the response features of interest over the parameter space of interest to screen the total number of parameters from 12 to about 5. For the 12 parameters of interest, 4 had 2 levels of interest while 8 had 3 levels. The total number of runs to build a full factorial RSM was therefore 104,976. To limit the required simulation time, a first set of 48 runs was completed from parameter samples selected using the Taguchi Orthogonal Array technique [3].

Because the transmission of shock across the mount to the payload components was the primary event of interest, errors between the predicted and measured statistical moments of the time history, shock response spectrum (SRS) and power spectral density (PSD) at each accelerometer location were used as features of interest. An analysis-of-variance analysis was performed on the 48 runs for each feature to compute the influence of each parameter on each feature. The features were evaluated based on whether a) the total contribution of the individual parameters was significant (e.g. the feature was significantly sensitive to at least 1 of the parameters) and b) whether the feature was amenable to a linear RSM fit (i.e. the linear fit had a high R^2 value).

A few of the features either were not amenable to linear screening or did not demonstrate significant sensitivity to any of the parameters. Generally, however, a trend was observed for features from all sensors indicating significant effects due to the following five parameters: one preload, three kinetic coefficients of friction, and the impulse magnitude. Thus the parameter space of interest was reduced from dimension 12 to dimension 5, allowing realistic generation of a higher-order RSM.

4. CONCLUSION/FUTURE WORK

Work to date has indicated that it is possible to reduce a high-dimension parameter space to a reasonable dimension using a moderate number of runs of a very large finite element model of a transient structural dynamics event. A higher-order RSM will be created using this lower dimension parameter space for the purposes of understanding the sensitivity of the response features to each of these parameters, and for the optimisation of these parameters to adequately represent the measurements from the actual test article. A second round of validation experiments will then be designed to further explore the parameter space and define the regime of validity of the model. The validated model can then be used with some confidence to predict events outside the regime of practical testing.

5. REFERENCES

[1] Bishop, C. M., **Neural Networks for Pattern Recognition**, Clarendon Press, Oxford University Press, Inc., New York, NY, 1998.

[2] Hoover, C. G., De Groot, A. J., Sherwood, R. J., "ParaDyn: A Parallel Nonlinear, Explicit, Three-Dimensional Finite-Element Code for Solid and Structural Mechanics--User Manual," Lawrence Livermore National Laboratory, Livermore, California, UCRL-MA, 2000, to appear.

[3] Hedayat, A.S., Sloane, N.J.A., Stufken, J., Orthogonal Arrays: Theory and Applications, Springer-Verlag, New York, NY, 1999.

PREDICTION OF DETERMINISTIC FUNCTIONS: AN APPLICATION OF A GAUSSIAN COKRIGING MODEL TO A TIME SERIES OUTLIER PROBLEM.

José Mira, María Jesús Sánchez and Francisco Javier Quijada

E.T.S. de Ingenieros Industriales
C/ José Gutierrez Abascal, 2
28006 Madrid (Spain)
e-mail: jmira@etsii.upm.es and mjsan@etsii.upm.es

ABSTRACT

In this paper we calculate the predictive distribution for a bivariate kriging model (or cokriging model). The model is successfully applied to the prediction of the sampling distribution of test statistics used in the detection of outliers in time series.

1. INTRODUCTION

Kriging models, a special case of random fields, are applied in Statistics to predict the value of one or more response variables for given space and time coordinates X_S, given the values of those responses for a different set of inputs X_D. If the response is univariate, we speak of a univariate kriging model, if it is bivariate of a cokriging or bivariate kriging model. Typical examples appear in Geostatistics, where the response is one or more properties of the mineral and X are the position of any location of the mine. For a better understanding of the problem let us assume there are two responses y_1 and y_2 corresponding to, say, hardness (y_1) and elasticity (y_2). Then, given the values of y_1 and y_2 for any set of locations X_D, when predicting the hardness for a new set of locations X_S, we would not only use the data on hardness for X_D, but also the data on elasticity in X_D and vice versa. This implies that there is not only autocorrelation for each response but also cross correlation between the two responses.

Handcock and Stein (1993) developed a univariate response model with regression term plus a zero mean stationary Gaussian process $Y = X\beta + u$, with a correlation structure defined in terms of a vector of parameters θ. They included several cases: first, the value of θ was estimated and "plugged in" so that the uncertainty of the estimation was not incorporated into the predictive distribution. Second, they incorporated this uncertainty by means of $f(y_S|y_D) = \int_\theta f(y_S|y_D,\theta) f(\theta|y_D) d\theta$. In this case $f(y_S|y_D,\theta)$ and $f(\theta|y_D)$ were obtained analytically but integration with respect to θ was numerical.

In this paper we calculate the predictive distribution for a bivariate response (bivariate random field) without regression term, i.e., with zero stationary mean. We then apply this model to the prediction of two deterministic functions, namely to the computation of the sampling distribution of two statistics used in the outlier detection in time series.

2. COMPUTATION FOR THE MULTIVARIATE CASE

Let $y(x)$ be a bivariate random field with a zero stationary mean for both responses, constant (stationary) variance for each response and an auto and cross correlation structure which is expressed in terms of a vector of parameters θ.

The model is based on the hypothesis of normality for the distribution of $y(x)$, conditional on the stationary standard deviations σ_1 and σ_2 and on non-informative priors for σ_1 and σ_2.

As in the univariate case, $f(y_S|y_D) = \int_\theta f(y_S|y_D,\theta) f(\theta|y_D) d\theta$ where $f(\theta|y_D)$ is the posterior distribution for θ and $f(y_S|y_D,\theta)$ is the predictive distribution, but conditional on the value of θ.

It is assumed that we know the two responses y_1 and y_2, for the set of m inputs of matrix X_D, these two responses are stored in vector y_D. We want to predict y_1 and y_2 for the new set of n inputs of matrix X_S, these unknown responses are vector y_S.

The main result of the paper consists in integrating out the two standard deviations σ_1 and σ_2, a problem which appears when computing $f(y_S|y_D,\theta) = \int_\sigma f(y_S|y_D,\theta,\sigma) f(\sigma|y_D,\theta) d\sigma$. This is done by means of the diagonalization of a quadratic form which appears on the exponential, followed by a conversion to polar coordinates and a computation of integrals of powers of trigonometric functions.

As mentioned above, $f(y_S|y_D) = \int_\theta f(y_S|y_D,\theta) f(\theta|y_D) d\theta$ is computed through Monte Carlo simulation using the analytical expressions for $f(y_S|y_D,\theta)$ and $f(\theta|y_D)$. The same applies to the mean and second order moment of $f(y_S|y_D)$, $E(y_S|y_D) = \int_\theta E(y_S|y_D,\theta) f(\theta|y_D) d\theta$ and $E(y^2{}_S|y_D) = \int_\theta E(y^2{}_S|y_D,\theta) f(\theta|y_D) d\theta$ where $E(y_S|y_D,\theta)$ and $E(y^2{}_S|y_D,\theta)$ have also been obtained analytically. $E(y_S|y_D)$ can be used as a point predictor and $\text{var}(y_S|y_D) = E(y_S^2|y_D) - (E(y_S|y_D))^2$ as a measure of the uncertainty of the predictions.

We have used the following stationary correlation structure: the autocorrelation function is $\rho(d) = e^{-\theta_1 d}$ and the cross –correlation function is $\rho(d) = \theta_3 e^{-\theta_2 d}$ where d is the euclidean distance between the inputs. These correlation functions must verify, both individually and jointly, the condition of positive definiteness, we use here the permissibility criteria of Christakos (1992), which, when applied, require that $\theta_1 > 0; \theta_2 > 0; 0 < \theta_3 < min(\frac{\theta_1}{\theta_2}, \frac{\theta_2}{\theta_1})$.

3. APPLICATION

We now apply the results above to the prediction of two deterministic functions: the 95% percentiles of the sampling distribution of the test statistics used to detect two different types of outliers in time series: *IO* (innovative) for the first function and *LS* (Level Shifts) for the second.

If y_t is a time series which follows an *ARIMA(p,d,q)* model, the models for an additive outlier (AO), innovative outlier (IO) and level shift (LS) can be written:

$$Z_t=y_t+w_iV_i(B)I_t^{(Ti)}$$

where $V_i(B)= 1$ for an *AO*, $1/\pi(B)$ for an *IO* and $1/(1-B)$ for a *LS*, $\pi(B)$ is the autoregressive representation for the *ARIMA* model and $I_t^{(Ti)}$ is an impulse variable which takes the value 1 if $t=T_i$ and 0 otherwise.

To test the existence of an outlier the following hypothesis are established: H_0: no outliers; H_1: there exists an *AO*; H_2: there exists an *IO* and H_3: there exists a *LS*. Given a time series with n time points, to test H_0 versus H_1, H_2 and H_3, three statistics $\lambda_{A,t}$ (for *AO*), $\lambda_{I,t}$ (for *IO*) and $\lambda_{L,t}$ (for *LS*) are calculated for each time point *t*; then, for $t=1,\ldots, n$ the maximum of $\lambda_{A,t}$ and $\lambda_{I,t}$ is calculated, and we also compute the maximum (η_{AI}) of these n maxima. Next, for $t=1,\ldots,n$ the maximum of the $\lambda_{L,t}$ (η_L) is calculated. Each of the two maxima is compared with a reference value which is the 95% percentile of its sampling distribution under H_0 (Sánchez and Peña, 1997); these percentiles are calculated by simulation and their values depend on the length n and on the parameters of the series; since computing the percentiles is expensive, specially for large series, we suggest here just calculating the percentiles for a subset of all possible combinations of n and the series parameters and then interpolate through our cokriging predictor for any other combination.

We shall consider only AR(1) as time series model, defined by a parameter (ϕ). Our two response variables in the cokriging predictor will thus be the 95% percentile for *IO* and the 95% percentile for *LS*, and the two input vector X will be the length of the series, *n*, and the value of ϕ.

4. RESULTS

In this section we show the results of a cross-validation exercise carried out using the cokriging predictors presented above.

As mentioned above, we have considered here only AR(1) models, which are defined through one parameter (ϕ) and have taken different values for the length of the time series (n); the dimension of the input variable X is thus two.

We have obtained the values of the two responses for the 42 design points which result from all the possible combinations of the values shown in table 1. We have then predicted the two responses for four new points (X_S).

Table 1: Values of the input variables.

N	30	50	100	150	250	500	
ϕ	0.2	0.4	0.6	0.8	-0.3	-0.5	-0.8

In table 2 we show the results: the first column shows the input values, the second the mean of the cokriging predictive distribution, which we take as point predictor; the third column shows the variance of the cokriging predictive distribution, which is a measure of the

uncertainty of the predictions; the fourth column are the true values, obtained by simulation; the fifth column are the relative errors and the last column are the run times for the predictors. The run times for the original function are of three hours in average. The first half of the *rows corresponds to the first response (IO) and the second half to the second response (*LS).

Table 2: Results for IO and LS

X_S	**Point Predictor (IO)**	**Predictor variance (IO)**	**True value (simulation) (IO)**	**Error (%)**	**Run time**
N=200, ϕ = 0.6	3.6105	0.0120	3.6280	1.75	3'18"
N=200, ϕ = -0.4	3.6534	0.0123	3.5702	-8.32	3'09"
N=100, ϕ = 0.5	3.3722	0.0122	3.3464	-2.58	3'28"
N=100, ϕ = -0.6	3.3226	0.0144	3.2938	-2.88	3'24"
X_S	**Point Predictor (LS)**	**Predictor variance (LS)**	**True value (simulation) (LS)**	**Error (%)**	**Run time**
N=200, ϕ = 0.6	2.8752	0.0191	2.8842	0.90	2'45"
N=200, ϕ = -0.4	2.6110	0.0197	2.5929	-1.81	3'09"
N=100, ϕ = 0.5	2.7700	0.0178	2.7409	-2.91	2'54"
N=100, ϕ = -0.6	2.4595	0.0272	2.5007	4.12	2'47"

We can see that the errors are small and thus validate the predictor.

5. CONCLUSIONS

Using the univariate case as a starting point, we have calculated the predictor for the bivariate case, including the mean and variance of the prediction. The application to the prediction of the sampling distribution (percentiles) of the statistics used to decide if there exist outliers in a time series was very successful. This is very encouraging in the direction of using random fields (kriging) as interpolating predictors in problems of mathematical statistics, a promising new field of application.

6. REFERENCES

1. Christakos, G. (1992). *Random Field Models in Earth Sciences.* Academic Press.
2. Handcock, M. and Stein, M. (1993). "A Bayesian Analysis of Kriging". Technometrics, Vol 35, N. 3.
3. Sánchez, M.J. and Peña, D. (1997). "The Identification of Multiple Outliers in ARIMA Models". Working Paper 97-76. Universidad Carlos III de Madrid.

GLOBAL SENSITIVITY ANALYSIS TECHNIQUES FOR THE ANALYSIS OF THE OIL POTENTIAL OF SEDIMENTARY BASINS.

Stefano Tarantola[(1)], Anna Corradi[(2)], Paolo Ruffo[(2)] and Andrea Saltelli[(1)]

[(1)]Institute for Systems, Informatics and Safety
Joint Research Center of the European Commission
TP. 361 - 21020 Ispra (VA) ITALY
E-mail: stefano.tarantola@jrc.it

[(2)]ENI – AGIP Division,
Via dell'Unione Europea 3
20097 San Donato Milanese (MI) - ITALY

ABSTRACT

Petroleum engineers analysing the oil potential of sedimentary basins are confronted with modelling tasks such as the computation of the temperature and pressure 3D fields, the generation and expulsion of hydrocarbons (HC), and the secondary migration of HC in the traps. The last task also involves, more than others, the definition of a methodology to perform the calibration to the known data (dry holes, discovered reserves, etc.).

In this paper, we focus on the modelling of the generation and expulsion of HC from a source rock in a particular sedimentary basin. We explore how some concepts deriving from the field of global sensitivity analysis can provide insights upon a better understanding of the models employed to simulate the generation and expulsion of HC from source rocks.

In this preliminary study, in addition to a visual scatter-plot analysis, we apply global quantitative techniques of sensitivity analysis. We employ the extended FAST method (Saltelli et al., 1999), which has been applied for the sensitivity analysis of expelled oil, gas and wet gas time histories to groups of uncertain factors (ie model parameters and input data).

1. INTRODUCTION

Global quantitative techniques for sensitivity analysis, that are based on the decomposition of the variance of the target model output, have received a considerable boost in recent years, due both to more efficient computational strategies and to a widening of their range of application.

In this paper we show a preliminary sensitivity study that has been conducted on a numerical model that simulates the generation and expulsion of HC from a source rock in a particular sedimentary basin. The numerical model employed in the study is called PMOD, it was originally developed at the Lawrence Livermore National Laboratory and it has been modified by ENI – AGIP Division, a brief description is given in the next section.

An interesting aspect of this preliminary study is that the PMOD model requires, in addition to a set of *standard* (ie scalar) parameters, also a collection of four time histories (temperature, pressure, effective stress and hydrostatic pressure), which are highly non-stationary and cross-correlated over millions of years before present.

This circumstance, rather unusual and complex to handle for the purpose of sensitivity analysis, but rather common in practical problems, has led us to ponder in detail how to work out a reliable and effective analysis. The procedure adopted in the study is described in Section 3.

2. THE SIMULATION MODEL PMOD

The 0-dimensional model PMOD has been used to calculate hydrocarbon expulsion. The code simulates oil generation, cracking, and other chemical reactions occurring during the pyrolysis of petroleum source rocks over a specified history of temperature and pressure. It simulates also compaction of the source rock and expulsion of hydrocarbons and water.

A point in the sedimentary basin under study has been selected and the PMOD model applied to it, obtaining as result the history of hydrocarbon expulsion out of the source rock from the beginning of the sedimentation (65 million years before present) through to the present time.

The quantities of interest for the sensitivity analysis are the cumulative expelled amounts of oil, gas (CH_4) and wet gas (CH_X) at selected time-steps.

Among all the input parameters of PMOD a number of them has been selected for the subsequent sensitivity analysis: chemical parameters (KEM/FIZ files), phi-stress curve, TOC (Total Organic Carbon), porosity, permeability, source rock thickness and time-series, that describe the evolutions of temperature, pressure, effective stress and hydrostatic pressure. These parameters are considered to be the most uncertain from a physical, geological and geochemical point of view in the study area.

The 'KEM/FIZ' files are input files to PMOD. They contain the stoichiometric and kinetic description of the chemical reactions taking place in the source rock and the chemical and physical properties of reactants and products. Eight 'KEM/FIZ' pairs of files have been used as alternative scenarios, in order to take into account the uncertainties both in the kinetics of the reactions and in fluid expulsion parameters.

Phi-stress curves describe the mechanical behaviour of the rock. As no data were available for the study area, three different curves, relative to similar sedimentary environments in other geographical areas, have been used.

TOC represents the total organic carbon content of the source rock. The variation of this parameter can change the timing of the beginning of expulsion. It is expert belief that TOC can have great influence on the overall efficiency of the expulsion process. TOC values are generally obtained from laboratory analyses of rock samples: the TOC range used in this study comes from experimental data.

Porosity and permeability are petro-physical properties of the rock, whose uncertainty can be due to lack of data or to up-scaling problems. Bibliography values of porosity and permeability in similar lithologies at similar depths have been used and combined into probability distributions.

For source rock thickness, an uncertainty of 50% has been considered with respect to the data obtained from the geological interpretation of this area.

Several sets of time-series of four variables (actually 32 sets) have been calculated with an ENI-AGIP Division internal 1D temperature and pressure modelling tool, they represent 32

different scenarios. Each set contains the description of the evolution through time of: temperature, pressure, effective stress and hydrostatic pressure in the selected point of the basin. All the time series were sampled for six time points, in million years before present (mybp): 30, 11.5, 8.5, 4.8, 1.9 and 0. All the 32 scenarios are acknowledged in the sensitivity analysis. This set up is representative of a credible range of uncertainty in the evolution through time of the four variables, as a consequence of the uncertainties in the sedimentation history of the basin and in its petro-physical properties.

NAME	GROUP	TYPE	RANGE of VALUES	PDF
"KEM/FIZ" files	A	Discrete	1,…,8	Uniform
"phi-stress" curves	A	Discrete	1,2,3	Uniform
TOC	A	Continuous	0.005 - 0.05	Uniform
Porosity	A	Continuous	Min=0.04; Mode at 0.05; Max=0.09	Triangular
Permeability	A	Continuous	1.e-9 – 1.e-6	Log-uniform
Source thickness	A	Continuous	907 – 1814 - 2721	Triangular
Time-series	B	Discrete	1,2,…,32	Uniform

Table 1: list of the uncertain input factors and their stochastic properties

3. SENSITIVITY ANALYSIS

A uniformly distributed statistical variable (the 'KEM/FIZ' factor) is defined and takes discrete values from 1 to 8. A sample from the distribution of the 'KEM/FIZ' factor is generated at run-time, i.e. at each run of PMOD, and the corresponding pair of 'KEM/FIZ' files is used as alternative scenario for the chemical and physical characterisation of the source rock.

In a similar fashion, an identification number is assigned to each one of 32 sets of time histories that have been calculated to describe the evolution through time of temperature, pressure, effective stress and hydrostatic pressure in the selected point of the basin. The identification number takes integer values from 1 to 32. At each run of PMOD, a sample is taken randomly between 1 and 32 and the corresponding set of time series is used as input to PMOD. This procedure is very easy to implement and has been used in this preliminary study.

A first sensitivity analysis is aimed at quantifying importance of the input time histories against all the other contributions to uncertainty. Therefore, the 7 uncertain factors have been partitioned into two groups (called A and B) as indicated in table 1. The extended FAST has been employed to compute the first order and the total sensitivity indices for each of the two groups (i.e. S_A, S_B, S_{TA}, S_{TB}) and for each of the six time points considered. The total cost of the analysis is of about 1,000 model executions: each model execution requires a few seconds to run. The results are shown in Table 2 for CH_4.

Fast first order indices						
Time (in 10 Myears)	CH4[1]	CH4[2]	CH4[3]	CH4[4]	CH4[5]	CH4[6]
Group A	0	0.17	0.33	0.43	0.79	0.75
Group B	0	0.12	0.11	0.02	0.01	0.02
Fast total effect indices						
Time (Myears)	CH4[1]	CH4[2]	CH4[3]	CH4[4]	CH4[5]	CH4[6]
Group A	0	0.78	0.86	0.93	0.96	0.96
Group B	0	0.78	0.58	0.40	0.09	0.14

Table 2: sensitivity analysis (first order and total effect indices) of the output "CH4" to the two groups of factors. Almost identical results have been obtained for "CHX" and "oil".

The first order indices indicate that group B is not influent over time, whereas group A shows an increasing importance (up to a maximum of 0.79 at point 5). At points 2, 3 and 4 the sum of the first order indices is very small (i.e. 0.3, 0.44, 0.44 respectively). This indicates a high level of non-additivity of the model, which is probably undergoing a complex transient. This transient is driven by both groups A and B, which have large values for their total indices (denoting remarkable interactions between A and B). Note how the total index for group B becomes smaller at time points 5 and 6, indicating that group B does not concur to interactions anymore (i.e. the transient is probably terminated), and that the system is almost entirely regulated by the parameters of group A.

Fast first order indices						
time (Myears)	CH4[1]	CH4[2]	CH4[3]	CH4[4]	CH4[5]	CH4[6]
KEM/FIZ files	0.00	0.03	0.07	0.08	0.03	0.03
phi-stress	0.00	0.06	0.08	0.02	0.01	0.02
TOC	0.00	0.07	0.12	0.26	0.64	0.63
Porosity	0.00	0.04	0.04	0.04	0.00	0.01
Permeability	0.00	0.04	0.04	0.04	0.03	0.02
Source thickness	0.00	0.05	0.02	0.03	0.01	0.01
Time series	0.00	0.08	0.08	0.04	0.02	0.03
Fast total effect indices						
time (Myears)	CH4[1]	CH4[2]	CH4[3]	CH4[4]	CH4[5]	CH4[6]
KEM/FIZ files	0.00	0.52	0.44	0.43	0.13	0.19
phi-stress	0.00	0.76	0.52	0.50	0.12	0.14
TOC	0.00	0.80	0.68	0.76	0.79	0.84
Porosity	0.00	0.67	0.35	0.38	0.07	0.12
Permeability	0.00	0.80	0.41	0.44	0.14	0.24
source thickness	0.00	0.52	0.34	0.38	0.12	0.22
time series	0.00	0.78	0.54	0.31	0.12	0.17

Table 3: sensitivity analysis (first order and total effect indices) of the output "CH4" to the seven factors. Almost identical results have been obtained for "CHX" and "oil".

Subsequently, another FAST analysis has been performed for the 7 factors taken singularly to investigate which factors of group A are driving the uncertainty of the output, especially in the time range (2, 3, 4). It has been found (see Table 3) that TOC is the only factor with an appreciable value of first order index (especially at time points 5 and 6). The TOC is also the only factor that has a large value of total index at all time points (except the first): the total indices for phi-stress, porosity, permeability and time series are quite large at time point 2, but then this value decreases

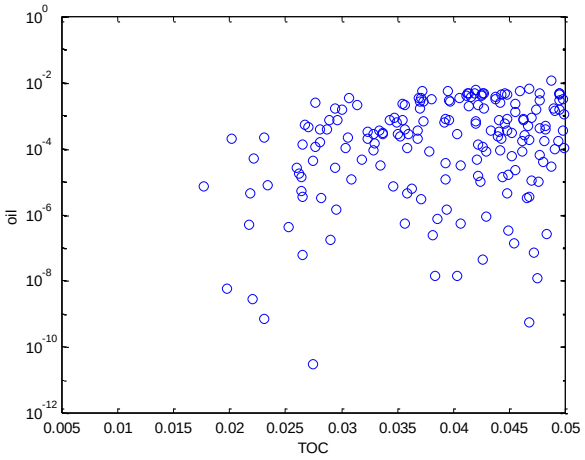

In conclusion, the highly non-linear behaviour of the model is shown by the very low value of the sum of the first order indices. The scatter plot given in figure 1 highlights that TOC acts as a threshold parameter: if the TOC values are below some threshold no expulsion can take place, even if high temperature and pressure values would facilitate oil expulsion.

Figure 1: scatterplot of oil expelled vs. TOC. Note the threshold effect of TOC

4. CONCLUSIONS

These analyses are essential to geologists, modellers and analysts to improve their knowledge on the mechanisms that govern the system over different regions of interest.

Different outputs of PMOD, such as the 'time of initial expulsion' for light oil, heavy oil, and gas, will be the object of future sensitivity analyses. These analyses will contribute to a better understanding of the physical system.

Monte Carlo filtering, and the GLUE approach that derives from it (Generalised Likelihood Uncertainty Estimation) are also promising tools to use in the presence of considerable model uncertainty. GLUE can further be combined with global sensitivity analysis in an effective fashion. This will also be the object of future work.

5. REFERENCES

Braun R. L., Burnham A. K., 1993, User's Manual for PMOD, a Pyrolysis and Primary Migration Model, Lawrence Livermore National Laboratory.

Saltelli A., Tarantola S., and Chan K., 1999, A quantitative, model independent method for global sensitivity analysis of model output, Technometrics, 41(1), 39-56.

AN APPLICATION OF TRANSFER FUNCTION TECHNIQUE TO MARINE DOSE ASSESSMENT

Renata Romanowicz and Peter C. Young

CRES, Environmental Science Department
Lancaster University, Lancaster, UK
Email: R.Romanowicz@lancaster.ac.uk; P.Young@lancaster.ac.uk

1. INTRODUCTION

The abundance of radionuclides in marine biota is usually characterised by coefficients called concentration factors. These coefficients are derived from data from coastal waters and are used as simple multiplicative factors to assess the risk from radionuclide discharges into the sea. This approach implicitly assumes that the transfer of radionuclides from sea water into fish follows a linear relationship, independent of time and space, which has no physical justification. This assumption is slightly improved in the case of so-called "non-conservative" radionuclides, e.g. ^{239}Pu, and ^{240}Am. However, the model used in that case is very simplified due to the small number of observations produced since this technique was introduced [1]. Since then many observational programmes have been performed and there is a need to introduce a more justified, data-based approach into the regulatory practise concerning the transfer of radionuclides into the food chain.

In this paper a transfer function approach is applied to modelling the transfer of radionuclides from sea-water to the marine biota. Concentrations of ^{137}Cs in sea-water and fish flesh in the Irish Sea near Sellafield are used to derive the transfer function parameters. The structure of the transfer function model and the values of its parameters are chosen using statistical and optimisation techniques within the DBM (Data-Based Mechanistic) modelling technique and the microCAPTAIN toolbox [2]. Concentrations of radionuclides not included in the calibration are used to validate the transfer function model predictions. The results are also compared with the predictions of radionuclide concentrations in fish obtained from an input of Sellafield discharges of ^{137}Cs into the Irish Sea. The uncertainties of the predictions are analysed using the Generalised Likelihood Uncertainty Methodology (GLUE) and expressed in the form of confidence limits for the predictions. As a result, the sensitivity of the prediction errors to the variations in the radionuclide discharges and observation errors are evaluated.

2. METHODOLOGY AND RESULTS

2.1. Available data

Available data include discharges of ^{137}Cs from the Sellafield pipe-line and the concentrations of radionuclide in different marine biota in the Sea and on the coast in Cumbria and Morecambe Bay. There are given mean annual radionuclide concentrations for particular locations within the Irish Sea in fish, mussels, winkles, crab and lobster. The

observations from different sources were combined together for the same species and the same location. For the purpose of the comparison of the model results with the observations, two sets of data were chosen for the radionuclide ^{137}Cs. They all come from MAFF annual reports, but consider different consumers.

2.2. Application of transfer function techniques to model transfer of radionuclide ^{137}Cs to fish

The time dependent annual observations of the marine biota make it possible to implement the transfer function approach [2] to the dose modelling. The single input single output transfer function model used for the off-line predictions has the form:

$$y_t = \frac{B(z^{-m})}{A(z^{-n})} u_{t-\delta} + \xi_t \qquad (1)$$

where y_t is the dose prediction at the end of year t, $u_{t-\delta}$ is the concentration of pollutant at the end of year t, δ denotes delay with which the concentrations are observed. ξ_t is the white gaussian noise and the polynomials $A(z^{-1})$ and $B(z^{-1})$ are defined by :

$$A(z^{-1}) = 1 + a_1 z^{-1} + ... + a_n z^{-n} \qquad A(z^{-n}) = 1 + a_1 z^{-1} + ... + a_n z^{-n}$$
$$B(z^{-1}) = b_0 + b_1 z^{-1} + ... + b_m z^{-m} \qquad B(z^{-m}) = b_0 + b_1 z^{-1} + ... + b_m z^{-m}$$

a_n, b_m, are model parameters and m=0,..,M; n=0,...,N

The operator z^{-n} denotes a shift backward in time, i.e. $z^{-m}u(t) = u(t-m)$, which is equivalent to introducing the process dynamics (in static model the process output does not depend on the past values, but only on the present). The value of the transfer function (TF) method depends on the amount of information available to define the model parameters. The microCAPTAIN toolbox and Data Based Mechanistic (DBM) modelling have been applied to identify the order of the TF and estimate the associated parameters [3]. The best optimised model for the discretisation period equal to one week has the form:

$$y(t) + 0.992\,y(t-1) = 14.26u(t) - 14.08u(t-1) + \xi$$

The resulting predictions of the concentration of ^{137}Cs in fish flesh based on sea-water measurements of ^{137}Cs for the validation data set are shown on Fig. 1. The figure also shows the 95% confidence limits for the predictions. It is worth noticing that the microCAPTAIN toolbox uses all the input measurement data, while the use of the simple transfer function method requires smoothing the data before hand. By characterising the data in this manner, the DBM approach demonstrates the analogy between TF and compartmental modelling techniques applied to transfer of pollutant in the food chain.

2.3. Transfer function and Generalised Likelihood Uncertainty Estimation technique applied to model transfer of radionuclides 137Cs from liquid discharges to fish

In the next step in the analysis, the discharges from Sellafield as used as an input to a TF model of the marine biota. The discharges are carried out under authorisation by British Nuclear Fuels (BNFL) and have the form of a liquid radioactive effluent released through a pipeline into the Irish Sea. Only annual discharge data are available to the public. The transfer function approach described in the previous section was applied to annually averaged ^{137}Cs concentration measurements in fish flesh.

The goal of this work is the evaluation of the sensitivity of the prediction errors to the variations in discharge and observation measurements. Two approaches are used. In the first approach, the TF model was derived for the discharges and observations equal to the given mean annual values interpolated into the monthly periods. The resulting predictions for the calibration and validation stage are given on Fig. 2. The second approach consists in derivation of prediction errors for the discharges and concentration observations varied normally from their specified values using full microCAPTAIN toolbox transfer function routines for each discharge realisation. 500 simulations of the transfer model for 48 years starting from 1952 are used in this Monte Carlo analysis. The resulting model predictions are used to evaluate the posterior distributions of concentrations of radionuclide in the marine biota and prediction errors. The predictions with 95% confidence limits for ^{137}Cs, fish, are shown on Figure 3 D. The posterior cumulative distributions for all three parameters of the TF model are shown on Figures 3A-C. In this case, the choice of TF parameters requires the solution of the inverse problem and therefore it is non-unique. Neither is unique the choice of a model structure. This choice should be supported by the research leading to better understanding of the mechanisms of transfer of radionuclides from the marine environment to marine species.

3. CONCLUSIONS

The work presented in this paper considers the generalisation of the uncertainty analysis applied to the marine dispersion models into the environmental assessment problems. Two aspects of the problem are described: (i) calibration of models on site specific data; and (ii) the availability and reliability of input data. Both of these aspects contribute to the modelling errors, which can be estimated only when the stochastic approach to the modelling is taken. In order to improve the marine dose model results, the dynamic dose model was introduced using the transfer function approach. It is based on the introduction of time series methodology to the error model analysis. The resulting predictions take into account the dynamics of the radionuclide transfer to the marine animal flesh and are generally superior to traditionally applied simple regression models. The examples show that a much better explanation of the data (model fit) is achieved by introducing the dynamic dose model and this gives greater confidence in the prediction studies.

4. REFERENCES

1. Hunt G.J., 1984, Simple models for prediction of external radiation exposure from aquatic pathways, *Radiation Protection Dosimetry*, **8**, 4 215-224.
2. Young, P. C. (1999a). Nonstationary time-series analysis and forecasting. *Progress in Environmental Science*, **1**, 3-48.
3. Young, P.C. (1999b). Data-based mechanistic modelling, generalised sensitivity and dominant mode analysis. *Computer Physics Communications*, **115**, 1-17.
4. Beven K.J., A. Binley, 1992, The future of distributed models: model calibration and uncertainty prediction, *Hydrol. Process.*, **6**, 279-298.
5. Romanowicz, R.J., Beven, K., and Tawn, J., 1994, Evaluation of Predictive Uncertainty in Nonlinear Hydrological Models Using a Bayesian Approach, in*: Statistics for the Environment 2, Water Related Issues*, eds. V. Barnett and K. F. Turkman, 297-315.

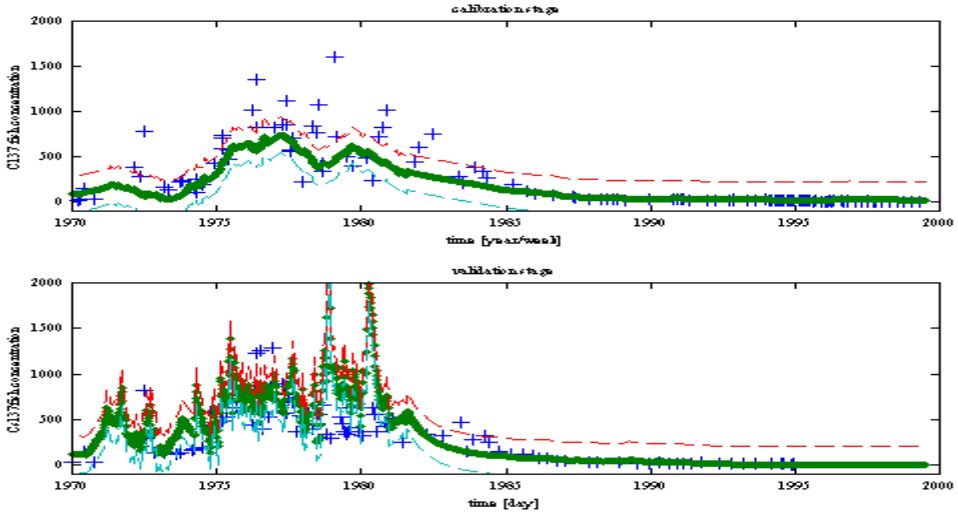

Figure 1. Transfer Function model for weekly data: y(t)+0.99y(t-1)=14.5u(t)-14.1u(t-1)+ξ

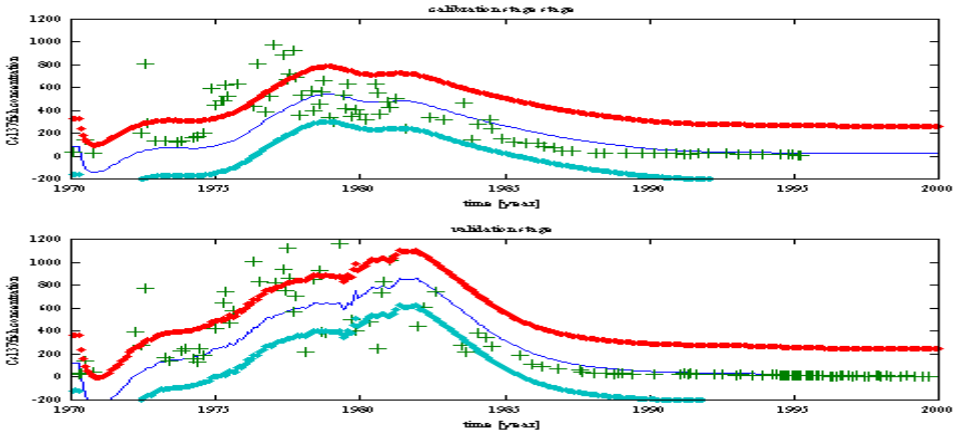

Figure 2. Transfer Function model for monthly data: y(t)+1.95y(t-1)+0.97y(t-2)=0.07u(t-4)+ξ

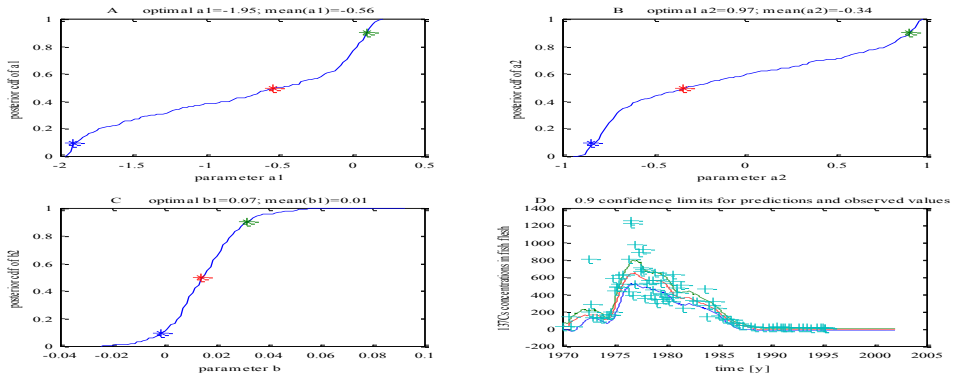

Figure 3. Sensitivity analysis of the transfer function model regarding discharge and observations uncertaintyA. – C.: Posterior cdfs for parameters; * denote 90% confidence limits and median. D.: Predictions of ^{137}Cs concentrations in fish with 90% confidence limits. (+) denotes observations.

SENSITIVITY ANALYSIS IN MODEL CALIBRATION: A CASE STUDY IN ENVIRONMENTAL MODELLING

*M. Ratto[(1)], S. Tarantola[(1)], U. Callies[(2)]**

[(1)] Joint Research Centre of the European Commission,
Institute for Systems, Informatics and Safety, TP 361,
21020 Ispra (VA), Italy
Email: marco.ratto@jrc.it

[(2)] Institute for Hydrophysics,
GKSS Research Centre,
Max Planck Str. 1, D-21502 Geestacht, Germany

1. INTRODUCTION

Temporal trends and spatial patterns in the state of the environment are often obscured by large year-to-year variation in climate conditions. Aim of this paper is to investigate how sensitivity analysis (SA) methods can be employed to achieve model reductions that facilitate the interpretation of temporal changes in the state of the environment. This includes model reductions undertaken to enable model calibration to empirical data. The SA approach is here applied to a water quality model. A new approach is applied here [1]. The approach consists of a combination of the Generalised Likelihood Uncertainty Estimation technique (GLUE) [2] and Global Sensitivity Analysis (GSA) [3]. The method is based on multiple model evaluations. The GSA is a quantitative, model independent approach and is based on estimating the fractional contribution of each input factor to the variance of the model output, also accounting for interaction terms. In GLUE, the model runs are classified according to a likelihood measure, conditioning each run to observations. In calibration procedures, strong interaction is observed between model parameters, due to model over-parameterisation. The use of likelihood measures allows an estimate of the posterior joint pdf of parameters. By performing a GSA to the likelihood measure, input factors mainly driving model runs with good fit to data are identified. Moreover GSA allows highlighting the basic features of the interaction structure.

2. THE METHOD

Many techniques for SA have been proposed (e.g. linear regression or correlation analysis, measures of importance, sensitivity indices, screening, etc.). A thorough description of such techniques can be found in [4]. The SA methods employed here is a new approach [1] based on a combination of the Generalised Likelihood Uncertainty Estimation technique (GLUE) and Global Sensitivity Analysis (GSA) techniques.

The GSA-GLUE method is based on multiple model evaluations. In GLUE [2], the model runs are classified according to a likelihood measure, conditioning each run to observations. The likelihood measure used here is defined by:

$$L(\underline{\theta}_i \mid \underline{Y}) \propto \exp\left(-\sigma_i^{\,2} / \sigma_{obs}^{\,2}\right) \qquad (1)$$

where

$$\sigma_i^2 = 1/2 \cdot Nobs \sum_{j=1}^{Nobs} \left(\hat{Y}_i(t_j) - \underline{Y}(t_j)\right)^2 \quad (2)$$

is the mean squared difference between predictions and observations for the *i*-th run and $\sigma_{obs}^2=\min(\sigma_i^2)$, i.e. the 'best' model run provides the estimate of the measurement error. At each run corresponds a particular factor set. Rescaling of the likelihood measures such that the sum of all the likelihood values equals 1 yields a distribution function for the factor sets. From this, the uncertainty estimation can be performed, by computing the model output cumulative distribution, together with prediction quantiles. An interesting feature of the GLUE approach is that correlation between factor values is reflected implicitly in the likelihood measure associated with the factor sets, so that no hypothesis about the correlation structure is necessary in defining the *a priori* distributions of the model factors. A covariance structure can be obtained *a posteriori* when each factors' combination is weighted via the likelihood measures. Moreover, the use of likelihood measures allows an evaluation of the interaction structure between model parameters: interaction is usually observed in calibration procedures, due to model over-parameterisation.

The GSA [3] is a quantitative, model independent approach and is based on estimating the fractional contribution of each input factor to the variance of the model output, also accounting for interaction terms. In order to calculate the sensitivity indices for each factor, the total variance *V* of the model output is decomposed as

$$V = \sum_i V_i + \sum_{i<j} V_{ij} + \sum_{i<j<m} V_{ijm} + \ldots + V_{12..k} \quad (3)$$

and dividing by *V*, sensitivity indices of singular factors and interaction terms of increasing order can be defined. Two measures will be applied here: $S_i = V_i / V = V[E(Y \mid X_i)]$ (the main effect of X_i) and $S_{Ti} = (V - V_{\sim i})/V = E[V(Y \mid X_{\sim i})]$ (the total effect of X_i, where $X_{\sim i}$ stands for all factors except X_i). Estimation procedures for S_i and S_{Ti} are an extended version of the Fourier Amplitude Sensitivity Test, FAST [4], the method of Sobol' [5]. By performing a GSA of the likelihood measure, input factors mainly driving model runs with good fit to data are identified. Moreover GSA allows highlighting the basic features of the interaction structure.

3. CASE STUDY: WATER QUALITY MODEL

This case study focuses on water quality in a major river, the Elbe River. A simple zero-dimensional model, the WAMPUM model, has been applied which describes the oxygen concentrations and major nutrient processes in the Elbe River at the Weir Geestacht [6]. A data set of daily data is available for model calibration [7]. Period of study is 120 days (May 1 to August 28 1997). The model is run with a time step of 30 minutes. Input data are meteorological time series and initial conditions for concentrations. Model outputs are time series of chlorophyll (CHL), phosphates (PO4), oxygen (O2).

3.1. Application of the GSA-GLUE technique

Six factors have been selected for the analysis, sampled from uniform distribution as shown in

Variable	Name	Min	Max	Reference
X_1	Depth (Water depth)	1.2	4	2.5
X_2	T_ref (Reference temperature)	0	30	14
X_3	k_light (Critical light intensity)	2	50	20
X_4	Tendency_scale_factor (for experimental purpose)	0.1	3	1
X_5	k_att_min (Non-algal light extinction coefficient)	0.1	1.5	1
X_6	k_att_shade (Algal self-shading coefficient)	0.002	0.01	0.005

Table 1. Factors of the analysis of the WAMPUM model.

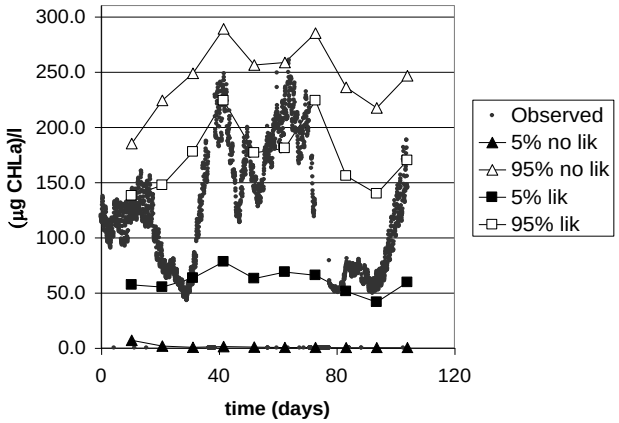

Figure 1. Confidence bands of chlorophyll applying GLUE with the likelihood weigths and when no likelihood measure is applied.

Table 1. The factors are statistically independent. Two outputs are considered: the time series (at 10 equally spaced times) of chlorophyill (CHL) and the likelihood measure. The likelihood measure is computed by considering the available observed chlorophyll concentration time series.

3.1.1. Uncertainty analysis

In Figure 1 the confidence band for the prediction of the chlorophyll time series is shown, based on the likelihood measure (1). This band is also compared with the case of plain Monte Carlo uncertainty prediction without conditioning to observations. The effect of applying likelihood weights is clear through the narrower confidence bound, where worst runs have a negligible contribution

3.1.2. Sensitivity analysis

FAST sensitivity indices for the time series of chlorophyll concentration are shown in Figure 2. Parameter X_4 is the most important parameter. It is the highest 1st order sensitivity index and also its total effect doubles the total effect of any other parameter. Among the remaining factors, X_1 is the only factor with significant main effect, while considering the total effect X_2 and X_6 are almost non-influential.

The sensitivity indices for the likelihood measure are shown in Figure 3. The only significant main effect (i.e. first order) is detected for X_4, while analysing total effect the couple: X_1 and X_4 have the most remarkable effect, X_3, X_5 and X_6 have intermediate effect and X_2 has a small impact. These results imply that a large interaction (signalled by the high difference between main effect and total effect) characterises the calibration of WAMPUM. This means that good runs (behavioural runs) are not driven by a particular factor, but by combinations of them. This kind of picture indicates that the model is over-parameterised and that the estimation problem is under-determined.

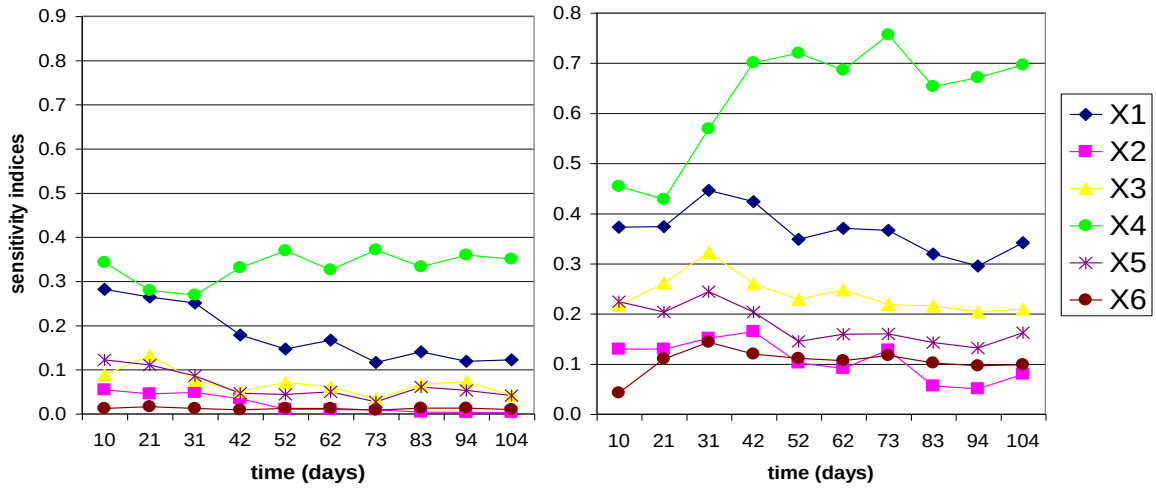

(a) (b)

Figure 2. (a) FAST first order sensitivity indices for chlorophyll concentration; (b) FAST total effect sensitivity indices for chlorophyll concentration

An important outcome of the analysis is that factor X_2 has a clearly smaller impact than other factors. This result could only be obtained applying GSA and in particular computing the total effect of factors and not only the main effect. In fact, considering only main effects in Figure 3, nobody could distinguish between the importance of X_2 and the other factors. Only considering total effect, we could state that X_2 has a negligible effect for the calibration of the WAMPUM model, while all other factors have a significant effect in the interaction structure. Finally, it seems useful to underline the difference between SA on raw data and on their likelihood. In particular, factors X_1, X_3, X_5, have an almost zero main effect for the likelihood measure, while for the physical output the main effect is more significant. This is due to the fact that they induce variability in the algae concentration, but for most of such runs the likelihood is null. So a small variance in the likelihood can correspond to a large variance in the raw data. In this sense the GSA-GLUE analysis is much more informative about the model with respect to the analysis of raw data only. Moreover, the predominance of X_4 in terms of total effect for the time series (Figure 2b) is drastically modified using the likelihood, where X_1 has the principal effect.

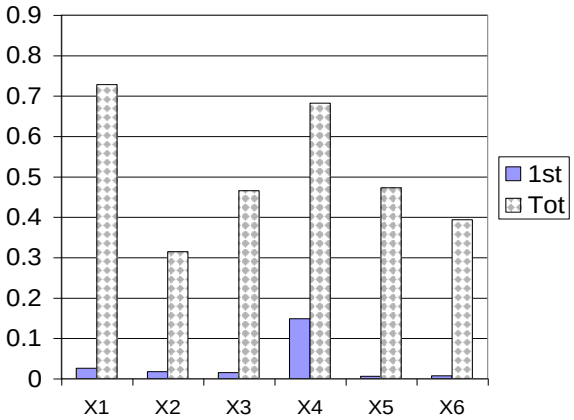

Figure 3. FAST sensitivity indices for the likelihood measure (1).

4. CONCLUSIONS

In the present paper, a SA based approach is applied for the calibration a water quality model. A GSA-GLUE approach has been applied, a new method addressing the problem of calibration for time- or spatially-distributed models. Model over-parameterisation usually implies that factors important for calibration hardly have an effect identifiable through elementary structures. On the other hand, a highly complex interaction structure is usually present. GSA provides quantitative criteria for choosing 'leading' factors based on main and total effect.

5. ACKNOWLEDGEMENTS

This work has been partially funded by European Commission, General Directorate Information Society, IST Program, through contract IST-1999-11313 (IMPACT project).

6. REFERENCES

[1] Ratto M., Tarantola S. Saltelli A., *Comp. Physics Commun.*, forthcoming (2001).

[2] Beven K., Binley A., *Hydrological Processes*, 6 (1992), 279-298.

[3] Saltelli, A., K. Chan, M. Scott, Editors, (2000), *Sensitivity analysis*, John Wiley & Sons publishers, Probability and Statistics series.

[4] Saltelli, A., S. Tarantola, K. P.-S. Chan, *Technometrics* **41** (1), 39-56 (1999).

[5] Sobol', I. M., *Mathematical Modelling & Computational Experiment* **1**, 407-414 (1993).

[6] Schröder F., Environm. Model. & Assessm., 2 (1997), 73-82.

[7] Petersen W., Bloecker G., Mehlhorn N. Schroeder F., *Vom Wasser*, 92, 37-50 (1999).

FUZZY CALIBRATION FOR A SOLIDS BUDGET MODEL IN A LAKE

C. Gualtieri, G. Pulci Doria

University of Napoli, Via Claudio 21

80125-Napoli (Italy)
Email: cagualti@unina.it ; pulci@unina.it

1. FOREWORD – MODEL PRESENTATION

Solids budget affects significantly environmental quality of a water body since the solids carry sorbed toxics that follow solids final fate within the aquatic environment. In particular, incoming solids loading can be flushed away with the outcoming flowrate or can be exchanged, meanwhile it is transported within the system, between water column and sediments through settling, resuspension and burial processes. These processes are particularly relevant in standing waters, such as lakes and reservoirs, and they are usually included in solids budget modeling frameworks. However, these models are difficult to be applied since a correct parameterization must face up to a lack of field data, that produces remarkable uncertainties on model outputs. Since steady-state solutions provide an estimate of the average water quality that will result if solids loading are held constant for a sufficiently long time period, in a previous paper [1] a dimensionless steady-state model for solids budget in a lake, which provides a general insight in exchange phenomena between water column and bed sediments, has been proposed; in that model water column and bed sediments were idealized as three well-mixed reactors: water column, active sediments layer and deep sediments layer (Fig.1).

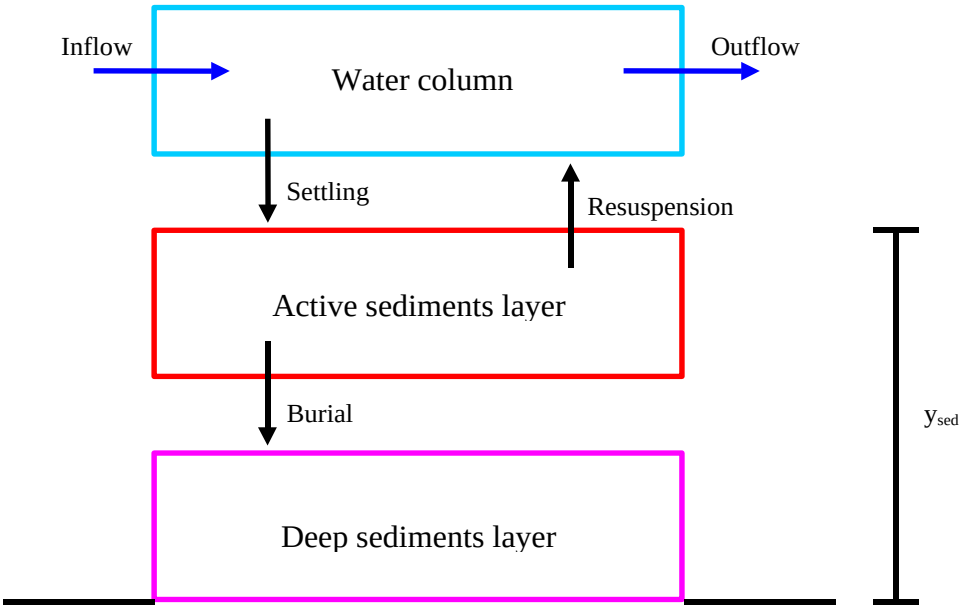

Fig.1 - Water column- bed sediments system in a lake

The active sediments layer represents the bed volume which is really involved in exchange phenomena with water column, i.e. settling and resuspension or scour; this layer could be considered having a constant thickness; thus, if water-sediment interface moves upward or downward as a result of settling/scour phenomena, the downer boundary of active sediments layer moves upward/downward too producing a downward/upward burial flux which accounts for solids loss from this layer to the deep sediments or vice versa. Model solutions were the transfer functions β_{lake} e β_{sed}, which specify how a system loading input is transformed into a water column and sediment layer concentrations. In fact, if $\beta_{fake} << 1$, it means that the lake's removal mechanism acts to greatly reduce the level of solids in the water column; conversely, if $\beta_{lake} \rightarrow 1$, it means that incoming solids tends to remain in the water column. These functions were derived applying dimensional analysis to mass balance equations for water column and active sediments layer, resulting in the following expressions:

$$\beta_{lake} = \frac{1}{1 + \frac{\eta}{\eta + 1}\frac{v_s}{v_f}} \tag{1a}$$

$$\beta_{sed} = \frac{\frac{v_s}{v_f}}{\frac{v_r}{v_f}\left[1 + \eta\left(1 + \frac{v_s}{v_f}\right)\right]} \tag{1b}$$

where η is $\eta = v_b/v_r$ and, if Q is water flowrate and A is lake area, $v_f = Q/A$ is the filling rate, that for each lake is known. Also, since $\eta > 1$, it is possible to skip the first unity at the denominator of (1b), which yields:

$$\beta_{sed} = \frac{\frac{v_s}{v_b}}{1 + \frac{v_s}{v_f}} \tag{2b}$$

As a result, key point in (1a)/(2b) is the characterization of exchange rate parameters v_s, v_r and v_b, i.e. settling, resuspension and burial velocities, respectively, and, consequently, of η. Notably, v_r is extremely difficult to measure, while both v_s and v_b could be measured directly [2] [3] and v_s could be also approximated from literature values. However, in many real contexts their values are not available. Therefore, since fuzzy sets theory is often used to characterize uncertainty about models parameters [4], this paper proposes an application of that theory to evaluate the uncertainty about these rates involved in the solids budget. Membership degree functions are defined for each rate and, consequently, for model solutions β_{lake} e β_{sed}.

2. APPLICATION OF FUZZY SETS THEORY TO MODEL SOLUTIONS

The theory of fuzzy sets can be applied when parameterization process is affected by relevant uncertainties. In fact, this theory assigns to all the uncertain parameters, instead of a single value, a variability range that is defined through a set of values, called fuzzy set. Within the set, parameter variability is stated using a degree membership function μ that can

assume any value in the range [0,1]. Thus, the values comprised in the fuzzy set are all true, but each one with a different grade of membership.

Therefore, as a first step, fuzzy parameterization requires the definition of membership degree function for each rate. i.e. v_s, v_r and v_b, and, consequently, for η.

Definition of membership function for settling rate v_s should be focused to the solids to whom toxics are sorbed. As a rough estimation, a range of 0.30÷2.40 m/day, which corresponds to 110÷890 m/year, could be suggested for settling velocity of solids in lakes and reservoirs; in fact, this range, which represents organic and clay particles, encompasses the majority of available field data. These types of solids are most relevant, since they have a greater capacity than larger, less flocculent particles to adsorb organic chemicals and heavy metals [5] [6]. Membership function μ_s can be considered as symmetric respect to a value of 500 m/year (Fig.2a).

Fig.2a - Membership function for v_s

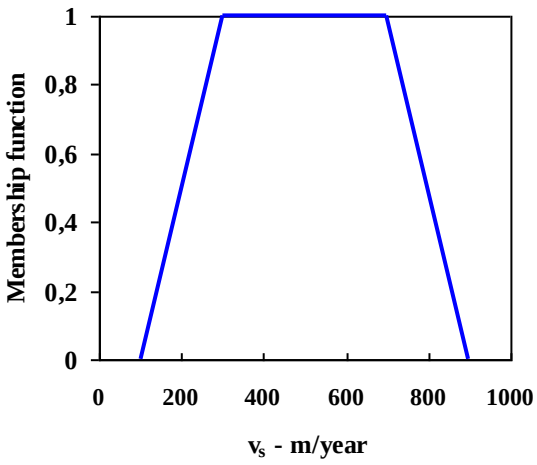

Fig.2b - Membership function for v_r

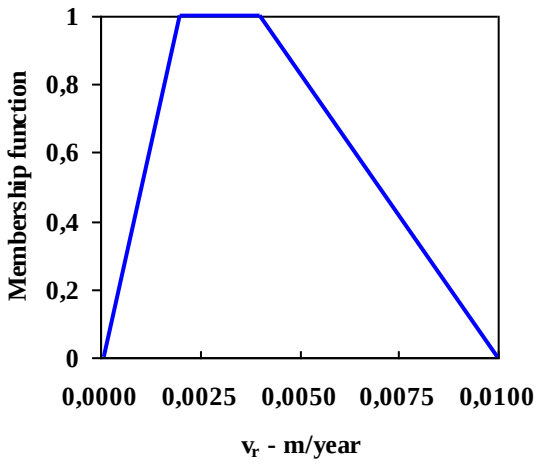

Resuspension is mostly due to short-term perturbations, such as storms and high winds; however, this process, in water quality modeling, is often modeled as a continuous process, that is characterized by a constant rate [7]. With some approximation, membership function for resuspension rate v_r can be defined in the range from 1×10^{-4} to 1×10^{-2} m/year, where maximum membership value is in the range from 2×10^{-3} to 4×10^{-3} m/year (Fig.2b).

Fig.2c - Membership function for v_b

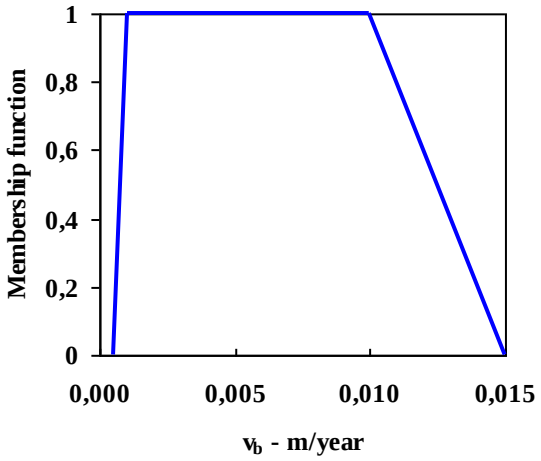

Fig.2d - Membership function for η

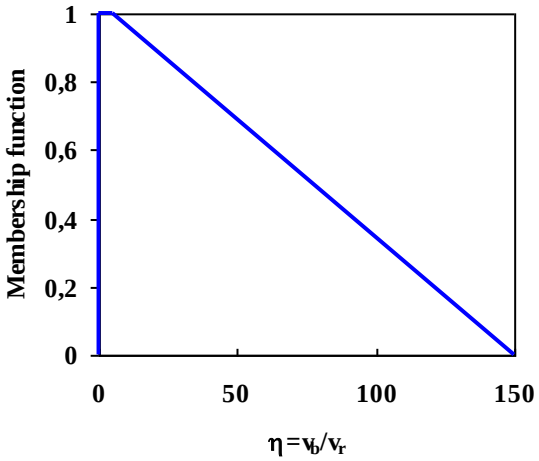

Finally, in sedimenting systems, such as deep lakes and reservoirs, burial rate v_b is positive and it lies in the range from 1×10^{-3} to 1×10^{-2} m/year, that are the values assumed for its membership function, where maximum value is achieved in the range 1×10^{-3} to 1×10^{-2} m/year (Fig.2c). Notably, all membership functions herein defined have a trapezoidal shape.

The functions now defined can be used to derive membership degree functions for model analytical solutions, i.e. (1a) and (2b); thus, a reasoning algorithm that links inputs and outputs should be applied. A correlation product encoding, that reduces the membership function using a scale factor which is function of input membership function values, has been assumed [4]. First of all, a membership function has been derived, using those for v_b and v_r, for η parameter, that is present in (1a). This function is shown in Fig.2d. Now, filling rate v_f must be defined to derive membership functions for (1a) and (2b). For example, filling rate for Lago Maggiore, one of the most important Italian lakes, is v_f=43.0416 m/year. Therefore, using this value membership functions for transfer functions β_{lake} and β_{sed} can derived (Figg.3a/3b). They have trapezoidal shape too, where maximum values identify a relatively narrow bands of responses of the system water column-sediments. Notably, for β_{lake}, membership function domain lies in the range [0.0459, 0.900] with maximum value from 0.0687 to 0.418, while β_{sed} belongs to the range [2006, 82154] with maximum value from 3764 to 40548. Therefore, typical response of the system is to yield, at steady-state, in the water column, a solids concentration comprised between 6.87% and 41.8% of incoming concentration.

Fig.3a - Membership function for β_{lake}

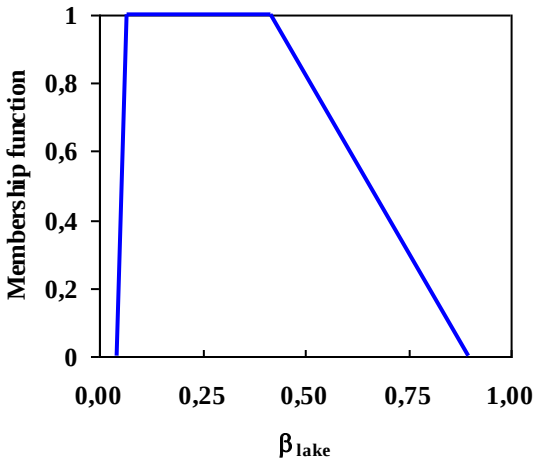

Fig.3b - Membership function for β_{sed}

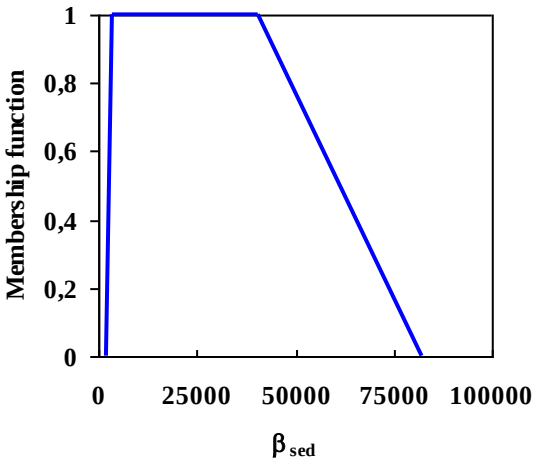

3. CONCLUSIVE REMARKS

Solids budget modeling can provide useful information about final fate within surface waters of environmental contaminants that are often sorbed onto the solids of water column and bed sediments. However, if modeling framework is relatively simple, careful attention should be paid to a proper parameterization in order to obtain reliable predictions.

This paper has proposed the application of fuzzy sets theory to parameterization of a dimensionless steady state model for solids budget in a lake. In fact, this theory allows to underline the influence that uncertainty about input parameters has on model results. Firstly, membership functions for exchange rate parameters have been defined. Then, membership functions for model solutions have been derived resulting in a useful identification of typical response of the system water column-bed sediments. Particularly, solids concentration in the water column is typically comprised from 6.87% and 41.8% of that of the inflow.

4. ACKNOWLEDGEMENT

The paper is a part of Italian MURST PRIN 2000 grant research *Interactions between whirling and turbulent fluxes and infrastructure in hydraulic engineering*.

5. REFERENCES

[1] Gualtieri C. and Pulci Doria G. (1998). *Non-dimensional steady-state solutions for solids budget in a lake*. IAWQ Conference *Application of models in water management*, Amsterdam, The Netherlands, September 24/25, 1998

[2] Gualtieri C. (1999). *Sediments burial velocity estimation in Venice Lagoon*. 28th IAHR Congress, Graz, Austria, August 22/27, 1999

[3] Ciaravino G. and Gualtieri C. (1999). *Probability distribution of filling velocity in italian lakes*. AIT Civil and Environmental Engineering Conference, Bangkok, Thailand, November 8/12, 1999

[4] Gualtieri C. and Fabbricino M. (1997). *Fuzzy method for landfill hazard ranking*. Sardinia '97/6th International Landfill Symposium, S.Margherita di Pula, Italy, October 13/17, 1997
[5] O'Connor D.J. (1988). Models of sorptive toxic substances in freshwater systems. II. Lakes and reservoirs. *J.Env.Eng.Div. ASCE,* **114**, 3, pp.533-551
[6] Thomann R.V. and Mueller J.A. (1987*). Principles of surface water quality modeling and control.* Harper Collins, New York
[7] Chapra S.C. (1997). *Surface water quality modeling.* McGraw-Hill, New-York

ON PREDICTION AND MODEL VALIDATION

Michael D. McKay, Richard J. Beckman, Katherine Campbell

Los Alamos National Laboratory,
Los Alamos, New Mexico, USA
Email: mdm@lanl.gov

1. INTRODUCTION

Quantification of prediction uncertainty is an important consideration when using mathematical models of physical systems. This paper proposes a way to incorporate "validation data" in a methodology for quantifying uncertainty of the mathematical predictions. The following sections outline a theoretical framework.

2. NOTATION

Let $y = m(x)$ be a model-predicted value and x a random variable with probability distribution $f(x;\theta)$. Let $g(y;\theta)$ denote the induced probability distribution of y. The parameter θ is assumed to characterize a scenario in the real world. The probability distribution $f(x;\theta)$ characterizes our (incomplete) knowledge of the values of model inputs for the scenario. For example, if the model input x is Wind Speed At Time Of Event, the probability distribution f could be Normal with θ being the mean and standard deviation we choose to associate with wind speed for the scenario. An important point in this development is that the scenario is characterized by θ from which the model input values x are determined as random variables.

The difference between a real-world response w and the model-predicted value y for the scenario θ is denoted by $d(x) = w - m(x)$ with $x \sim f(x;\theta)$. The difference or error term d, in its general form, is thought to include terms that refer to "modeling error" or "model-structure error", as well as to other considerations that might make w a random variable, like "observation error." (We postpone the expansion of d and the treatment of θ itself as a random variable.) If the joint probability distribution of d and y at the value q were known, it could be used to establish a prediction region for w. We intend to use the validation data to estimate that distribution.

3. VALIDATION DATA

Suppose that the validation data are n observations w_i from scenarios θ_i. For these observations, we might hypothesize the description

$$w_i = y_i(x) + d(x),\ x \sim f(x;\theta_i),\ \ i = 1,\ldots,n,$$

where it is important to recognize that the w_i are random variables for which the data represent realizations. Figure 1 depicts a relationship among realizations

w_i*, y_i, and $d_i = w_i$ *- y_i. The probability distributions $g(y;\theta_i)$ are symbolized on the vertical axis. The distributions for θ_i, conditional on the values w_i *, are symbolized by the vertical bars in the graph.

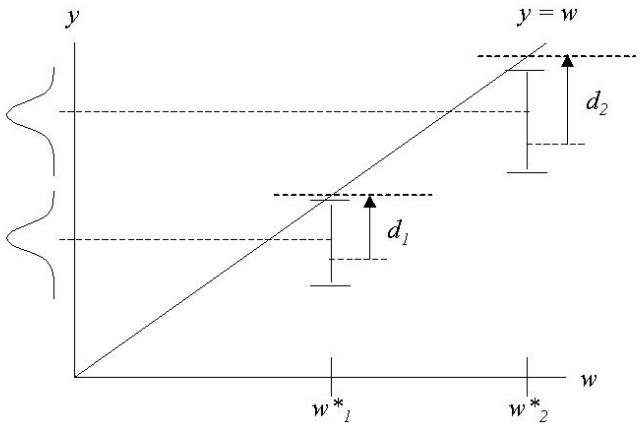

Figure 1. Two observations of *w*, corresponding probability distributions of *y* and *d*.

In order to estimate the joint probability distribution of θ and y for some future scenario $\tilde{\theta}$ we will need to make some assumptions about *d*. When *n* is large enough relative to the dimension of *x*, assumptions about the form of *d* might include things like it being a response surface or a random (gaussian) process in *x*. Another possibility is that *d* might be a function of only a small number (relative to *n*) of inputs that dominate model predictions.

This paper investigates another alternative. The function *d* depends on the scenario description θ through the probability distribution *f*. For cases where the dimension of θ space (and that of *x*) is large, we suggest replacing *d* by a series of functions of reduced dimension, transformations of θ. For example, we begin by replacing $d(x;\theta)$ by the function $d_y(E[y;\theta])$. Further possibilities, not discussed in this short paper, include the addition of functions of selected components of θ, as well as of other model-calculated response variables. Then, the validation data are described by

$$w_i = y_i(x) + d_y(E[y_i]),\ \ x \sim f(x,\theta_i),\ \ i = 1,\ldots,n.$$

In this form, the difference function d_y is to be estimated as a function of *y* and evaluated at $E[y]$. The complexity induced by the dimensionality of *x* is confined to the (estimation) probability distribution of d_y as a dependency on θ.

Let g_i denote the probability distribution of y_i at θ_i, which is induced by *x* and may be estimated via simulation. Consider as data $\{w_i^*, g_i \mid i = 1,\mathrm{L}\ ,n\}$ and the derived variables $d_i = w_i$ *- y_i with their associated probability distributions $h(d;\theta_i)$. Figure 2 depicts a relationship among $E[y]$, d, $h(d)$, and the "observed" value $d^* = E[d] = w^* - E[y]$, say.

The probability distributions $h(d;\theta_i)$ are symbolized on the vertical axis and by the vertical bars in the graph.

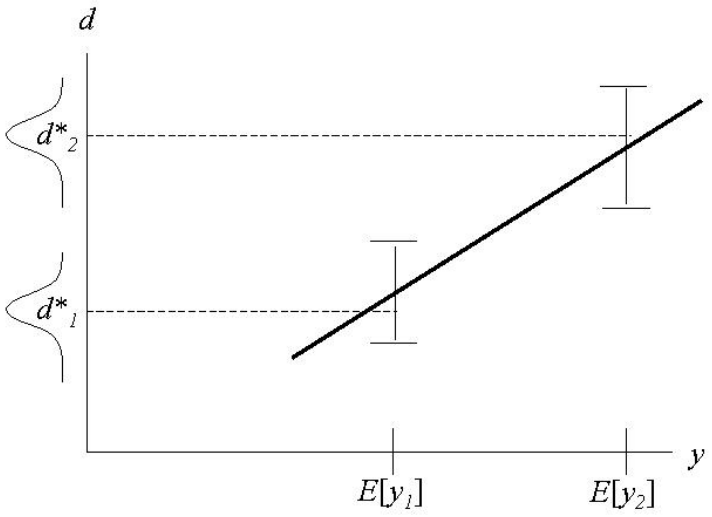

Figure 2. Two "observations" of *d*, corresponding probability distributions and estimated function $\hat{d}$.

From these data, we propose to develop a functional relationship between d^* and $E[y]$ for the validation data points indexed by θ_i. For example, we could model $d^*(y) = a + by + e$ where the error term e has mean value 0 and variance $V[y,\theta_i]$. The parameters *a* and *b* would be estimated with weighted least squares. The form of the estimated predicted difference becomes $\hat{d}(y) = \hat{a} + \hat{b}y$.

4. PREDICTION

Finally, we would describe a future observation $\tilde{w}$ for scenario $\tilde{\theta}$ by

$$\tilde{w} = y(x) + \hat{d}(E[y]) + e,\ x \sim f(x,\tilde{\theta}),\ e \sim n(0, V[y;\tilde{\theta}])$$

Uncertainty in $\tilde{w}$ could be quantified from the estimation distribution of $\hat{d}$ and the probability distributions of *x* and *e*, in a way similar to that used in regression analysis with, for example, a prediction interval.

5. EXAMPLE

We present the following very simple, artificial example to illustrate the notation and method. Suppose that the model is

$$y = m(x) = x_1 + x_2 \ \textit{with}\ x \sim n[\theta = (\theta_1, \theta_2), I],$$

Suppose that the response in the real world is generated according to

$$w = \theta_1 + 2\theta_2 .$$

Let the validation data be $n = 4$ values $\{w^*_1, \mathrm{L}\ , w^*_4\} = \{0,2,1,3\}$, corresponding to 4 values $\{\theta_1, \ldots, \theta_4\} = \{(0,0),(0,1),(1,0),(1,1)\}$. The values of $E[y] = \theta_1 + \theta_2$ for the validation data points are $\{0,1,1,2\}$. The values of $d^* = w^* - E[y]$ are $\{0,1,0,1\}$. Estimating a linear relationship between $E[y]$ and d^*, we have

$$\hat{d}(y) = \frac{1}{2} y .$$

The prediction of a future observation is

$$\tilde{w} = y(x) + \tfrac{1}{2}(\tilde{\theta}_1 + \tilde{\theta}_2) + e,\ x \sim n(x;\tilde{\theta}),\ e \sim n(0,2)$$

with point estimate

$$E[\tilde{w}] = E[y(x)] + \frac{1}{2}(\tilde{\theta}_1 + \tilde{\theta}_2) = \frac{3}{2}(\tilde{\theta}_1 + \tilde{\theta}_2)$$

The error in the point estimate is seen to be

$$d = (\tilde{\theta}_1 + 2\tilde{\theta}_2) - \frac{3}{2}(\tilde{\theta}_1 + \tilde{\theta}_2) = \frac{1}{2}(\tilde{\theta}_2 - \tilde{\theta}_1)$$

6. DISCUSSION

Clearly, it is a very strong the assumption that the difference term $d(x)$ can be replaced by a function of $E[y]$. Because there are very reasonable examples where the approach produces absurd results, investigation of conditions under which the assumption is viable are needed. The motivation for the assumption is straight forward, however. Suppose that there are only a few validation data points and that the number of model inputs is quite large. Further, suppose that the principal contribution to *d* comes from either incomplete representations of reality in $m(x)$ or even from omission of important considerations. In that case, trying to determine empirically a suitable functional form for *d*, where necessary input variables might not be included in *x*, would seem to be a daunting task. As a possibility for dimension reduction, we choose to use a transformation of the inputs *x*, namely, the response variable *y*. We propose to exploit any trend in a plot of *w* versus $E[y]$ for the validation data points. Additionally, we propose to exploit any trends in plots of additional components of multivariate response vectors *y* and *w* to construct the difference term. The degree to which success is achieved will certainly be model dependent.

STATISTICAL UNCERTAINTY ANALYSIS AS A TOOL FOR MODEL VALIDATION

Doug Fraedrich and Robert Gover

Naval Research Laboratory
Washington DC 20375 USA
Email: fraedric@ninja.nrl.navy.mil

SUMMARY

This paper applies a new concept from the epistemological literature to model validation. The concept of a *Severe Test* is defined and then shown how it dictates a model validation methodology. Sensitivity analysis proves to be a key element in both planning a *Severe Test* and analysing subsequent data.

1. INTRODUCTION

The practice of model validation is essentially a scientific endeavor (establishing the relationship between model predictions and reality) while the study of the model validation process is essentially an epistemological one. Recent advances in the field of epistemology have emphasized a testing approach toward validating scientific theories as opposed to the more conventional "evidential - relationship" approach [1] favored by previous schools of thought. This new testing approach, called *Error Statistics*, stresses the role of the theory (or in this case, model) in designing the experiment that results in a *Severe Test* of the model.

A *Severe Test*, in the context of model validation, is defined as a test that will have a high probability of indicating good prediction accuracy if the model is truly accurate and a high probability of indicating poor prediction accuracy if the model is truly inaccurate. This is equivalent to stating that the test will have a small probability of indicating a poor prediction accuracy if it is truly accurate (we will label this as a Type I error) and a small probability of indicating a good prediction accuracy if in fact is in truly inaccurate (Type II error).

The method of *Error Statistics* requires that one identifies the possible or logical mechanisms that can result in the above epistemological Type I and II errors, and then designs an experiment and analysis method to test for their existence. Type II errors can occur if: 1) the validation was performed with the same data as was used to build the model [known as *ad hoc* validation]; 2) the model was tested over a smaller or different domain than which the model is intended to be used over; or 3) a small number of data points were collected and they indicate good prediction accuracy by chance. The probability of these types of errors occurring can be reduced by: 1) using a statistically independent data set for validation 2) ensure the dataset spans the domain of the model's intended use [i.e. sample design] and 3) collect an adequate number of data points [i.e. sample size].

Type I errors can exist if: 1) large residuals between the model's output and measured data are caused by errors in the measured data; or 2) large residuals are caused by measurement errors in the INPUT variables propagating through an accurate model, which result in a

mismatch between the model output and measurements (as well as sample size and design issues as before). Sensitivity analysis (SA) is an invaluable tool to reduce the probability of these Type I errors. This paper will describe how to use SA in a methodology for model validation that yields reduced probability of a Type I error.

2. METHODOLOGY

The model under test is represented as an input-output relation: $\underline{S} = f(\underline{x}, \underline{y}, \underline{z})$ where $\underline{S}$ is the endogenous variable (scalar or vector) which is a function of three types of exogenous variables. The x's are controllable (in a validation experiment), and the y's are uncontrollable. The z's are variables that remain constant between validation and future prediction. If the values of the z variables are changed, the model must be re-validated over this new domain. The total uncertainty between the measured and modelled values of S is referred to as U_t. This is partitioned into several logical components [2,3]:

$$U^2_t = U^2_m + U^2_x + U^2_y + U^2_z + U^2_f \quad (1)$$

Where U_m is the measurement error in S (from the validation experiment), U_f is due to errors in the underlying conceptual model f, and U_x, U_y and U_z refer to uncertainties in S due to measured errors in the inputs from the validation test which propagate through the model. The relative errors, U_m , U_x , U_y and U_z are directly estimated and U_f is derived using Equation 1. For future predictions, the prediction error is:

$$U^2_p = U^2_z + U^2_f \quad (2)$$

For Equations 1 and 2 to hold, the various terms must be both statistically independent and distributed normally. (If normality does not hold, Equation 1 is approximately valid for small values of the U_i's.) Normality can be tested quantitatively on the directly measurable terms (e.g. U_t and U_m) by performing a Shapiro-Wilk normality test [4]. For the U_x , U_y and U_z terms, a Monte Carlo analysis can be run by injecting normally distributed errors in the inputs (x's, y's and z's) of the appropriate magnitude into the model. The distribution of the output can then be tested for normality.

Regarding independence, the model error term U_f is expected to be independent of the measurement related terms (U_m, U_x, U_y, U_z) as long as the same data was not used to both build and validate the model. For the measurement related terms, independence can be assessed by checking for common error sources, such as: 1) Common measurement instrumentation, 2) Common calibration standards, 3) Common noise sources (such as noisy line voltage or EMI) or 4) Operator bias (for analog instruments.) If independence is not established for individual variables within a logical component of Eq. 1, then the methods of [5] can be readily applied to account for these correlation effects.

The various terms in Equation 1 are estimated using methods outlined below.

I. Design Validation Test

A. Decide on an acceptable level of U_f.
B. Perform backwards Uncertainty Analysis to define maximum levels of error in U_m, U_x, U_y and U_z.
C. Perform Sensitivity Analysis to decide which x's are most important. These variables should be varied systematically in the validation test using standard Design of Experiment techniques [6].

II. Perform Test

A. Perform Test.

B. Perform Error Analysis to define measurement errors in S's, (Um) and also x's, y's and z's [7].

III. Perform Validation Analysis

A. Compute variance of difference between measured and predicted values of S (U2t).

B. Use results from Error Analysis (IIB) to perform Uncertainty Analysis to estimate U2x, U2y and U2z.

IV. Compute Uf term (using Eq. 1) and then Prediction Error Up (using Eq. 2).

Thus, uncertainty is ascribed to modelling errors only if they exist. If the model is truly accurate but large values of total uncertainty are observed which are due to measurement error or propagated errors, uncertainty will be appropriately assigned. If the model errors are indeed large, total uncertainty will not be explained by either measurement or propagated errors and thus a large uncertainty will be assigned to the model. The result is a *Severe Test* of the model.

3. RESULTS

The above methodology was used by NRL to perform a validation on a model that predicts the infrared radiometric properties of Navy ships [8]. The output S is infrared intensity. The x variables are ship speed and heading and the y variables are weather observations. Details of the ship design (e.g. geometrical, thermal and optical) are the z variables and do not change between validation and prediction.

Infrared field measurements were made on a U.S. Navy ship and compared to predicted values; the overall relative uncertainty U_t was 24%, which was estimated from 21 pairs of data points. Normality was tested on both the U_t and U_m terms. For the U_t term, the P-value from a Shapiro-Wilk test was 0.17, indicating that we cannot reject the Null Hypothesis (at the 5% level) that the underlying distribution is normal. The P-value for the measurement error term U_m was even better, 0.57 [9]. The propagated terms were tested via Monte Carlo simulation; an example P-Value from this procedure is 0.81. With the exception of two of the y_i's (air temperature and sea temperature) none of the x's, y's or z's share a common error source with each other or S and are treated as independent. The thermocouples that measure air and sea temperature use the same calibration sources and therefore correlated bias errors are expected. However, the magnitude of this error is estimated to be 0.2% and is justifiably ignored.

Measurement errors of IR intensity, S (U_m) and all of the x's, y's and z's were estimated and the terms U_x, U_y and U_z were then computed by performing a sensitivity analysis on the model. Model error, U_f , was then derived using Eq. 1. The apportionment of the different terms in Eq. 1 are shown in Figure 1. It is seen in Figure 1 that the measurement error and propagated terms, which are usually ignored, are of comparable magnitude to the model error (which is what needs to be estimated.) The resultant estimate of prediction error (U_p) is 19%, compared to the total uncertainty of 24%. Thus, this procedure results in a reduction of Type I error.

4. DISCUSSION

The epistemological concept of a *Severe Test* is successfully applied to model validation. The *Severe Test* ensures that good prediction accuracy is indicated only when the model is truly accurate and poor prediction accuracy is indicated only when the model is truly inaccurate. Sensitivity analysis is a powerful and necessary methodological tool to apportion the total measured uncertainty between the various logical components. This partitioning enables to reduction the probability of Type I error, namely assigning a large prediction error to an accurate model.

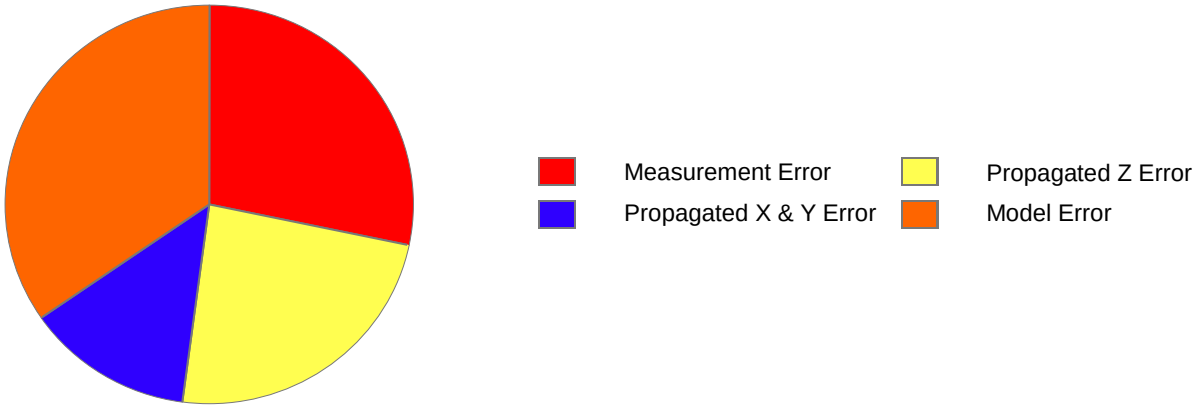

Figure 1. Apportionment of Uncertainty

5. ACKNOWLEDGEMENTS

The authors are grateful to Dr. Allen Goldberg for many insightful discussions on this topic. Also, Mr. Craig Miller is acknowledged for performing the simulation runs.

6. REFERENCES

1. D. Mayo, *Error and the Growth of Experimental Knowledge,* University of Chicago Press, Chicago, IL USA, 1996.
2. H. Coleman and F. Stern, *Uncertainties and CFD Code Validation*, Journal of Fluids Engineering, Vol. 119, 1997.
3. D. Fraedrich and A. Goldberg, *A Methodological Framework for the Validation of Predictive Simulations*, European Journal of Operational Research, V. 124, 2000.
4. S. Shapiro, M. Wilk and H. Chen, *A Comparative Study of Various Tests for Normality* Journal of the American Statistical Association, Vol. 63, 1968.
5. K. Brown, H. Coleman, W. Steele, and R. Taylor *Evaluation of Correlated Bias Approximations in Experimental Uncertainty Analysis*, AIAA Journal, V 34, 1996.
6. D. Montgomery, *Design and Analysis of Experiments*, Wiley, New York, USA 1996.
7. International Organization for Standardization *Guide to the Expression of Uncertainty in Measurement,* ISBN 92-67-10188-9 ISO Geneva, 1993.
8. D. Vaitekunas and D. Fraedrich, *Validation of the NATO-Standard Ship Signature Model (ShipIR),* Proceedings SPIE Vol. 3699, 1999.
9. D. Fraedrich, *Methods in Calibration and Error Analysis for Infrared Imaging Radiometers*, Optical Engineering, Vol. 30, 1991.

SENSITIVITY ANALYSIS METHODS APPLIED TO RADAR RANGE TRACKER BEHAVIOR

A. Goldberg, S. Wolk, and R. Gover

Naval Research Laboratory TEW Division (Code 5750)
Washington DC 20375, USA

1. INTRODUCTION

The Naval Research Laboratory has developed an interesting application of model sensitivity analysis (SA) to radar range tracking in multiple target and diffuse target situations. The application is notable mathematically in that the tracker equations involved are fundamentally stochastic, non-linear and time-dynamic. The SA is performed at runtime on each solution sample path using auxiliary equations derived from the simulation's own dynamical equations. These auxiliary SA indicators are able to rank target importance in governing tracker behavior and indicate whether or not a genuine track condition exists or if the results are merely due to chance. Far greater testing efficiency is achieved by this method than physical testing or traditional modeling involving the tracker dynamics alone. Similarly, the process of model validation is simplified and strengthened because a clear an indication is provided per run of which targets or target features govern the outcome.

2. SYSTEM DYNAMICAL BEHAVIOR

The system of interest here is a radar target tracker that attempts to follow a specific target among a field of several possible alternatives. Think of a ship at sea as the target and a guided missile's radar seeker as the tracker. The tracker uses feedback control to maintain a small three-dimensional cell over the desired target as it moves. The cell represents the missile's estimated location of the missile's quarry. The cell is made small deliberately to help eliminate extraneous targets from influencing the tracker behavior. When an alternate target, such as a decoy, crosses through the cell, the intrinsic non-linear dynamics of the tracker follow the combination of both targets until one or another reach the boundary of the cell. See Figure 1. At such a moment, the tracker dynamics "make" a decision and the outcome is a selection of only one remaining target as being tracked from that time forward. It is important to analyze or simulate such a situation to determine the likelihood of tracker deception by an alternate target. It is even more important to understand

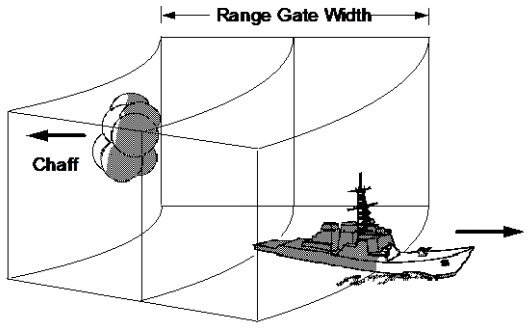

Figure 1. Ship and Decoy Competing Within Tracker Cell

why the deception occurred and how reliable alternate targets are at achieving this deception. This latter pursuit is tantamount to sensitivity analysis (SA).

For simplicity, we'll focus on the range tracker loop alone, setting aside azimuth and elevation tracking behavior. The basic model is [1], [2]:

$$\frac{d\rho}{dt} = \nu + e^{-2\eta}\int |E(t,\sigma)|^2 w_D(\sigma-\rho)d\sigma\,, \tag{1}$$

$$\frac{d\nu}{dt} = e^{-2\eta}\int |E(t,\sigma)|^2 w_D(\sigma-\rho)d\sigma\,, \tag{2}$$

$$\frac{d\eta}{dt} = e^{-2\eta}\int |E(t,\sigma)|^2 w_S(\sigma-\rho)d\sigma - 1\,. \tag{3}$$

The range tracker consists of two coupled non-linear feedback loops represented by differential equations. One of them, the range error loop, involves a pair of differential equations, and its job is to maintain an accurate estimate of target range, ρ, and estimated velocity, ν. The second loop, the automatic gain control (AGC), involves a first order differential equation, and its job is to stabilize the loop gain exponent, η, affecting the range estimator loops. Both feedback loops are driven by information supplied by the radar about the external world. This information signal, E, the so-called complex video envelope supplied by the radar, may be written as a raster signal parameterized by two time variables, t and σ. The variable t keeps track of radar pulses (sweeps), while σ denotes distance in the range dimension (range position within each sweep). The complex video envelope is thus also denoted $E(t,\sigma)$. The tracker's range estimate is denoted by ρ, which coincides with the cell position in range, its velocity is denoted by ν, and its AGC voltage denoted by η. The model involves three integrals with the kernel functions w_S and w_D. The kernel functions, design characteristics of the tracker, specify the precise method used by the tracker to derive the error laws. To represent a small cell tracker, these two functions are of compact support.

Each target in the environment is comprised of numerous scattering surfaces that reflect and redirect radar energy back to the radar receiver. The amplitude and phase of this scattered energy is determined for each scatterer by its directivity pattern and orientation with respect to the radar and the sea surface. The complex video envelope, $E(t,\sigma)$, is the superposition of the radar scattering returns from all the scattering surfaces of the targets in the range cell. It is stochastic in nature. The magnitude of $E(t,\sigma)$ is the driving function for the range gate tracker, and its stochastic fluctuations (along with the initial conditions of ρ and ν) determine the outcomes of our experiments.

3. IMPACT OF INDIVIDUAL TARGETS / SENSITIVITY ANALYSIS

In a real physical radar situation, the radar can only experience the environment as a total effect from all targets in the field of view. This is also true of conventional models, even high fidelity models that attempt to simulate the real environment and radar electronics. While such modeling may be extremely faithful to the physical problem at hand, it obscures the impact of each target (or each element within a target) upon the tracker response. By means of auxiliary equations, as described in what follows, far greater clarity is achieved. The superposition of individual scattering elements in $E(t,\sigma)$ permits us to write:

$$\int |E(t,\sigma)|^2 w_D(\sigma-\rho)d\sigma = \sum_i a_i(t) f\left(\rho - d_i^1\right) + \sum_j b_j(t) f\left(\rho - d_j^2\right) + [\ldots], \qquad (4)$$

where $f(\ )$ is the error law for a single unit amplitude scatterer, $a_i(t)$ and d_i^1 are the radar cross sections (RCS) and position, respectively, of the i^{th} ship scatterer, $b_j(t)$ and d_j^2 are the RCS and position, respectively, of the j^{th} decoy scatterer, and […] denotes cross terms. In our simulations, the range tracker experiences the entire integral in (4), including the cross terms. However, important simplifications can be made in order to derive efficient meaningful measures of individual target sensitivity. The dominant scatterers that comprise both of our targets are widely separated and target translation and rotation are relatively rapid. In addition, the second order range tracker dynamics provide smoothing over a succession of pulses. Because of this, the cross-terms occurring in (4) can be neglected in this sensitivity analysis. (As it turns out, the full composite target calculation in (4) is available at any time to substantiate the quality of this simplification.) The resultant approximation is:

$$\int |E(t,\sigma)|^2 w_D(\sigma-\rho)d\sigma \approx \sum_i a_i(t) f\left(\rho - d_i^1\right) + \sum_j b_j(t) f\left(\rho - d_j^2\right). \qquad (5)$$

The RHS of (5) can be seen as the sum of the individual target error characteristics, the ones that would be observed if only a single target was present. These individual target responses are what we mean by the auxiliary calculations. It is important to realize that the real physical system never gains access to individual terms expressed in (4) or (5). These sub-expressions are a prelude to sensitivity analysis.

For the sake of basic illustration in this paper, the equilibria associated with range estimate ρ are directly traceable to the zero crossings in (4) and its approximation (5). The trajectories of the zero crossings (equilibria) can be plotted in a simple fashion as the targets fluctuate and separate from one another. Which target is getting the attention can be discovered by comparing the individual target pictures with that of the composite. To illustrate these ideas, output from our simulation is presented in Fig. 2. These plots show range gate position and equilibria as a function of range-to-go for the case of two separating targets. The central points to be made here are that the trajectory of the range gate is governed by local conditions, and that auxiliary calculations can be made expressly to identify the model variables that most strongly influence these local conditions.

To understand Fig. 2, imagine a missile radar on the left, approaching a ship and a decoy that are separating in downrange. The downrange view is referenced to the ship center of gravity, located at 0. Time, or equivalently, range-to-go, evolves from the bottom of the plot to the top. The decoy is initially at far range. It moves to near range, passing over the ship, with final position some distance in front the ship.

The equilibria points for the composite error function, which includes both ship and decoy targets, are shown in Fig. 2(a). Asterisks represent stable equilibria, and open circles represent unstable equilibria. The continuous line in Figs. 2(a)-(c) is the trajectory of the range gate, ρ, as it tracks signal energy in accordance with (1) – (3). The range gate position follows the local stable equilibrium except in regions where the latter is moving too rapidly for the former to follow. The location of the equilibria points, an analytical calculation that is not performed by the range gate tracker, gives us powerful insight into the dynamical

behavior of the range tracker. Even so, the composite ship/decoy picture, Fig 2(a), does not isolate the influence of the individual targets on the range tracker trajectory.

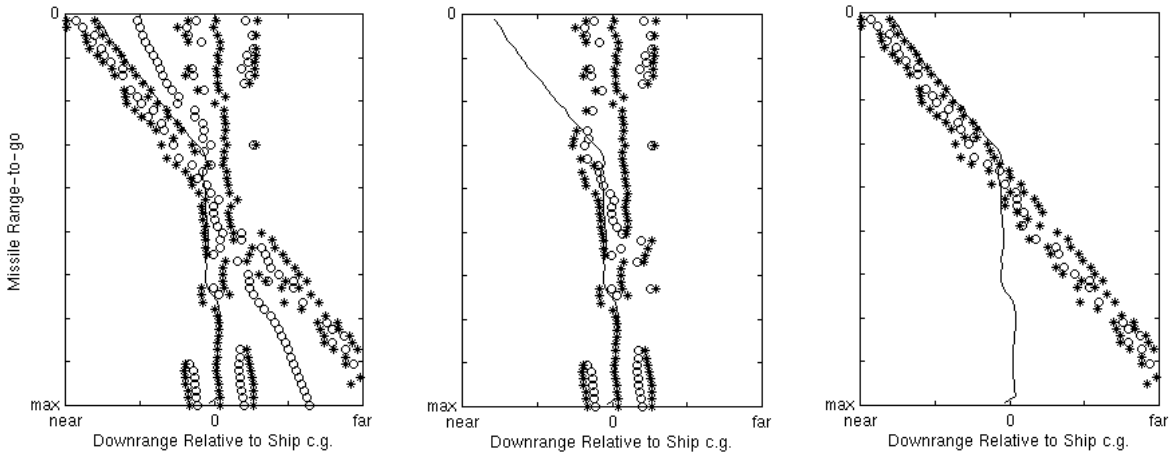

(a) Ship and Decoy (b) Ship only (c) Decoy only

Figure 2. Range gate trajectory and stable and unstable equilibria for two separating targets.

Figures 2(b) and 2(c), respectively, illustrate the stable and unstable track points for the ship only and for the decoy only that are derived from the auxiliary calculations. Between maximum and intermediate ranges-to-go, the range gate is solidly tracking the ship. Then the targets separate and a bifurcation emerges. Two loci of stable track points develop, and the range tracker must choose between them. Ultimately, the decoy is tracked. While Fig. 2 presents a global view of stability, in each region the range gate is actually responding only to the attractor or attractors (in the case of a bifurcation) local to the range gate position. Initially, range gate position is driven by only a subset of the ship scatterers. At bifurcation, it is strongly influenced by both local ship and decoy scatterers. At small ranges-to-go, the range gate is only affected by a subset of the decoy's scatterers.

4. CONCLUSIONS

We have identified of the most important driving variables for a nonlinear, stochastically driven simulation (a range gate tracker). We have identified the importance of model variables by inserting explicit, auxiliary calculations that identify the targets that most strongly influence each trajectory. Model validation is simplified and strengthened because a clear indication is provided per run of which targets or target features govern the outcome.

5. REFERENCES

[1] Abed, E.H., Goldberg, A.J., Gover, R.E., Nonlinear modeling of gated range tracker dynamics with application to radar range resolution. IEEE Trans. AES, 27(1991); also Report. NRL/TR/5753-92-9371, Naval Research Laboratory, Washington, D.C., Sept. 1992

[2] A.J. Goldberg, R.E. Gover and E.H. Abed, "Nonlinear Deterministic and Stochastic Radar Tracker Modeling and Analysis," NRL/FR/5750--96-9824, Naval Research Laboratory, Washington, D.C., Nov. 1996

VERY FAST PROBABILISTIC DOSE CALCULATIONS AND UNCERTAINTY ANALYSES

Allan Hedin

Swedish Nuclear Fuel and Waste Management Co.
SKB, P.O. Box 5864, SE-102 40 Stockholm, Sweden
Email allan.hedin@skb.se

1. INTRODUCTION

Probabilistic radionuclide transport and dose calculations are central in the evaluation of performance of nuclear waste repositories. It has recently been shown how the numerical models used for such calculations in a safety assessment of a deep repository for spent nuclear fuel in Sweden can be well approximated by closed form analytic expressions [1]. This paper demonstrates how the analytic model is used to extend the preliminary probabilistic analyses reported in the mentioned safety assessment.

In the KBS 3 concept for storage of spent nuclear fuel, the waste is placed in 5 cm thick corrosion resistant copper canisters with a cast iron insert giving mechanical strength. The canisters are surrounded by 35 cm bentonite clay and deposited in individual deposition holes at a depth of approximately 500 m in crystalline bedrock.

In the recently completed safety assessment SR 97 [2] of this concept, it is shown that *initially intact* canisters are expected to keep their isolating capacity for millions of years. An important scenario in the assessment treats *initially defective* canisters, e g due to imperfect sealing. Such deficiencies are today deemed unlikely but must be further evaluated by results from the development of fabrication methods for the canisters.

The consequences of the canister defect scenario are evaluated by numerical radionuclide transport and dose calculations. The numerical models for radionuclide transport in canister, buffer and geosphere have recently been approximated by closed form analytic expressions [1]. The analytic model was evaluated in a number of single realisations covering together the data uncertainties identified in SR 97. The agreement with the numerical models is good, both regarding maximum releases and overall time dependencies. For nuclides that dominate the total dose, the agreement is within a factor of two.

Figure 1 shows the results of probabilistic calculations with the two models. The numerical results are those presented in SR 97. Three sites in different parts of Sweden, all with real bedrock data, are evaluated. The same input, determined by detailed evaluation of data uncertainties in SR 97 [3], are used for both models. The calculation end-point is the maximum total annual dose to man in the time interval up to one million years after repository closure. The regulatory target is the expectation value of this quantity, which must not exceed $1{,}5 \cdot 10^{-4}$ Sv/yr for the situations discussed in this paper. (The Swedish compliance regulations were issued recently; discussions of their interpretation are on-going.)

The agreement is again good, with deviations in expectation values and standard deviations within a factor of two for all three sites. 5000 realisations per site were run with both models.

Commercially available software was used for the calculations with the analytic model. The numerical models and the probabilistic frame-work for them have been developed by SKB over the past decade. The numerical calculation required three weeks of computer time on dual SUN Ultra SPARC II CPUs whereas the corresponding analytic calculation was completed in less than an hour using an ordinary office PC.

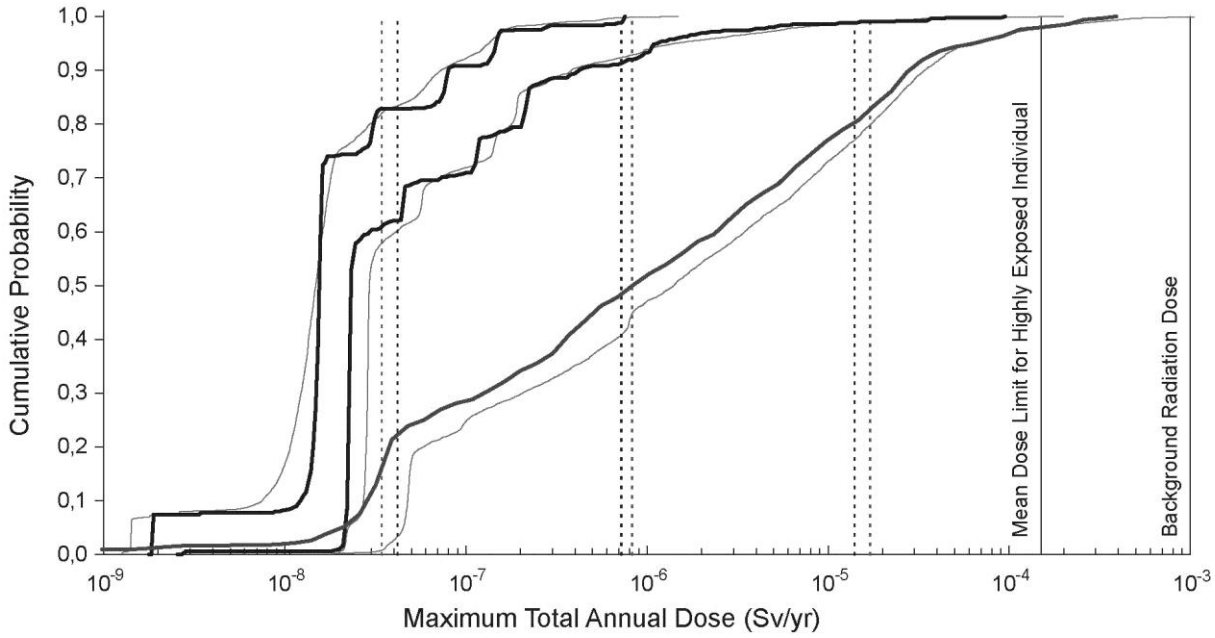

Figure 1. Cumulative distribution functions of maximum total annual doses for the three sites studied in SR 97 obtained with numerical (thin, grey) and analytic (thick, black) models. The dashed, vertical lines represent the expectation values of the distributions, which should be compared to the mean dose limit. The three sites Aberg, Beberg and Ceberg are about one, two and three orders of magnitude below the limit, respectively.

2. EXTENDED PROBABILISTIC CALCULATIONS

The probabilistic analyses in SR 97 were of a simplified and preliminary nature. In the following, results of extended probabilistic calculations using the analytic model are presented, giving insights into the probabilistic properties of the system.

For most input parameters, probability density functions (PDFs) were not determined in the SR 97 study, but only a reasonable, best estimate value, and a pessimistic, most unfavourable value, given current knowledge [3]. In the probabilistic calculations, the PDFs were simplistically taken to be bimodal distributions with p(reasonable) = 0.9 and p(pessimistic) = 0.1. This assumption is based on a general evaluation of the data for the calculations and was deemed to be on the pessimistic side. Hydrology data are an important exception; PDFs were determined through detailed groundwater modelling of the three sites.

An obvious complement to the simple approach taken in SR 97 is an exploration of different types of PDFs. A replacement of all bimodal PDFs by log-normal distributions, while preserving expectation values and variances, altered the shapes of the low dose parts of the distributions, whereas the high dose ends and most importantly the expectation values and standard deviations are rather similar to results with bimodal distributions, see Table 1.

Table 1. Expectation values (EV) and standard deviations (SD) of maximum total annual dose distributions for the cases discussed in this paper.

Site	Aberg		Beberg		Ceberg	
	EV (Sv/yr)	SD (Sv/yr)	EV (Sv/yr)	SD (Sv/yr)	EV (Sv/yr)	SD (Sv/yr)
Numerical model Base case	$1.7 \cdot 10^{-5}$	$6.3 \cdot 10^{-5}$	$8.2 \cdot 10^{-7}$	$6.9 \cdot 10^{-6}$	$3.3 \cdot 10^{-8}$	$7.7 \cdot 10^{-8}$
Analytic model Base case	$1.5 \cdot 10^{-5}$	$4.7 \cdot 10^{-5}$	$7.1 \cdot 10^{-7}$	$3.4 \cdot 10^{-6}$	$4.1 \cdot 10^{-8}$	$7.5 \cdot 10^{-8}$
Analytic model log-norm PDFs	$2.2 \cdot 10^{-5}$	$1.0 \cdot 10^{-4}$	$1.2 \cdot 10^{-6}$	$1.2 \cdot 10^{-5}$	$4.0 \cdot 10^{-8}$	$7.9 \cdot 10^{-8}$
Analytic model I-129 + Ra-226	$2.1 \cdot 10^{-5}$	$1.2 \cdot 10^{-4}$	$1.4 \cdot 10^{-6}$	$1.5 \cdot 10^{-5}$	$3.9 \cdot 10^{-8}$	$8.9 \cdot 10^{-8}$
Analytic model Geochem. corr.	$1.9 \cdot 10^{-5}$	$7.0 \cdot 10^{-5}$	$1.4 \cdot 10^{-6}$	$7.2 \cdot 10^{-6}$	$1.5 \cdot 10^{-7}$	$6.5 \cdot 10^{-7}$
Analytic model Biosphere corr.	$1.4 \cdot 10^{-5}$	$5.0 \cdot 10^{-5}$	$5.2 \cdot 10^{-7}$	$2.6 \cdot 10^{-6}$	$3.6 \cdot 10^{-8}$	$6.8 \cdot 10^{-8}$

Uncertainty analyses using rank order correlations reveal that the hydrological indata has the dominating influence on the output uncertainty. Also the biosphere input data and the likelihood of initial canister defects are important, two areas where much research is being carried out at present.

Scatter plots show that, for all sites, either only I-129 or only Ra-226 of the 32 nuclides analysed, contribute significantly to the total dose in almost all realisations. A re-run with only these two nuclides yields an almost unchanged result, see Table 1, meaning that a number of nuclide specific input parameters do not significantly impact the resulting dose distributions.

The geochemical properties of a site influence several parameters in the transport calculations, which could thus be expected to be partially correlated. To determine an upper bound on the effects of such correlations, the bimodal PDFs of all geochemistry dependent transport parameters in canister, buffer and geosphere were forced to take either their reasonable ($p = 0.9$) or pessimistic ($p = 0.1$) value simultaneously. Even this full correlation yields mostly minor effects on both the shape of the resulting dose distributions and on their statistics, see Table 1. The effect is most pronounced for the Ceberg site, where doses from Sn-126 become significant with fully correlated geochemistry related data.

Similarly, the biosphere input data for different nuclides may be assumed to be correlated since several conditions in the biosphere influence all nuclides in a similar manner. Also in this case, a full correlation reveals only a minor influence on the distributions and their statistics, see Table 1. This finding is compatible with the dominance of only one nuclide in almost all realisations.

3. DISCUSSION

This paper demonstrates how, in this particular case of radionuclide transport modelling, complex numerical models can be replaced by analytic approximations which can subsequently be used to study the probabilistic properties of the system. Calculation speed is thereby improved by almost three orders of magnitude. Both approaches do however rely on data from elaborate and time consuming modelling of both groundwater flow and the turn-over of radionuclides in the biosphere.

The simple calculation exercises reported here, point out fields of research where further knowledge may yield improved calculated performance (biosphere studies, canister sealing technique) and other fields where this is not likely to be the case.

Most of the width of the output distributions is caused by hydrology parameters, which are influenced by both uncertainty and spatial variability of the hydraulic properties of the bedrock. This emphasises the importance of the quality of i) the groundwater modelling yielding input to the transport calculations and ii) the site data on which groundwater modelling is based. Moreover, the naturally occurring spatial variability puts a limit on the extent to which calculated performance may be enhanced through improved knowledge of the site.

Furthermore, it has been shown that correlations, which might be expected for physical reasons but are difficult to quantify, have in general a limited influence on the calculation end-point and how an upper bound of these influences can be determined.

Concerning PDFs for parameters where these are difficult to determine objectively, correct expectation values and variances are crucial, whereas the type of distribution assumed is of secondary importance.

Considering that this probabilistic modelling exercise is based on bedrock data from three different sites in Sweden, and on extensively evaluated data for the near field barriers, the above conclusions can be expected to be valid also for other sites, which are about to be investigated as candidates for a deep repository. This will have to be confirmed by renewed both analytic and numerical calculations for these sites. Analytic expressions of this kind are however not meant to replace numerical models. The analytic expressions will always have to be verified against numerical models, for the data set and calculation cases under consideration in a particular calculation exercise.

4. REFERENCES

1. Hedin, A; Integrated Analytic Radionuclide Transport Model for a KBS 3 Repository; Swedish Nuclear Fuel and Waste Management Co; To be submitted to *Nuclear Technology* 2001.
2. Deep repository for spent nuclear fuel; SR 97 – Post-closure safety. Parts I and II. Swedish Nuclear Fuel and Waste Management Co., Stockholm 1999.
3. Andersson, J; SR 97 – Data and Data Uncertainties; SKB Technical Report TR-99-09; Swedish Nuclear Fuel and Waste Management Co., Stockholm 1999.

AN OPTIMIZATION ALGORITHM BASED ON STOCHASTIC SENSITIVITY ANALYSIS

Hiroyuki Okano[(1)] *and Masato Koda*[(2)]

IBM Research, Tokyo Research Laboratory
1623-14 Shimotsuruma, Yamato,
Kanagawa 242-8502 (Japan)
Email: okanoh@jp.ibm.com

Institute of Policy and Planning Sciences
University of Tsukuba Tenno-dai, Tsukuba,
Ibaraki 305-8573 (Japan)
Email: koda@shako.sk.tsukuba.ac.jp

SUMMARY

A new optimization algorithm based on stochastic sensitivity analysis is described and its performance is evaluated. The relationship between the performance and the roughness of objective landscapes is also discussed by using the notion of fractal dimension.

1. INTRODUCTION

When an objective function to be minimized is differentiable or has certain smooth property, many optimization techniques are available, e.g., gradient methods, mathematical program-ming, etc. For discrete problems, problem-specific approaches are often required because solutions need to utilize problem-specific neighbourhood structures. In this paper, a new gradient-based optimization algorithm that uses stochastic sensitivity analysis is presented. The algorithm, referred to as Stochastic Noise Reaction (SNR) [1], can locally minimize arbitrary objective functions, such as non-differentiable or discrete functions, whenever their objective landscapes have a certain roughness (smoothness) in a stochastic sense. Because the computation of a gradient is problem-independent, SNR may cope with the discrete problems efficiently independent of the neighbourhood structures. In [1], SNR was shown to be applicable to combinatorial optimization problems. This paper focuses on its performance analysis compared to a deterministic algorithm and another stochastic algorithm, i.e., Simulated Annealing (SA). The present paper also focuses on the relationship between their performances and the roughness of the objective landscapes. Because of limitations of space, only the continuous functions $\tanh^2(x)$ and XOR are treated for the numerical experiments.

2. METHODOLOGY

Consider an optimization problem: Minimize $f(x)$ subject to $x \in S$, where a state x is an n-dimensional column vector, and the feasible domain S is a set in R^n. Conventional Gradient-based methods iteratively update the current solution (state) x so that the objective function $f(x)$ is locally minimized as follows:

$$x \leftarrow x + \mu \frac{\delta x}{|\delta x|}, \quad \delta x = -\nabla f(x), \quad \nabla f(x) = \left(\frac{\partial f(x)}{\partial x_1}, \frac{\partial f(x)}{\partial x_2}, \ldots, \frac{\partial f(x)}{\partial x_n} \right)^T . \qquad (1)$$

Unlike the deterministic algorithms that use partial derivatives for sensitivity information, SNR approximates each component of a gradient vector by using additive Gaussian white noise. In SNR, a Gaussian white noise sequence, $\xi_i \in N(0,1)$, is injected into each variable x_i, and each component of a corresponding sensitivity derivative is approximated by

$$E\left[\frac{\partial f(x)}{\partial x_i}\right] = \frac{1}{M}\sum_{j=1}^{M} f(x^j)\xi_i^j, \quad x_i^j = x_i + \xi_i^j, \tag{2}$$

where $E[\cdot]$ denotes the expectation operator, M is a loop count for taking the average, ξ_i^j denotes the j-th noise in the noise sequence injected into the i-th variable, and x_i^j is a realization of a stochastic variable of x_i into which ξ_i is injected. Note that, in (2), Novikov's theorem $E[\delta H(\xi)/\delta\xi_i] = E[H(\xi)\xi_i]$ has been used, where $H(\xi)$ is an arbitrary functional of a Gaussian white noise sequence ξ_i, $i = 1,2, \cdots, n$, and $\delta H(\xi)/\delta\xi_i$ denotes the functional derivative. Note also that, in (2), all of the n components of gradient vector are computed at the same time.

SNR is performed following the algorithmic framework described in Fig. 1. In Step 4, a step width μ_k is gradually decreased from $\mu_{\max}$ to $0.1\mu_{\max}$. Step 12 adjusts each state variable x_i to the value range $[x_{\min}, x_{\max}]$.

1. Initialise the current solution $x := x^0$.
2. Initialise the best solution $x^{best} := x$.
3. For $k := 1,2,\cdots,N$ do begin
4. $\mu_k := \mu_{\max}(1 - 0.9(k-1)/(N-1))$.
5. Initialise decent direction $\delta x := 0$.
6. For $j := 1,2,\cdots,M(=100)$ do begin
7. Generate a noise vector ξ^j.
8. $\delta x_i := \delta x_i - f(x^j)\xi_i^j$.
9. If $f(x^{best}) > f(x^j)$ then $x^{best} := x^j$.
10. end;
11. $x := x + \mu_k \delta x/|\delta x|$.
12. $x_i := \max\{\min\{x_i, x_{\max}\}, x_{\min}\}$.
13. If $f(x^{best}) > f(x)$ then $x^{best} := x$.
14. end;
15. Output x^{best}.

Figure 1. Algorithmic framework of SNR.

2.1. Measure of roughness: fractal dimension

In this study, the roughness of an objective landscape (also referred to as an energy landscape or a fitness landscape in different contexts) is measured by the value of H inherent in the following relationship, called a *power-law* relation [2]:

$$E[(f(\tilde{x}) - f(x))^2] \propto d(\tilde{x}, x)^{2H}, \tag{3}$$

where $d(\tilde{x}, x)$ is a distance function. Note that the power-law relation (3) depicts an evidence of fractal property. Intuitively, in fractal functions, good solutions are distributed around good ones, and local-search- or gradient-based heuristics work well for such functions. The value of H is computed by plotting $E[(f(\tilde{x}) - f(x))^2]$ and $d(\tilde{x}, x)^{2H}$ for randomly sampled pairs of solutions on a log-log scale and fitting a straight line to the data. When the data does not fit a line, it is fit to portions of the data within small distances (Fig. 2). When the value of H is small, the objective landscape is harsh, while the landscape is moderate when H is large.

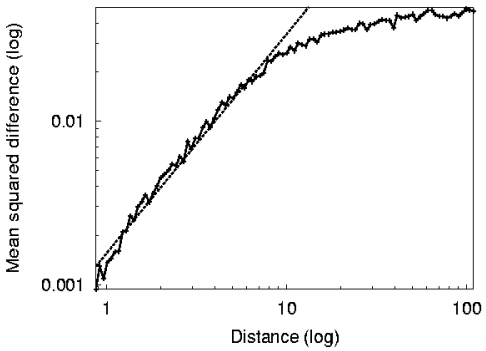

Figure 2. Mean squared functional differences against distances between randomly sampled data pairs for XOR.

2.2. Other methods used for comparison

A deterministic algorithm with the framework described in Fig. 1, called DA in this paper, is used for comparison with SNR. In DA, Steps 5 to 10 are replaced by $\delta x = -\nabla f(x)$. Simulated annealing (SA) was also considered. In SA, Step 4 is replaced by $T = 0.999^k$, i.e., geometric cooling, and Steps 5 to 11 are replaced by a neighbourhood generation step, $\tilde{x} \in N(x,b)$, and a transition step. Each neighbourhood solution in $N(x,b)$ is defined as $x_i + \varepsilon_i$ for randomly selected b variables, where $\varepsilon_i \in [-1,+1]$. The parameter $1 \le b \le n$ specifies the size of the neighbourhood. In the transition step, the generated solution $\tilde{x}$ is accepted, i.e., $x \leftarrow \tilde{x}$, if $\Delta f = f(\tilde{x}) - f(x) < 0$ or with probability $e^{-\Delta f / T}$.

3. NUMERICAL EXPERIMENTS

3.1. Application to $\tanh^2(x)$

SNR was applied to minimize $f(x) = \tanh^2(x)$, which has a narrow valley around its global minimum at $x = 0$. The values of N and $\mu_{\max}$ were set to 100 and 0.5, respectively; i.e., $\sum_{k=1}^{N} \mu_k = 27.5$. Theoretically, SNR starting from $x^0 \in [-27.5,+27.5]$ should find the global minimum. Figure 3 shows average values of x^{best}, plotted against x^0. The simulations starting from $x^0 \in [-20,+20]$ converged to $x = 0$ with high probability. SNR did not converge to the global minimum from the region where $df(x)/dx \approx 0$, i.e., when the sensitivity information of SNR fails to provide the correct descent direction.

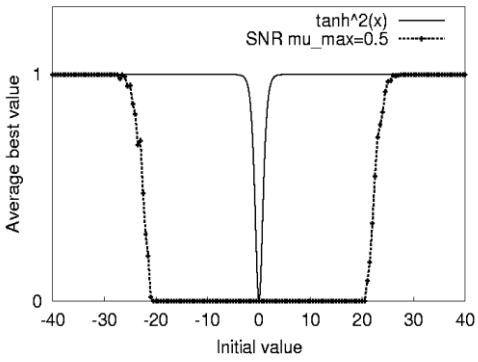

Figure 3. Initial and average best values by SNR minimizing $\tanh^2(x)$.

3.2. Application to the logical XOR function

SNR, DA, and SA were applied to XOR (the logical XOR function), which is modelled as a layered neural network that has $m = 2$ input units, m hidden units, and one output unit. It has additional threshold units in the input and the hidden layers, respectively. Each

component of x represents a connection weight in the network; therefore, the dimension of x is $(m+1)^2$; i.e., $n=9$. The signal transmission function used in the neural network is $S(y)=\tanh(s\cdot y)$ where s is a constant to control the slope of the function around the origin and is set to 0.5. The maximum number of iterations was set to $N=100$ for SNR and DA, and 3000 for SA.

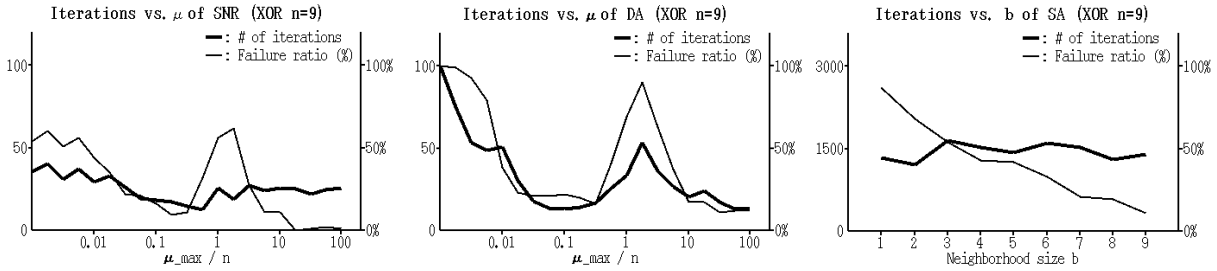

Figure 4. Results of SNR (left) and DA (centre) for XOR, plotted against $\mu_{\max}/n$, and result of SA (right) for XOR, plotted against the neighbourhood size b.

Figure 4 shows results of SNR, DA, and SA. Thick lines show the average numbers of iterations required for convergence, and thin lines show ratios of failed simulations, i.e., fractions of simulation runs that could not learn the XOR pattern. The graph shapes of SNR and DA are similar. They were both minimized around $\mu_{\max}/n=0.2$, and further reduced when $\mu_{\max}$ is large. This may be because the number of local minima is small, while SNR and DA generate many solutions in the feasible domain in almost random fashion when $\mu_{\max}$ is large. The performance of SNR is better than DA in this case. (This is generally not true for higher dimensional functions, and DA is usually preferable when a function is differentiable.) The performance of SA simply depended on the neighbourhood size. Note that the result of SA also depends very much on the maximum number of iterations, and so that the result in Fig. 4 could be improved if the number is larger. The results are presented only to illustrate the trend of the performance with respect to the neighbourhood size.

3.3. Relationship to the roughness of the objective landscape

The parameter s in the neural network was changed between 0.1 and 5.0 to control the fractal dimension of XOR. When s was set to 0.1, the parameter H was about 0.97, which means that the landscape is moderate, and it was about 0.43 when s was set to 5.0, which means the landscape is harsh. The parameter $\mu_{\max}/n$ was fixed at 0.2 for both SNR and DA, and the parameter b of SA was fixed at 5. Figure 5 shows the relationships between the failure ratios and the roughness of the objective landscape of SNR, DA, and SA. The figure depicts that the two stochastic search algorithms, SNR and SA, are less sensitive to the roughness of the objective landscape

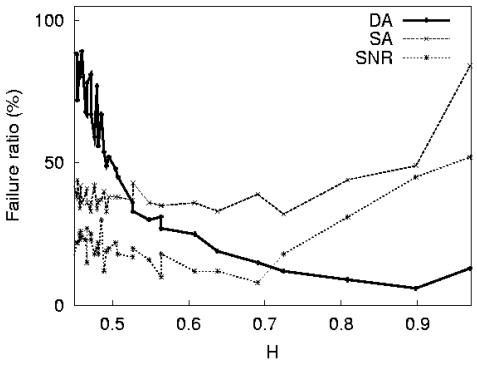

Figure 5. Relationship between performances of SNR, DA, and SA and the roughness of the objective landscape of XOR.

when the landscape is harsh, while DA is more affected. When the landscape is moderate, DA outperformed the stochastic search algorithms. The remarkable point is that SNR and SA exhibit similar relationships, although an explicit hill-climbing mechanism is not provided in SNR. This is because SNR levels the sensitivity information around a current solution in the gradient approximation (Steps 5 to 10) in a stochastic sense.

4. DISCUSSION

It was shown that the stochastic sensitivity approach provides correct descent direction unless the sensitivity is nil (Fig. 3). The convergence property of the present stochastic method, SNR, was comparable to that of the deterministic algorithm, DA (Fig. 4). SNR outperformed DA when the objective landscape was harsh, and the convergence property of SNR was similar to SA (Fig. 5). The performance of SA depended on the neighbourhood size; i.e., SA requires larger neighbourhood as the problem dimension increases. Note that SNR can be scalable to higher dimensional problems without much additional effort.

5. REFERENCES

[1] H. Okano and M. Koda, "A New Noise-Based Gradient Method and Its Applications," *IBM Research Report*, RT0390, 2000.

[2] G. B. Sorkin, "Efficient Simulated Annealing on Fractal Energy Landscapes," *Algorithmica*, Vol. 6, pp. 367-418, 1991.

DO GENETIC ALGORITHMS PARAMETER OPTIMIZATION STRATEGIES CONVEY ANY INFORMATION ON THE IMPORTANCE OF THE PARAMETERS?

Marzio Marseguerra, Luca Podofillini, Enrico Zio

Department of Nuclear Engineering, Polytechnic of Milan
Via Ponzio 34/3, 20133 Milan, Italy
Email: marzio.marseguerra@polimi.it

ABSTRACT

In this paper, we investigate the evolution strategy followed by a Genetic Algorithm (GA) in finding the optimal estimates of the effective parameters in a lumped nuclear reactor model of literature. It is shown that the GA evolves towards convergence in such a way to stabilize first the most important parameters of the model and later those which influence little the model outputs. In this sense, besides estimating efficiently the parameter values, the optimization approach also allows us to provide a qualitative ranking of their importance in contributing to the model output. The results thereby obtained are in good agreement with those derived from a variance decomposition-based sensitivity analysis.

1. INTRODUCTION

Genetic algorithms are numerical search tools used for the optimization of a multivariate function (called fitness or objective function) [1-3]. The search of the optimal solution is basically performed proceeding from one group (population) of possible points in the search space to another, according to procedures that resemble those of natural selection and genetics and designed such as to steer the search towards better solutions. While evolving through its generational steps, the algorithm examines and evaluates several solution points in the search space, before converging to the best solution. The significant amount of data thereby handled contains relevant information on the search space and on the model characteristics so that it seems worthwhile to make an effort to appropriately process these data so as to extract additional, spin-off results.

This work aims at analysing the evolutionary process of the genetic algorithms in order to infer qualitative information on the importance of the optimization control variables with respect to the objective function. More precisely, in our study we start from the observation that in the process of convergence some variables tend to set earlier than others. A tempting conjecture, to be verified, is that the genetic algorithms optimization strategy proceeds by adjusting first the most important variables, i.e. those which mostly influence the objective function, and worries only at a later stage about tuning the other less important variables which determine only minor variations to the fitness function. If this conjecture were true, then we could expect to be able to extract information on the importance of the control variables governing the objective function from the analysis of the evolution process towards convergence.

In the next Section, we look into the genetic algorithms' evolution procedure. In Section 3 the nuclear reactor model application is illustrated. A short discussion ends the paper.

2. ANALYSIS OF THE GENETIC ALGORITHM'S EVOLUTION

In our work, the analysis of the GA process towards convergence is performed on a suitably devised archive containing a given number of different best solutions, each solution being a vector of values of the control variables, and consists in investigating, for each control variable, how the first and second order statistics of the archived best solutions set behave through the successive generations. Of particular relevance is, thus, the construction and management of the archive.

After each generation, the best chromosome-solution's fitness value is compared to those of the individuals already present in the archive:

- if the archive's capacity is not filled up, then the current generation best chromosome is inserted;
- otherwise, if the current generation best chromosome's fitness value is larger than, and sufficiently different from, that of any of the already archived chromosomes, the current generation best chromosome is added to the archive and the archived chromosome with smallest fitness is discarded.

Thus, the archive set-up amounts to considering all chromosomes-solutions ever encountered throughout the generations, ranking them in increasing order of fitness, discarding the replicas (i.e. those chromosomes which appear in the list more than once) and keeping only a given number of the different individuals with the highest fitness values in the list.

3. APPLICATION TO A SIMPLIFIED NUCLEAR REACTOR MODEL

We consider the simple Chernick's nuclear reactor model [4, 5] to be used for predicting on line the reactivity variation necessary to adapt the power production to the loads of the electrical grid. In order to predict the system behavior starting from a given time t_0, we use pseudo experimental (i.e. obtained by simulation) power and reactivity data taken from the past reactor history back to a time t^{**} preceding t_0 by, say, five days (several characteristic times of the Xe and I dynamics). The interval (t^{**}, t_0) is further divided into two subintervals: (t^{**}, t^{*}) during which we only use the reactor power, and (t^{*}, t_0) during which both the reactor power and the reactivity changes with respect to the value at t^{*} are used as experimental data. The model equations, written in terms of the available data, i.e. the reactor power $P = \Sigma_f \phi$ and the reactivity variation $\Delta\rho(t) = \rho(t) - \rho(t^{*})$, are:

$$\Lambda \frac{dP}{dt} = [\rho(t^{*}) + \Delta\rho - \frac{\sigma_X}{c\Sigma_f} Xe - \frac{\gamma}{\Sigma_f} P]P \qquad (1)$$

$$\frac{dXe}{dt} = \gamma_x P + \lambda_I I - \lambda_x Xe - \frac{\sigma_x}{\Sigma_f} XeP \qquad (2)$$

$$\frac{dI}{dt} = \gamma_I P - \lambda_I I \qquad (3)$$

where ρ is the reactivity; $\Phi(cm^{-2}s^{-1})$ is the flux; $Xe(cm^{-3})$ and $I(cm^{-3})$ are the Xenon and Iodine concentrations, respectively; Σ_f (cm^{-1}) is the effective fission macroscopic cross section; $\sigma_x\,(cm^2)$ is the effective Xenon microscopic cross section; γ_x and γ_I are the Xenon and Iodine fission yields, respectively; λ_x (s^{-1}) and $\lambda_I\,(s^{-1})$ are the Xenon and Iodine decay rates; $\Lambda\,(s)$ is the effective neutron mean generation time. The temperature and Xenon feedbacks are modeled via the introduction of two lumped parameters, namely: the temperature feedback coefficient, $\gamma\,(cm^2 s)$ and the adimensional conversion factor of Xenon concentration to reactivity, *c*.

In this model, the assumed values for the known nuclear constants are $\gamma_x = 0.003$, $\gamma_I = 0.061$, $\lambda_x = 2.09*10^{-5}$ s^{-1}, $\lambda_I = 2.87*10^{-5}$ s^{-1} and the values to be estimated are the quintuplet of effective parameters $\frac{\sigma_x}{\Sigma_f}$, $\frac{\gamma}{\Sigma_f}$, c, $\Lambda, \rho(t^*)$ plus the Xe and I concentration at t^*. The model is admittedly very simple but the use of effective parameters to be periodically updated renders it potentially very reliable. Thus, the strength of this approach mainly rests in the capability of estimating the effective parameters. In addition to the effective parameters, the initial concentrations of Xe and I should also be estimated.

For the genetic algorithm, we consider chromosomes made up of five genes, each one coding one of the five effective parameters. Table 1 contains the relevant data. Each population is composed of 1000 chromosomes. As objective function to be optimized, we consider the inverse of the average squared residuals R between the experimental power history and the computed one normalized to the nominal power, summed over a succession of 2001 discrete time points $t_i \in (t^*, t_0)$.

The values found by the genetic algorithm are reported in the second-to-last column of Table 1. The resulting power profile from t^* to t_0 turns out to be in very good agreement with the corresponding (pseudo)experimental profile. Now, at the present time t_0, we have available a 'good' model, all its effective parameters and the Xe and I values, so that we can predict the reactivity changes needed to satisfy future power load variations.

Table 1**: genetic algorithms data and parameters values for the reference power load profile**

	Simulation phase	Genetic Algorithms			
Parameter	True value	Range (±50%	# bits	GA value	Relative error (%)
C	1.3606	0.6-2.0	10	1.2938	5.0
γ/Σf*1016	8.3802	4.0-12.0	10	8.7148	4.0
σx/Σf*1018	3.5358	1.75-5.25	10	3.5290	0.2
Λ*102	8.3000	4.0-13.0	10	9.8652	20.8
ρ0*102	1.5063	0.75-2.5	10	1.3695	10.6

Note that the described genetic algorithms procedure leads to very good results even though one of the parameters, namely the generation time Λ, has a relative error close to 20% (Table 1), thus suggesting a scarse sensitivity of the results to such parameter. The larger error in the estimation of the mean generation time Λ is due mainly to the fact that in eq. (1) Λ multiplies the derivative of the power which is zero most of the time, except during the power variations: since these last only half an hour, not much information is provided for the estimation of Λ.

3.1. Analysis of the genetic algorithm's evolution process

The purpose of this analysis is to extract some information on the relative sensitivity of the model to the different parameters. Figure 1 shows the behaviour of the square of the coefficient of variation as a function of the generations. The variable σ_x/Σ_f is shown to converge first, followed by $\rho(t^*)$, γ/Σ_f, and *c*. The parameter Λ is shown to converge much slowlier, thus confirming a relatively smaller sensitivity of the model to such parameter. Similar conclusions can be drawn by an analysis of the behaviour through the successive generations of the sample means of the parameter values characterizing the individuals in the archive (here not reported for brevity).

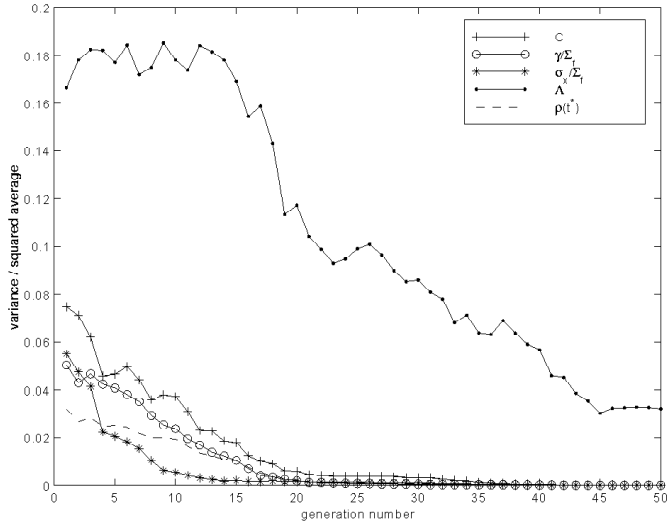

Figure 1: square of the coefficients of variation as a function of the generations

The qualitative sensitivity ranking thus far obtained is in agreement with the results obtained by a standard variance decomposition analysis [6], whose sensitivity coefficients values are defined as $\eta^2_{X_s} = V[E(y|x_s)]/V[y]$. These coefficients measure how much of the unconditional variance V[y] of the model output y is accounted for, by the variance of the expected value of y conditioned on the input parameter x_s. The values obtained are $2.47\cdot10^{-3}$, $2.06\cdot10^{-3}$, $1.32\cdot10^{-3}$, $1.00\cdot10^{-3}$, $3.15\cdot10^{-4}$ for the parameters σ_x/Σ_f, $\rho(t^*)$, γ/Σ_f, *c*, Λ, respectively.

4. CONCLUSIONS

Genetic algorithms are optimization methods based on procedures which resemble those of natural selection and genetics. While performing its steps, the method evaluates several solution points within the search space, thus offering the possibility of disclosing the characteristics of the underlying model object of the optimization.

In this paper we have shown that the genetic algorithm convergence procedure at first is effective in settling the most important variables to their best values, and only afterwards in focussing on the tuning of the less important variables. Thus, the succession of convergences of the variables throughout the generations gives a qualitative indication of the importance of the variables with respect to the function objective of the optimization.

5. REFERENCES

1. J.H. Holland, (1975). *Adaptation in Natural and Artificial Systems*, University of Michigan Press, Ann Arbor, MI.
2. D.E. Goldberg, (1989). *Genetic Algorithms in Search, Optimization, and Machine Learning*, Addison-Wesley Publishing Company.
3. L. Chambers, (1995). *Pratical Handbook of Genetic Algorithms*, Vol. 1 and 2, CRC Press.
4. M. Marseguerra, E. Zio, (2000). *Genetic Algorithms for Estimating Effective Parameters in a Lumped Reactor Model for Reactivity Predictions*, accepted for publication in Nuclear Science and Engineering.
5. J.Chernick, (1960). *The Dynamics of a Xenon-Controlled Reactor*, Nuclear Science and Engineering **8**, pp. 233-243.
6. M.D. McKay, (1995). *Evaluating prediction uncertainty*. Tech. Rep. NUREG/CR-6311, U.S. Nuclear Regulatory Commission and Los Alamos National Laboratory.

EMULATOR-BASED GLOBAL OPTIMISATION USING LATTICES AND DELAUNAY TESSELATION

R A Bates[(1)] & L Pronzato[(2)]

[(1)] Dept. of Statistics, University of Warwick, Coventry CV4 7AL, UK.

[(2)] Laboratoire I3S, CNRS--UNSA, bât. Euclide Les Algorithmes, 2000 route des Lucioles, BP 121 06903 Sophia-Antipolis Cedex, France

1. SUMMARY

Emulators are fast statistical approximations of engineering systems or simulators used to increase the speed of analysis for design optimisation. This paper presents a method intended for global optimisation of engineering systems using design of experiments and emulators in a unified fashion. The Rosenbrock optimisation example describes the method.

2. INTRODUCTION

The use of Design of Experiments (DoE), modelling and optimisation in engineering is well-established for cases where a product or process is too complex for a complete whole-system model to be identified, or, where a model is available, but computationally too expensive to evaluate[1]. The idea is to use DoE to test the system, or a computer simulation of the system, at specific combinations of input factors, gather the results and use this data to build a more efficient empirical approximation to the system which can then be used for optimisation. These approximate models are variously called meta-models, low-fidelity models, surrogates or emulators, but their purpose remains the same: to approximate the system response. Areas where this technology is useful can be characterised by: (i) high number of (important) input factors, $\mathbf{x}=x_1,\ldots,x_d$, (ii) several system responses (multi-objective), $\mathbf{y}=y_1,\ldots,y_d$, (iii) possibly highly constrained input and response spaces, (iv) high cost of evaluating design points $\mathbf{s}_i=s_1,\ldots,s_d$. In this paper we focus on complex systems that match the above characteristics, specifically the combined use of experimentation, modelling and optimisation, in order to present an efficient and holistic method of optimisation for use in engineering design.

3. SEQUENTIAL DESIGN AND OPTIMISATION

Performing experiments is costly and the goal is often straightforward optimisation so it is reasonable to proceed sequentially. What is required is to calculate the expected improvement in the current minimum value of y when the next design point is evaluated. It could well be the case that, in parts of the design space that are poorly modelled, the expected improvement is very high. The generalised expected improvement criterion $I^g(\mathbf{x})$, as described in [4,5], can be used to indicate the best location of additional design points to improve the emulator model. It is defined as the expected value of

$$I^g(x) = \begin{cases} [y_{\min} - y(x)]^g & \text{if.} y(x) < y_{\min} \\ 0 & \text{otherwise} \end{cases} \quad (1)$$

where $g \geq 0$ is an integer-valued parameter that controls how globally the function searches the design space (in this paper g is set to 2), and where, in the DACE model, the prediction $y(\mathbf{x})$ is a Gaussian random variable, with known mean $\eta(\mathbf{x})$ and variance $v(\mathbf{x})$. Thus the search for an optimal point in the design space is guided by the emulator model. An algorithm for combined sequential experimentation, modelling and optimisation is as follows: (i) compute an initial space-filling experiment (e.g a lattice design), (ii) fit an emulator to the experimental data, (iii) select a new design point that maximises the expected improvement of the model, (iv) evaluate the design point and return to (ii), (v) stop adding points when the expected improvement drops below a pre-defined threshold value. In this way the quality of the emulator is refined until it reaches the desired level of prediction accuracy. The emulator can then be used to predict the optimal point that can be confirmed with a final experiment. In practice there are some problems to be resolved before this procedure can be of use. The first is that, as the algorithm converges, design points tend to be placed very close together, leading to conditioning problems in model fitting. For example, using the DACE emulator, the covariance matrix rapidly tends towards being singular, which affects predictions such that the algorithm does not converge. Another problem is in ensuring a global search of the design space. If the function for expected improvement is used to determine the next design point it may become trapped in a local minimum and not explore the whole design space for the best point. In order to overcome these difficulties one possibility is to restrict the selection of design points to a candidate set defined by an integer lattice. This means that the design points will always be a certain minimum distance apart, and also that the design space can be more fully explored to find the best next point in the sequence.

4. LATTICE-BASED EXPECTED IMPROVEMENT

Integer lattices are used widely in numerical integration due to their excellent space-filling properties in high dimensions. In order to demonstrate the approach outlined in this paper, the well-known 2-dimensional Rosenbrock function ($y = 100(x_2-x_1^2)^2 + (1-x_1)^2$) is used as a test case with $x_1, x_2 \in [-2 , +2]$. The minimum value for y is 0 and can be found at x_1=1, x_2=1. A lattice in d=2 dimensions with N=100 points is used as a candidate set and n=7 well-spaced points are chosen from it by hand as an initial experimental design, $S=\mathbf{s}_1,\ldots,\mathbf{s}_n$ and used to obtain response values $Y=y_1,\ldots,y_n$, $y_i=y(\mathbf{s}_i)$, i=1,…,n. An initial DACE model is fitted to the [S,Y] pairs and $I^g(\mathbf{x})$ is evaluated at each of the remaining points in the candidate set to determine the next design point, which is then evaluated and removed from the candidate set. In all 10 additional points were evaluated, the algorithm terminating due to the threshold condition $I^g(\mathbf{x}) < 10^{-3}$ (see (1)). The final DACE model predicted the optimal point to be at x_1=0.989, x_2=0.974 with a function value of $\hat{y}^*$=-0.42 compared with an actual value of y^*=0.0013. This result should be compared with the actual minimum of y=0 at x_1=1, x_2=1.

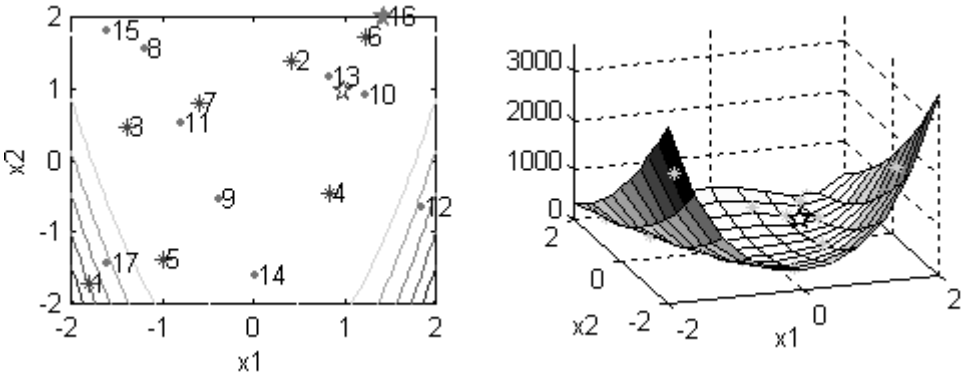

Figure 1: Optimisation results for Rosenbrock function

Fig.1 shows the results of optimising the Rosenbrock function using $I^g(\mathbf{x})$.

The left-hand plot shows the contours of the original Rosenbrock function with the initial design points (asterisks), the added points (dots), the best design point evaluated so far (solid star) and the optimal emulator point (hollow star). The right-hand plot shows a surface plot of the final DACE emulator with all the design points superimposed as asterisks.

5. DELAUNAY TESSELATION

Assume that the search domain correspond to a *d*-dimensional box. In order to avoid the computational cost of a global (continuous) search in this space, and the clustering of the design points that may lead to problems in model fitting, the design space is divided into smaller cells such that the expected improvement criterion is unimodal (or even concave) in each cell. The cells are constructed by Delaunay tesselation [9], with vertices given by the design points. The optimisation algorithm is modified as follows: (ii-a) compute the Delaunay tesselation of the domain and perform a *local* maximisation of the expected improvement in each Delaunay cell C_i (each cell is a *d*-dimensional simplex). Let $\mathbf{x}_i$, the point that maximises the expected improvement in C_i, be considered as a possible new design point, (iv-a) refit an emulator to the current experimental data, update the Delaunay tesselation, perform a *local* maximisation of the expected improvement in each newly created or modified Delaunay cell, recompute the expected improvement at $\mathbf{x}_i$ if C_i was already in the tesselation; return to (iv) with the best point. The fact that the uncertainty on the prediction increases with the distance to the design points usually makes the expected improvement unimodal in the cells, hence the possibility of using a fast local search method at the new steps. The number of local searches at step (iv-a) generally remains reasonably small since the optimisation is only performed in the new/modified cells. Fig. 2 presents an application of the method to the Rosenbrock function in the domain $[-2,2]^2$ (normalized to $[0,1]^2$). The dots correspond to the points $\mathbf{x}_i$

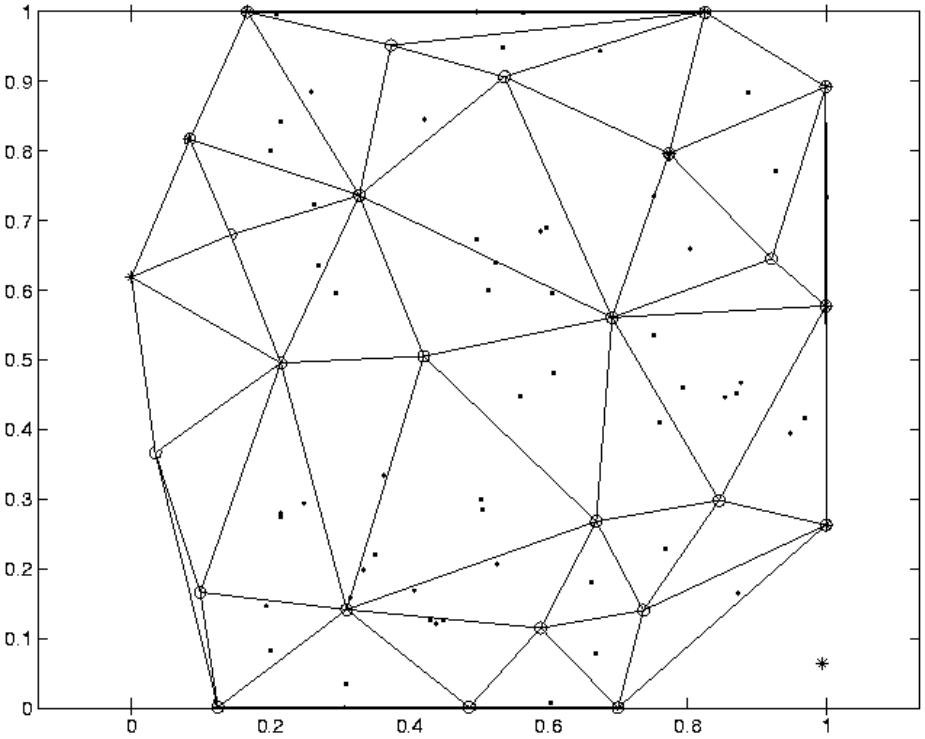

Figure 2: Optimisation of Rosenbrock function using Delaunay Tesselations

maximising the expected improvement in the cells constructed by the algorithm, the circles correspond to the design points. The star indicates the location of the next design point, where the function would have been evaluated if the algorithm had not been stooped due to a small value of the expected improvement at this point. The initial design corresponds to a LHS design with 7 points. The threshold used at step (v) is $10^{-3}(y_{max}-y_{min})$, with y_{max} and y_{min} the maximum and minimum values of y on the current design points. The algorithm stops after introducing 20 additional points, and suggests a minimum for y at x_1=1.0948, x_2=1.1870. The associated function value is $\hat{y}^*$ =0.0224.

6. DISCUSSION

Although only in 2 dimensions, the results show that expected improvement combined with lattice search, or Delaunay tesselation of the search domain, might be a suitable approach for optimisation problems involving functions computationally expensive to evaluate. The use of a lattice-based candidate set enabled the search to be conducted globally, while maintaining stability in the emulator building stages of the algorithm. One consequence of the lattice approach is that the ultimate step of the algorithm must allow the emulator to specify a final optimum value which is not constrained to be on the candidate set, as the true optimum point will probably not be contained within this set. A final local (continuous) optimisation of the response (or expected improvement) must therefore be made to confirm the result. Additional examples in higher dimensions with a simple quadratic function have also proved successful, and the results of this will be reported separately. However, in high dimensions this requires the evaluation of the expected improvement at a large number of sites (the points of the lattice). The use of Delaunay tesselation allows one to resort to *local* search when maximising the expected improvement, while maintaining a *global* search of the space. The combination of the two approaches is currently under study and should be beneficial. The tesselation may be used to search only in appropriate sub-regions, while searching on a lattice may help to maintain the design informative enough for a good exploration of the system response (note that the expected improvement approach is only one-step-ahead).

7. REFERENCES

[1] W. J. Welch et al. Screening, predicting, and computer experiments. Technometrics, 34(1):15-25,1992.

[2] MD McKay, WJ Conover & RJ Beckman. A comparison of three methods for selecting values of input variables in the analysis of output from a computer code. Technometrics, 21:239-245, 1979.

[3] J Sacks, WJ Welch, TJ Mitchell & HP Wynn. Design and analysis of computer experiments. Statistical Science, 4:409-435, November 1989.

[4] J. Mockus. Bayesian Approach to Global Optimization, Theory and Applications. Kluwer, Dordrecht, 1989.

[5] M Schonlau, WJ Welch & DR Jones. Global versus local search in constrained optimization of computer models. In N Flournoy, WF Rosenberger & WK Wong, editors, New Developments and Applications in Experimental Design, Lecture Notes, Monograph Series, 34:11-25. IMS, Hayward, 1998.

[6] A Okabe, B Books & K Sugihama. Spatial Tesselations. Concepts and Applications of Voronoi Diagrams. Wiley, NewYork, 1992.

FAST SIMULATORS FOR ASSESSMENT AND PROPAGATION OF MODEL UNCERTAINTY

J.O. Berger[1], M.J. Bayarri[2], and G. Molina[1]

[1]Institute of Statistics and Decision Sciences
Duke University, Durham,
NC 27708-0251, USA
Email: berger@stat.duke.edu, german@stat.duke.edu

[2]Dept. of Statistics and Operations Research
University of Valencia, Burjassot,
Valencia, 46100, SPAIN
Email: bayarri@uv.es

1. INTRODUCTION

Investigating sensitivity of model output is particularly challenging when the model is expensive to run, and when model inputs must be determined from limited data on the real process. Both of these problems can sometimes be addressed by the creation of "fast simulators" that (hopefully) mimic the relevant features of the model in regards to inputs and resulting sensitivity.

Such simulators can have a number of uses. The use that will be emphasised here is that of solving the inverse problem – i.e., determining needed model inputs based on data from the real process – as well as accounting for the associated uncertainty in inputs. The fast simulator can also prove useful in helping to adjust to situations of missing or incomplete data.

We will investigate these issues in the context of a traffic microsimulator discussed in subsection 1.1. The fast simulator will be a probabilistic network that is exercised by Markov chain Monte Carlo methods.

1.1. Traffic Simulation

The microsimulator CORSIM [5] is a computer model of street and highway traffic. It represents individual vehicles, which enter the road network at random times, move according to local interaction rules describing governing phenomena, such as vehicle following and lane changing, and turn (or not) at intersections according to prescribed probabilities. There is inherent randomness in CORSIM: vehicles arrive at random and move randomly, albeit with rather simplified governing distributions. For example, arrival time distributions are limited largely to Gamma distributions and vehicle turning movements are independent vehicle-to-vehicle and link-to-link.

CORSIM is currently in wide use as the platform for a variety of traffic management and research purposes. One of these [4] is measuring the performance of traffic signal timing plans (in cooperation with the Chicago Department of Transportation). The traffic network studied is depicted in Figure 1, and consists of a 52-intersection neighbourhood in Chicago. Of specific interest will be use of CORSIM to model and analyze traffic in this network during the "rush hour" period (on a normal day).

Of interest in this paper are two of the most significant (unknown) inputs to CORSIM: (i) demand and (ii) turning probabilities. *Demand, D,* consists of parameters that determine the numbers of vehicles that enter the system from external streets, while the *turning*

probabilities, P, refer to the probabilities that a vehicle turns right, turns left, or goes through a given intersection. Demand and turning probabilities are street and intersection specific, so that *D* is actually a vector of 16 numbers (for the studied system), while *P* is an 84-dimensional vector of probabilities. These must be determined from observational data, consisting of counts, *C,* made on the real-world traffic network. The available data is further discussed in Section 2.1.

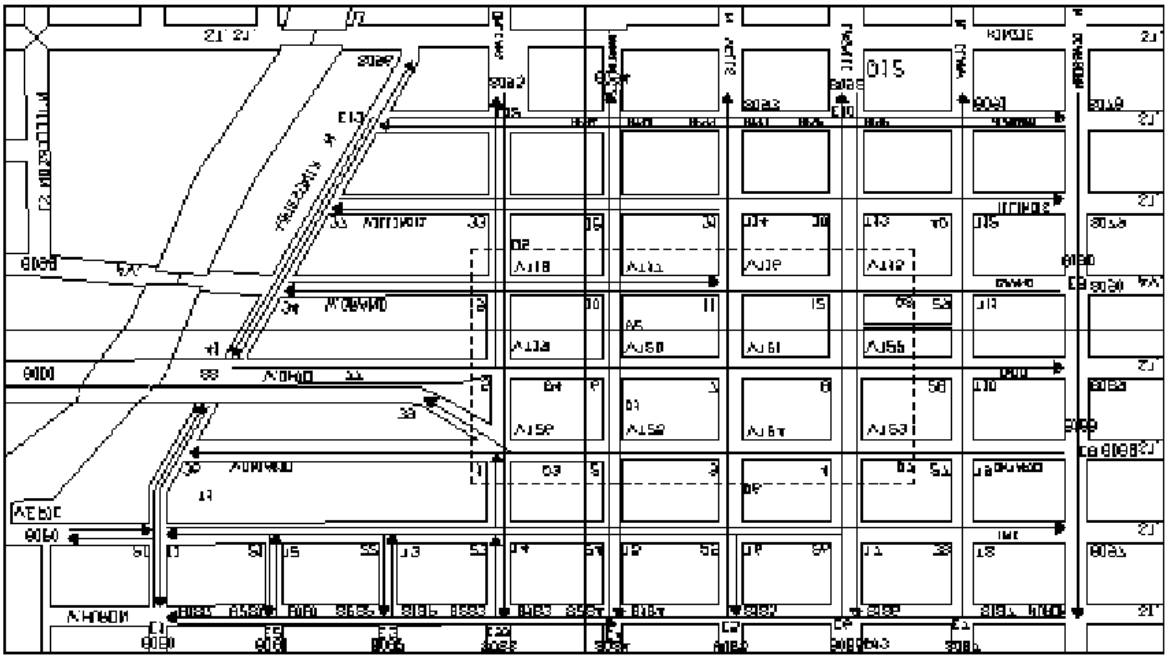

Figure 1. The traffic network (a Chicago neighbourhood) under study.

1.2. Inferential Focus

The basic problem we consider is the statistical inverse problem of using the data, *C,* to determine the inputs, *D* and *P,* to the simulator. In practice, this is often done by an informal process of "tuning," namely adjusting *D* and *P* until the output of the simulator seems similar to the observed data. The most serious deficiency of this approach is that the uncertainty in the tuning process is not accounted for. For the situation we consider (and for most complex computer models), there are very considerable uncertainties in the inputs to the model. Sources of uncertainty for CORSIM include quite large measurement errors in the data, *C,* and the uncertainty inherent in the simulator (since it produces random outputs, even given the inputs *D* and *P*). Determining these uncertainties, and doing so in such a way that they can be utilised for future predictions from the simulator, is thus our primary goal.

In principle, the Bayesian approach allows accomplishment of this goal. One views the (random) simulator output as a probability distribution, given *D* and *P,* and relates this to the actual observations *C* through a measurement error model. Specifying a prior distribution for *D* and *P* then allows use of Bayes theorem to obtain their posterior distribution, given the data *C,* to be denoted by $\pi(D,P|C)$. This distribution automatically incorporates all the uncertainty in the simulator inputs *D* and *P.* The challenge of determining $\pi(D,P|C)$ is discussed in the next section.

Uncertainty in simulator predictions can then be assessed by treating $\pi(D,P|C)$ as the "random input distribution" for the simulator, and making repeated runs of the simulator, initialised by draws from this distribution. This is not significantly more expensive than running the basic simulator in our situation; being a random simulator, its predictions can, in any case, only be ascertained through repeated runs, and starting each run with *D* and *P* chosen from $\pi(D,P|C)$ is virtually as cheap as starting each run with *D* and *P* fixed. Note that we are not addressing possible simulator bias here; we are simply addressing the issue of inherent sensitivity of simulator output to uncertainty in the inputs.

1.3. The Fast Simulator

A single run of CORSIM, on a typical PC platform and in the setting discussed in Section 1.1, typically takes 2 to 3 minutes. While much faster than many complex computer models, this is still too slow to use the simulator directly to obtain $\pi(D,P|C)$. The reason is that the only available method for direct determination of the posterior is the Markov chain Monte Carlo (MCMC) approach [1,3]. In our problem, however, there are upwards of 200 unknown and highly dependent parameters under analysis, and 2-3 minute simulator run-times will not allow an MCMC analysis in a situation of such complexity.

We proceed, therefore, by creating a simpler stochastic network that mimics the traffic simulator, with respect to the key features *D* and *P* under study. Simulation from this network is fast enough that it can be used for determination of $\pi^*(D,P|C)$, where we use "*" to indicate that this is the posterior that would correspond to the simplified network. One then has a separate model validation problem of assessing whether the fast simulator is an adequate approximation to the original traffic simulator, in the sense that $\pi^*(D,P|C)$ is a good approximation to $\pi(D,P|C)$, but we do not consider this problem here.

2. CONSTRUCTING THE FAST SIMULATOR

2.1. The Data

The data, *C*, is a vector of counts of vehicles. Let C_{ijk} denote the count of vehicles at intersection *i* (any of the 52 intersections), arriving from direction *j* (either N-north; S-south; E-east; or W-west), and making movement *k* (either R-right turn; L-left turn; or T-through). Thus C_{21NT} is the count of vehicles arriving at intersection 21 from the North, and continuing through the intersection. It is also convenient to define $C_{ij} = C_{ijR} + C_{ijL} + C_{ijT}$; this represents the total observed number of vehicles entering intersection *i* from direction *j*. The counts fall into three classes of data

Demand counts: These are counts, made over a two-hour period, by observers placed on the streets entering the traffic neighbourhood in Figure 1, and correspond to certain of the C_{ij} above. Some of these counts are suspected of being quite inaccurate, with errors potentially as high as 50%.

Turning counts: These are counts, made by observers over shorter time intervals (at most 20 minutes), of the numbers of R, L and T vehicles at each intersection. Some of these counts are missing and even those that are present can be quite inaccurate.

Camera counts: At the intersections in Figure 1 that lie within the central dashed rectangle, cameras were placed that recorded all vehicles passing through the intersection over the two-

hour period. The recordings were later analysed to exactly determine the numbers of R, L and T vehicles at each of these intersections. These counts can be treated as exact.

2.2. The Likelihood

The basic elements of the stochastic network to be constructed are numbers N_{ijk} that correspond to the true numbers of vehicles passing through the traffic network. Thus the C_{ijk} are viewed as arising from the N_{ijk}, but possibly with measurement error. The counts C_{ij} arising from the streets entering the traffic neighbourhood are likewise viewed as arising from the true numbers N_{ij}. The three different types of data are modelled probabilistically as follows.

Demand counts: It is assumed that the C_{ij}, arising from the streets entering the traffic neighbourhood, follow a discrete normal distribution with mean $(1+b)\,N_{ij}$ and variance $\sigma^2\,(N_{ij}+1)$, where b is an unknown "observer bias" and σ^2 is an unknown "variance inflation factor." (By a discrete normal distribution, we mean the distribution on the non-negative integers that has density proportional to the normal density.) The assumed proportionality of the variances of the C_{ij} to the true underlying counts, N_{ij}, is based on the fact that either binomial or Poisson error models for the C_{ij} have such proportional variances; while neither model can be used here (since incorporation of an unknown mean bias is also important), it is reasonable to follow this variance proportionality. (The addition of 1 to the N_{ij} is simply to eliminate possible problems with zero counts.) Letting C_1 denote the vector of these incoming C_{ij} and N_1 the corresponding vector of N_{ij}, we have thus specified the density $f(C_1 \mid N_1, b, \sigma^2)$.

Turning counts: These are determined over much shorter intervals (at most twenty minutes) than the C_{ij}, and are of a different nature than the demand counts. Hence we model them as arising from a discrete normal distribution with a different bias and variance inflation factor. Denote this density as $f(C_2 \mid N_2^*, b^*, \sigma^{*2})$, where C_2 is the vector of observed turning counts and N_2^* is the corresponding vector of true numbers of vehicles. We have distinguished N_2^* here from N_2, the vector of true numbers of vehicles over the longer two-hour period.

Camera counts: Again, the counts obtained from the camera recordings are viewed as exact. Thus we can view these counts as exactly specifying the corresponding values of N_{ij}.

2.3. The Prior Distribution

Section 2.2 specifies the density of the observed vector of vehicle counts *(C)* given the true vehicle numbers (N and N_2^*), b, b^*, σ^2, and σ^{*2}. This is the "likelihood" corresponding to the data.

The actual inputs that are needed for the CORSIM model are the turning probabilities P_{ijk} (i.e., the probability that a vehicle arriving at intersection i from direction j makes movement k) and the vehicle interarrival times λ_{ij} (which we earlier denoted generically by D), at the streets entering the neighbourhoods. The vehicle input distributions utilised in CORSIM are Erlang-2 distributions with rates λ_{ij} (i.e., Gamma distributions with scale parameters λ_{ij} and shape parameters 2). Thus we need to relate these actual parameters of interest to N.

The N_{ij} corresponding to the streets entering the neighbourhoods can simply be viewed as arising from the Erlang-2 distributions and we assume these to all be independent; thus we

have specified the density $\pi(N_1 \mid \lambda)$, where N_1 refers to the vector of incoming N_{ij} and λ is the vector of the λ_{ij}.

Next, vehicles arriving at an intersection from a given direction will be treated as independent, so that (N_{ijR}, N_{ijL}, N_{ijT}) follows a multinomial distribution with total sample size $N_{ij} = N_{ijR} + N_{ijL} + N_{ijT}$, and probabilities ($P_{ijR}$, P_{ijL}, P_{ijT}). Assuming independence across intersections, this specifies the density $\pi(N_2 \mid P)$, where N_2 denotes the vector of all true turning numbers (over the two-hour period) and P the vector of all turning probabilities.

It is important to realise that there are numerous constraints among the N_{ijk} and $N_{ij.}$ For instance, the total number of vehicles entering an intersection must equal the number leaving the intersection. Furthermore (and of crucial effect), the camera counts lead to known values of some of the N_{ij}, and these known values induce other constraints. For the neighbourhood of Figure 1, there are a total of 37 constraints that must be included. Let $\mathcal{N}$ denote the region implied by all these constraints, and $\mathbf{1}_{\mathcal{N}}$ denote the indicator function on this region

We also have to deal with N_2^*, the vehicle numbers from the short time intervals corresponding to the actual observations C_2. While N_2^* and N_2 are clearly somewhat dependent, the comparatively small time interval corresponding to the N_2^* makes an assumption of independence at least reasonable as an approximation.

Finally, we must specify the prior distribution $\pi(\lambda, P, b, b^*, \sigma^2, \sigma^{*2})$. We (independently) utilise the standard noninformative prior distributions $1/\lambda_{ij}$, $1/\sigma^2$, and$1/\sigma^{*2}$ for the various scale parameters, choose a constant prior distribution for b and b^* over their domains, and assign the turning probabilities for a given triplet the Jeffreys prior $(P_{ijR} P_{ijL} P_{ijT})^{-1/2}$.

2.4. The Posterior Distribution

By Bayes theorem, the posterior distribution, $\pi(N_1, N_2, N_2^*, \lambda, P, b, b^*, \sigma^2, \sigma^{*2} \mid C)$, of all unknowns given the data C, is simply proportional to the product of the likelihood and the prior, i.e.

$$f(C_1 \mid N_1, b, \sigma^2)\, f(C_2 \mid N_2^*, b^*, \sigma^{*2})\, \pi(N_1 \mid \lambda)\, \pi(N_2 \mid P)\, \pi(N_2^* \mid P)\, \pi(\lambda, P, b, b^*, \sigma^2, \sigma^{*2})\, \mathbf{1}_{\mathcal{N}}.$$

Although $\pi(\lambda, P, b, b^*, \sigma^2, \sigma^{*2})$ was improper, it can be shown that the posterior distribution is proper, even when (as is the case with the CORSIM data) some of the counts are missing. (The ability to deal with missing data is one of the strengths of the Bayesian approach.)

We have completed specification of what is commonly called a Bayesian network [2]. The nodes of the network can be thought of as the *ij* pairs (an intersection number, together with the relevant directional input of vehicles). The numbers of vehicles going between nodes are sums of the N_{ijk}, with the N_{ij} being the vehicles arriving into the network from "external nodes" representing the Erlang-2 input distributions. Note that N_1 and N_2, while (mostly) unknown, are not of immediate interest; the goal is to obtain the posterior distribution of the inputs needed for the CORSIM model, which are λ and P. As is common in Bayesian analysis, however, the N_i are introduced as "latent variables" for the purpose of simplifying the distributional structure of the Bayesian network and the ensuing computations.

3. MCMC COMPUTATION

The chief difficulty in the analysis is dealing with the constraints specified by $\mathbf{1}_{\mathcal{N}}$. Indeed, the most important step in the computation is to effect a reparameterization of N_1 and N_2 so that unneeded variables are eliminated and the constraints take a simple form. Indeed, we were unsure that an effective MCMC analysis could be implemented here, until a scheme for carrying out this reparameterization was found. (In principle, one could simply numerically compute the constraint at each step of the MCMC procedure via linear programming, but this would be too time consuming because of the large number of iterations that are needed.) Space precludes a description of the reparameterization here.

After the reparameterization, one can proceed by Gibbs sampling (see [1,3]). The full conditional distributions of the λ_{ij}, $(P_{ijR}, P_{ijL}, P_{ijT})$, (b, σ^2), and (b^*, σ^{*2}) are Gamma, Dirichlet, and (twice) Normal-Inverse-Gamma, respectively, with easily specified parameters. The full conditional distributions of the various N have no simple form, but are discrete distributions over specified ranges. Hence they can also be easily sampled. We are currently proceeding with a full implementation of this analysis. To date, however, it has been implemented only under the simplifying assumptions that $\sigma^2 = 1$ and $\sigma^{*2} = 0$.

The output of the MCMC analysis is a large sample of (dependent) realisations from the posterior distribution. For use in CORSIM, one thus simply records this sample of (λ, P), and uses the sample directly as the input values for the exercise of CORSIM. In practice, only a few hundred values of the (λ, P) vectors will typically be utilised in a CORSIM prediction, whereas the MCMC runs will typically result in, say, 100,000 realisations of (λ, P). Hence, one need typically only save, say, every 500^{th} realisation of (λ, P) from the MCMC run; the resulting 200 realisations will then also be much less dependent, desirable when used as the inputs for CORSIM.

4. CONCLUSIONS

To see the effects of the joint posterior analysis of the data, Figure 2 presents histograms of values of the N_{ij} for two of the incoming streets of the neighbourhood, along with the corresponding observed counts, C_{ij} (indicated by the vertical line). These histograms reveal two central points. First, the joint posterior analysis can cause marked shifts in the distribution of the actual numbers of vehicles, away from the observed counts. Second, the variability in the distribution of the actual numbers is quite significant, and will result in a very significant increase in the variability of CORSIM predictions. Neither of these could have been realised by "tuning" the model to fit the data or even by "univariate" statistical analyses of aspects of the data.

It should also be emphasised that, in effect, we constructed a "fast simulator" that reflects certain features of the CORSIM model. The developed probabilistic network contains all intersections of the CORSIM model, and also reflects the vehicle counts and turning probabilities involved in passing between intersections. However, the vehicles are essentially viewed in this fast simulator as passing through the neighbourhood instantaneously; thus important details, such as queue times, are missing. The fast simulator is, therefore, not a replacement of the CORSIM model from the perspective of traffic management. But it does serve the central purpose of allowing for the observational data to appropriately influence the input distributions to CORSIM, leading to improved assessment of uncertainty in CORSIM prediction.

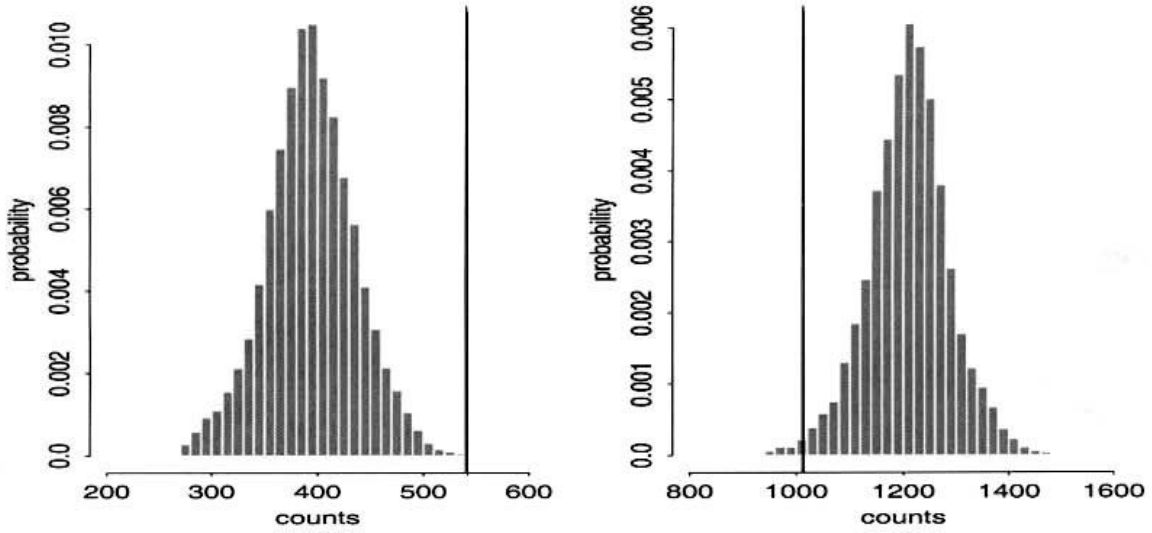

Figure 2. Histograms indicating the posterior distributions of two of the N_{ij}.

Acknowledgements. Research was supported by the U.S. National Science Foundation, Grant DMS-0073952.

5. REFERENCES

[1] Chen, M.H., Shao, Q.M. and Ibrahim, J.G. (2000). *Monte Carlo Methods in Bayesian Computation.* New York: Springer-Verlag.

[2] Cowell, R.G., Dawid, A.P., Lauritzen, S.L. and Spiegelhalter, D.J. (1999). Probabilistic Networks and Expert Systems, New York: Springer-Verlag.

[3] Robert, C.P. and Casella, G. (1999). Monte Carlo Statistical Methods. New York: Springer-Verlag.

[4] Sacks, J., Rouphail, N.M., Park, B., and Thakuriah, P. (2000). Statistically-based validation of computer simulation models in traffic operations and management. Technical Report 112, National Institute of Statistical Sciences (US).

[5] US Federal Highway Administration (1997). CORSIM User's Manual. FHWA, US. Department of Transportation Office of Safety and Traffic Operation R&D, Intelligent Systems and Technology Division, McLean, VA

INFORMATION CONTENT OF A SIMPLE WATER QUALITY MODEL: SENSITIVITY WITH RESPECT TO MODEL STRUCTURE

U. Callies, F. Schroeder, K. Bülow

GKSS-Forschungszentrum, Max-Planck-Str.
21502-Geesthacht (Germany)
Email: ulrich.callies@gkss.de ; friedhelm.schroeder@gkss.de ; katharina.buelow@gkss.de

SUMMARY

A simple water quality model is fitted to continuous observations collected at the weir at Geesthacht on the Elbe river. A case study addresses the questions of a) what kind of information about the impact of external forcing on the temporal evolution of chlorophyll concentrations can be obtained from using a mechanistic model's uncertain output and b) how this information changes when the model's structure is simplified. Model output is considered informative if its linear re-scaling based on linear multivariate least squares regression methods is efficient in reproducing the observed data. Canonical correlation analysis (CCA) is employed to analyse this post-calibration process in terms of pairs of correlated patterns in the spaces of data and model output, respectively. Using observed water temperature (which is model input) as an additional explanatory variable in the calibration scheme allows for the assessment of the incremental amount of information in model output when already knowing the time dependent model input. The sensitivity of the model's information content with respect to details of the model formulation is investigated.

1. INTRODUCTION

To be able to identify anthropogenic changes of observed water quality in a river, the proportion of observed variability that is due to internal dynamical variability or time dependent external meteorological forcing must be estimated. Normalisation of observed data may be attempted so as to facilitate the comparison of observed data from different places or periods with different meteorological conditions. Mechanistic modelling can be helpful for this task.

Models for predicting water quality typically contain many input parameters the exact values of which are not well known. In fitting such models to observations, it is often the case that using significantly different parameter sets results in very similar model outputs, indicating that the model is overparameterised. Monte Carlo techniques can be used to identify that region in the space of model input parameters that implies good model performance [6]. Here, it is suggested that Bayesian network technology [2] might provide a convenient way to portray the shape of this region and thereby allow for a systematic approach to tuning overparameterized models.

Mechanistic models and their resultant mathematical structures portray processes that involve different variables at the same time. Thus, the temporal evolution of characteristic patterns may be traced. The main idea underlying this study is that even when a model is

badly calibrated, essential mechanistic processes may still be represented, although the shapes of the covariance patterns or their amplitudes may be wrong. If such deficiencies can be corrected by post-calibrating model output based on multivariate regression techniques, a mechanistic model may still be considered as being useful. It is investigated how the application of model output post-calibration affects parameter sensitivities.

2. METHODOLOGY

2.1. Representation of Parameter Uncertainty by Bayesian Networks (BNs)

BNs [2] use the language of conditional probabilities portrayed by directed links between nodes in a graphical network to represent associations between variables. The notation is intuitively conceivable and at the same time underpinned by strict probabilistic mathematics. To choose the network topology (which is not unique as a given joint probability distribution can be factored in different ways) means to impose a certain order on the set of variables. Thus, the language of directed Bayesian graphs can profitably be employed to support the perception of "causal" interactions between model parameters.

2.2. Model Post-Calibration

The observations-predictions correlation is used as a measure to assess the amount of information that is available from the mechanistic model. CCA [1] is applied to concentrate information on the kind of association between the observed data vector (chlorophyll, phosphate, oxygen) and the corresponding vector of model output by identifying pairs of patterns whose time evolution is optimally correlated. This information about independent pairs of correlated patterns in the spaces of observations and model predictions, respectively, allows for the decomposition of the matrix of regression coefficients that is used for model calibration into additive components.

3. RESULTS

3.1. Definition of the Case Study

The theoretical concept will be illustrated in a case study of water quality data of the Elbe river. The main focus is on simulating observed chlorophyll-a concentrations.

3.1.1. Data

Weir Geesthacht is located about 50 km upsteam of Hamburg on the Elbe river. Since 1996 many relevant water quality parameters (pH, oxygen, nutrients) and external forcing parameters (water temperature, radiation) have been observed on a continuous basis [3]. For the present study a period of 120 days starting with the first of May 1997 has been selected.

3.1.2. Model WAMPUM

A zero-dimensional version of the water quality model WAMPUM [5] developed at GKSS has been used. The following compartments are represented in the model: oxygen, biomass of phytoplankton, carbon, nitrogen and phosphorus. No transport term has been activated.

3.2. Sensitivities

Five model input parameters have been selected for a sensitivity study. Four of theses parameters enter the formulation of the algae growth rate:

- Water depth
- Light intensity at which algae growth rate is 71% of the maximum growth rate
- Non-algal light extinction coefficient (by mineral compounds)
- Algal self-shading coefficient

As a fifth parameter for experimental purposes (originally not contained in WAMPUM) a "tendency scale factor" has been introduced that allows to adjust the overall time scales of growth and depletion rates. Monte-Carlo-experiments with 4000 realisations for the five-dimensional vector of model input parameters have been performed. Results of the sensitivity study are reported in a companion paper [4]. Only few constraints for successful combinations of model input parameters can be discerned in pairwise scatterplots. Analysing the constrained model parameters in terms of conditional probabilities, however, clearly reveals a multidimensional structure of parameter interaction.

As to be expected, using linear post-calibration for correcting raw model output has a major impact on the classification of Monte-Carlo-runs in terms of their success. Surprisingly, the overall connectivity between parameters in the subset of successful parameter combinations seems not to be weakened by allowing for post-calibration of model output. Further research is needed to decide whether this result can be confirmed in other applications.

3.3. Truncation of The Model Structure

Four of the selected model parameters enter a formula that parameterizes the impact of radiative forcing on algae growth. One may ask whether, given the observed evolution of meteorological forcing, the specific formulation of this non-linear module of the mechanistic model is essential for explaining variability of algae populations.

A very simple experiment consists of setting the light demand of algae in the model to zero so that light attenuation by mineral compounds and self-shading of the algae in the model become irrelevant. The performance of the truncated model's output is extremely poor. Even re-calibrating the model output does not improve its quality to a significant degree. The situation becomes very different, however, when post-calibration of model output is based on raw model output variables plus the observed water temperature rather than on model output alone. In contrast, using observed temperature alone as a predictor for algae bio mass (when using linear least squares regression formulas), is again not successful.

Individual canonical variates obtained by CCA mostly have characteristic scales of temporal variability. A striking result obtained for the present example is that time series of canonical variates in the space of observations are not changed much by the model truncation. Significant changes are observed only for the canonical variates in the space of predictors (raw model output, eventually plus observed temperature). Similarly, including water temperature into the set of explanatory variables has no major effects on canonical variates in the space of data.

4. DISCUSSION

Model predictions of water quality are associated with high degrees of uncertainty that may reside in parameter specifications but also in assumptions about the overall model structure. The representation of simple model overparameterization can be considerably facilitated by using BN-technology. Once a BN has been fitted, new samples of dependent model input factors can readily be drawn from the joint likelihood function represented by the BN.

The main objective of this paper was to explore a theoretical concept to better assess the amount of information that can be obtained from uncertain output of a mechanistic water quality model. The basic idea was that linearly re-scaling model output should not change its information content. A least squares post-calibration scheme of multivariate model output (chlorophyll, phosphate, oxygen) has been subjected to CCA. Characteristic time series of canonical variates in space of observations were found to be independent of model details. Model post-calibration formulated in terms of correlated canonical variates might therefore be used to statistically relate observed natural processes and corresponding structures in the model output to each other.

It is to be expected that mechanistic processes are correlated better with external forcing than with changes of individual variables. For this reason water temperature (being one aspect of external forcing that enters the mechanistic model as input) has been included into the data vectors that are subjected to CCA. The implications of including temperature are different for different pairs of correlated patterns which indicates a chance for statistically isolating the impact of temperature on individual processes. This would be an important contribution to the technique of data normalization with regard to external meteorological forcing.

5. ACKNOWLEDGEMENTS

This work has been carried out within the European Commission project IMPACT (contract no. IST – 1999 - 11313). Data sets have been made available by Gerd Blöcker. For fitting BNs a demo version of the Pronel BN learner 1.0.1 has been used (available from Hugin Expert A/S, http://www.hugin.dk).

6. REFERENCES

[1] Johnson, R. A. and D. W. Wichern, 1992: *Applied Multivariate Statistical Analysis*. Prentice Hall, Englewood Cliffs, New Jersey.

[2] Pearl, J., 1988: Probabilistic Reasoning in Intelligent Systems: *Networks of plausible Inference*. Morgan Kaufman Publishers, San Mateo.

[3] Petersen, W., Blöcker, G., Mehlhorn, N. and F. Schroeder, 1999: Einfluß der veränderten Schadstoffbelastung in der Elbe auf den Sauerstoffhaushalt. *Vom Wasser* **92**, 37-50.

[4] Ratto. M., Tarantola, S., and U. Callies, 2001: Sensitivity Analysis in Model Calibration: A case Study in Environmental Modelling. *In this volume.*

[5] Schroeder, F., 1997: Water quality in the Elbe estuary: Significance of different processes for the oxygen deficit at Hamburg. *Environmental Modeling and Assessment* **2**, 73-82.

[6] Spear, R. C., 1997: Large Simulation Models: Calibration, Uniqueness and Goodness of Fit. *Environmental Modelling & Software* **12**, 219-228.

STABILITY OF SAMPLING-BASED SENSITIVITY ANALYSIS RESULTS

J.C. Helton, F.J. Davis

Sandia National Laboratories
P.O. Box 5800, Albuquerque, NM 87185-0779
Email: jchelto@sandia.gov; davis@anrc-research.org

1. INTRODUCTION

Sampling-based (i.e., Monte Carlo) approaches to uncertainty and sensitivity analysis are popular and widely used [1]. The most commonly used sampling techniques are simple random sampling [2] and Latin hypercube sampling [3]. Both theory [3-5] and some empirical comparisons [3, 6] indicate that Latin hypercube sampling provides more robust results in sampling-based analyses than simple random sampling. In this presentation, sensitivity analysis results obtained with both random and Latin hypercube sampling for a model of two-phase fluid flow are compared.

2. ANALYSIS PROBLEM

The model for two-phase flow under consideration [7] was used in the 1996 performance assessment (PA) for the Waste Isolation Pilot Plant (WIPP) [8,9]. The model, which is often referred to as BRAGFLO after the computer program that implements it, is based on a system of nonlinear partial differential equations and is evaluated numerically with finite difference procedures. As a single evaluation requires approximately 1-4 hours of processing time on a Vax Alpha, the number of evaluations that can be performed in an uncertainty and sensitivity analysis is necessarily limited.

The BRAGFLO program was used to model several different configurations of the repository in the 1996 WIPP PA (Table 6, [10]). The configuration considered in this analysis involves a single drilling intrusion that passes through the repository and penetrates a region of pressurized brine beneath the repository (i.e., an E1 intrusion in the terminology of the 1996 WIPP PA). The analysis of this configuration involved 31 uncertain variables (Table 1) that were sampled by Latin hypercube sampling in the 1996 WIPP PA. In particular, three replicated samples of size 100 each were used [11], with the Iman and Conover restricted pairing technique [12] employed to control correlations within the individual replicates. Uncertainty and sensitivity analysis results were found to be quite stable across replicates in this analysis [9].

This study compares regression-based sensitivity analysis results obtained with three replicated random samples of sizes 25, 50 and 100, respectively, and also with three replicated Latin hypercube samples (LHSs) of sizes 25, 50 and 100. The LHSs of size 100 are the three replicated samples used in the 1996 WIPP PA; the remaining samples were generated and analyzed specifically for this study.

Table 1. Example Sampled Variables (see Table 1 [11] for additional information and definitions of the remaining 27 sampled variables: *ANHBCEXP*, *ANHBCVGP*, *ANHCOMP*, *ANHPRM*, *ANRBRSAT*, *ANRGSSAT*, *BPINTPRS*, *BPPRM*, *HALCOMP*, *HALPOR*, *HALPRM*, *SALPRES*, *SHBCEXP*, *SHPRMASP*, *SHPRMCLY*, *SHPRMCON*, *SHPRMDRZ*, *SHPRMHAL*, *SHRBSAT*, *SHRGSSAT*, *WASTWICK*, *WFBETCEL*, *WGRCOR*, *WGRMICI*, *WGRMICH*, *WRBSAT*, *WRGSSAT*)

BHPRM—Logarithm of intrinsic borehole permeability (m^2). Distribution: Uniform. Range: −14 to −11 (i.e., permeability range is 1×10^{-14} to 1×10^{-11} m^2). Mean, median: −12.5.
BPCOMP—Logarithm of bulk compressibility of brine pocket (Pa^{-1}). Distribution: Triangular. Range: −11.3 to −8.0 (i.e., bulk compressibility range is $1 \times 10^{-11.3}$ to 1×10^{-8} Pa^{-1}). Mean, mode: −9.80, −10.0. Correlation: −0.75 rank correlation with *BPPRM* (brine pocket permeability).
BPVOL—Brine pocket volume (m^2). Distribution: Discrete, with 32,000, 64,000, 96,000, 128,000 and 160,000 m^3 having probabilities of approximately 0.19, 0.31, 0.31, 0.16 and 0.03, respectively.
WMICDFLG—Pointer variable for microbial degradation of cellulose. Distribution: Discrete, with 0, 1, 2 having probabilities of 0.5, 0.25 and 0.25, respectively. *WMICDFLG* = 0, 1, 2 implies no microbial degradation of cellulose, microbial degradation of only cellulose, and microbial degradation of cellulose, plastic and rubber, respectively.

3. EXAMPLE RESULTS

A typical comparison is given in Table 2. As in this example, there is often little agreement on the variables identified as being important with samples of size 25, although the results with LHSs of size 25 tend to identify more physically significant variables than is the case with random samples of size 25.

As the sample sizes increase, more physically significant variables are identified and the stability of the results increases. Here, stability refers to the amount of variation in the important variables identified with different samples of the same size. Often, there is little variation in the identification of the dominant variables with samples of size 100 (and sometimes even of size 50). Thus, there is apparently little to be gained from the use of a sample size larger than 100 in regression-based sensitivity analyses of the problem under consideration.

The results obtained with LHSs of size 50 and 100 tend to be somewhat more stable than those obtained with random samples of corresponding size. However, on the whole, regression results with random and LHSs of sizes 50 and 100 tend to be surprisingly similar. This is probably due to the fact that the uncertainty in the outcomes of most analyses derive from the uncertainty in a small subset of the uncertain variables used as input. Low R^2 values in the regression models for samples of size 100 appear to be due more to the inappropriateness of the rank regression model in use than to an inadequate sample size. Specifically, there are relationships between sampled and predicted variables that cannot be captured with a rank regression model.

Table 2. Comparison of Stepwise Rank Regression Analyses with Replicated Random and Latin Hypercube Samples of Size 25, 50 and 100 for Cumulative Brine Flow over 10,000 yr from Brine Pocket into Bottom of Lower Disturbed Rock Zone (*BNBHLDRZ*)

	Random Samples: Analyses for *BNBHLDRZ*								
	Replicate 1			**Replicate 2**			**Replicate 3**		
Size	**Variable[a]**	**R^{2b}**	**SRRC[c]**	**Variable[a]**	**R^{2b}**	**SRRC[c]**	**Variable[a]**	**R^{2b}**	**SRRC[c]**
25	*SHRBRSAT*	0.41	–0.59	*WGRMICI*	0.26	–0.51	*ANHPRM*	0.26	0.51
	HALPOR	0.55	–0.47				*SHPRMDRZ*	0.45	0.43
	WRGSSAT	0.65	–0.34						
50	*BPCOMP*	0.51	0.73	*BPCOMP*	0.66	0.89	*BPCOMP*	0.47	0.74
	BHPRM	0.59	0.28	*BPVOL*	0.72	0.30	*WMICDFLG*	0.57	–0.41
				WMICDFLG	0.78	–0.24	*WGRMICI*	0.63	–0.23
				BHPRM	0.82	0.23	*SALPRES*	0.67	0.22
				BPINTPRS	0.85	0.16			
100	*BPCOMP*	0.55	0.61	*BPCOMP*	0.56	0.77	*BPCOMP*	0.44	0.65
	BHPRM	0.62	0.29	*WMICDFLG*	0.66	–0.30	*WMICDFLG*	0.56	–0.34
	BPVOL	0.67	0.24	*BHPRM*	0.72	0.25	*BHPRM*	0.65	0.30
	WMICDFLG	0.70	–0.17	*BPVOL*	0.78	0.25	*WRGSSAT*	0.69	–0.17
	BPINTPRS	0.72	0.14	*BPINTPRS*	0.81	0.17	*BPINTPRS*	0.72	0.17
	BPPRM	0.74	–0.19	*ANHBCVGP*	0.82	–0.11	*BPVOL*	0.75	0.16
				SHPRMHAL	0.83	–0.11			

	Latin Hypercube Samples: Analyses for *BNBHLDRZ*								
	Replicate 1			**Replicate 2**			**Replicate 3**		
Size	**Variable[a]**	**R^{2b}**	**SRRC[c]**	**Variable[a]**	**R^{2b}**	**SRRC[c]**	**Variable[a]**	**R^{2b}**	**SRRC[c]**
25	*BCOMP*	0.81	0.92	*BPCOMP*	0.53	0.69	*WASTWICK*	0.23	0.45
	BPVOL	0.89	0.28	*ANHPRM*	0.66	–0.36	*BHPRM*	0.51	0.58
							SHPRMCON	0.68	–0.42
50	*BPCOMP*	0.50	0.80	*BPCOMP*	0.61	0.55	*BPCOMP*	0.50	0.56
	BHPRM	0.62	0.27	*BPVOL*	0.67	0.23	*WMICDFLG*	0.60	–0.35
	BPVOL	0.71	0.32	*WGRMICH*	0.72	0.20	*BPINTPRS*	0.69	0.29
	WMICDFLG	0.77	–0.25	*BPPRM*	0.75	–0.28			
100	*BPCOMP*	0.51	0.58	*BPCOMP*	0.56	0.72	*BPCOMP*	0.49	0.70
	BHPRM	0.63	0.34	*BHPRM*	0.64	0.31	*BHPRM*	0.64	0.36
	WMICDFLG	0.68	–0.21	*WMICDFLG*	0.72	–0.29	*WMICDFLG*	0.74	–0.30
	BPVOL	0.71	0.17	*BPINTPRS*	0.77	0.20	*BPVOL*	0.77	0.17
	BPPRM	0.73	–0.23	*BPVOL*	0.79	0.15	*SHRBRSAT*	0.29	–0.14
	WGRCOR	0.75	–0.13	*SHRBRSAT*	0.80	–0.12			

[a] Variables listed in order of selection in regression analysis (α = 0.02 to enter, α = 0.05 to remain), with *ANHCOMP* and *HALCOMP* excluded from entry into regression model because of –0.99 rank correlation within the pairs (*ANHPRM*, *ANHCOMP*) and (*HALPRM*, *HALCOMP*).

[b] Cumulative R^2 value with entry of each variable into regression model.

[c] Standardized rank regression coefficients (SRRCs) in final regression model.

4. FUTURE WORK

This study compared a large number of sensitivity analyses of the form indicated in Table 2 and briefly summarized in the preceding section. Summarizing and then communicating the impressions gained in these comparisons is difficult due to the number and variety of

comparisons involved. Future work will investigate the use of techniques based on coefficients of concordance calculated on Savage scores [13] as a means presenting concise comparisons of variable rankings obtained with different sample sizes, sampling techniques, and sensitivity analysis procedures.

5. REFERENCES

[1] Helton, J.C. 1993. "Uncertainty and Sensitivity Analysis Techniques for Use in Performance Assessment for Radioactive Waste Disposal," *Reliability Engineering and System Safety*. Vol. 42, no. 2-3, pp. 327-367.

[2] Fishman, G.S. 1996. *Monte Carlo: Concepts, Algorithms, and Applications*. New York: Springer-Verlag New York, Inc.

[3] McKay, M.D., R.J. Beckman, and W.J. Conover. 1979. "A Comparison of Three Methods for Selecting Values of Input Variables in the Analysis of Output from a Computer Code," *Technometrics*. Vol. 21, no. 2, pp. 239-245.

[4] Stein, M. 1987. "Large Sample Properties of Simulations Using Latin Hypercube Sampling," *Technometrics*. Vol. 29, no. 2, pp. 143-151.

[5] Owen, A.B. 1992. "A Central Limit Theorem for Latin Hypercube Sampling," *Journal of the Royal Statistical Society. Series B. Methodological*. Vol. 54, no. 2, pp. 541-551.

[6] Iman, R.L. and J.C. Helton. 1988. "An Investigation of Uncertainty and Sensitivity Analysis Techniques for Computer Models," *Risk Analysis*. Vol. 8, no. 1, pp. 71-90.

[7] Vaughn, P., J.E. Bean, J.C. Helton, M.E. Lord, R.J. MacKinnon, and J.D. Schreiber. 2000. "Representation of Two-Phase Flow in the Vicinity of the Repository in the 1996 Performance Assessment for the Waste Isolation Pilot Plant," *Reliability Engineering and System Safety*. Vol. 69, no. 1-3, pp. 205-226.

[8] Helton, J.C., D.R. Anderson, H.-N. Jow, M.G. Marietta, and G. Basabilvazo. 1999. "Performance Assessment in Support of the 1996 Compliance Certification Application for the Waste Isolation Pilot Plant," *Risk Analysis*. Vol. 19, no. 5, pp. 959 - 986.

[9] Helton, J.C. and M.G. Marietta. 2000. "Special Issue: The 1996 Performance Assessment for the Waste Isolation Pilot Plant," *Reliability Engineering and System Safety*. Vol. 69, no. 1-3, pp. 1-451.

[10] Helton, J.C., F.J. Davis, and J.D. Johnson. 2000. "Characterization of Stochastic Uncertainty in the 1996 Performance Assessment for the Waste Isolation Pilot Plant," *Reliability Engineering and System Safety*. Vol. 69, no. 1-3, pp. 167-189.

[11] Helton, J.C., M.-A. Martell, and M.S. Tierney. 2000. "Characterization of Subjective Uncertainty in the 1996 Performance Assessment for the Waste Isolation Pilot Plant," *Reliability Engineering and System Safety*. Vol. 69, no. 1-3, pp. 191-204.

[12] Iman, R.L. and W.J. Conover. 1982. "A Distribution-Free Approach to Inducing Rank Correlation Among Input Variables," *Communications in Statistics: Simulation and Computation*. Vol. B11, no. 3, pp. 311-334.

[13] Iman, R.L. and W.J. Conover. 1987. "A Measure of Top-Down Correlation," *Technometrics*. Vol. 29, no. 3, pp. 351-357.,

COMPARISON OF GLOBAL SENSITIVITY ANALYSIS TECHNIQUES AND IMPORTANCE MEASURES IN PROBABILISTIC SAFETY ASSESSMENT

E. Borgonovo[1],G.E. Apostolakis[1], S. Tarantola[2] and A. Saltelli[2]

[1] Room 24-221
Nuclear Engineering Department
Massachusetts Institute of Technology
77 Massachusetts Av.,
Cambridge, MA 02139-4307, USA

[2] S. Tarantola and A. Saltelli
Institute for Systems, Informatics and Safety
Joint Research Center of the European Commission
TP. 361 - 21020 Ispra (VA)
ITALY

1. INTRODUCTION

Probabilistic Safety Assessment (PSA) computes the risk of complex technological systems. The core damage frequency (CDF) and the large early release frequency (LERF) are usually the risk metrics of interest in nuclear power plants (NPP). Epistemic uncertainty affects the use of PSA model results. In fact, because of the lack of knowledge in the parameter values, the risk metrics become uncertain and described by epistemic distributions (Apostolakis, 1995).

In this paper, we discuss the use of Global Sensitivity Analysis (GSA) techniques for the determination of the parameters that contribute to the uncertainty in R the most. This information cannot be gained through the use of traditional importance measures (IMs), since: (1) IMs are defined for components and basic events and not for parameters, (2) IMs assume the parameters at their nominal value, and are therefore Local Methods. In Section 2 we discuss that, because of epistemic uncertainty, GSA must be performed through the PSA model parameters, and not at the basic event level. In Section 3 we present the defnition of the PSA IMs and GSA techniques used in this work. In Section 4 we present the approach to compare PSA IMs results to GSA results, to understand whether uncertainty driversare also important risk contributors. Results will be discussed for the application of these techniques and the proposed approach to the PSA large loss of coolant accident (LOCA) sequence of a research reactor.

2. EFFECT OF EPISTEMIC DEPENDENCE

The generic risk metric R, is represented in standard PSA codes as:

$$R = h(\, f_{IE_i}, q_j \,) \tag{9}$$

where: f_{IE_i} = frequency of the generic initiating event i, and, $q_j = \mathrm{p}(\mathrm{BE_j})$ probability of the generic basic event. We refer to eq. (9) as the basic event representation or basic event level of the PSA model. For a one-out-of-two system, where R is the system unavailability, eq. (9) becomes:

$$R = q_1 \cdot q_2 \tag{10}$$

where q_1 and q_2 are the unavailabilities of the two components.

Suppose now that the two components are nominally identical. Then the numerical values of q_1 and q_2 are equal because of epistemic dependence, i.e., $q_1=q_2=q$ (Apostolakis, 1995; Apostolakis and Kaplan, 1981). Thus, R as a function of the parameters is:

$$R = q^2 \tag{11}$$

This equation enables the correct computation of the variance and expected value of R, as opposite to eq. (9) (Apostolakis and Kaplan, 1981). More in general, we denote with:

$$R=g(x1,x2,\ldots,xn) \tag{12}$$

the expression of the risk metric as a function of the PSA model parameters. The presence of epistemic uncertainty requires that uncertainty and GSA are performed on eq. (12), the parameter level, as opposite to eq. (9), the basic event level.

3. IMS AND GSA TECHNIQUE DEFINITIONS

PSA IMs are used to identify parameters or basic events that are important to safety. The following PSA IMs have been used in this work: the Differential Importance Measure (DIM) (Borgonovo and Apostolakis, 2000), the Fussell-Vesely (FV) IM, and the Risk-Achievement Worth (RAW) IM (Cheok, Parry and Sherry, 1998). DIM is defined for both parameters and basic events. DIM(x_i) is the fraction of the local change in R that is due to a change in parameter x_i. In this case DIM is computed on eq.[12]. Similarly, for basic events, DIM(q_i) is the fraction of the local change in R due to a change in probability q_I, and is computed on eq.[9]. FV and RAW are defined for basic events, i.e. on eq.[9]. FV(BE_j) is the fraction of the risk metric that is associated to basic event j. RAW(BE_j) is the ratio of the risk that is produced when basic event j happens over the nominal risk. It can be proven that it is possible to extend the definition of FV to the parameter level [eq. (12)]. In this case, FV(x_i) is the fraction of the risk that is associated to parameter x_i.

GSA techniques focus on the output uncertainty. In this work, we analyzed the aplplication of the extended FAST (Saltelli, Tarantola and Chan, 1999) to a PSA model for the identification of the parameters that contribute to uncertainty the most. We also compared the results of the extended FAST to the following techniques, applied to the same PSA model:

- The Morris Screening Method (Morris, 1991)
- The Pearson Correlation Coefficient (PEAR), the Standardized Linear Regression Coefficients (SRC), the Partial Correlation Coefficient (PCC) and the corresponding techniques based on rank transformation (SPEAR), (Saltelli and Marivoet, 1990)
- The Smirnov test

4. COMPARISON OF IMS AND GSA TECHNIQUES

Suppose that R is of the form:

$$R=q_1+q_2 \tag{13}$$

with q_1 perfectly known, and equal to 0.1, and q_2 with mean 0.0001 and variance 10^{-3}. The nominal value of R is: $R_0=0.10001$. Applying PSA IMs we get that q_1 is the most important risk contributor, while the uncertainty in R is driven entirely by q_2, which is the most

important uncertainty contributor according to any of the previously mentioned GSA techniques. In this case, it is fairly easy to conclude that uncertainty in R is not driven by important risk contributors.

However, to determine whether uncertainty contributors are also relevant to the risk is not straightforward when dealing with PSA models that are characterized by a large number of parameters and for which R is not known analytically. Furthermore, standard PSA codes compute IMs at the basic event level, trhough eq. (9). We showed that GSA is properly performed at the parameter level. Thus some intermediate steps are necessary to connect the results of standard codes to the results of GSA. We propose the following:

1- Associate to each parameter the corresponding basic events

2- Compute the corresponding average rankings and re-scale the rankings according to the number of parameters.

3- Translate the IM and GSA rankings into Savage scores (Campolongo and Saltelli, 1997)

4- Compute the correlation coefficient on the scores

We finally note that, when comparing GSA results to the results obtained with parameter DIM and FV steps 1 and 2 are not necessary.

5. RESULTS

The previously mentioned GSA techniques were applied to the PSA Large LOCA sequence of a research reactor. The sequence consisted of 45 basic events, 31 parameters and 289 Minimal Cut Sets. The frequency of the initiating event, F_{LLOCA}, was identified as the most important parameter with respect to the uncertainty in R by using the extended FAST technique. Discrete agreement was found using non-parametric techniques based on rank transformation. However, convergence was not obtained for non-parametric techniques based on raw data, due to the model non-linearity. Poor performance of the Morris and the Smirnov test was registered. The application of the steps illustrated in Section 4 showed that uncertainty is not driven by parameters related to PSA elements important to safety. However, F_{LLOCA} ranked first using both GSA and IMs. This means that, collecting data on F_{LLOCA}, the analyst would be able to acquire information on an important risk contributor, while effectively reducing the uncertainty in the risk metric.

6. CONCLUSIONS

In this work, several GSA techniques were analyzed for application to PSA models. To understand whether the most important uncertainty contributors are important to safety, the comparison of PSA IM and GSA technique results was performed. The application to the Large LOCA sequence of a research reactor showed that uncertainty drivers were not important to safety for this model, with the exception of the frequency of the initiating event.

7. ACKNOWLEDGMENT

We thank Mr. J. Phillips and Ms. T. Thatcher of the Idaho Engineering Environmental National Laboratory, Idaho Falls, USA for providing the PSA model that enabled the analysis.

8. REFERENCES

Apostolakis G.E., 1995: " A Commentary on Model Uncertainty," *Proceeding of the Wokshop on Model Uncertainty: its Characterization and Quantification*, published by Center for Reliability Engineering, University of Maryland, College Park, Maryland, USA.

Apostolakis G.E. and Kaplan.S., 1981 : "Pittfalls in Risk Calculations," *Reliability Engineering*, 2, 135-145.

Borgonovo E. and Apostolakis G.E., 2001: "A New Importance Measure for Risk-Informed Decision-Making," *Reliability Engineering and System Safety*, to appear, 2001.

Campolongo F. and Saltelli A., 1997: "Sensitivity Analysis of an Environmental Model: an Application of Different Analysis Methods," *Reliability Engineering and System Safety*, 57, 49-69.

Cheok M.C., Parry G.W. and Sherry R., 1998: "Use of Importance Measures in Risk-Informed Regulatory Applications," *Reliability Engineering and System Safety*, 60, 213-226.

Morris M.D., 1991: "Factorial Sampling Plans for Preliminary Computational Experiments," *Technometrics*, 33 (2), 161-174.

Saltelli A., Tarantola S. and Chan K. P.-S., 1999: "A Quantitative Model-Independent Method for Global Sensitivity Analysis of Model Output," *Technometrics*, 41, 1, 39-56.

RISK-BASED ENVIRONMENTAL REMEDIATION OF CONTAMINATED SITES: UNCERTAINTY ANALYSIS APPLIED TO RISK ANALYSIS MODEL

Nadal, Nadia[(1)]; Carlon, Claudio[(2)]; Critto, Andrea[(1)]
Marcomini, Antonio[(1)]; Pastres, Roberto[(3)]

(1)Dept. of Environmental Sciences and
(3)Dept. of Physical Chemistry,
University Ca' Foscari,
Calle Larga S. Marta 2137 Venice, Italy.
Email: lanadal@yahoo.it ; critto@unive.it
marcom@unive.it ;pastres@unive.it

(2) Consorzio Venezia Ricerche, V. della Libertà 5-12
Parco Scientifico Tecnologico
VEGA, Marghera-Venice, Italy.
Email: carlon@unive.it

SUMMARY

The Risk Assessment applied to contaminated sites is a procedure to determine site specific cleanup goals. Three contaminated sites were the object of the stepwise risk assessment procedure undertaken according to the American Society for Testing and Materials. The second and third tiers were performed by applying an analytical and a numerical model respectively. With the numerical model either a deterministic or probabilistic risk analysis were performed. Sensitivity analysis was also undertaken to determine the input parameters uncertainty that exhibit most influence on probabilistic risk estimation and to identify each parameter which needs a deeper characterisation, such as, in our case the hydrogeological parameters.

The probabilistic risk estimation confirmed its fundamental role in the risk assessment; the use of deterministic third tier only provided site specific cleanup goals that are not protective for the human health.

1. INTRODUCTION

Human health risk analysis of a contaminated site is a technical procedure based on the source-pathway-receptor scheme. It is composed of four phases: the site characterisation, the exposure analysis, the toxicological assessment, and the risk characterisation [1].

The risk assessment applied to contaminated sites, besides risk characterisation, determines remediation site specific target levels (SSTLs), which are the acceptable soil contamination that produce an acceptable risk level [2].

RBCA [2] is an internationally recognised risk assessment procedure. It is a three tiered approach moving from conservative assumptions and simple predictive models to more site specific parameter values and complex probabilistic models, which might provide less stringent SSTLs beside more expensive and time consuming analysis.

In this work, the tiered analysis has been applied to three case studies to verify the dependence of risk-based clean-up goals upon site-specific characteristics and to outline advantages and limits of a more accurate probabilistic risk analysis.

It has to be noticed that the risk analysis applied to contaminated sites is a quite new discipline. In fact, the contaminated sites started to be a problem when several industrial areas near the cities were dismissed. The deterministic risk estimation was the main goal for risk assessors till a few years ago. Recently, the US Environmental Protection Agency [3] focused the attention on probabilistic risk analysis in order to include the uncertainty estimation into the risk assessment. Probabilistic risk assessment is not a novel procedure. It was applied in different risk assessment fields as lakes acidification, nuclear and traffic accidents. However, there is a growing awareness among scientists and decision makers of the value of integrating these uncertainties into the human health risk analysis of contaminated sites. Although the use of probabilistic methods are strongly recommended [4], only some of the most used commercial software packages apply the probabilistic analysis.

Finally, it is authors' opinion that in the risk analysis of contaminated sites the third level models should need a sensitivity analysis (SA). In fact, SA is a tool to determine the areas of uncertainty (illustrated in methodology section) most affecting the probabilistic risk estimation. Moreover, it can identify the parameters of each area which need a deeper characterisation.

The current software packages allow to estimate the uncertainty of the risk but they are not designed to perform a sensitivity analysis in respect to its sources. This appears to us as a limitation of this generation of software packages for risk assessment, which should be overcome by the next one. To this regard, the direct implementation of advanced tools for performing a quantitative SA or a more flexible approach to the generation of Monte Carlo samples of input factors, which would allow the user to carry out the SA using its own tools, would represent a step forward. However, in order to get a first idea of the importance of each factor, we carried out a global sensitivity based on linear methods of the risk predicted by an analytical model, which makes use of the same formulations but assumes steady-state conditions. Based on the results of this analysis, which we intend to repeat on the numerical model, only uncertainties of the hydrogeological parameters and of soil contaminants concentrations were considered in the following uncertainty analysis.

2. METHODOLOGY

The tiers two and three of risk assessment were performed by using the software RBCA Tool Kit [5] and API-DSS [6] respectively. The RBCA Tool Kit is implemented exclusively in a deterministic mode using conservative assumptions about exposure scenarios for simulating the contaminants fate and transport. It employs analytical algorithms to quantify the contaminant concentration at the exposure point in a steady state equilibrium with the concentration at the source. The API-DSS can be implemented in either a deterministic or a probabilistic approach (through a Monte Carlo simulation method). It employs numerical models to simulate the transport of pollutants in the environment. The third level of risk analysis requires a number of site specific parameters larger than second level.

The probabilistic analysis, allowing the estimation of the risk uncertainty was performed according to US-EPA guidelines [3,7]. The following areas of uncertainty were identified:

- uncertainty on hydrogeological parameters (permeability, porosity, etc.) and contamination levels. This uncertainty refers to site-specific data;
- uncertainty on human exposure factors (frequency and duration of exposure, etc.). Since risk assessment refers to hypothetical future scenarios, conservative values for

these factors are indicated by the model or obtained by US-EPA Exposure Factors Handbook;

- uncertainty on physico-chemical properties of the chemicals of concern. The properties of individual compounds were obtained by Oak Ridge National Laboratory database (http://risk.lsd.ornl.gov) and Mackay et al. [8];
- uncertainty on toxicological properties of contaminants. Toxicological properties have been obtained by US-EPA Integrated Information System (http://www.epa.gov/iris) and Oak Ridge National Laboratory databases.

This work was focused on the site-specific uncertainty associated to the hydrogeological parameters and the soil contaminant concentrations.

3. RESULTS

The risk posed by most of substances (see Table 1) through the inhalation route and groundwater ingestion pathway were greater in the second tier than in the third. It is due to the different modelling methods employed by RBCA and API-DSS. The RBCA assumes a constant contaminant source for simulating steady state conditions, while API-DSS simulates the decreasing over the time of the contaminant source and the resulting variation of vapour and leachate emission. API-DSS estimated a contaminant intake and the related risk lower than RBCA.

Table 1. Carcinogenic risks estimated for one of the three case studies

Chemicals	Second Tier RBCA			Deterministic Third Tier API-DSS			Probabilistic Third Tier API-DSS					
	Soil ingestion, Dermal contact	Inhalation	Ground water ingestion	Soil ingestion, Dermal contact	Inhalation	Ground water ingestion	Soil ingestion, Dermal contact		Inhalation		Groundwater ingestion	
							Median	95% Perc.	Median	95% Perc.	Median	95% Perc.
Benzo(a) Anthracene	7.1E-07	2.5E-08	**1.7E-06**	**2.0E-06**	1.4E-08	0	8.9E-07	**6.4E-06**	2.6E-09	2.0E-08	1.6E-08	3.6E-07
Benzo(a)pyrene	**1.3E.05**	**1.1E-06**	**1.6E-05**	**3.6E-05**	2.5E-07	0	**1.4E-05**	**5.3E-05**	8.5E-08	2.8E-07	1.4E-08	5.1E-07
Benzo Fluorantheni	7.1E-07	2.1E-07	**1.2E-06**	**2.0E-06**	1.4E-08	0	**1.0E-06**	**4.3E-06**	1.4E-08	2.9E-08	9.3E-07	**3.6E-06**
Crysene	**1.9E-06**	9.5E-07	**6.3E-05**	4.2E-07	3.8E-08	0	1.6E-07	8.3E-07	9.4E-09	4.8E-08	6.4E-07	9.3E-07
Dibenzo(a,h) Anthracene	**1.7E-06**	4.9E-08	3.1E-07	**4.7E-06**	3.3E-08	0	**2.6E-06**	**1.1E-05**	9.1E-09	4.7E-08	0	**4.4E-06**
Indeno (1,2,3,c,d)pyrene	**1.8E-06**	1.7E-07	**1.6E-06**	**5.0E-06**	3.5E-08	0	**2.4E-06**	**1.0E-05**	8.4E-09	4.4E-08	3.7E-11	1.1E-08
Arsenic	**6.4E-05**	**2.5E-05**	**3.5E-06**	**1.3E-04**	**1.8E-05**	0	**5.2E-05**	**1.9E-04**	**6.1E-06**	**2.2E-05**	0	0
Cadmium	NA	**2.3E-06**	NA	NA	**1.6E-06**	NA	NA	NA	2.5E-07	**1.6E-06**	NA	NA

The non acceptable risks are in bold (>1.0E-06)
NA = Non applicable because the toxicological parameters are not defined

The groundwater ingestion pathway risk estimation outlined relevant differences between probabilistic and deterministic analysis performed at the third tier. As reported in Table 1, negligible risk from the deterministic analysis turned out to be not acceptable after undertaking the uncertainty analysis. The uncertainty associated to the hydrogeological and contamination input parameters, indicated by the difference between the median and the 95th

percentile of the probabilistic risk estimate, showed an uncertainty of about one order magnitude (i.e. factor ten).

The SA conducted with the analytical model RBCA outlined the non effect of hydrogeological parameters, as groundwater rate, at the steady state. Analysing the contaminants transport over the time, it was pointed out the importance of groundwater rate when greater than 10^{-6} m/s. Under this condition, low contaminant soil-water distribution coefficients (K_d)(i.e. K_d = 15 l/kg for Cadmium) became important.

The relative contribution of different exposure pathways to the total exposure can differ in tier two and three. For all three case studies, the greatest risk contribution in tier two came from the groundwater ingestion, the soil ingestion and the dermal contact with soil. At the third level, since most of the substances did not reach the well, the greatest risk contribution was posed by soil ingestion and dermal contact. Once the contaminants reached the well, for the most mobile substances (such as naphthalene and phenanthrene that are non carcinogens), the groundwater ingestion posed a relevant risk. It can be observed that SSTLs resulting from the second tier level show the necessity of a remediation intervention addressed to both soil and groundwater pathways. After conducting the third risk analysis level, a cleanup intervention is required for soil pathway only.

The risk-based SSTLs derived from the risk analysis procedure were compared with the generic threshold values proposed by the Italian Regulation for the Remediation of Contaminated Sites [D.M. 471/99]. The application of regulatory threshold limits leads either to too restrictive clean up targets, or to not sufficiently protective targets. Generally the threshold limits were too restrictive for non-carcinogenic substances, and not enough protective for carcinogenic chemicals.

4. DISCUSSION

Risk assessment proved to be a very effective tool for setting up the experimental information and selecting the remediation strategies. Comparing the tiered approach results, it is shown that further investigation and a smaller number of conservative assumptions, produces less restrictive remediation targets compared with less site-specific risk analysis.

The uncertainty analysis was very effective for the risk analysis based on site specific parameters and numerical models, especially for the groundwater ingestion pathway when the deterministic analysis estimated negligible risk values for most the contaminants. The regulatory agencies in charge of public health protection should be aware of both risk and uncertainty estimations.

The application of global and quantitative SA methods to the problems outlined in this paper would be of great help for identifying the parameters responsible of the majority of the total uncertainty.

It was proved that the application of general regulatory threshold limits can lead to over- or underestimation of the human health risk

5. REFERENCES

1. U.S. EPA. Risk assessment guidance for Superfund, Volume 1, Human Health Evaluation Manual. EPA/540/1-89/002. Washington DC. (1989).
2. ASTM - American Society for Testing and Materials. Standard Provisional Guide for Risk-Based Corrective Action. PS 104 Philadelphia. (1998).
3. U.S. EPA. Policy of Use of Probabilistic Analysis in Risk Assessment at the U.S. Environmental Protection Agency. EPA/ORD/NCEA. Washington D.C. (1997).
4. Carlon, C. Risk assessment of contaminated sites. PhD Thesis, University of Ferrara. Italy. (1999).
5. Groundwater Services Inc. TIER 2 RBCA Tool Kit. Guidance Manual for Risk-Based Corrective Action. Houston, Texas. (1995).
6. American Petroleum Institute. Decision Support System for Exposure and Risk Assessment. Version 1.0. Geraghty e Miller, Inc. Washington D.C. (1994).
7. U.S. EPA. Guiding Principals for Monte Carlo Analysis. EPA/630/R-97/001. Washington D.C. (1997).
8. Mackay, D.; Ying Shiu, W.; e Ching Ma, K. Illustrated Handbook of physical-chemical properties and environmental fate for organic chemical. Lewis Publishers. (1992).

ON THE USE OF SENSITIVITY ANALYSIS FOR UNRAVELING PROBABILISTIC PERFORMANCE ASSESSMENT RESULTS AT YUCCA MOUNTAIN

S. Mishra, N.E. Deeds and B.S. RamaRao

Duke Engineering & Services, 9111 Research Blvd., Austin, Texas 78758 (USA)
E-mail: sxmishra@dukeengineering.com

1. INTRODUCTION

The total system performance assessment (TSPA) model for predicting the behavior of the potential high-level radioactive waste repository at Yucca Mountain represents a complex system with hundreds of parameters. Many of the parameters are uncertain and/or variable, and their interaction with one another can also be complex and/or highly nonlinear. It is difficult to obtain an understanding of exactly how the model works and what the critical uncertainties and sensitivities are from a simple examination of model results. Sensitivity analysis provides a structured framework for unraveling the results of probabilistic performance assessments by examining the sensitivity of the TSPA model results (and their uncertainties) to the uncertainties and assumptions in model inputs. This paper describes the application of two sensitivity analysis techniques, regression analysis and classification tree analysis, to the recently concluded TSPA study for Yucca Mountain [1].

2. METHODOLOGY

Regression analysis is a commonly used tool for identifying key contributors to the spread in probabilistic model results by fitting a stepwise linear rank regression model between model output and all randomly sampled inputs [2]. In this approach, a sequence of regression models is constructed starting with a single selected input parameter (usually the parameter that explains the largest amount of variance in the output), and including one additional input variable at each successive step (usually the parameter that explains the next-largest amount of variance). This is repeated until all of the statistically significant input variables have been included in the model. Relative importance ranking is accomplished using the partial rank correlation coefficient, which measures correlation between the output and the selected input variable after the linear influences of the other variables in regression have been eliminated [2]. Importance can also be quantified by ranking parameters on the basis of how their exclusion would degrade the explanatory power of the regression model [3]. The importance-ranking metric used for in this study is the uncertainty importance factor, defined as the loss in explanatory power (R^2-loss) divided by the coefficient of determination (R^2) of the regression model.

Classification tree analysis, a subset of classification and regression tree analysis (CART), is a method for determining what variables or interactions of variables control extreme outcomes in multivariate data sets [4]. CART can be used to generate decision rules that determine whether a given observation would produce a "high" or "low" dose depending on

the values of the most important variables. A binary decision tree is at the heart of the CART analysis. The decision tree is generated by recursively finding the variable splits that best separate the output into groups where a single category dominates. The domination of a single category resulting from a split is called the "purity" of that split. For each successive fork of the binary decision tree, the CART algorithm searches through the variables one by one to find the purest split within each variable. The splits are then compared among all the variables to find the best split for that fork. The process is repeated until all groups contain a single category. In general, the variables that are chosen by the algorithm for the first several splits are the most important. The application of CART for analyzing probabilistic model results has hitherto not been reported in the literature.

3. YUCCA MOUNTAIN TSPA MODEL

The total-system model for Yucca Mountain consists of detailed and/or abstracted process models addressing the following components of the disposal system: (1) water flow through the unsaturated zone, (2) waste package degradation, (3) waste form dissolution and radionuclide mobilization from the engineered barriers, (4) radionuclide transport through the geosphere and biosphere, and (5) potentially disruptive events and processes. A probabilistic framework was used to account for uncertainty and/or variability in model parameters, with conservative/bounding values and/or models being utilized when data were deemed insufficient for a defensible stochastic characterization of uncertainty. The TSPA model was executed with 300 Latin hypercube samples of the 240+ stochastic parameters, and the total dose rate history was computed separately for the nominal scenario (components 1-4) and disruptive scenario (component 5). For reasons of brevity, only a few sensitivity analysis results for the nominal scenario are presented below.

4. RESULTS AND DISCUSSION

McNeish et al. (2000) have shown that there is a broad range in projected dose rates over the 100,000 year simulation period, with most of the realizations producing negligible dose during the first few tens of thousands of years. Regression analysis of such data is difficult because of the limited number of non-zero dose producing realizations, as well as the large number of stochastic inputs in the model. Therefore, regression analysis was restricted to those time slices (at 10,000 year increments) for which at least 100 realizations produced dose in excess of 10^{-5} mrem/yr. Stepwise rank regression models between total dose and a set of statistically significant input variables were built for each case, and the most important variables were identified based on the value of their uncertainty importance factor. As an example, **Figure 1** shows a bar chart of such results generated for the 70,000-year data, indicating that the most important variables are the stress corrosion cracking (SCC) outer and middle lid stress profile indexes and the Alloy-22 outer lid median general corrosion rate. These are variables that determine the rate at which the metallic barriers of the waste package (surrounding the waste canisters) degrade**.** **Figure 2** shows how uncertainty importance factors change with time for the key uncertain variables. Note the slow but steady increase in importance for saturated zone groundwater flux with time – indicating the gradual importance of the natural system once the degradation of the engineered barriers has progressed.

Next, we present an application of classification tree analysis to the same data set to determine which variables control extreme outcomes. The multiple realizations of total dose,

at any given time slice, were first categorized as "high" if the values were in the top 10th percentile, or "low" if the values were in the bottom 10th percentile. The CART algorithm then identified those variables most capable of explaining the separation of these realizations into the appropriate categories. **Figure 3** shows a decision tree summarizing the classification tree analysis in terms of the two most important variables for the 70,000-year data. Here, the variables related to SCC middle and outer lid stress profile indexes provide the most explanatory power in the categorization problem. High values for both the stress profiles indexes leads to high doses, and conversely, low values for both stress profile indexes leads to low doses. This trend is also demonstrated in the partition plot shown in **Figure 4**, where high and low dose producing outcomes are separated into the top right and bottom left quadrants. The partition plot is actually an input-input scatter plot which shows the occurrence of clusters in the bivariate parameter space of the two most important variables, with the dividing lines indicating where the split between the categories occurs.

We also examined the variability in predicted waste package failure distributions to obtain further insights into the workings of the TSPA model. A scatter plot of total dose and fraction waste packages failed at 100,000 years is shown in **Figure 5,** with a focus on those realizations where more than 80 percent of the packages have failed. The two shaded regions in the figure demarcate "high" dose outcomes (dose greater than 100 mrem/yr) from "low" dose outcomes (dose less than 15 mrem/yr). A CART analysis of this data, as depicted in **Figure 6**, indicates that infiltration scenario and saturated zone groundwater flux are the two most important parameters in explaining the categorization. The important point to note here is that even when a large percentage of the waste packages have failed, certain combinations of natural system parameters can provide effective waste isolation. This analysis demonstrates the power of the CART analysis in "mining" the data to provide insights into cause-effect relationships that are not readily apparent otherwise.

5. ACKNOWLEDGMENTS

This work was funded by the Yucca Mountain Site Characterization Project under contract number DE-AC01-91RW00134

6. REFERENCES

1. McNeish, J.A. et al., 2000. *Total System Performance Assessment – Site Recommendation*. Civilian Radioactive Waste Management System, Management and Operating Contractor, Yucca Mountain Project, Las Vegas, NV.
2. Helton, J.C., 1993. "Uncertainty and Sensitivity Analysis Techniques for Use in Performance Assessment for Radioactive Waste Disposal." *Reliability Engineering & System Safety*, 42 (2-3), 327-367.
3. RamaRao, B.S., S. Mishra, S.D. Sevougian and R.W. Andrews, 1998. "Uncertainty Importance of Correlated Variables in the Probabilistic Performance Assessment of a Nuclear Waste Repository." Proceedings of *SAMO98, Second International Symposium on Sensitivity Analysis of Model Output*, Venice, Italy, April 19-22.
4. Breiman, L., J.H. Friedman, R.A. Olshen and C.J. Stone, 1984. *Classification and Regression Trees*. Wadsworth and Brooks/Cole, Monterey, CA.

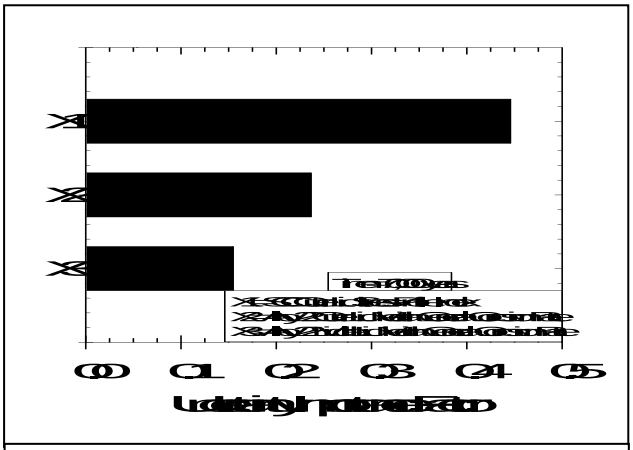

Figure 1. Bar Chart of Uncertainty Importance Factors for Key Variables at 70,000 years.

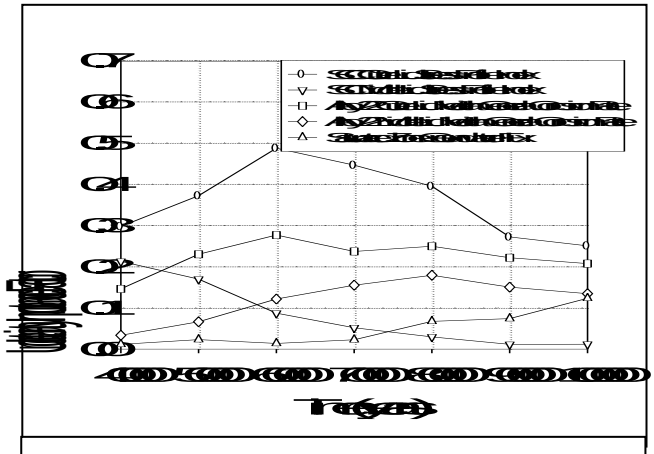

Figure 2. Time-Varying Uncertainty Importance Factors for Key Variables.

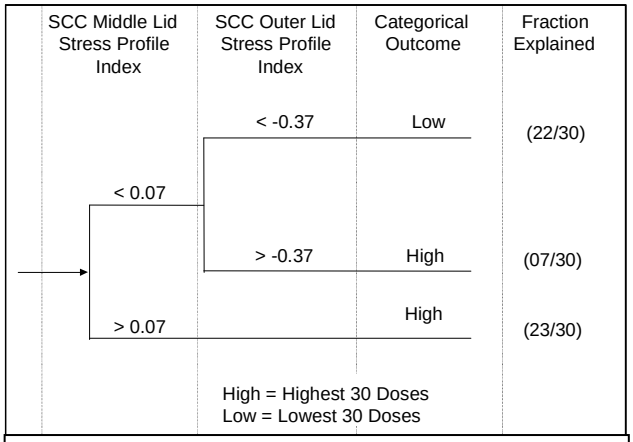

Figure 3. Decision Tree Summarizing CART Analysis for Key Variables at 70,000 years.

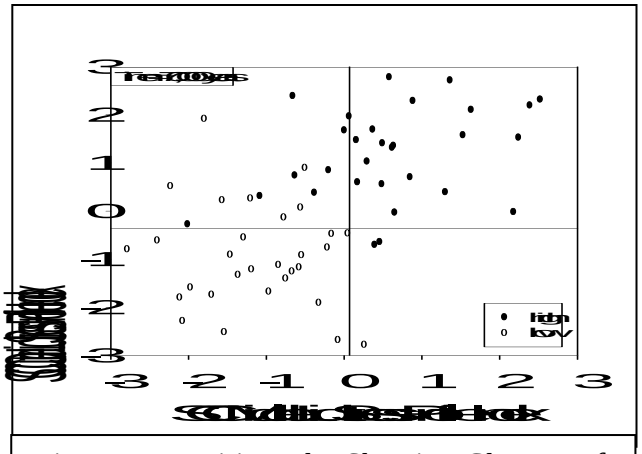

Figure 4. Partition Plot Showing Clusters of High- and Low-Dose Outcomes at 70,000 years

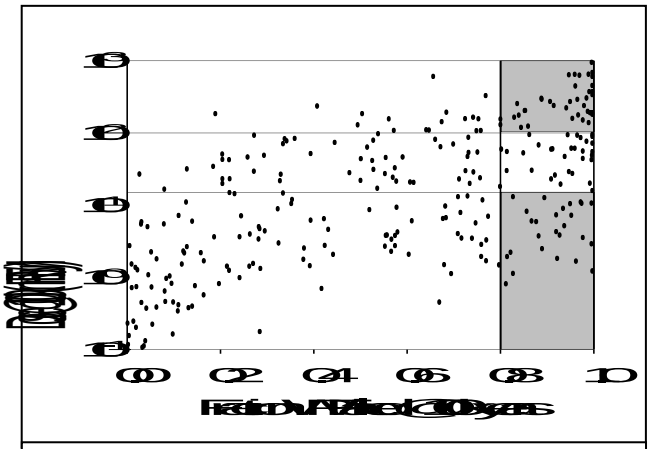

Figure 5. Scatter Plot of Total Dose and Fraction Waste Packages Failed at 100,000 years.

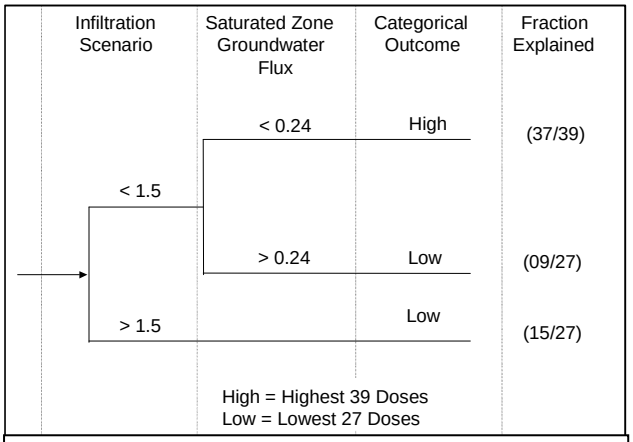

Figure 6. Decision Tree Summarizing CART Analysis for the Clusters Shown in Figure 5.

SENSITIVITY ANALYSIS FOR HIGH PERCENTILES OF OCHRATOXIN-A EXPOSURE DISTRIBUTION

I. Albert, J.P. Gauchi

National Institute for Agricultural Research
Research Center of Jouy-en-Josas, Biometrics Unit
Domaine de Vilvert, 78352-Jouy-en-Josas (France)
Email: **Isabelle.Albert@jouy.inra.fr** ; **Jean-Pierre.Gauchi@jouy.inra.fr**

SUMMARY

High percentile estimations of the exposure to the mycotoxin Ochratoxin-A (OTA) in food, for the French population, were calculated in a previous study by a Monte Carlo type simulation method from real consumption and contamination data [1]. In this paper, from the same data (but only for the children class), we focus on sensitivity analysis (SA) of the high 95^{th} and 99^{th} percentiles (the simulation outputs), relatively to the variation of the parameters of the fitted probability density functions (the simulation inputs), necessary for having a relevant and stable estimation of these percentiles. After some preliminary trials, we postulated a quadratic polynomial model and we used an experimental design approach depending on a resolution-V fractional factorial design of 6561 experiments to lead to an optimal estimation of the polynomial model parameters. The factors ranges were established by bootstrap sampling taking into account the consumption dependencies by the Iman & Conover method [2] and, eventually, taking into account the parameter correlation of the fitted probability densities. Finally, we have validated and useful parsimonious polynomial models for each desired percentile showing a major influence of the distribution parameters of the two foods « Cereals » and « Pork », and eventually three with « Fruit Juices », in the sensitivity of the percentiles.

1. INTRODUCTION

The mycotoxin Ochratoxin-A (OTA) is a contaminant of grain stored in poor conditions, and through the food chain also contaminates several other foodstuffs, typically pork and poultry meat. Several toxicological studies [3] have shown the carcinogenic effect of this mycotoxin, particularly for the kidney, in rats. In humans, epidemiological studies indicate that this mycotoxin could be involved in the endemic nephropathy of the Balkans and cancer of the urinary tract which is associated with it [4]. For these reasons, this mycotoxin remains under the close surveillance of the « Conseil Supérieur d'Hygiène Publique » in France and thus evaluating human exposure to this mycotoxin is an important public health question. A consumption survey (ASPCC-CREDOC, INCA survey) organised by the DGAl – a department of the French Minister of Agriculture – has been conducted from June 1993 to June 1994 on 1161 individuals (children, women and men) to notably estimate risk assessment exposure to OTA in food. During seven days, the participants were questioned on their consumption of several types of food. For more detailed information on the origin of these data we refer the reader to Verger [5]. Our SA is restricted to the children class

(individuals younger than 15) and to the eight types of food « Cereals », « Dried Raisins », « Other Dried Fruits », « Pork », « Poultry », « Fruits Juices », « Wines » and « Coffee », keeping in mind that certain cover several foods. The contamination data come from elements independent of the consumption survey: they originate from "SCOOP task 3.2.2" reports (European Community) taking several member states into account. Descriptive statistics and histograms of these data can be found in Gauchi [1].

2. METHODOLOGY

An elementary exposure to OTA is defined by the product of a food consumption (normalized by the individual weight) by the contamination level of this food. A global exposure is the sum of several elementary exposures. A Monte Carlo type simulation method (the *MP-P* method) was defined and used in [1] to evaluate the global exposure to OTA and notably the 95th and 99th percentiles of the OTA exposure distribution. As this *MP-P* method depends on the values of the parameters of the probability density functions (*pdf*) fitted to consumption and contamination data, it is crucial to quantify the sensitivity of these high percentiles (the model outputs) to the variation of these parameters (the model inputs). Our SA is based on the joint tools: a quadratic polynomial postulated for modelling the variation of those model outputs and a resolution-V fractional factorial simulation design of 6561 experiments. The factors of this design are the fitted *pdf* parameters. We clarify the process in the following.

2.1. Polynomial model

After some preliminary trials, we assumed a full quadratic polynomial regression model for the model outputs studied . This regression model is based on 32 main factors, their 496 two-factor interactions and their 32 quadratic terms. The 32 factors are the *pdf* parameters: 16 parameters of the Gamma distributions relative to the eight consumed foods (each of these distributions is described by three parameters but the influence of the threshold parameter was not studied), and 16 parameters of the two-parameter Gamma distributions relative to the eight food OTA contaminations. The general form of the assumed model is:

$$y = \beta_0 + \sum_{j=1}^{32} \beta_j z_j + \sum_{j=1}^{31} \sum_{k=j+1}^{32} \beta_{jk} z_j z_k + \sum_{j=1}^{32} \beta_{jj} z_j^2 + \varepsilon , \qquad (1)$$

where the β are unknown parameters, the factors z are the consumption and contamination *pdf* parameters and ε is an error term for which no particular probability distribution is assumed and we only suppose its expectation is zero. The model (1) is a second degree (quadratic) polynomial in *z*. In the following, the model (1) was successively applied to the 95th and 99th empirical percentiles .

2.2. Simulation design

In a view to estimate optimally the parameters β, an appropriate simulation design was chosen. As the three-factor interactions and over are assumed negligible, it is well-known that a full factorial design of 3^{32} experiments is not necessary, especially as it should take a redhibitory time. Instead of this unfeasible design we built a resolution-V fractional factorial [6] simulation design of 6561 experiments. We remind that a resolution-V design allows us to estimate independently the parameters of the main effects of the factors (the z_j), of the 496

two-factor interactions (the $z_j z_k$), and of the 32 quadratic effects (the z_j^2). The factor levels were coded as -1 , 0 and +1.

2.3. Factor ranges

The factors z, *i.e.* the parameters of the consumption and contamination *pdf*, were the inputs of the SA. Thus, we had now to set their variation ranges. The aim was to make the inputs vary in a reasonable range but large enough to observe the response output varying. However we had only one data set for the consumptions and only one for the contaminations, and therefore no hypothesis of the factor variations could be made; no supplementary surveys or contamination analysis were available. Thus, with the aim to simulate a meaningful range for each factor we had the idea to determine it by a nonparametric bootstrap approach [7] achieved on the consumption and contamination samples. For each bootstrap sample the shape and scale parameters of a Gamma distribution were calculated. In a first approach, we didn't take into account the correlation between the shape parameter and the scale parameter to explore a larger domain of variation. In a second approach, we considered the correlation between the shape parameter and the scale parameter. In this approach, the parameters pairs were preserved: for each consumption and contamination sample, from 10,000 bootstrap samples, we obtained 10,000 parameter pairs. Their scatter plot showing an elliptical appearance, we determined a variation domain by calculating a 95%-concentration ellipse. In this ellipse, three squared variation domains were designed for the shape and scale parameters, the first one in the lower part of the ellipse (zone I), the second one in the middle part (zone II) and the third one in the upper part (zone III). So in this approach, three polynomial models were determined for each percentile.

3. RESULTS

We present here the results of the second approach which is more sophisticated. We fitted the model (1) to the 6561 experiments for the 95^{th} and 99^{th} percentiles in the three zones I, II and III. After a step of variable selection (depending on the sum of squares of each variable) and a validation step (examination of the residuals and simulation experiment tests), we obtained the reduced models given in Table 1, where the multiple correlation coefficient R^2 is given for all the models also.

95%-concentration elliptical zone	Percentile	Final Model	R^2
I (« LOW »)	95th	$\hat{y} = 28.1 - 8.2z_1 + 5.4z_2 + 1.2z_3 - z_4$	0.97
	99th	$\hat{y} = 61.5 - 18.1z_1 + 7.3z_2 + 2.7z_3 - 2.2z_4$	0.96
II (« MEDIUM »)	95th	$\hat{y} = 20.1 - 3.1z_1 + 2.6z_2 + 2.6z_3 - 0.7z_4 - 0.5z_5$	0.97
	99th	$\hat{y} = 39.1 - 6z_1 + 3.6z_2 + 4.9z_3 - 1.5z_4 - 0.5z_5$	0.94
III (« HIGH »)	95th	$\hat{y} = 16.7 - 1.7z_1 + 1.3z_2 + 0.7z_3 - 0.5z_4$	0.94
	99th	$\hat{y} = 30.4 - 3.2z_1 + 1.9z_2 + 1.3z_3 - z_4$	0.89

Table 1 : Polynomial models of the 95th and 99th percentiles in the three zones of the 95%-concentration ellipse with z_1 = « Cereals » contamination scale parameter; z_2 = « Cereals » contamination shape parameter; z_3 = « Cereals » consumption shape parameter ; z_4 = « Cereals » consumption scale parameter ; z_5 = « Pork » consumption scale parameter

4. DISCUSSION

Finally, we have parsimonious polynomial models for each percentile studied. These models should be used to obtain percentile estimations easily. The results between the 95th and 99th percentile are very close, except that the percentage of explained variability is a little bit smaller for the 99th percentile. The results of the three zones are similar, except that the larger zone, the « MEDIUM » one, shows one more significant term, the « Pork » consumption scale parameter. Note that, in the first approach where we didn't take into account the correlation between the shape parameter and the scale parameter, the domain of the factor variation was larger and the influence of the « Fruit Juices » food appeared.

It is difficult to compare our results with others because it does not exist such a study achieved by other research groups for the contamination by OTA, to our knowledge. The others estimations of the OTA exposure percentiles were very empirical. But we can say that we find a major influence of the « Cereals », « Pork » foods which are known by the epidemiologists and toxicologists to play an important role in the health risks in connection to OTA.

5. REFERENCES

1. Gauchi, J.P., (2001). Quantitative assessment of exposure to the mycotoxin Ochratoxin-A in Food. Submitted to Risk Analysis.
2. Iman, R.L., Conover, W.J. (1982). Commun. Statist.-Simula. Computa ., *11*, 3, 311-334.
3. Pfohl-Leszkowicz, A. (1999). Les mycotoxines dans l'alimentation : évaluation et gestion du risque. TECDOC, Paris
4. Moll, N., & Moll., M. (1995). Sécurité alimentaire du consommateur. TECDOC, Paris.
5. Verger, P., (1999). Exposure assessment to certain contaminants, working group « Contaminants ». Internal Technical Report, march 1999. INRA, Paris.
6. Box, GEP., Hunter, W.G., Hunter, J.S. (1978). Statistics for experimenters.
7. Efron, B., Tibshirani, R.J. (1993). An Introduction to the Bootstrap. Chapman & Hall.

POSTER SESSION

CALIBRATION AND SENSITIVITY ANALYSIS IN REACTIVE TRANSPORT MODELS FOR TIDAL WATERS. APPLICATION TO RADIONUCLIDE DISPERSION IN THE SUEZ CANAL[3].

J.M. Abril

Dpto. Física Aplicada I, University of Seville.
E.U.I.T.A. Carretera de Utrera km 1, 41013.- Sevilla (SPAIN)
E-mail: abril@cica.es

SUMMARY

During the last decade we have been developing conceptual and numerical models to study the dispersion of radionuclides in marine and estuarine environments. We are using approaches from the Computational Fluid Dynamics to solve the instantaneous water state and the dynamics of suspended solids and bottom sediments. This provides the physical scenario where the electrolytic reactions between dissolved radionuclides and the solid phase take place. The model structure is constructed so that each new sub-model is implemented over the previously established and validated basis. The final stage is a kinetic-reactive transport model for tidal waters. In this work we illustrate the calibration procedure and the sensitivity analysis in a modelling study of the dispersion of radioactive material in the Suez Canal waters.

1. INTRODUCTION

The fate of dissolved pollutants in the aquatic ecosystem will be strongly dependent on their chemical affinity to particulate matter in suspended loads and bottom sediments. Their dispersion has to be studied at different spatial and temporal scales [1]. As shown in this reference, a complete study requires a sequence of independently calibrated models dealing with hydrodynamics, transport of dissolved pollutants, suspended loads, sediment dynamics, and electrolytic reactions in aqueous suspensions. The final stage is a kinetic-reactive transport model for tidal waters.

A considerable amount of international trade is transported in Egypt through the Suez Canal including radioactive material. This results in increased public concern about hazardous safety in transport The hydrodynamics of the Suez Canal is complex and not jet well studied. During an IAEA Project, a relevant data set for hydrodynamics was prepared in collaboration with the Suez Canal Authority. Two field tracing experiments by using rhodamine B were carried out in the southern Suez Canal to study the dispersion of conservative pollutants. Some measurements of suspended loads concentrations served to adapt a submodel for suspended matter dynamics. Aquarium tracing experiments allowed us to find out suitable kinetic parameters to simulate the electrolytic reactions. Sensitivity analysis of the model predictions with respect to model parameters were done in connection with its calibration.

[3] **Work partially supported by the IAEA Co-operation Project with Egypt EGY/07/002 and by I+D contract with ENRESA.**

2. METHODOLOGY

In previous works we presented a detailed modelling study of the Suez Canal hydrodynamics using both 1D and 2D modelling approaches [2]. The continuity and momentum equations were numerically solved by using a finite-differences method. Some 100 hours of tidal elevations wee recorded and digitized at several stations within the canal. This served to provide suitable boundary conditions and for model calibration. The bed-friction coefficient in the momentum equation is the only parameter to be calibrated. This coefficient can vary with the spatial coordinates, but it may be inside a realistic range of values. The model is run several times varying this coefficient and comparing the computed time series of water elevations and velocities against the recorded ones. This comparison applies for several locations within the spatial domain till get a reasonable agreement for all of them.

Two tracing experiments were accomplished by using rhodamine [3]. The collected water samples were measured by luminescence spectrometry. Even within the narrow and regular canal, important two-dimensional effects appeared due to the asymmetry in the cross-sectional area and thus, in the lateral velocity profile. The advective-diffusive equation for a conservative tracer is solved by using a 2D-mesh and the previously computed velocity field. Different formulations of the dispersion coefficients in the longitudinal and lateral directions were tested, comparing computed concentrations at the sampling time with the measured values.

Most of the time, the suspended load concentrations and the instantaneous sedimentation rates show a dynamic equilibrium governed by the tidal changes in the settling and resuspension velocities [1]. The corresponding differential matter conservation equation can be solved coupled to the hydrodynamics and dispersion modules. The new parameters (settling and resuspension velocities) can be calibrated comparing computed time series of suspended loads against the recorded ones at several locations within the spatial domain [1].

The electrolytic reactions between the dissolved radionuclides and the suspended particulate matter can be formulated as a two-steps reaction with saturation [4]. Kinetic transfer coefficients can be found out from appropriate tracing aquarium experiments by using natural aqueous suspensions [5]. The top layer of the bottom sediments also uptakes dissolved radionuclides, from the water column and from the interstitial waters [1]. The penetration depth depends on the cohesiveness of the sediments and is a parameter to be calibrated. As the small grain size fraction on the top layer of bottom sediments can be resuspended by water currents, we distinguish two grain fractions in the sediments and we need an additional fitting parameter to adapt the kinetic coefficients to both grain size fractions, including the effect of the porosity. Granulometric, density and porosity analysis of bottom sediments are required. Sensitivity analysis of the model predictions with respect to model parameters can be performed prior to calibration, to investigate what parameters have a chance to be calibrated.

3. RESULTS

The calibration of our hydrodynamics model allowed us a reasonable description of water dynamics in the whole Suez Canal. Some examples of this are shown in Fig. 1. The dispersion model for conservative pollutants could be calibrated from the two field tracing experiments. Some details are given in Fig. 2. From some field measurements we adapted our

suspended matter submodel [1] to this new scenario. We used kinetics transfer coefficients derived from aquarium experiments carried out by using estuarine waters [5].

We applied our dispersion model to simulate the dispersion of hypothetical discharges (107 Bq each) of ^{239}Pu (a highly particle-reactive radionuclide) and ^{137}Cs (and almost conservative isotope) at Shallufa station. We stated the penetration depth for Pu in the top sediment layer as 5 mm, being this depth a parameter for calibration.

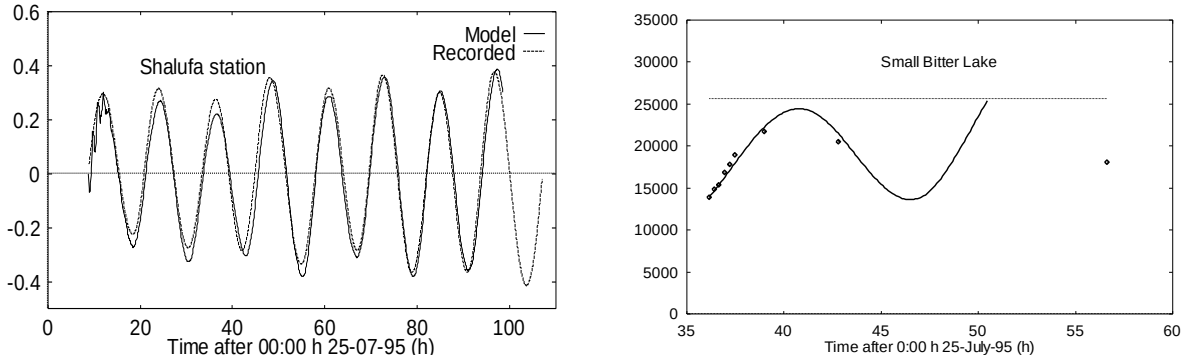

Figure 1.- A) Comparison between computed and recorded water elevations at Shallufa station, in the southern Suez Canal. B) Computed and measured path of the rhodamine cloud corresponding to the first field tracing experiment

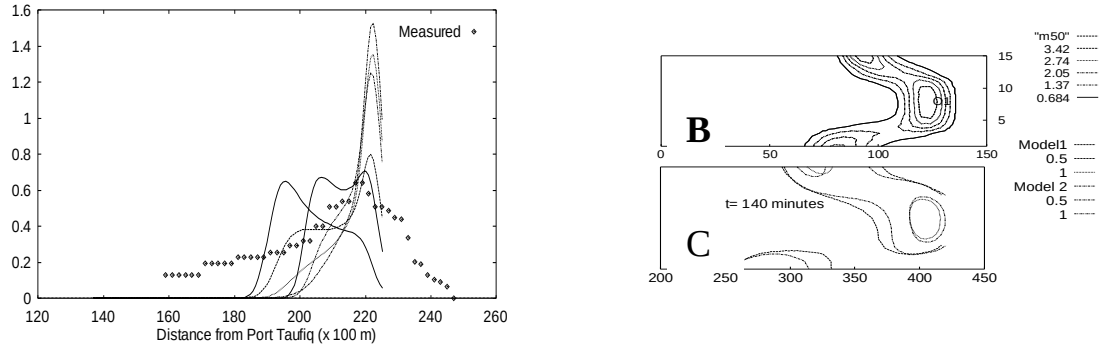

Figure 2.- A) Comparison between computed (at several longitudinal cross-sections) and measured concentrations of rhodamine. B) Computed spatial distribution of concentrations (in mg/m^3) at the sampling time. C) Comparison between computed concentrations (in mg/m^3) from two different formulations of the diffusion coefficient.

Sensitivity tests were done for the case of Pu, where the uptake by sediments is most important. In a second run of the model we divided by 5 the two correction factors for the direct kinetics transfer coefficients for sediments. This reduced by a factor 5 the concentrations in sediments and the effects are also apparent in the spatial distribution and time series of concentrations (see Fig. 3 and 4).

4. DISCUSSION

The kinetic-reactive transport model involves a set of independently calibrated and validated models. Hydrodynamics models are well established and they can be adapted and calibrated for each specific aquatic system. The study of the dispersion of mobile species requires further work, but ever more the literature data bank increases, and site specific field tracer experiment can be accomplished to calibrate the dispersion coefficients. The understanding and reliable modelling of the suspended loads and sediment dynamics is in progress. Appropriate laboratory experiments can provide the required kinetic parameters to reliably describe the electrolytic reactions in the aqueous suspension and bottom sediments. Sensitivity analysis is an useful technique in model calibration.

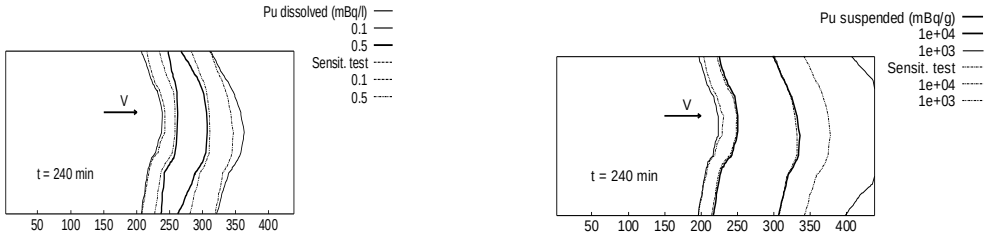

Figure 3.- Sensitivity test for the correction factors for the direct kinetic transfer coefficients in sediments. Comparison between the computed spatial concentrations of Pu in dissolved and suspended matter 4 hours after injection. "Sensit.test" reduces by 5 the correction factors.

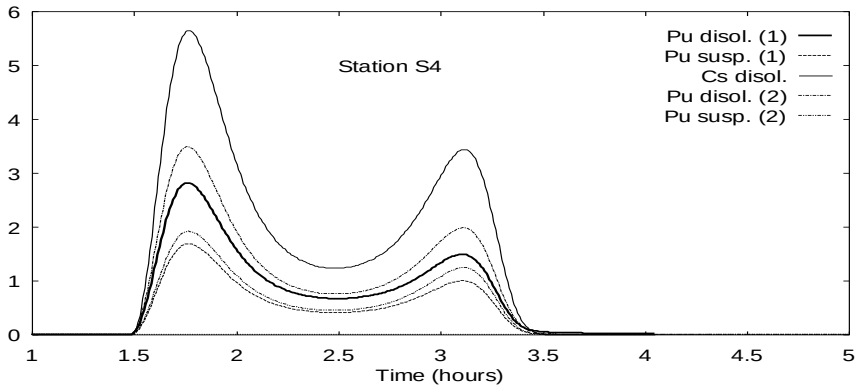

Figure 4.- Computed time series of Pu and Cs concentrations in dissolved phase at 4.9 km south of the injection point. Label Pu(2) corresponds to the same reduction in the correction factors that in Fig. 3.

5. ACKNOWLEDGEMENTS

This work was initiated in the NCNSRC, in Cairo, under an IAEA Project. I am indebted to all the colleagues from this Centre, specially to Dr M. Abdel-Aal.

6. REFERENCES

[1] Periáñez, R., Abril, J.M, & García-León, M. (1995) *J. Environ. Radioact*. **30**, 253-270.
[2] Abril, J.M. & Abdel-Aal, M. (2000). *Estuarine and Coastal Shelf Sciences*.50, 489-502.
[3] Abril, J.M., Abdel-Aal, M. Al-Gamal, S.A., Abdel-Hay, F.A. & Zahar, H.M. (2000). *Estuarine and Coastal Shelf Sciences*. **50**, 503-513.
[4] Abril, J.M. & Abdel-Aal, M. (2000). Ecological Modelling. **128**, 1-17.
[5] El-Mrabet, R., Abril, J.M., Manjón, G. & García-Tenorio, R. (2001). *Water Research* (accepted)

SENSITIVITY ANALYSIS APPLICATION: DYNAMIC THERMAL CHARACTERIZATION OF THE BUILDING

San Isidro M.J., Zarzalejo L.F.

CIEMAT,Avda. Complutense 22, 28040-Madrid (Spain).
Email: mj.sanisidro@ciemat.es ; lf.zarzalejo@ciemat.es

1. INTRODUCTION

The objective of this paper is the dynamic characterization a posteriori of the building as thermal performance. It could be a complementary way to the traditional simulations in building design phase, which provides us the dynamic thermal evolution of a building that is being used. For this proposes, we need real measurements (monitorization) of the main variables that take part in this system.

In the thermal behaviour of our building we must take account as input some external variables, like meteorological data, and the variation of internal conditions, indoor temperature and energy gains (heating-cooling systems and casual gains). In terms of block diagram we can imagine our system as a black box with an external input (weather conditions and adjacent areas temperature) which has a response that, with internal excitation added, feedback the system (Fig. 1).

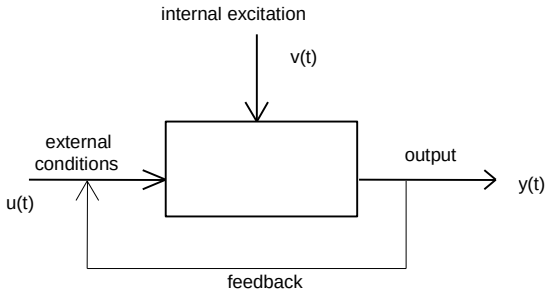

Fig 1. Application Description.

We could describe this system following the energy balance equation:

$$Mc\frac{dT}{dt} = UA_e(T_e - T) + UA_i(T_i - T) + A_sQ_s + Q_{aux} + Q_{int}$$

where:

- M_c refers to the thermal inertia of the building.
- T refers to the indoor temperature of the characterization area
- T_e refers to the outdoor temperature
- T_i refers to the temperature of the indoors adjacent areas.
- UA_e refers to the thermal looses coefficient respect to the outdoor.
- UA_i refers to the thermal looses coefficient respects to the indoor adjacent areas.
- A_s refers to the solar area of the characterization zone.
- Q_s refers to solar radiation energy gains.
- Q_{aux} refers to mechanical comfort system thermal gains.
- Q_{int} refers to casual internal thermal gains.

2. METHODOLOGY

The used procedure, to reach our objective, is based on the linear Transfer functions between our output and the main important inputs. But, our system presents two problems that make impossible to use linear functions directly: inputs are correlated and each one of them have important seasonal contribution.

In order to solve these aspects, it is necessary to carry out:

- *A principal component analysis* on the set of input variables. This kind of analysis is concerned with explaining the variance-covariance structure through a few linear combination of the original variables. The advantages of the principal components of a system are based on: they represent the directions with maximum variability, provide a simpler and more parsimonious description of the covariance structure and the set of principal components builds an uncorrelated system $\{z_i\}$.
- *To lead the System towards the stationarity.* The input variables involve in our system (temperature, solar radiation) are clearly not stationary due to seasonal component. It makes to suppose that their principal components $\{z_i\}$ follow being not stationary. We can find, by spectral analysis, the contribution of the seasonal part of each $\{z_i\}$. In this way, Fourier analysis on each $\{z_i\}$ guide us to know which are the most important frequencies $\{w_i\}$. These frequencies are chosen taking account that they represent at least the 85% of the total periodogram. Without loosing generality it is possible to suppose that each new variable $\{x_i\}$, that results from eliminating the seasonal part to $\{z_i\}$ is stationary except to some degree of differentiation.

$$X_t = Z_t - \sum_{i=1}^{K} \left(A_i \cos w_i t + B_i \operatorname{sen} w_i t\right) + \varepsilon_t$$

But these important frequencies relatives to the z-variable produce a seasonal part on the indoor temperature $\{T_t\}$ that also is eliminated

$$Y_t = T_t - \sum_{i=1}^{K} \left(A'_i \cos w_i t + B'_i \operatorname{sen} w_i t\right) + \varepsilon_t$$

2.1. Identification of transfer function models by prewhitening the input

Suppose the suitable differenced input process x_t is stationary and is capable of representation by some member of the general linear class of autorregresive-moving average models. Then, given a set of data, we can carry out our usual identification and estimation methods to obtain a model ARMA for the x_t process $\phi_x(B)\theta_x^{-1}(B)x_t = \alpha_t$. Which, to a close approximation, transforms the correlated input series x_t to the uncorrelated white noise series α_t. If we now apply this same transformation to y_t to obtain $\phi_x(B)\theta_x^{-1}(B)y_t = \beta_t$

Then the model may be written $\beta_t = v(B)\alpha_t + \varepsilon_t$ .On multiplying on both sides by α_{t-k} and taking expectations, we obtain $\gamma_{\alpha\beta}(k) = v_k\sigma_\alpha^2$ where $\gamma_{\alpha\beta}(k) = E[\alpha_{t-k}\beta_t]$ is the cross covariance at lag +k between α and β.

In terms of the cross correlation, $v_k = \dfrac{\rho_{\alpha\beta}(k)\sigma_\beta}{\sigma_\alpha}$ $\quad k = 0,1,2,\ldots$

Hence, after *prewhitening* the input, the cross correlation function between the prewhitened input and correspondingly transformed output is directly proportional to the impulse response function $\{v_i(B)\}$.

3. CASE STUDY

Our real system is an office room placed in Ciemat building 42 (Madrid, latitude 40.45ºN, longitude 3.73ºW, altitude 670m.), this office is placed in the first plant of the building and it only has an external East facade, and it is shaded from outside by some trees.The dimensions are: 3.81x5.02x2.70 m.

The monitorization period was carried out during September and October months of 1998. The variables measured were:

- The office indoor temperature
- The corridor temperature
- External temperature
- Solar global radiation

Not cooling-heating system was used during this period.

The inputs that take into account in the procedure are solar radiation $\{Q_s\}$, the difference between the office indoor and the external temperature $\{\Delta T_e\}$, and the difference between the office indoor and the corridor temperature $\{\Delta T_i\}$. The output corresponds to the office indoor temperature $\{T\}$.

3.1. Results

The component principal analysis lead us to two components, the eigenvectors and their corresponding eigenvalues for each component are:

$$v_1 = (-0.6830, -0.6963, 0.2205) \qquad v_2 = (-0.2191, -0.0927, -0.9713)$$

$$\lambda_1 = 1.6385 \qquad \lambda_2 = 0.9723$$

These two components produce 87.02% of the variability of the initial inputs.

In this way the new variables will be:

$$z_1 = -0.6830 * Q_s - 0.6963 * \Delta T_e + 0.2205 * \Delta T_i \qquad z_2 = -0.2191 * Q_s - 0.0927 * \Delta T_e - 0.9713 * \Delta T_i$$

The most important frequencies for each z_i are:

$$z_1 \Rightarrow \quad 0.2493, 0.2743, 0.5236$$

$$z_2 \Rightarrow \quad 0.0499, 0.0748, 0.0249, 0.0997, 0.2743, 0.1496, 0.1247, 0.3241$$

The stationary part of z_1 behavior as Autorregresive model of order 2.

$$x_1(t) = 1.0303 * x_1(t-1) - 0.2469 * x_1(t-2) + \alpha_1(t)$$

The stationary part of z_2 behavior as Autorregresive model of order 4.

$$x_2(t) = 0.8760 * x_2(t-1) - 0.3574 * x_2(t-2) + 0.095 * x_2(t-3) - 0.1155 * x_2(t-4) + \alpha_2(t)$$

Where x_i is the corresponding variable to z_i when its seasonal part has been eliminated. Eliminating from the output variable Y each one of the important frequencies relatives to each

input, it is obtained two variables {y1,y2} relatives to the contribution of each input respect to the output. In this way, is calculated the β_i

$$\beta_1(t) = y_1(t) - 1.0303 * y_1(t-1) + 0.2469 * y_1(t-2)$$

$$\beta_2(t) = y_2(t) - 0.8760 * y_2(t-1) + 0.3574 * y_2(t-2) - 0.095 * y_2(t-3) + 0.1155 * y_2(t-4)$$

In the Fig. 2 and 3, it is possible to see the cross-correlation function, for the first 40 lags, between each prewhitened input $\{\alpha_i\}$ and its corresponding transformed output $\{\beta_i\}$. It makes to think in a possible parameterization of each one function.

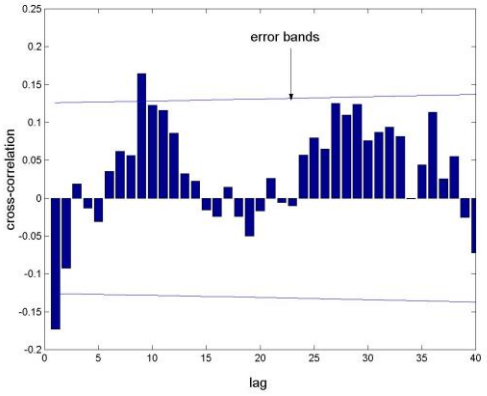

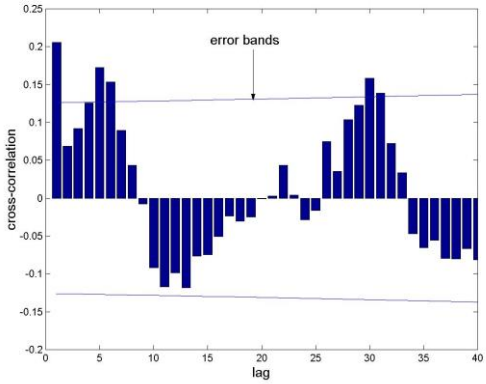

Fig 2: Cross-correlation between α_1&β_1 **Fig 3:** Cross-correlation between α_2&β_2

In the first case, the transfer function behaviour as an Autorregresive of the first order, and its first important lag corresponds to k=0. $y_1(t) = 0.733 * y_1(t-1) - 0.1469 * x_1(t)$

In the second case, the transfer function behaviour as an Autorregresive of the second order, and the first important lag corresponds to k=0. $y_2(t) = 1.1696 * y_2(t-1) - 0.2980 * y_2(t-2) + 0.1946 * x_2(t)$

Taking into account the weight $\{\lambda_i\}$ for each principal component $\{x_i\}$, it is possible to say that $y(t) = \frac{1}{2}[\lambda_1 * y_1(t) + \lambda_2 * y_2(t)] + n(t)$ Where n(t) is the residual between the measurement and simulated output. In Fig.4 it is possible to see the fitting between the measurement and simulated indoor temperature, after undoing the changes made in all the process

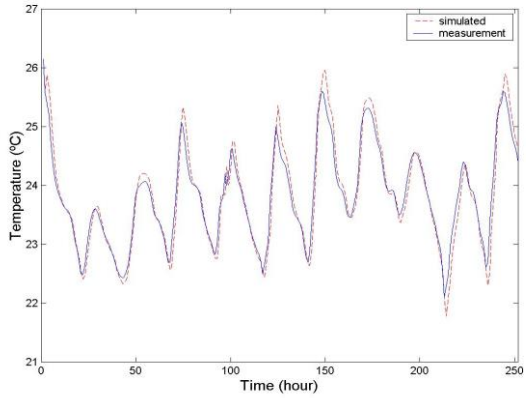

Fig.4: The measurement and simulated indoor temperature

4. REFERENCES

[1] Box G.;Jenkins G. "Time Series Analysis forecasting an control", Holden-Day, California.1976.

[2] Priestley M.B. "Spectral Analysis and Time Series", Academic Press, San Diego. 1981.

[3] Edited by J.J. Bloem "System identification applied to building performance data". Joint Research Center Euopean Commision EUR 15885 EN.1995.

SENSITIVITY ANALYSIS OF A LEONTIEF MODEL

V. Beletskyy, A. Chemeris**, E. Nowatskaya***

Computer Science and Informatics Department, Technical University of Szczecin, ul. Zolnierska 49, 71-210 Szczecin, Poland
Email: bielecki@wi.ps.pl

** Institute of Simulation Problems in Power Engineering, National Ukrainian Academy of Sciences, General Naumov St. 15, Kiev, Ukraine
Email: chemeris @sabbo.net

ABSTRACT

A Leontief model and a tool for its sensitivity analysis are presented. The main goal of building the model is to investigate interindustries processes in the Ukrainian economy. The model was built on the base of the Ukrainian national account date and interindustries Input-Output tables. The model is implemented as a program in the Visual Basic for Excel with using the GAMS(General Algebraic Modelling System) language and a GAMS solver. The tool for the investigation of the model sensitivity analysis is a special program that generates changes in input parameter values, solves linear equations, and calculates multipliers i.e. the changes in the endogenous variables in response to those in exogenous ones. Results of sensitivity analysis of the model are presented.

1. INTRODUCTION

The static input-output(I-O) model based on the linear structure of inter-industry production linkages pioneered by Wassily Leontief [1] marked the beginning of multi-sector planning. Leontief models are by far the most developed models that attempt to derive quantitative economy-wide implications of the interdependence of industries. These models have been successfully applied in many countries for economic policy making. I-O models describe a multi-sector economy where there are:

i. *Producing sectors.* Many outputs generating industries form the supply side of the economy. Goods and services produced by other sectors are used up as intermediate inputs by producing sectors to generate new products, which go into final consumption or used as intermediate inputs within the supply sector for further production.

ii. *Consuming sectors.* The target of production is to satisfy final demand by consuming sectors. These are known as the final demand sectors (households or private consumption, government purchases, exports and building of inventory stocks or saving). Generally, represented by households as the owners of resource factors (labour, capital, land) which they sell to producing sectors for income (wages, interest, rent, etc.), they then use that income to purchase consumption or investment goods and services from producers.

iii. *Resource factors.* Not produced within the system (e.g. labour and land). These resource factors typically do not explicitly appear as part of the I-O tables.

iv. *Intermediate inputs.* These are goods and materials produced by other supply sectors and absorbed back into the system to generate other products. Examples are steel, cotton, fertilisers, wheat, etc.

In compact form an I-O model can be written as

$$X = AX + d \quad . (1)$$

Where X is a vector of sectoral outputs(x_i is gross output of sector i), A is the I-O coefficient matrix(a_{ij} is the amount of product i required to produce one unit of j) and d is the vector of final demands(d_i is *final demand* for product i).

I-O models are concerned with solving for sectoral output levels (X) that satisfy final demands for those outputs (d) given the inter-industry structure of production (A). In other words, model (1) can determine the production plan that is consistent with a desired final demand vector (d) given the inter-sectoral transaction matrix (A), i.e. also meets indirect intermediate demands necessary to generate the target net output (d).

Depending on data availability and the desired degree of detailed sectoral analysis, I-O models can handle any level of disaggregation in the supply and demand sectors of the economy. Producing sectors can be disaggregated into several commodity sub-sectors, e.g. energy into petroleum, biomass, electric, and so forth.

The I-O model built for the Ukrainian economy includes the following sectors: electro energy, gas and petroleum, coal, other fuel, black metallurgy, coloured metallurgy, chemical, machinery, forest industry, other industry, building, agriculture, transport, trade, science, the other sectors. Imports and exports were added as well as division of final consumption between private households and government purchases.

2. MODEL IMPLEMENTATION

The implementation of the I-O model illustrates figure 1.

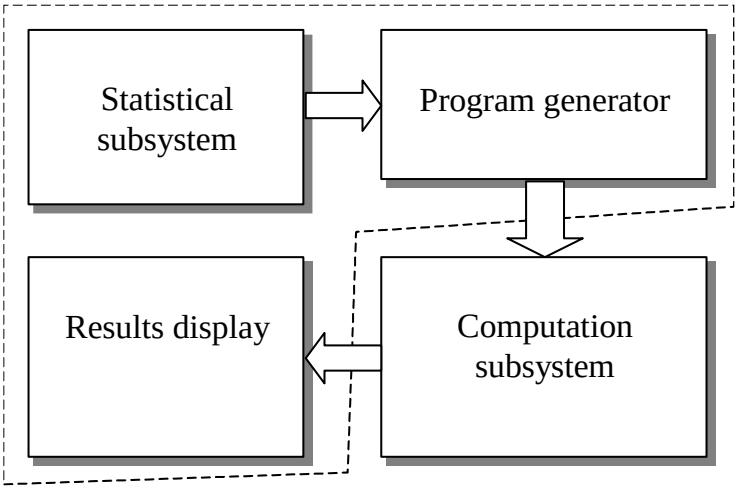

Fig.1

The statistical subsystem stores statistical date in the form of Input-Output tables for 1993-1998 years and calculates the matrix A coefficients. The program generator builds a GAMS program using the matrix A coefficients. This program describes an Input-Output model for a chosen year. GAMS (General Algebraic Modelling System) is a high-level computer language for the compact presentation of large and complex models, allowing changes to be

made in model specifications simply and safely, and permitting model descriptions that are independent of solution algorithms[2]. GAMS is available for use on personal computers, workstations, main-frames, and supercomputers. It lets the user concentrate on modelling, eliminating the need to think about purely technical, machine-specific problems. The computation subsystem solves linear equations of the I-O model. We use for this goal the MINOS solver. The solver yields values for the sixteen sectoral outputs.

Calculating multipliers was chosen as a basic technique for carrying out sensitivity analysis of the model, i.e. calculating the changes in the endogenous variables in response to those in exogenous ones. A multiplier myi for an output variable yi is calculated by the formula:

$$myi = ((yi(xi+\Delta xi) - yi(xi))/yi(xi))/(xi/\Delta xi),$$

where xi - an input variable, Δxi - an increment of xi. The multiplier myi shows how yi changes (in percents) as a result of 1 percent change in xi .

A user interface permits to choose any coefficient of the matrix A and determine an interval in which the coefficient can be vary [parmin, parmax]. Next the program forms (n+1) values of the coefficient: parmin, parmin+h, parmin+2h,..., parmax; where h=(parmax-parmin)/n and solves linear equations of the model for each coefficient value. The results display subsystem stores all the values of sectoral outputs and builds diagrams to demonstrate the dependence of outputs on a chosen coefficient.

The program was designed in Excel environment using the MINOS solver as the computation subsystem. The statistical subsystem, the program generator and the data display subsystem were realised in an Excel workbook as sheets and Visual Basic modules. All parts of the program are integrated by a user interface. A user can view all the sectors of the model, choose an investigated coefficient, set an interval in which the coefficient can be vary and start computation. After finishing all the computation loops, the results of calculation are written down into a special Excel sheet where the automatic diagram drawing is performed.

3. RESULTS

The goal of sensitivity analysis was to investigate how increasing/decreasing basic energy products (electro, gas and petroleum, and coal) required to produce one unit of a sector product at the same demands influences the Ukrainian economy. With this purpose a family of tables and diagrams was built on the date of 1997. Each diagram represents the dependence of a multiplier of gross output of sector i on increasing/decreasing a coefficient aij, were j corresponds to one of the energy sectors.

On the base of these results, the sectors that have the most influence on the energy sectors were detected, i. e. the sectors decreasing/increasing in which the amount of electro energy required to produce one unit of sectors production at the same demands yields the most change at the electro energy sector. The results are as follows. The coal sector has the most influence on the electro energy sector. The other sectors effect on the electro energy sector in the following decreasing order: gas and petroleum, coloured metallurgy, chemical, electro energy, science, other industry, machinery, black metallurgy, forest industry, transport, the other sectors, building, agriculture, trade, other fuel.

The ordered decreasing influence of the sectors on the gas i petroleum sector is as follows: gas and petroleum, transport, trade, chemical, electro energy, machinery, other industry,

science, coloured metallurgy, black metallurgy, forest industry, building, the other sectors, agriculture, coal, other fuel.

On the coal sector we have received the following ordered decreasing influence of the sectors: coal, electro energy, forest industry, machinery, black metallurgy, transport, chemical, other industry, trade, coloured metallurgy, gas and petroleum, the other sectors, science, agriculture, building, other fuel.

The results were passed to the Ukrainian Economy Ministry and Energy Sectors Ministries. Currently authors are carrying out research to handle impacts of structure adjusting in the Ukrainian economy by means of sensitivity analysis of the Leontief model.

4. CONCLUSION

Authors intend to extend the model to handle income distribution issues, trade policy, impacts of structural adjustment and industrial growth. Such extensions required relaxing the assumptions of linearity (to allow for substitution possibilities in production and consumption) and exogeneity of final demand and prices (to capture policy instruments present in decentralised economies with functioning markets). Those modifications led to the emergence of the family of non-linear programming and Walrasian computable general equilibrium models[3, 4] that we will describe and investigate by means of GAMS.

5. REFERENCES

[1] Leontief, W. *Studies in the structure of the American economy*. New York: Oxford University Press, 1953.

[2] Brook A., Kendrick D., Meeraus A.: GAMS, RELEASE 2.25. A USER's GUIDE, GAMS Development Corporation, 1996.

[3] Don H., van de Klundert T., van Sinderen J. (red): Applied General Equilibrium Modeling, Kluwer Academic Publishers, Dordrecht, 1991.

[4] Ballard C.L., Fullerton D., Shoven J., Whalley J.: A General Equilibrium Model for Tax Policy Evaluation. Chicago etc.: University of Chicago Press., 1985.

SENSITIVITY OF MONTE CARLO SIMULATIONS TO INPUT DISTRIBUTIONS

B S RamaRao[1], Srikanta Mishra[1], Jerry McNeish[2], Robert W Andrews[2]

[1]Duke Engineering and Services, 9111 Research Boulevard, Austin, TX 78758, USA
E-mail: bsramara@dukeengineering.com

[2]Duke Engineering and Services, 1211 Town Center Drive, Las Vegas, NV 89144, USA

SUMMARY

The sensitivity of the results of a Monte Carlo simulation to the shapes and moments of the probability distributions of the input variables is studied. An economical computational scheme is presented as an alternative to the replicate Monte Carlo simulations and is explained with an illustrative example.

1. INTRODUCTION

The post-Monte Carlo sensitivity analysis techniques used in performance assessment of nuclear waste repositories are directed towards identifying the important parameters based on their contribution to the uncertainty (variance) of the performance measure (e.g., dose). The United States Nuclear Regulatory Commission's revised regulatory criteria emphasize the "probability-weighted mean dose" as a performance measure. Also, the analysts are uncertain about the shapes and moments of the probability density functions (PDFs) of the input variables. This study focuses on methods to evaluate and display the sensitivities of the regulatory criterion, the mean dose, to the shapes and moments of the probability density functions of the input variables. Replicate Monte Carlo simulations can resolve this sensitivity, but are impractical for the complex models with a large number of inputs, as in the Yucca Mountain modeling studies. An alternative computational scheme, without recourse to additional Monte Carlo runs, is available [1,2] and is proposed for use in this study. This method belongs to a "re-weighting" scheme, and involves simple post-processing of the inputs and outputs of the Monte Carlo simulations. This numerical method is particularly suited to the Latin Hypercube Sampling scheme (LHS) used in the uncertainty modeling studies. The method is briefly described here and an example application is presented and the applicability of the proposed method is discussed.

2. METHODOLOGY

In a Latin Hypercube sampling scheme, the PDFs of each input variable are divided into N equi-probable intervals, where N is the number of samples and one sample is drawn from each interval randomly. When the PDF of a specific input variable is altered, the same intervals and the same samples are retained as in the original LHS; but the probabilities of those intervals change from their values of $1/N$ in LHS to different values in the new PDF. This procedure is illustrated in Figure.1. The modified probabilities (q_m) are used to compute the

unbiased estimates of different moments of the output variable (Eq.1), and the cumulative distribution function, *F* (Eq. 2).

$$E\left(Y^r\right)=\sum_1^N q_i Y_i^r \quad \textbf{(1)}$$

$$F(z)=P(Y\le z)=\sum_1^N q_i U(z-Y_i) \quad \textbf{(2)}$$

where, $U(t)=1;t\ge 0$ and $\mathrm{U(t)}=0;t<0$. Here, Y_i denotes the value of the output variable *Y* for the *i* th sample, and *E*(.) denotes the expected value.

This procedure can be extended to cases of two or more variables with new PDFs, where q_i is obtained as the product of the modified probabilities in each of the new PDFs. In this case care needs to be exercised to normalize the resulting weights. The algebraic details are provided in [1] and a code to implement this scheme, named PDFSENS is developed and documented [3].

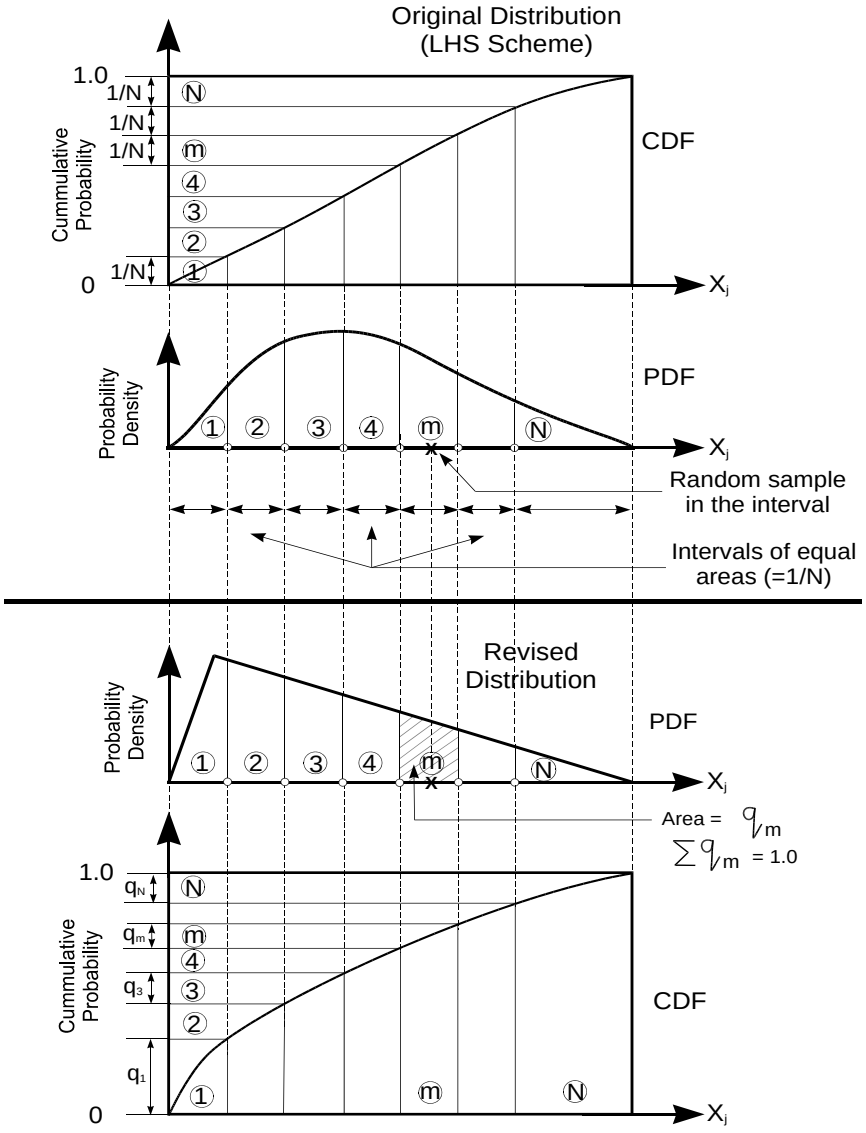

Figure 1. Original and Revised Probability Distribution Functions for the Variable X_j

3. APPLICATION: RESULTS AND DISCUSSION

The methodology is illustrated using an analytical "screening" model of health risk arising from water-borne radionuclide migration [4]. This simple model contains components representing source release, geosphere transport and biosphere transport for a single member radionuclide chain. The source term is described by an initial containment time followed by radionuclide release at a rate specified as a fraction of the current nuclide inventory, with radioactive decay occurring all along. The geosphere term includes one-dimensional transport with advection, dispersion, equilibrium sorption and decay. The biosphere term is based on a stream being the principal groundwater pathway, and includes the rate of drinking water intake by an individual, the stream flow rate, the activity-to-dose factor, and the risk factor for radiation induced cancer fatality. As described in the original reference, intermediate expressions for the source term, the geosphere term and the biosphere term can be combined using the Laplace transformation technique to yield a time-dependent consequence, $C(t)$, given by:

$$C(t) = \frac{1}{2} B k M_o e^{-\lambda(T_0+t)} e^{L/2d} e^{-RL^2/4dvt} e^{-vt/4dR}$$
$$\left[\phi\left\{ \left(\frac{RL^2}{4dvt} \right)^{1/2} + \left(\frac{vt}{4dR} - kt \right)^{1/2} \right\} + \phi\left\{ \left(\frac{RL^2}{4dvt} \right)^{1/2} - \left(\frac{vt}{4dR} - kt \right)^{1/2} \right\} \right] \quad (3)$$

where $\phi(z) = \exp(z^2)\mathrm{erfc}(z)$, and the other symbols are as defined later. Note also that the consequence, $C(t)$, is a risk term which expresses the probability of deaths per year beyond the initial containment period (i.e., for $t > T_o$).

This simple model is used to compute human health risk (and its associated uncertainty) after 20 000 y of waste emplacement due to the migration of a single radionuclide from a hypothetical repository. The uncertain parameters in the model are taken to be: (1) fractional release rate, k; (2) groundwater velocity, v; (3) retardation R; and (4) the path length L. The other parameters are taken to be fixed. Table 1 provides the list of stochastic parameters and their ranges used for the alternative PDFs. In respect of the truncated normal distributions, these ranges, i.e., the minimum and the maximum correspond to the 0.1 and 99.9 percentiles respectively. For generating the Monte Carlo simulations of the output variable C, all the stochastic variables are assigned truncated normal distributions. The parameters k, R, ν, and L are selected for studying the effects of modified distributions on the output mean. The other parameters are held constant in these simulations: initial Inventory M_O= 1.0E+16 Bq, containment time T_O= 0 years, decay constant λ =3.25E-6/year, dispersivity d =20 m, and biosphere conversion factor B_O = 1.0E-18 deaths/Bq. More details of this and other examples are provided [3].

Table 1. Ranges of Stochastic Variables

Variable	Minimum	Maximum
Release Rate k (y^{-1})	1.0E-06	1.0E-05
Retardation R	3.16	31.6
Groundwater Velocity ν (m y^{-1})	0.0316	0.316
Geosphere Path L (m)	168.7	561.7

In this case, the normal distributions are replaced by triangular distributions with the same range (with the mid-point as the mode), for one variable at one time, without re-simulation, based on the re-weighting scheme described here. The results from the re-weighting scheme are compared with the re-simulation scheme using the modified distribution. Table 2 shows the results.

Table 2. Results from Re-Weighting and Re-Simulation Schemes (100 Samples)

Variable	Y_{mean}	
	Re-Weighting Scheme.	**Re-Simulation Scheme**
K	0.0414	0.0423
R	0.0507	0.0516
ν	0.0436	0.0463
L	0.0437	0.0464

The results show that re-weighting scheme produces results in reasonable agreement with re-simulation. The deviations range from 2% to 8%. This may be treated as a validation of this methodology. Accuracy of similar order is noted in respect of higher order moments and for the cumulative distribution function but are not included here.

4. CONCLUSION

The examples presented here suggest that re-weighting scheme offers a computationally efficient scheme for computing the expected value of a simulated result under revised probability distributions. However, the method may not provide good results, if the revised probability distributions entail ranges far different from that of the original distribution. Also, the method may fail for the case of very small sample size and for the case of highly skewed probability distributions.

5. ACKNOWLEDGMENTS

This work was funded by the Yucca Mountain Site Characterization Project under contract number DE-AC01-91RW00134.

6. REFERENCES

Iman, R L, 1980. Risk Methodology for Geologic Disposal of Radioactive Waste: Small Sample Sensitivity Techniques for Computer Models, With an Application to Risk assessment. NUREGCR-1397/ SAND801397, Sandia National Laboratories, Albuquerque, NM. 211289.

Beckman, Richard J., McKay, Michael D. Monte Carlo Estimation Under Different Distributions Using the Same Simulation. Technometrics, Vol 29, No. 2, 1987.

CRWMS M&O, 2000: Software Routine Report for PDFSENS (10190-SRR-1.0-00), Civilian Radioactive Waste Management System, Management and Operation Contractor

Robinson, P.C. and Hodgkinson, D.P. 1986 Exact Solutions for Radionuclide Transport in the presence of Uncertainty. UK Atomic Energy Agency Report No. AERE R 12125.

INFLUENCE OF THE GE INACTIVE LAYER THICKNESS ON DETECTOR CALIBRATION SIMULATION FOR ENVIRONMENTAL RADIOACTIVE SAMPLES USING THE MONTE CARLO METHOD

J. Ródenas[1], A. Pascual[1], I. Zarza[1], V. Serradell[2], J. Ortiz[2], L. Ballesteros[2]

[1] Departamento de Ingeniería Nuclear
[2] Laboratorio de Radiactividad Ambiental
Universidad Politécnica de Valencia
Apartado 22012 E-46071 Valencia, Spain
E-mail: jrodenas@iqn.upv.es

1. INTRODUCTION

One of the most powerful tools used for environmental radioactivity measurements is a gamma spectrometer, which usually includes a HP Ge detector. The detector should be calibrated in efficiency for each considered geometry. Simulation of the calibration procedure with a validated computer program becomes an important auxiliary tool for an environmental radioactivity laboratory being that it permits one to optimise calibration procedures and reduce the amount of radioactive wastes produced. The Monte Carlo method is applied to simulate the detection process and obtain spectrum peaks for each modelled geometry [1, 2].

An accurate detector model should be developed in order to obtain a good accuracy in the output of the calibration simulation [3]. An important parameter in the detector model is the thickness of any absorber layer surrounding the Ge crystal, particularly the inactive Ge layer.

In this paper, a sensitivity analysis on the inactive Ge layer thickness is performed using MCNP 4B code [4]. Results are compared with experimental measured efficiency. A sensitivity analysis is also performed on the aluminium cap thickness.

2. METHODOLOGY

One of the major problems to perform any detector calibration simulation is the lack of accurate data about Ge crystal. In other words, many details of the detector geometry are not well known. Calculated efficiency is very sensitive to the germanium dead layer, a layer of inactive germanium, not useful for detection, but strongly attenuating photons [3].

When data provided by detector manufacturers are used in the simulation, some strong discrepancies appear between calculated and measured efficiencies. They can be attributed to the existence of a transition zone between the inactive layer and active Ge in the crystal [5]. Photons absorbed in the transition zone will not contribute to the full energy peak count rate. Thus, concerning detector efficiency, the transition zone behaves as an inactive layer.

Therefore, a sensitivity analysis on the inactive Ge layer thickness is performed varying this thickness in our detector model. Calculations have been performed for all of the radionuclides included in a calibration gamma cocktail solution for each thickness of the inactive Ge layer. Results have been compared with experimental measurements. A Marinelli

beaker has been considered for this analysis as it is one of the most commonly used recipients for this type of measurements.

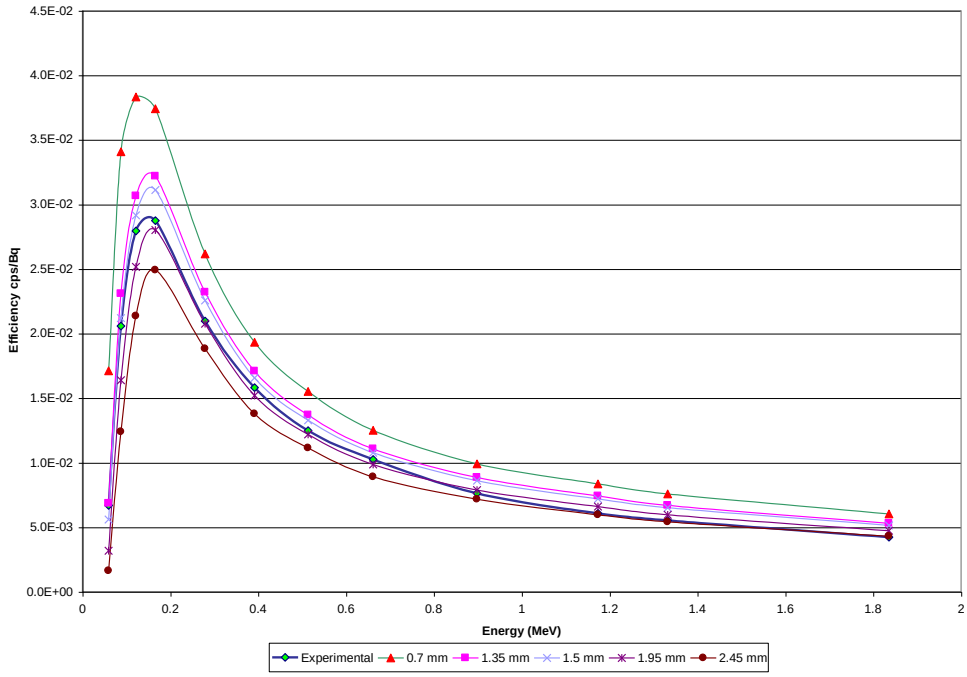

Fig. 1 Variation of efficiency with ene**rgy**.

3. RESULTS

To develop the sensitivity analysis proposed, four values for the inactive Ge layer thickness have been considered besides the value (0.7 mm) provided by the manufacturer. Calculated efficiencies for each considered inactive Ge layer thickness as well as experimental values are plotted in terms of energy in Fig. 1. The MCNP to experimental efficiency ratios are listed in Table 1.

Table 1 Ratio of calculated to experimental efficiency.

Nuclide	**Energy (MeV)**	**Inactive** germanium **layer thickness (mm)**				
		0.7	**1.35**	**1.5**	**1.95**	**2.45**
Am-241	0.060	2.56	1.02	0.84	0.47	0.24
Cd-109	0.088	1.66	1.12	1.03	0.80	0.60
Co-57	0.122	1.37	1.10	1.04	0.90	0.76
Ce-139	0.166	1.30	1.12	1.08	0.97	0.87
Hg-203	0.279	1.25	1.11	1.08	0.99	0.90
Sn-113	0.392	1.22	1.08	1.05	0.96	0.87
Sr-85	0.514	1.24	1.10	1.06	0.98	0.89
Cs-137	0.662	1.22	1.08	1.05	0.96	0.87
Y-88	0.898	1.30	1.16	1.13	1.03	0.94
Co-60	1.173	1.37	1.22	1.18	1.08	0.98
Co-60	1.333	1.37	1.21	1.18	1.08	0.98
Y-88	1.836	1.42	1.25	1.21	1.12	1.02

4. DISCUSSION

When the dead layer thickness is increased, an additional shielding as well as a smaller detector active volume, are introduced into the model, hence efficiency decreases. However, this effect is not the same for all energies. For the lowest energies (Am-241 to Ce-139), the best agreement with experimental data is shown for a 1.35 mm dead layer. This agreement is improved (except for Am-241) when a 1.5 mm layer is considered. For this value the behaviour is acceptable except for the extreme values. Increasing the inactive layer thickness up to 1.95 mm we obtain a better agreement for higher energies. However, the discrepancy for the lowest one is strongly increased. Finally, a thicker layer (2.45 mm) is modelled to obtain the best agreement for the highest energy, but deviations for medium and lower energies make this value unacceptable.

TABLE 2 **CALCULATED TO EXPERIMENTAL EFFICIENCY RATIO FOR DIFFERENT ACTIVE VOLUMES**.

Nuclide	**Energy (MeV)**	**Active** germanium **volume (cm^3)**				
		124.435	**123.961**	**122.791**	**122.091**	**121.310**
Am-241	0.060	0.8367	0.8367	0.8369	0.8370	0.8372
Cd-109	0.088	1.0298	1.0299	1.0300	1.0300	1.0297
Co-57	0.122	1.0440	1.0438	1.0433	1.0430	1.0427
Ce-139	0.166	1.0837	1.0836	1.0824	1.0812	1.0799
Hg-203	0.279	1.0945	1.0888	1.0761	1.0691	1.0603
Sn-113	0.392	1.0746	1.0655	1.0476	1.0370	1.0244
Sr-85	0.514	1.1021	1.0910	1.0637	1.0513	1.0369
Cs-137	0.662	1.0927	1.0790	1.0508	1.0353	1.0187
Y-88	0.898	1.1805	1.1657	1.1284	1.1086	1.0911
Co-60	1.173	1.2355	1.2197	1.1822	1.1575	1.1326
Co-60	1.333	1.2403	1.2222	1.1798	1.1580	1.1321
Y-88	1.836	1.2814	1.2594	1.2142	1.1863	1.1662

TABLE 3 **EFFICIENCY AND RATIO OBTAINED FROM VARYING ALUMINIUM LAYER THICKNESS**.

Nuclide	**Energy (MeV)**	ALUMINIUM LAYER THICKNESS							
		0.77 mm		**1.27 mm**		**1.77 mm**		**2.27 mm**	
		Efficiency	**C/E Ratio**	**Efficiency**	**C/E Ratio**	**Efficiency**	**C/E Ratio**	**Efficiency**	**C/E Ratio**
Am-241	0.060	5.80E-03	0.87	5.59E-03	0.84	5.38E-03	1.04	5.18E-03	0.78
Cd-109	0.088	2.18E-02	1.06	2.12E-02	1.03	2.07E-02	1.03	1.95E-02	0.95
Co-57	0.122	2.99E-02	1.07	2.91E-02	1.04	2.84E-02	1.03	2.77E-02	0.99
Ce-139	0.166	3.18E-02	1.11	3.11E-02	1.08	3.04E-02	1.02	2.98E-02	1.04
Hg-203	0.279	2.29E-02	1.09	2.26E-02	1.08	2.21E-02	1.02	2.17E-02	1.03
Sn-113	0.392	1.68E-02	1.06	1.66E-02	1.05	1.63E-02	1.02	1.60E-02	1.01
Sr-85	0.514	1.35E-02	1.08	1.33E-02	1.06	1.31E-02	1.01	1.29E-02	1.03
Cs-137	0.662	1.09E-02	1.06	1.08E-02	1.05	1.06E-02	1.01	1.05E-02	1.02
Y-88	0.898	8.69E-03	1.14	8.60E-03	1.13	8.50E-03	1.01	8.42E-03	1.11
Co-60	1.173	7.25E-03	1.19	7.18E-03	1.18	7.11E-03	1.01	7.04E-03	1.16
Co-60	1.333	6.56E-03	1.19	6.50E-03	1.18	6.44E-03	1.01	6.39E-03	1.16
Y-88	1.836	5.17E-03	1.22	5.13E-03	1.21	5.08E-03	1.01	5.04E-03	1.19

The effects on the efficiency of shielding and detection active volume and especially its dependence on energy, have been confirmed by varying the Ge active volume but maintaining the same inactive layer. When the active volume is decreased, efficiency decreases for all energies except for the lowest one for which it slowly increases. Furthermore for E<200 keV efficiency decreases very slowly. These results are shown in Table 2 by listing the MCNP to experimental efficiency ratio for different values of Ge active volume. The original volume considered in previous calculations (Fig. 1 and Table 1) is 122.791 cm^3.

Finally, a sensitivity analysis on the aluminium cap thickness was performed using the 1.5 mm inactive Ge layer model. Results are listed in Table 3. It can be seen that the influence of this parameter is less important. Still, it can be noted that an increasing absorber layer produces a better agreement with experimental efficiencies for higher energies but a strong deviation for the lower ones.

5. CONCLUSIONS

The sensitivity analysis performed shows that an increasing value of absorber layers causes a decreasing calculated efficiency. However, this behaviour is different for lower and higher energies. It is also different for Al and Ge as when the inactive Ge layer is increased, not only a thicker shielding but also a lower detection volume is included in the model.

A better agreement between calculated and measured efficiencies is obtained using, in the detector model, a value for the inactive Ge layer thickness greater than that provided by the detector manufacturer (at least twice this value).

Small increments on this value of inactive Ge layer thickness show less discrepancies from experimental measured efficiency for lower source energies, while a thicker layer seems to be necessary to match experimental efficiency for higher energies. This can be attributed to the fact that the shielding effect is greater for lower energies, while the effect of decreasing the active volume is similar for all the energy range with less influence for lower energies.

6. REFERENCES

[1] J. Ródenas, V. Rius: **Application of Monte Carlo method to the simulation of Ge-detector calibration**. TOPSAFE'98, Valencia (Spain), 15-17 April 1998.

[2] J. Ródenas, A. Martinavarro, V. Rius: **Validation of the MCNP code for the simulation of Ge-detector calibration**. Nuclear Instruments & Methods in Physics Research A 450 (2000) 88-97.

[3] J. Ródenas, J. Ortiz, L. Ballesteros, V. Serradell: ***Analysis of the Simulation of Ge-Detector Calibration for Environmental Radioactive Samples in a Marinelli Beaker Source Using the Monte Carlo Method****. International Conference on Advanced Monte Carlo for Radiation Physics, Particle Transport Simulation and Applications. MC 2000, Lisbon (Portugal), 23-26 October 2000.*

[4] J. F. Briesmeister (Editor): **MCNP - A General Monte Carlo N-Particle Transport Code, Version 4B**, LA-12625-M, Los Alamos National Laboratory, Los Alamos, New Mexico, March 1997.

[5] A. Clouvas, S. Xanthos, M. Antonopoulos-Domis, J. Silva: **Monte-Carlo based method for conversion of *in-situ* gamma ray spectra obtained with a portable Ge Detector to an incident photon flux energy distribution**. Health Physics 74(2): 216-230; 1998.

PREMIUM SENSITIVITY USING BIMODAL PRIOR DISTRIBUTIONS

E. Gómez, J.M. Pérez and F.J. Vázquez Polo

Dpto. Métodos Cuantitativos. Univ. de Las Palmas de G.C. 35017 Las Palmas de G.C.(Spain)
Email: emilio@empresariales.ulpgc.es; josema@empresariales.ulpgc.es;
polo@empresariales.ulpgc.es

SUMMARY

We study the situation where collective risk model in credibility theory has two types of risks that can be modelled by two structure functions (prior distributions). This model can be used in two ways. First is the good/bad risks models. In this case, two kinds of risks are present in the population: α_1% with low probability of a claim or loss amount, and the other α_2% are bad risks with high claim or loss amount probability. Second way can be useful if we have a bimodal prior distribution for the population. A bayesian sensitivity analysis for this model is presented and we provide a result for calculating variation range of bayesian premium in this situation. A Numerical example is provided.

Keywords and phrases: Credibility theory, net premium principle, bimodal structure function, Bayesian robustness, classes of priors.

1. INTRODUCTION

In this paper, bayesian approach is applied to estimate net premiums. Let Θ be a random variable, and $X_i|\Theta=\theta,\ i=1,2,...,t$, the claims or loss amount in subsequent years. We assume that given θ the X_i´s are conditionally independent and identically distributed random variables.

One goal of credibility theory is to estimate the conditional mean $E[X|\theta]$, which is known as the net premium principle. The loss distribution of a given risk is characterized by its conditional mean, but that mean is generally unknown. Therefore, assume that the value θ is fixed for a given risk, althought it is generally unknown. The probability density function of Θ is given by $\pi(\theta)$; this is the prior distribution in bayesian analysis, also called *structure function*, the distribution that represents one's uncertainty about the parameter Θ before observing claim data for a given risk.

In this paper we study the situation where the collective has two types of risks; α_1% are good risks with a low probability of a claim or loss amount, and the other α_2% are bad risks with a high claim or loss amount probability that can be modelled by two structure functions (prior distributions) $\pi_1(\theta)$ and $\pi_2(\theta)$. Therefore our prior distributions of θ is given by $\pi_0(\theta)=\sum_{i=1}^{2}\alpha_i\pi_i(\theta)$, with $\alpha_1,\alpha_2\in\mathcal{R},\alpha_1+\alpha_2=1$. Bayesian analysis requires two models;

the sampling density $f(x|\theta)$ and the prior $\pi_0(\theta)$, which is given in our model by a convex sum of probability distributions. Since prior specification is typically imprecise, recent attention focuses towards local sensitivity which measures the effect of perturbations of the inputs to the final answer.

2. CALCULATION OF PREMIUM IN A CLASSICAL BAYESIAN ANALYSIS

A premium calculation principle assigns to any risk *X* (with probability function $f(x|\theta)$, where *x* takes values in the sample space $\mathcal{X}$ and θ considered a realization of a parameter space Θ) a real number, which is the premium. In the case of the net premium principle the premium (Heilmann, 1989) is given by $\mathcal{P}(\theta) = E_{\mathcal{X}}[X|\theta] = \int_{\mathcal{X}} xf(x|\theta)dx,\ \theta \in \Theta.$

In experience ratemaking the actuary takes a claim experience $\mathcal{M}$=*m* from the random variables $X_1, X_2, ..., X_t$ and uses this information to estimate the unknown fair premium $\mathcal{P}(\theta)$. Now, let $\pi_0(\theta) = \sum_{i=1}^{2} \alpha_i \pi_i(\theta)$ denote the prior density function of θ, which is given by a convex sum of two prior distributions; the good and bad risks distributions. The posterior distribution of θ given the likelihood *m* is given by

$$\pi_0(\theta|m) = \frac{f(m|\theta)\pi_0(\theta)}{\int_\Theta f(m|\theta)\pi_0(\theta)d\theta} = \sum_{i=1}^{2} \alpha_i' \pi_i(\theta), \text{ where } \alpha_i' = \frac{\alpha_i\, p(m|\pi_i)}{\sum_{i=1}^{2} \alpha_i\, p(m|\pi_i)}$$

and $p(m|\pi_i) = \int_\Theta f(m|\theta)\pi_i(\theta)d\theta$ is the marginal distribution of $\mathcal{M}$ with respect to prior π_i. Using net premium principle, bayesian net premium (Heilmann, 1989; Eichenauer et al., 1988) is given now by $\mathcal{P}^*_{\pi_o}(m) \equiv \int_\Theta \mathcal{P}(\theta)\pi_0(\theta|m)d\theta, = \sum_{i=1}^{2} \alpha_i \mathcal{P}^*_{\pi_i}(m).$ Assume now that the number of claims generated annually depends upon chance, while the amount of the individual claim is taken as fixed. Suppose that the number of claims follows a Poisson distribution with parameter θ and the prior distribution of this parameter is a convex sum of two gamma density functions, this is $\pi_0(\theta) = \sum_{i=1}^{2} \alpha_i Ga(a_i, b_i) = \sum_{i=1}^{2} \alpha_i (a_i^{b_i} / \Gamma(b_i))\theta^{b_i - 1} e^{-a_i \theta}$, where $a_i, b_i > 0$. If we know the claims $x_1, ..., x_t$ of periods 1 to *t* of the random variables $X_1, ..., X_t$ and $m = (1/t)\sum_{i=1}^{t} x_i$, bayesian net premium is given by $\mathcal{P}^*_{\pi_o}(m) \equiv \sum_{i=1}^{2} \alpha_i' \frac{b_i + tm}{a_i + t}.$ Now we consider claims amounts instead claims and suppose that the likelihood is the exponential distribution, this is $f(x) = \theta e^{-\theta \cdot x}$, and prior distribution is the same that the other example above. In this case, bayesian net premium is given by $\mathcal{P}^*_{\pi_o}(m) \equiv \sum_{i=1}^{2} \alpha_i' \frac{a_i + tm}{b_i + t - 1}.$ In this paper, range of bayesian net premium is found over the class $\Gamma_\varepsilon^j = \left\{ \pi = (1-\varepsilon)\sum_{i=1}^{2} \alpha_i \pi_i + \varepsilon \sum_{i=1}^{2} \beta_i q_i, q_i \in \mathcal{Q}_i \right\},\ (j = 1,2),$ with $\mathcal{Q}_i^1 = \{$All probability

distributions} and $\mathcal{Q}_i^2 = \{q_i(\theta) : q_i$ is unimodal with the same mode θ_i, as that of $\pi_i\}$, where θ_i is the modal value for the distribution of expected value of claims (or loss amount), $\pi_i(\theta)$. Using Γ_ε^1, if similar conclusions are obtained, no additional information is required; however, if conclusions differ markedly, we must obtain more information. In this case we could acquire partial information about the prior (for example, the bimodality) and consider all prior distributions that are compatible with this information, using Γ_ε^2. Before presenting the results a preliminary is required which is given in the following theorem.

Theorem. *Suppose B>0 and* $f_i(x_i), g_i(x_i)$, $i = 1,2$ *are continuous functions with* $g_i(x_i) \geq 0$, *then*

$$\sup_{dF_1, dF_2} \frac{A + \sum_{i=1}^{2} \int f_i(x_i) dF_i(x_i)}{B + \sum_{i=1}^{2} \int g_i(x_i) dF_i(x_i)} = \sup_{x_1, x_2} \frac{A + \sum_{i=1}^{2} f_i(x_i)}{B + \sum_{i=1}^{2} g_i(x_i)}.$$

The same result holds with sup replaced by inf.

$$\inf_{\pi \in \Gamma_\varepsilon^1} \mathcal{P}_\pi(m) = \inf_{\theta \in \Theta} \mathcal{R}(\theta), \text{ with } \mathcal{R}(\theta) = \frac{(1-\varepsilon)\left[\sum_{i=1}^{2} \alpha_i p(m|\pi_i)\right] \mathcal{P}_{\pi_0}(m) + \varepsilon g(\theta) f(m|\theta)}{(1-\varepsilon)\left[\sum_{i=1}^{2} \alpha_i p(m|\pi_i)\right] + \varepsilon f(m|\theta)}.$$

If $f_2(x_2) = g_2(x_2) = 0$, *then,* $\inf_{\pi \in \Gamma_\varepsilon^2} \mathcal{P}_\pi(m) = \inf_{z_1 \geq 0, z_2 \geq 0} \mathcal{R}(z_1, z_2)$, *with*

$$\mathcal{R}(z_1, z_2) = \frac{(1-\varepsilon)\left[\sum_{i=1}^{2} \alpha_i p(m|\pi_i)\right] \mathcal{P}_{\pi_0}(m) + \varepsilon \sum_{i=1}^{2} \beta_i H^{q_i}(z_i)}{(1-\varepsilon)\left[\sum_{i=1}^{2} \alpha_i p(m|\pi_i)\right] + \varepsilon \sum_{i=1}^{2} \beta_i H^{q_i}(z_i)}, \quad \textit{where}$$

$$H^{q_i}(z_i) = \begin{cases} (1/z_i) \int_{\theta_i}^{\theta_i + z_i} g(\theta) f(m|\theta) d\theta, & z_i > 0, \\ g(\theta_i) f(m|\theta_i) d\theta, & z_i = 0 \quad (i = 1,2). \end{cases} \textit{and}$$

$$H^{i}(z_i) = \begin{cases} (1/z_i) \int_{\theta_i}^{\theta_i + z_i} f(m|\theta) d\theta, & z_i > 0, \\ f(m|\theta_i) d\theta, & z_i = 0 \quad (i = 1,2). \end{cases}$$

3. ILUSTRATIONS

We conclude the paper by including an example which serve to illustrate the ideas, theorems and corollaries exposed above. We shall use same weights as prior distribution for contaminations, i.e. $\beta_i = \alpha_i, i = 1,2$.

EXAMPLE. Specifically, let $X_1|\theta$ has a Poisson distribution with parameter θ and $\pi_0(\theta) = 0.8Ga(2,4) + 0.2Ga(3,30)$, and $X_2|\theta$ has an exponential distribution with parameter θ and $\pi_0(\theta) = 0.6Ga(60,11) + 0.4Ga(10,6)$. Standard bayesian premium appears in Table 1 and 2 for each sample mean under consideration (*m=4*, *m=7* and *m=12*).

Table 1: Poisson-gamma case.

m	$\mathcal{P}^*_{\pi_1}(m)$	$\mathcal{P}^*_{\pi_2}(m)$	α_1'	α_2'	$\mathcal{P}^*_{\pi}(m) = \sum_{i=1}^{2} \alpha_i' \mathcal{P}^*_{\pi_i}(m)$
4	3.666	5.384	0.998	0.002	3.670
7	6.166	7.692	0.07	0.93	7.585
12	10.333	11.538	0.001	0.999	11.538

Table 2: Exponential-gamma case.

m	$\mathcal{P}^*_{\pi_1}(m)$	$\mathcal{P}^*_{\pi_2}(m)$	α_1'	α_2'	$\mathcal{P}^*_{\pi}(m) = \sum_{i=1}^{2} \alpha_i' \mathcal{P}^*_{\pi_i}(m)$
2	2	4	0.864	0.136	2.270
4	3.333	5	0.164	0.836	4.727
5	4	5.5	0.073	0.927	5.391

This particular situation corresponds to the case in which $\varepsilon = 0$, i.e. no errors in the process of elicitation. Furthemore, if $\alpha_2 = \beta_2 = 0$ we are in the unimodality setting (see Gómez et al., 2000 and Sivaganesan et al., 1989). In both cases, most robusted situation occurs when the difference between bayesian net premiums for good and bad risks are higher (*m=12* in the Poisson case and *m=5* in the exponential case). In the other hand, less robusted situation appears in the case *m=4* and *m=2* for the two cases considered when there is the higher difference between bayesian net premiums for both good and bad risks.

4. SUMMARY AND CONCLUSIONS

A basic assumption of credibility theory is that the values of the parameters of the probability distribution of loss are unknown. In such case premium that company charges is the bayesian premium. This premium requires that the actuary can define a probability distribution for the values of unknown parameters of this loss process, prior distribution. In our model, prior distribution, π_0, is given by a convex sum of two prior distributions π_1 and π_2. This leads to the question of bayesian robustness which has been treated in this paper using the ε-contamination class. We have seen that bimodality effects are very important in modelling subjective beliefs about risk parameter when is necessary. We have used gamma density for the prior distribution because it is very flexible and conjugated with Poisson and Exponential distributions. If we use another distributions that are not conjugated we can use recent development in Markov chain Monte Carlo (MCMC) methods to facilitate exploration of posteriori magnitudes. A slight modification of the section 3 unimodal class would be to

consider all symmetric bimodal distributions as contamination of prior distribution. This is possible by replacing $(1/z)\int_{\theta_0}^{\theta_0+z}(\cdot)d\theta$ by $(1/(2z))\int_{\theta_0-z}^{\theta_0+z}(\cdot)d\theta$.

Finally, all results and theorem treated here can be used for another premium calculation principles (Heilmann, 1989) as Exponential, Esscher and Variance, among others.

5. REFERENCES

Eichenauer, J;Lehn, J. and Rettig, S. (1988). A Gamma-Minimax Result in Credibility Theory. *Insurance: Mathematics and Economics*, **2**, 49-57.

Gómez, E, Hernández, A. and Vázquez, F. (2000). Robust Bayesian Premium Principles in Actuarial Science. *Journal of the Royal Statistical Society. (Series D, The Statistician)*, **49**, 2, 241-252.

Heilmann, W. (1989). Decision theoretic foundations of credibility theory. *Insurance: Mathematics & Economics*, **8**, 77-95.

Sivaganesan, S. and Berger, J.O. (1989). Ranges of posterior measures for priors with unimodal contaminations. *The Annals of Statistics*, **17**, 2, 868-889.

MARKOV CHAIN MONTE CARLO POSTERIOR SAMPLING WITH THE HAMILTONIAN METHOD

Kenneth M. Hanson

Los Alamos National Laboratory, MS P940, Los Alamos, NM 87545 (USA)
Email: kmh@lanl.gov, WWW: http://public.lanl.gov/kmh/

1. INTRODUCTION

A major advantage of Bayesian data analysis is that provides a characterisation of the uncertainty in the model parameters estimated from a given set of measurements in the form of a posterior probability distribution [1]. When the analysis involves a complicated physical phenomenon, the posterior may not be available in analytic form, but only calculable by means of a simulation code. In such cases, the uncertainty in inferred model parameters requires characterisation of a calculated functional. An appealing way to explore the posterior, and hence characterise the uncertainty, is to employ the Markov Chain Monte Carlo technique. The goal of MCMC is to generate a sequence random of parameter **x** samples from a target pdf (probability density function), $\pi(\mathbf{x})$. In Bayesian analysis, this sequence corresponds to a set of model realisations that follow the posterior distribution [2].

There are two basic MCMC techniques. In Gibbs sampling, typically one parameter is drawn from the conditional pdf at a time, holding all others fixed. In the Metropolis algorithm, all the parameters can be varied at once. The parameter vector is perturbed from the current sequence point by adding a trial step drawn randomly from a symmetric pdf. The trial position is either accepted or rejected on the basis of the probability at the trial position relative to the current one. The Metropolis algorithm is often employed because of its simplicity.

The aim of this work is to develop MCMC methods that are useful for large numbers of parameters, n, say hundreds or more. In this regime the Metropolis algorithm can be unsuitable, because its efficiency drops as $0.3/n$ [3]. The efficiency is defined as the reciprocal of the number of steps in the sequence needed to effectively provide a statistically independent sample from π.

2. METHODOLOGY

An alternative MCMC technique is what I will call the Hamiltonian method. It is often referred to as the hybrid method because it alternates between Gibbs and Metropolis steps, but that name is not distinctive. For each parameter x_i, another parameter p_i is introduced, which represents the parameter's conjugate momentum variable [4]. A Hamiltonian is constructed as a potential term $\varphi = -\log(\pi(\mathbf{x}))$, plus a kinetic energy term:

$$H = \varphi(x) + \sum \frac{p_i^2}{2m_i} \qquad (1)$$

where m_i is a fictitious mass. The goal is to draw random samples from the new pdf that is proportional to exp(-*H*). Each iteration of the algorithm starts with a Gibbs sampling to pick a new momentum vector from the uncorrelated Gaussian in the momenta corresponding to the second term in *H*. Then a trajectory in (**x**,**p**) space is followed such that *H* is constant using the leapfrog technique, which consists of the following three substeps:

$$p_i(t+\frac{\tau}{2}) = p_i(t) - \frac{\tau}{2}\frac{\partial\varphi}{\partial x_i}\ \mathbf{x}(t) \qquad \textbf{(2)}$$

$$x_i(t+\tau) = x_i(t+\tau) + \tau\frac{p_i(t+\frac{\tau}{2})}{m_i} \qquad \textbf{(3)}$$

$$p_i(t+\tau) = p_i(t+\frac{\tau}{2}) - \frac{\tau}{2}\frac{\partial\varphi}{\partial x_i}\ \mathbf{x}(t+\tau) \quad . \qquad \textbf{(4)}$$

The parameter τ represents an increment in time. After *m* leapfrog steps corresponding to a total trajectory time of $T = m\tau$, a Metropolis acceptance/rejection decision is made to guarantee that the sequence is in statistical equilibrium with the target pdf. Clearly large steps in the parameter space are possible with only a few evaluations of φ and the gradient of φ. Note that the gradient of φ can often be done in a time comparable to the (forward) calculation of φ by applying adjoint differentiation to the computer code used to calculate φ [5]. In practice, the length of the Hamiltonian trajectories must be randomised to realise adequate sampling of π(**x**). Once an MCMC sequence has been generated, the properties of π(**x**) may be characterised by considering just the **x** samples. The momentum aspects of the extended pdf, exp(-*H*), are marginalised out because they are independent of the **x** dependence.

3. RESULTS

Figure 1 shows typical paths followed by the Hamiltonian MCMC algorithm for a one-dimensional target pdf, which is a Gaussian with unit standard deviation. The vertical jumps correspond to the Gibbs sampling of momentum from the Gaussian pdf, exp(-p^2), for unity mass. The circular arcs correspond to the trajectories of constant *H* followed in five steps of the leapfrog method using $\tau = 0.4$, yielding a total trajectory length of $T = 5\tau = 2$.

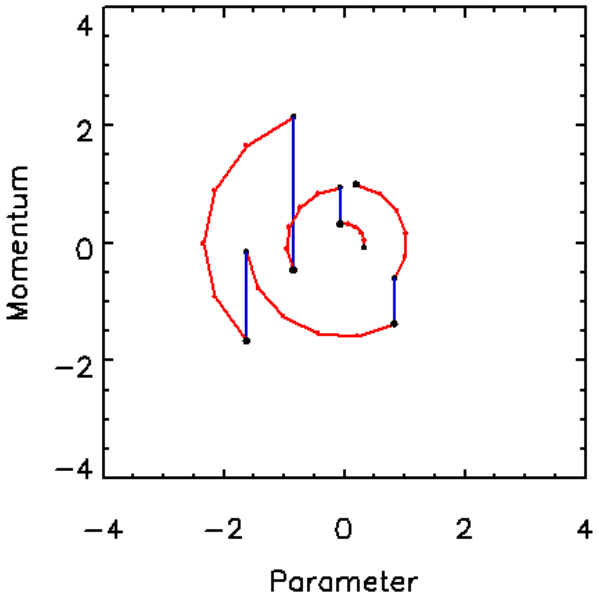

Figure 1. Example of several trajectories in the momentum-parameter space for the Hamiltonian method for a 1D Gaussian distribution. For each trajectory, the momentum is drawn from the assumed Gaussian momentum distribution (vertical jumps), which is followed by several steps along a trajectory of constant Hamiltonian value (circular paths).

Figure 2 shows the behaviour of the Hamiltonian method for an asymmetric two-dimensional Gaussian distribution with a standard deviation of four in one direction and unity in the other. For this example, the maximum value for τ is 0.4. The total length of each Hamiltonian trajectory is randomly chosen from a distribution that is uniform from 0 to T_{max} = 5 and τ is adjusted for a minimum number of number of leapfrog steps. The important aspect of this example is that the full width of the target pdf is easily reached in relatively few (15) trajectories consisting of 91 leapfrog steps. This kind of distribution causes difficulty for the Metropolis algorithm with an isotropic trial distribution because it essentially follows a random walk.

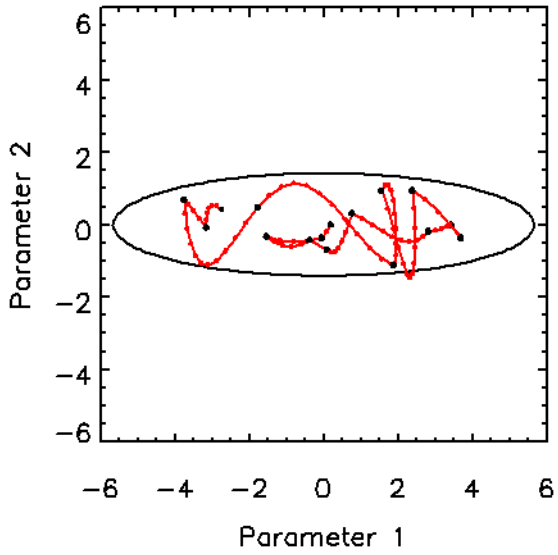

Figure 2. Hamiltonian trajectories for a two-dimensional asymmetric uncorre-lated Gaussian pdf, demonstrating the ability of the Hamiltonian trajectories to readily transverse the length of the target pdf.

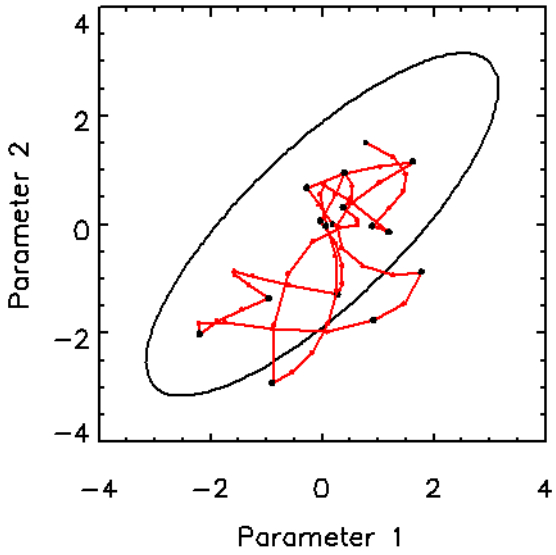

Figure 3. Trajectories in a 2D subspace from a 16-dimensional correlated Gaussian pdf. The contour shown is at the two-standard-deviation level for the marginalised distribution.

The motivation here is to handle pdfs of high dimensionality. Figure 3 shows how the Hamiltonian method copes with a 16D Gaussian distribution with a fair degree of correlation among the variables. The covariance matrix of the target pdf is a circulant matrix with rows whose elements are –0.2, 0.0, 0.4, 1.2, 2.5, 4.0, 5.0, 4.0, 2.5, 1.2, 0.4, 0.0, -0.2, with the maximum value on the diagonal [6]. The figure shows that the Hamiltonian method does a good job of sampling this pdf with only 15 trajectories, or 61 function and gradient evaluations. The maximum Hamiltonian length is 3 for this example.

The efficiency of Hamiltonian method is found to be optimised for τ = 0.4 and T_{max} = 8. The MCMC algorithm is tested by running the algorithm 1000 times with 50 Hamiltonian trajectories in each run. The efficiency of the algorithm is calculated as the ratio of the mean square deviation from the mean of the parameter variance expected for ideal independent sampling method to that observed for the 1000 runs. The efficiency of the Hamiltonian method under these conditions is 45% per Hamiltonian trajectory or 2.1% per function evaluation. The latter number assumes that the computation time for gradient computation of φ is the same as for φ itself, which is often possible when the gradient is calculated using a code that represents the adjoint differentiation of the simulation code [5]. In the examples shown in Figs. 1 and 2, the Hamiltonian trajectories maintain constant H so that the

Metropolis rejection rate is nearly zero. However, in this example, about 8% of the trajectories are rejected.

4. DISCUSSION

The previous problem involving a target distribution with modest correlations was treated in [6]. Using an isotropic trial distribution in the Metropolis algorithm, the efficiency was determined to be 0.11%. When the trial distribution is adaptively modified to have a covariance structure similar to that of the target pdf, the efficiency improved to 1.6%. This latter efficiency is close to the upper limit on efficiency of the simple Metropolis algorithm for a 16D isotropic pdf, 1.9%.

Comparison of these results with those for the Hamiltonian method indicates that the Hamiltonian method has the advantage of providing good efficiency without the need to supply an estimate of the covariance method. Furthermore, as the number of dimensions increases, the efficiency of the simple Metropolis algorithm will drop as 0.3/n. On the other hand, for pdfs in 64 dimensions with the same pdf, the efficiency of the Hamiltonian method is 1.9% per function evaluation and for 128 dimensions, it is 1.7%. Thus, the Hamiltonian MCMC method appears to be well suited for sampling pdfs of high dimension.

Almost the entire drop in efficiency comes from the Metropolis rejection of the Hamiltonian trajectories, which is the deterministic part of the algorithm. The implication is that improvements in the Hamiltonian method can be achieved through improvement in calculating the deterministic Hamiltonian trajectories. As with it any MCMC method, it is also possible to improve the performance of the Hamiltonian method for correlated and asymmetric pdfs through the usual means of adapting the algorithm to include estimates of the covariance structure of the target pdf [2].

5. ACKOWLEDGEMENTS

For insightful discussions, I would like to thank Frank Alexander, Greg Cunningham, David Haynor, Jim Gubernatis, Julian Besag, and Malvin Kalos. This work was supported by US-DOE under contract W-7405-ENG-36.

6. REFERENCES

[7] Gelman, A, Carlin, JB, Stern, HS, Rubin, DB (1995), *Bayesian Data Analysis*, Chapman & Hall, London.

[8] Gilks, WR, Richardson, S, Spiegelhalter DJ (1996), *Markov Chain Monte Carlo*, Chapman & Hall, London.

[9] Gelman A, Roberts, GO, Gilks, WR (1996), Efficient Metropolis jumping rules, *Bayesian Statistics 5*, Bernardo, JM, et al., eds., Oxford Univ. Press.

[10] Neal, RM (1996), *Bayesian Learning for Neural Networks*, Springer, New York.

[11] Hanson, KM, Cunningham, GS, Saquib SS (1998), Inversion based on computational simulations, *Maximum Entropy and Bayesian Methods*, pp. 121-135, Kluwer Academic, Dordrecht.

[12] Hanson, KM, Cunningham, GS (1998), Posterior sampling with improved efficiency, *Medical Imaging: Image Processing, Proc. SPIE* **3338**, pp. 371-382.

SENSITIVITY ANALYSIS OF THE TSUNAMI WARNING POTENTIAL

R.D. Braddock

Faculty of Environmental Sciences, Griffith University
Nathan, Qld 4111, Australia
Email: r.braddock@mailbox.gu.edu.au

ABSTRACT

Tsunamis are normally generated by underwater earthquakes. The earthquakes are normally easily detected by seismographs. However, the earthquake may not always generate a tsunami. Further, the severity of the earthquake is not linearly related to the severity of the tsunami. The tsunami may be detected by a deep-sea pressure transducer communicating through a surface rider buoy, through satellites to a tsunami warning centre. The detectors are expensive to build and maintain, need to be placed near surface-rider buoys, and the placement of these detectors needs to be optimal. The provision of adequate warnings from the network of detectors, called the tsunami warning potential, depends on the network of the deployed detectors, the number of detectors used, and the response times of the detectors, warning centre, and of the emergency services which need to convey the warning. The warning potential is also a function of the number in the population at risk. The sensitivity of the warning potential is analysed for first-order effects, particularly with respect to time delays arising from detection and operation of the emergency services to deliver the warning to the population. The sensitivity of the warning potential to population shifts is also considered. Areas for improvement are identified, together with suggestions of how the system can be optimised.

1. INTRODUCTION

In the past, tsunamis have caused considerable loss of life and destruction of property in coastal areas [5]. Various tsunami warning systems have been designed and used to detect the generation of a tsunami, and to warn of its approach to coastal regions [2]. Currently, seismic observations are used to detect the occurrence of earthquakes, act ‘at a distance’, and communications are rapid.

The real-time detection of a tsunami is usually through direct observation. This is a hazardous operation, as the observer needs to be near the destructive zone, and the means of communication are often destroyed, disrupted or utilised by non-essential traffic. Fortunately, tsunamis are far less damaging in the open ocean and may be detected by suitable sea-floor-mounted detectors [1]. These detectors use acoustic coupling to communicate to the surface, to wave-rider buoys which can then communicate via satellite [1].

The detectors and wave-rider buoys are expensive to make and are currently limited in number. Some six possible sites have been selected, after consideration of regular NOAA ship passages and other maintenance and cost factors (Tsunami Hazard Mitigation Federal/State Working Group, 1996 [THM]). The problem is to locate a small number of detectors at a

selection of the possible communication-buoy locations, so as to give the maximum warning of the generation of a tsunami, i.e. the maximise the warning potential function. This problem has been formulated and solved; it leads to an integer programming problem which can be solved using standard enumeration techniques [6].

The solution for the optimal warning potential function depends on parameters such as population numbers at risk, and response times for detection of the tsunami and for conveying the warning to the population. These parameters can be considered to vary continuously in their ranges. The maximum warning potential function also depends on the number of buoys which are deployed, and this is a discrete variable with up to six buoy locations.

The aim of this paper is to investigate the sensitivity properties of the maximum warning potential function to its input parameters. This will assist in determining the subset of more influential parameters with respect to sensitivity. The results will provide valuable feedback to the operation of a tsunami warning system.

2. METHODOLOGY

2.1. Model

The locations of the six wave-rider buoys are denoted by b_w, w = 1, ..., 6. The latitudes and longitudes for these positions are given in [1, 3] and the data will not be repeated here. The representative locations of the generation points are denoted by g_u, u = 1, ..., 18 [3]. Major representative population centres were selected to provide a general estimate of the population at risk in the Pacific Ocean. These are located at points denoted by p_v, v = 1, ..., 27 (see [3] for data). The population at each point p_v is denoted by π_v, v = 1, ..., 27.

Let $$y_w = \begin{cases} 0, & \text{if buoy location } b_w \text{ is not occupied by a detector} \\ 1, & \text{if buoy location } b_w \text{ is occupied by a detector} \end{cases}$$

The total number of detectors, Y, may be limited by capital costs or by maintenance costs. The vector $\underset{\sim}{y}$ of 0's and 1's then represents a particular deployment of detectors.

Now consider the generation of a tsunami at time t = 0 at the generation point g_u. Let

$$T_{u,v} = t_u^*(\underset{\sim}{y}) + t_d + r_v - t_{u,v}\,, \qquad (1)$$

where

$t_u^*(\underset{\sim}{y})$ is the travel time of the tsunami from g_u to the nearest occupied wave-rider buoy,

t_d is the detection time for processing, detecting and signalling to confirm the generation of the tsunami,

r_v is the reaction time of the emergency services and population to move to safety,

$t_{u,v}$ is the travel time of the tsunami from the generation point to the population.

Note that $t_u^*(\underset{\sim}{y})$ and $t_{u,v}$ can be calculated from travel time charts [2,3]. Also let

$$e_{u,v}(\underset{\sim}{y}) = \begin{cases} 0, & T_{u,v} > 0 \\ \pi_v, & T_{u,v} \le 0 \end{cases} \tag{2}$$

The total warning potential is then defined as

$$E(\underset{\sim}{y}) = \left[\sum_{u=1}^{18} \sum_{v=1}^{27} e_{u,v} \right] \Big/ \left(18 \sum_{v=1}^{27} \pi_v \right) \tag{3}$$

Then the problem can be formalised as

$$\Im = \underset{\underset{\sim}{y}}{\text{Max}} \; E(\underset{\sim}{y})$$

subject to

$$\sum_{w=1}^{6} y_w \le Y. \tag{4}$$

The optimal solution may be found using curtailed enumeration [6].

2.2. Sensitivity analysis

The function $\Im$ depends on $t_u^*(y)$, t_d, r_v and $t_{u,v}$, all of which are continuous, and on Y, which is discrete. The travel times $t_u^*(y)$ and $t_{u,v}$ are generally accurate to within $\pm$ 5%. The detection time t_d varies between 20 minutes to 50 minutes [1]. The reaction time for the general population varies between 1 to 5 hours, depending on time of day, and on the education and training of the emergency services and general population.

The population at risk, π_v are technically discrete but sufficiently large to be taken as continuous. The population numbers are only estimates and will be assumed to be variable by $\pm$ 50% on the data in [3]. The number of buoys is definitely discrete, and $\Im$ varies discontinuously on Y.

A first-order-effects sensitivity analysis was performed on the function $\Im$ using the One-at-a-Time (OAT) Morris method [4]. The parameters used in the analysis are shown in Table 1 and the ranges used are given above. It was found that the results were very similar with respect to variations in the travel times, t_u^* and t_{uv}. The travel time t* is used to represent a generic travel time factor with a value range of $\pm$ 5%. The response times, r_v, were assumed to be independent of location, and were replaced with a uniform response time r*.

3. RESULTS

The results of the OAT analysis are given in Table 1, where the means (μ), standard deviations (δ) and Morris ranking are given. The Morris ranking is calculated as the Euclidean distance in the (μ, δ) plane, and the ranking is ordered according to this distance. The results are also summarised on the (μ, δ) plot shown in Figure 1.

Table 1. Sensitivity analysis of the tsunami warning potential

Factor Number	Factor	μ (Morris Mean)	δ (Morris standard deviation)	Morris rank
1	t_d	0.009	0.005	11
2	t*	0.011	0.042	4
3	r*	0.105	0.331	2
4	Y	0.092	0.347	1
5	π_1	0.001	0.002	16
6	π_2	0.004	0.003	14
7	π_3	0.001	0.000	25
8	π_4	0.013	0.009	7
9	π_5	0.003	0.006	13
10	π_6	0.019	0.010	6
11	π_7	0.000	0.000 –	NR
12	π_8	0.001	0.000	16
13	π_9	0.001	0.002	20
14	π_{10}	0.001	0.001	20
15	π_{11}	0.000	0.000	NR
16	π_{12}	0.002	0.001	16
17	π_{13}	0.054	0.037	3
18	π_{14}	0.002	0.001	16
19	π_{15}	0.001	0.000	25
20	π_{16}	0.001	0.000	25
21	π_{17}	0.001	0.000	25
22	π_{18}	0.000	0.000	NR
23	π_{19}	0.010	0.008	9
24	π_{20}	0.001	0.001	20
25	π_{21}	0.001	0.001	20
26	π_{22}	0.011	0.010	8
27	π_{23}	0.001	0.001	20
28	π_{24}	0.002	0.003	15
29	π_{25}	0.024	0.013	5
30	π_{26}	0.011	0.005	10
31	π_{27}	0.003	0.008	12

The results show that Factors 3 and 4 are ranked highest with respect to the sensitivity of the tsunami warning potential. Factor 3 is the response time of the emergency services, and whilst ranked second on the Morris ranking, it is almost equivalent to Factor 4. Factor 4 relates to the number of warning buoys in the system, and this is a discrete variable. The warning potential increases rapidly when Y is small, but then displays the economic law of diminishing return. Thus, when most wave buoy sites are occupied, little increase in warning potential is obtained by adding another buoy.

The third most important factor, Factor 17, corresponds to the population at risk in Tokyo, Japan. This is also the largest population centre in the data used to construct the warning potential. The Euclidean, or Morris, distance measure is much smaller than for the factors

ranked at 1 and 2, and it is much less important in the sensitivity analysis. All of the other population centres have a lower Morris distance, and the warning potential is relatively insensitive to variations in the estimated population. Some have not been ranked in Table 1 due to the very small values of μ and δ obtained in the analysis.

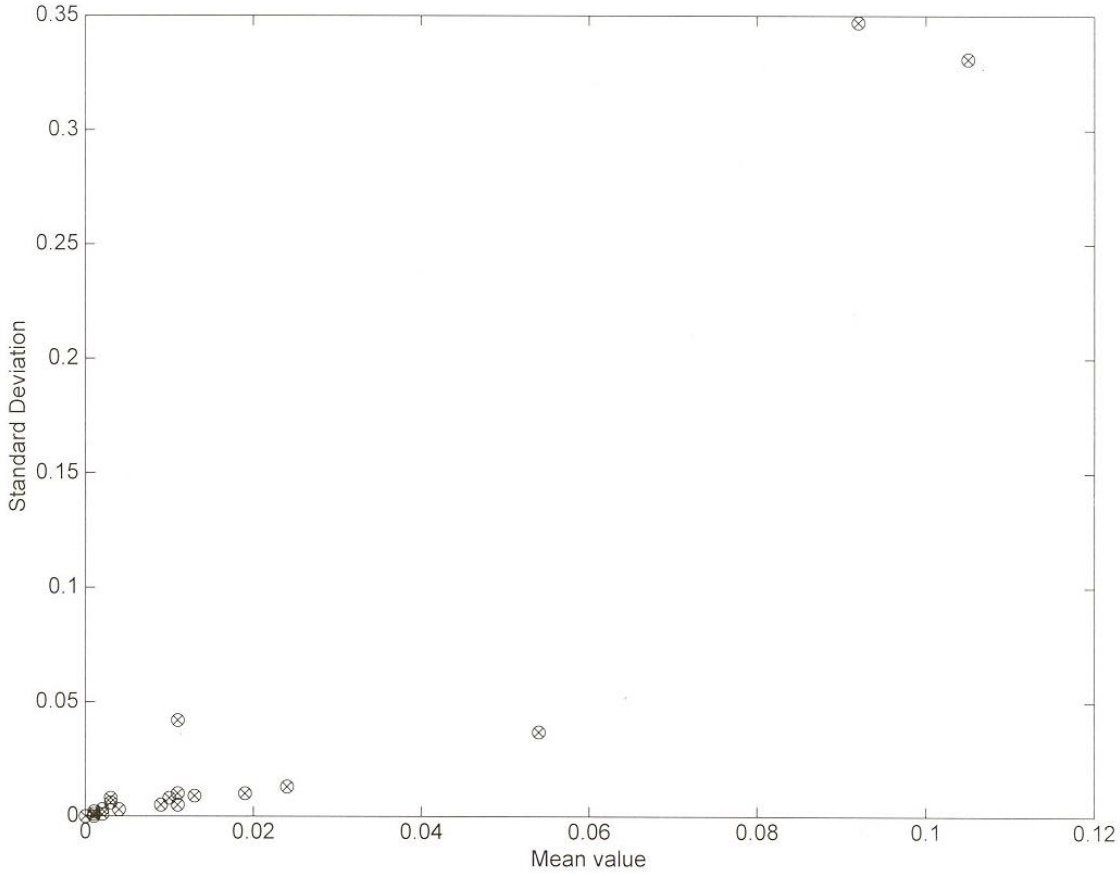

Figure 1. Sensitivity plane (μ, δ) for the tsunami warning potential

The calculation of the population at risk was only an approximation. It was used to illustrate the optimisation calculations to determine the optimum number of detectors [B and C]. This sensitivity analysis indicates that the use of population estimates is justified in calculating the tsunami warning potential.

The factor t* is ranked fourth in importance by the Morris ranking system. This term represents the sensitivity of the warning potential to errors in the calculation of travel times of the tsunami. Note that the Euclidean or Morris distance between Factor π_{13} (ranked at 3) and t* (ranked 4) is considerable. Errors in the bathymetry and in calculating travel times will have little effect on the estimated values of the tsunami warning potential.

4. DISCUSSION

The tsunami warning potential is sensitive to the number of detectors used and to the response times of the emergency services in warning and moving the population at risk.

Increasing the number of operational detectors is mainly an economic problem; the technology exists and has been proven in use.

Conveying warnings to populations at risk is a problem in many areas, particularly for natural disasters. For tsunamis, there is a need for the population at risk to be educated as to the nature of tsunamis and in the evasive action to be taken. There also need to be effective means of alerting the population.

5. REFERENCES

[1] Bernard, E.N. and Milburn, H.B. (1991) Improved Satellite-Based Emergency Alerting System, **J. Atmos. Oceanic Tech. 8**, 879-883.

[2] Blackford, M. and Kanamori, H. (1995) Tsunami Warning System, Workshop Report, NOAA - Technical Memorandum ERL PMEL-105, PB95-187175, 95 pp.

[3] Braddock, R.D. and Carmody, O. (2001) Optimal Location of Deep-Sea Tsunami Detectors, Intl. Trans. in Ops. Res. 7, 1-11.

[4] Campolongo, F. (1998) "Sensitivity Analysis in Model Building", PhD thesis, Griffith University, Australia.

[5] Folger, T. (1994) Waves of Destruction, Discover No. 5, pp. 66-73.

[6] Winston, W.L. (1991) Operations Research - Applications and Algorithms, PWS - Kent Publishing Company, Bost

SOLAR RADIATION AND RELATIONSHIP WITH OTHER METEOROLOGICAL VARIABLES

Zarzalejo L. F. & San Isidro, M. J

Solar Energy in Buildings Project. CIEMAT.
Avda. Complutense 22, 28040 Madrid. SPAIN
Email: lf.zarzalejo@ciemat.es; mj.sanisidro@ciemat.es

ABSTRACT

The main goal of this paper is to be able to performance the solar radiation as a function of another meteorological variables: temperature, relative humidity and zenithal angle. To obtain this objective the linear Transfer function models will be used to represent these dynamic systems, where the output is solar radiation variable and the inputs are temperature, relative humidity and zenithal angle.

1. INTRODUCTION.

Meteorological information is critical to the assessment of the energy performance of many different types of system, especially those systems where indoor environmental control is important like buildings.

Thermal capacity associated with buildings, climatic conditions, environmental factors, etc. are very important in determining the internal dynamic thermal response to the varying external conditions. Then the assessment of dynamic thermal storage effect forms a key aspect of the design of thermal energy systems, and performance is closely linked with weather variations. Such problems can only be handled by examining the dynamic characteristics of the natural energy supply system in relation to the dynamics of the external natural environmental factors creating the various internal demands, impacting on the dynamic thermal response characteristics of the basic system, be it a building, or other.

Data of different complexity are needed at different stages of the design process. Bioclimatic analysis is an important tool used in the early stages of indoor environmental design to establish climatic priorities in design. Monthly mean climatic data on maximum and minimum dry bulb temperature, and associated humidity are plotted onto suitable charts related to human comfort, so the building design solution space can be more clearly identified in terms of principle. The implications are that external data are needed at the hourly level rather than at the monthly level, if dynamic implications described are to be properly studied. The higher level of complexity is the supply of full hourly data series for simulation [1, 2, 3] (containing hourly values of a wide range of relevant observed variables). Due to is very difficult to obtain some of these variables simultaneously, we propose in this paper a method to reproduce global solar radiation from temperature and humidity.

2. THE THEORETIC PROCEDURE

We will study a system defined by temperature, relative humidity and zenithal angle as input variables and solar global radiation as output. Due to this system is not lineal (inputs are correlated and each one of them have important seasonal contribution) and it makes impossible to use linear Transfer functions directly, it is necessary to generate a new system of input variables [4, 5].

In order to solve these aspects, it is necessary to carry out:

- *A principal component analysis* on the set of input variables. This kind of analysis is concerned with explaining the variance-covariance structure through a few linear combination of the original variables. The advantages of the principal components of a system are based on: they represent the directions with maximum variability, provide a simpler and more parsimonious description of the covariance structure and the set of principal components builds an uncorrelated system $\{z_i\}$.
- *To lead the System towards the stationarity.* The input variables involve in our system (temperature, relative humidity and Zenithal angle) are clearly not stationary due to seasonal component. It makes to suppose that their principal components $\{z_i\}$ follow being not stationary. We can find, by spectral analysis, the contribution of the seasonal part of each $\{z_i\}$. In this way, Fourier analysis on each $\{z_i\}$ guide us to know which are the most important frequencies $\{w_i\}$. These frequencies are chosen taking account that they represent at least the 85% of the total periodogram. Without loosing generality it is possible to suppose that each new variable $\{x_i\}$, that results from eliminating the seasonal part to $\{z_i\}$ is stationary except to some degree of differentiation [4].

$$X_t = Z_t - \sum_{i=1}^{K} \left(A_i \cos w_i t + B_i \operatorname{sen} w_i t\right) + \varepsilon_t \qquad \text{where:} \quad A_i = \frac{2}{N}\sum_{t=1}^{N} Z_t \cos w_i t \quad B_i = \frac{2}{N}\sum_{t=1}^{N} Z_t \operatorname{sen} w_i t$$

But these important frequencies relatives to the z-variable produce a seasonal part on the solar radiation $\{R_t\}$

$$Y_t = R_t - \sum_{i=1}^{K} \left(A'_i \cos w_i t + B'_i \operatorname{sen} w_i t\right) + \varepsilon_t \qquad \text{where:} \quad A'_i = \frac{2}{N}\sum_{t=1}^{N} R_t \cos w_i t \quad B'_i = \frac{2}{N}\sum_{t=1}^{N} R_t \operatorname{sen} w_i t$$

2.1. Identification of transfer function models by prewhitening the input

Suppose the suitable differenced input process x_t is stationary and is capable of representation by some member of the general linear class of autorregresive-moving average models [4, 5]. Then, given a set of data, we can carry out our usual identification and estimation methods to obtain a model ARMA for the x_t process $\phi_x(B)\theta_x^{-1}(B)x_t = \alpha_t$. Then, to a close approximation, we can transform the correlated input series x_t to the uncorrelated white noise series α_t. If we now apply this same transformation to y_t to obtain $\phi_x(B)\theta_x^{-1}(B)y_t = \beta_t$

Then the model may be written $\beta_t = v(B)\alpha_t + \varepsilon_t$. On multiplying on both sides by α_{t-k} and taking expectations, we obtain $\gamma_{\alpha\beta}(k) = v_k\sigma_\alpha^2$ where $\gamma_{\alpha\beta}(k) = E[\alpha_{t-k}\beta_t]$ is the cross covariance at lag +k between α and β.

In terms of the cross correlations, $v_k = \dfrac{\rho_{\alpha\beta}(k)\sigma_\beta}{\sigma_\alpha}$ $\qquad k = 0,1,2,...$

Hence, after *prewhitening* the input, the cross correlation function between the prewhitened input and correspondingly transformed output is directly proportional to the impulse response function.

3. CASE STUDY

During September and October months of 1998 solar global radiation, dry bulb temperature and relative humidity were measured in the DER-CIEMAT building (Madrid, 40.45ºN - 3.73ºW - 667m.). From ten days of these measurements we have applied the previous theoretical procedure.

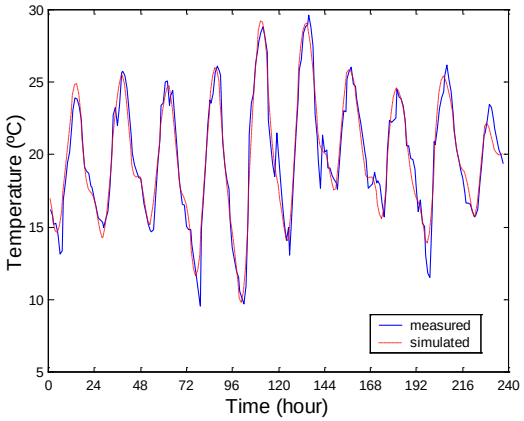

Fig. 1.- Dry bulb temperature.

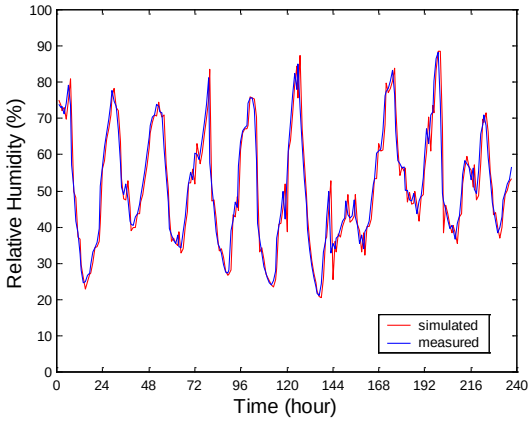

Fig. 2.- Relative humidity.

A previous analysis of temperature and humidity provide us both of them are behaviour as normal distribution and they could be described by an order two autorregresive model:

$$T(t)=0.6626*T(t-1)-0.2353T(t-2) \qquad H(t)=1.4208*H(t-1)-0.4285*H(t-2)$$

as it shows Figs. 1 & 2.

3.1. Results

The principal component analysis provide us two principal components ; the eigenvectors and their corresponding eigenvalues for each component are:

$$\mathbf{v_1} = (0.7040, -0.6919, 0.1604) \qquad \mathbf{v_2} = (0.0370, -0.1897, -0.9811)$$

$$\lambda_1 = 1.8646 \qquad \lambda_2 = 0.9872$$

These two components produce 95.06% of the variability of the initial inputs.

In this way the new variables will be:

$$z_1 = 0.7040 * T - 0.6919 * Hr + 0.1604 Az \qquad z_2 = 0.0370 * T - 0.1897 * Hr - 0.9811 * Az$$

Where:

T refers to dry bulb temperature

Hr refers to relative humidity

Az refers to zenithal angle of sun

The most important frequencies for each $\mathbf{z_i}$ are

$\mathbf{z_1} \Rightarrow$ **0.2493, 0.2743, 0.1995, 0.5236, 0.3241, 0.0499, 0.0249, 0.1496, 0.0244**

$\mathbf{z_2} \Rightarrow$ **0.2493, 0.2743, 0.2992, 0.2244, 0.1995, 0.3241, 0.3491, 0.3740**

The stationary part of z1 behaviour as Autorregresive model of order 2.

$$\mathbf{x_1(t) = 0.7418 * x_1(t-1) - 0.2469 x_1(t-2) + \alpha_1(t)} \qquad \mathbf{x_2(t) = 0.9226 * x_2(t-1) - 0.1658 x_2(t-2) + \alpha_2(t)}$$

Where $\mathbf{x_i}$ is the corresponding variable to $\mathbf{z_i}$ when its seasonal part has been eliminated. Eliminating from the output variable Y each one of the important frequencies relatives to each input, it is obtained two variables $\{y_1, y_2\}$ relatives to the contribution of each input respect to the output. In this way, is calculated the β_i

$$\mathbf{\beta_1(t) = y_1(t) - 0.7418 * y_1(t-1) + 0.2469 * y_1(t-2)} \qquad \mathbf{\beta_2(t) = y_2(t) - 0.9226 * y_2(t-1) + 0.1658 * y_2(t-2)}$$

In the Fig. 3 and 4, it is possible to see the cross-correlation function, for the first 40 lags, for each prewhitened input $\{\alpha_i\}$ and its corresponding transformed output $\{\beta_i\}$. Note that the most important lags of the impulse response function between α_1 and β_1 are:{0, 11,19,35} and the corresponding between α_2 and β_2 is {12}.

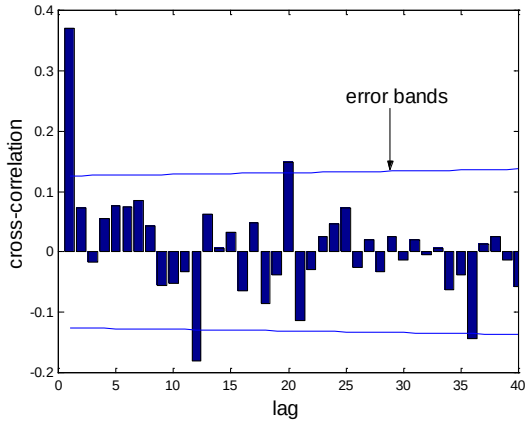

Fig. 3.- Cross-correlation between $\alpha 1 \& \beta 1$

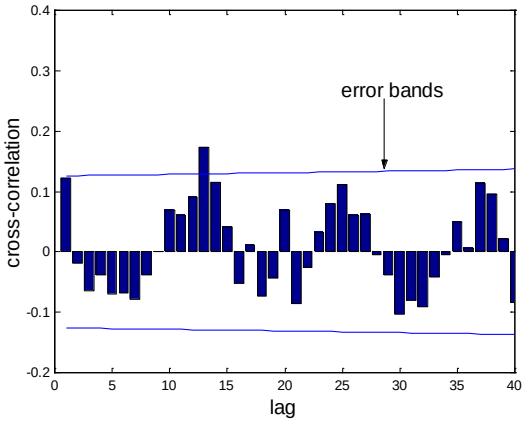

Fig. 4.- Cross-correlation between $\alpha 2 \& \beta 2$

These above results lead us to say that:

$$\mathbf{y(t) = 0.4961 * x_1(t) - 0.2418 * x_1(t-11) + 0.1986 * x_1(t-19) - 0.1932 * x_1(t-35) + 0.7341 * x_2(t-12)}$$

except to some error (that can be due to random or some variable not considered).

The last stage consists to recover the physical initial variables coming back the previous steps. In the Fig. 5 you could see measured and simulated values of solar global radiation. We can consider this methodology as a start point to forecast, to fulfil, to resample, etc. some physical measurement.

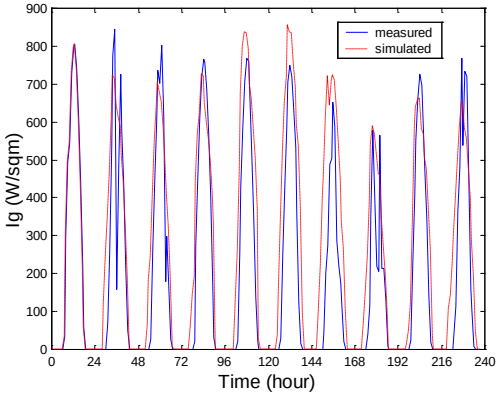

Fig. 5.- Global solar radiation.

4. REFERENCES

1. LUND, H., ***EC work on short reference years (SRY)***, in *Proc. Conf. Adv. European Solar Radiation Climatology*, Conf. C43, UK-ISES 19. London, (1986)
2. ***Test Reference Years (TRY), Weather Data Sets for Computer Simulations of solar energy systems and Energy Consumption in Buildings***. Commission of the European Communities, Directorate General XII for Science, Research and Development (1985).
3. ZARZALEJO, L.F., TÉLLEZ, F.M., PALOMO, E. et al, ***Creation of Typical Meteorological Years (TMY) for Southern Spanish cities.*** Pasive cooling of buildings. International Symposium; Athens, June 1995.
4. BOX G.;JENKINS G., ***Time Series Analysis forecasting an control***, Holden-Day, California.1976.
5. PRIESTLEY M.B. ***Spectral Analysis and Time Series***, Academic Press, San Diego. 1981.

SENSITIVITY ANALYSIS IN MEDICAL DECISION PROBLEMS

C. Pérez[(1)], J. Martín[(1)] y P. Müller[(2)]

[(1)] Universidad de Extremadura
Carretera de Trujillo s/n, 10071 Cáceres, Spain
E-mail; {carper,jrmartin}@unex.es

[(2)]Duke University, Durham
North Carolina, USA
Email: pm@isds.duke.edu

1. INTRODUCTION

In this paper we review important concepts of sensitivity of the optimal decision in a decision problem with respect to the underlying utility function, the prior model and the sampling model. The discussion is based on Martín and Ríos Insua (1996) and Martín *et al* (2001). To address sensitivity with respect to the model we introduce an extension of the results in Martín and Ríos Insua (1996). We show how these concepts are applied to medical decision problems. While the concepts are general, particular implementations need to always be problem specific. Using the structure of a given problem the analyst has to decide which sensitivity measures are relevant and efficiently computed. In the context of two medical decision problems, which we argue are representative for a wide range of important applications, we discuss some general principles and common computational strategies.

Bayesian decision theory and inference describes a decision problem by a set of possible alternatives $a \in A$, a set of states, or parameters, $\theta \in \Theta$, a prior distribution $\pi(\theta)$, a model, or likelihood $l(x|\theta)$, for the observed data x, and a utility function $u(a,\theta,x)$. For illustration, in Example 1, a will describe on which days between pre-treatment and chemotherapy to collect stem cells from a new patient; θ parameterizes a model $l(x|\theta)$ for the profile of a patient's CD34 count over the days before chemotherapy; $x = (x_1,...,x_I)$ are observations from previous patients; and $u(a,\theta,x) = -c_1\, n_a - c_2\, Pr(A|a,\theta)$, where n_a is the number of scheduled stem cell collections under design a, and A is the event of collecting a certain target number of stem cells. In this example, the utility function does not directly depend on the data x. In such cases we will sometimes write $u(a,\theta)$. The optimal decision a^* is the action which maximizes the posterior expected utility.

Among the many fine reviews of Bayesian decision theory are, for example, Berger (1994), French and Xie (1995), Ríos Insua and Ruggeri (2000) and references therein.

Practical implementation of utility maximization is hindered by the fact that a^* could possibly be very sensitive to the chosen prior $\pi(\cdot)$, model $l(\cdot|\cdot)$ and utility function $u(\cdot)$. A skeptical decision maker will require in addition to the optimal solution some description of the sensitivity of a^* with respect to reasonable changes and uncertainties in the specification of prior, utility and model. Berger (1994) provides an excellent summary of some recent Bayesian literature in this area. Most authors, e.g. Wasserman (1992) and Ruggeri (1993), focus on prior sensitivity. Sivaganesan (1993) and Dey *et al*. (1996) study the sensitivity with respect to prior and likelihood. Greenhouse and Wasserman (1996) and Carlin and Pérez (2000) discuss applications to medical problems.

In Section 2 we introduce the application examples. In Section 3 we review basic concepts of Bayesian sensitivity analysis. In Section 4.1 we summarize the practically relevant parts concerning prior robustness of the optimal decision. In Section 4.2 we extend the results about prior robustness to model robustness. Section 4.3 considers sensitivity with respect to the chosen utility function. We conclude with a brief discussion section.

2. EXAMPLES

We apply the proposed sensitivity measures to two examples of medical decision making.

Example 1: Optimal apheresis schedules: Palmer and Müller (1998) consider optimal apheresis designs for cancer patients undergoing high-dose chemotherapy. Between a pre-treatment and start of the chemotherapy stem cells are collected to allow later reconstitution of white blood cell components. Depending on the chosen pre-treatment the first stem cell collection process (apheresis) is scheduled on the fifth or seventh day after pretreatment, respectively. The design problem is to decide for which of the remaining days further aphereses should be scheduled. Clearly the optimal solution should propose stem cell collections on days with high-predicted stem cell concentrations. The prediction is based on observations of stem cell levels (represented by CD34 antigen levels) from past patients. Palmer and Müller (1998) solved the problem for a particular model based on a rescaled gamma curve for the mean profile of each patient and a hierarchical prior probability model.

Example 1 has some key features of a wide class of problems in medical decision making: (i) A parametric, hierarchical model to fit data from previous patients; (ii) The model is estimated by Markov chain Monte Carlo posterior simulation; (iii) The loss function contains one term relating to sampling cost and another term relating to the posterior (predictive) probability of some event of interest.

Example 2: Optimal screening schedules for breast cancer: Parmigiani (1993) considers the problem of optimal screening schedules for a chronic disease, for example breast cancer. Design parameters are the age at which to begin regular screening and the frequency of screenings. Parmigiani (1993) define a four-state semi Markov process to describe the history of a chronic disease. The four states are “disease is absent or present but not detectable” (A), “detectable pre-clinical” (B), “clinical” (C) and “death“ (D). Deciding on an optimal screening schedule requires specifying in the utility function a tradeoff between the cost of screening and the probability of early detection of breast cancer. The recommended optimal screening schedule is very sensitive to the choice of these trade off parameters. Therefore a full sensitivity analysis, for example in the framework introduced in this paper, is crucial.

3. BAYESIAN SENSITIVITY ANALYSIS

In Bayesian Decision Theory and Inference, actions are ranked by expected utility/loss. The optimal decision a^* is the action which maximize in a expected posterior utility, $T(a;u,\pi,l)$. However, T might be sensitive to changes in specification of prior, model and utility. The assessment of (u,π,l) is far from simple, and the decision maker might demand ways of checking the impact of the given choices on the conclusion, i.e. a study of the sensitivity of T with respect to changes in (u,π,l).

We consider two distinct aspects of sensitivity in the decision problem:

The change of expected utility at a^* as a function of the triple (u,π,l), i.e. the operator $(u,\pi,l) \rightarrow T(a^*; u,\pi,l)$. Many recent papers in Bayesian robustness studied this problem focusing on changes in the prior π only, allowing π to range in various classes Γ of probability distributions, see e.g. Ríos Insua and Ruggeri (2000). In the full version of the paper we summarize some results from Martín and Ríos Insua (1996) concerning robustness with respect to changes in π. We extend their results to apply to changes in the model $l(\cdot|\cdot)$.

Changes in expected utility when we replace the optimal decision a^* by a suboptimal alternative b. If there is a triple (u,π,l) such that $(T(a^*; u,\pi,l) - T(b; u,\pi,l)) < 0$, then under these inputs the action b is preferred to the current optimal act a^*. We study the operator $(u,\pi,l) \rightarrow T(a^*; u,\pi,l) - T(b; u,\pi,l)$ when the utility function ranges over a parametric class.

We shall study prior and model sensitivity, i.e. the first operator, from a local point of view. To quantify local sensitivity with respect to prior changes, Martín and Ríos Insua (1996) propose to consider the derivative T'_π of $T(a^*; u,\pi,l)$ with respect to π defined by:

$$T(a; u,\pi+h,l) - T(a; u,\pi,l) = T'_\pi(h) + o(||h||),$$

where the norm $||h||$ is defined as bounded variation norm: $||h|| = \sup_A |h(A)|$. For the remaining discussion it suffices to think of $T'_\pi(\cdot)$ as a rate of change in expected utility if we change the prior probability measure from π to $\pi+h$. The use of such derivatives in Robust Bayesian Analysis was introduced by Diaconis and Freedman (1986) and developed, among others, by Ruggeri and Wasserman (1993) and Gustafson (2000).

4. RESULTS

We sketch briefly the results:

4.1. Prior sensitivity

We shall study changes in expected utility when varying the prior probability model π: decision a^* utility u and the model l remain fixed. The practical impact of the computed prior sensitivity measures is that large values tell the decision maker that any conclusion should be strictly viewed as applicable to the particular prior assumptions. Some more careful prior elicitation might be in order. On the other hand, low values imply that the conclusions can be considered reasonably robust against changes in the prior probability model.

We assume that the information about the probability distribution allows us to constrain it to a convex class Γ and applied some results from Martín and Ríos (1996) to Example 2.

4.2. Model sensitivity

We now change perspective and consider the change in expected utility when both, prior π and model l, vary over a certain class. From a decision theoretic point of view model l and prior π are indistinguishable in the sense that the optimal decision depends on either only through the product $l(x|\theta) \times \pi(\theta)$. In other words, the appropriate way to define a class of changes in prior and model jointly is to consider a class within which the posterior $p(\theta|x) \propto l(x|\theta) \times \pi(\theta)$ can vary. This implicitly defines uncertainty on prior and model.

As in the last section, we will define a measure of sensitivity by the supremum over a certain class of a derivative with respect to a change in the posterior distribution. We obtain some results for problem with a structure similar to Example 1.

4.3. Sensitivity with respect to the utility function

In this section we study the change in $T(a^*; u,\pi,l) - T(b; u,\pi,l)$ as we vary the loss function and b. We focus on utility functions of the form

$$T_r(d) = -r \times n_d - f(d)$$

which include a tradeoff between one term related to sampling cost and another term containing the posterior (predictive) probability of some event of interest. Our interest in this section is to know how much can vary the term related to sampling cost without change the optimal decision. We use a parametric class of loss functions with parameter r. We illustrate the ideas with Example 1.

5. CONCLUSIONS

We adapt Bayesian sensitivity analysis techniques to medical decicision problems. In this class of problems it is particularly important that uncertainty in the inputs should not drastically affect the optimal decision, and to understand the nature of the impact if it does. The utility (or loss) funciton in such problems typically include components related to the different points of view of the involved decision makers (patients, doctors, administrators, etc). The proposed sensitivity analysis helps to study the impact of different believes and choices on the final conclusion.

6. ACKNOWLEDGEMENTS

This work has been partially supported by project IPR00A075 from Junta de Extremadura.

7. REFERENCES

Berger, J.O. (1994) An overview of robust Bayesian analysis, *Test*, 3, 5-124.

Carlin, B.P. and Pérez, M.E. (2000) Robust Bayesian Analysis in Medical and Epidemiological Settings, in Ríos Insua and Ruggeri (eds.) *Robust Bayesian Analysis,* 351-372, Springer.

Dey, D., Ghosh, S. and Lou, K. (1996) On local sensitivity measures in bayesian analysis, *IMS Lecture Notes, 29.*

Diaconis, P. and Freedman, D. (1986) On the consistency of Bayes estimates, *Annals of Statistics*, 14, 1-67.

French, S. y Xie, Z. (1994) A perspective on recent developments in Utility Theory, in Ríos (ed.) *Decision Theory and Decision Analysis: Trends and Challenges*, Kluwer A. P.

Greenhouse, J. and Wasserman, L. (1996) A practical robust method for bayesian model selection: a case study in the analysis of clinical, *IMS Lecture Notes, 29.*

Martín, J. and Ríos Insua, D. (1996) Local Sensitivity Analysis in Bayesian Decision Theory', *IMS Lecture Notes, 29.*

Martín, J., Ríos-Insua, D. and Ruggeri (2001) Stability of Bayesian decisions, *Unpublished manuscript.*

Palmer, J. and Müller, P. (1998) Bayesian Optimal Design in Population Models of Hematological Data, *Statistics in Medicine*, 17, 1613-1622.
Parmigiani, G. (1993) On Optimal Screening Ages, *Journal of the American Statistical Association*, 89.
Ríos Insua, D. and Ruggeri, F. (2000) *Robust Bayesian Analysis*, Springer.
Ruggeri, F. (1993) Local and global sensitivity under some classes of prior, in Vilaplana and Puri (eds.) *Recent advances in Stat. and Prob.*, 233-243.
Ruggeri, F. and Wasserman, L. (1993) Infinitesimal Sensitivity of Posterior Distributions, *Can. Jour. Stats*., 21, 195-203.
Sivaganesan, S. (1993) Robust Bayesian diagnostics, *J. Statist. Planning and Inference*, 35, 171-188.
Wasserman, L. (1992) Recent methodological advances in robust Bayesian Inference', in Bernardo, De Groot, Lindley, Smith (eds.) *Bayesian Statistics 4*, Oxford U.P.

APPLICATION OF SENSITIVITY ANALYSIS TO OIL REFINERY EMISSIONS

JM Whitcombe and R Braddock

Affiliation: Faculty of Environmental Sciences
Griffith University, Nathan Qld 411
Email: josh.whitcombe@mailbox.gu.edu.au, r.braddock@mailbox.gu.edu.au

ABSTRACT

Catalyst emissions from Fluidizing Catalytic Cracking Units have the potential to impact significantly on the environmental compliance of oil refineries. Traditionally it has been assumed that gas velocity and fine particles significantly impact on emission levels. Through the use of a simple fluidized bed model, sensitivity analysis was conducted to identify the key operating parameters that influence emission rates. It was found that it is actually the coarse size fractions and particle characteristics such as size and density that are the most influential factors for emission rates. Further work is needed to identify how these parameters can be altered during normal operations to reduce catalyst emissions.

1. INTRODUCTION

The petroleum industry currently employs Fluidizing Catalytic Cracking Units (FCCU's) as the major tool in producing the gasoline needs from crude oil. FCCU's typically consist of a rising main where the chemical reactions between catalyst and hydrocarbon occurs, a reactor to separate the product and catalyst and a regenerator to re-charge the used catalyst. The regenerator is a fluidized bed used to combust coke from the used catalyst, with cyclones to remove particles from the flue gas stream before venting to the atmosphere. The recharged catalyst then re-circulates through the rising main and the process is continued. Refer to [1] for details on fluidization engineering.

In recent years, fine particle emissions from industry have been identified as important contributors to poor environmental and health standards across the United States [2]. With increasing demands for cleaner air, catalyst emissions from FCCU's have the potential to impact significantly on the environmental efficiency of the overall refining operation [3]. Currently, FCCU's are designed and operated in such a way as to maximise output and profitability of the refinery [4]. Thus there is a need for the relationships between current operational strategies and air pollution to be better understood.

2. METHODOLOGY

Matlab was used to develop a model to predict catalyst emissions from the fluidized bed, through the use of operating parameters of the system. The objective of the model was to produce qualitative trends, rather than to be a tool for representative emission estimates.

2.1. Model Background

Fluidization is an extremely large area of research, in which a wide number of different approximations and models are used to predict all aspects of the system. However, fluidization is still to a large extent not fully understood [5]. The complexity and accuracy of each model is dependent on the conditions and underlying assumptions used to develop and construct each model. To overcome this, a detailed literature review was completed to identify the key areas important to fluidization. From here a simple model was developed to link a large number of individual equations, dealing with such phenomena as entrainment, elutriation, cyclone efficiency, and bed effects, in order to develop a basic emission model for an FCCU fluidized bed. Further detail can be found in [6]. Worked examples from the literature were used to validate the model and test the accuracy of the output. Once the model was operating correctly, real life FCCU operating conditions were used to track emission trends.

2.2. Sensitivity Analysis

The New Morris Method, as developed by Campolongo [7], was used to test the model's input parameters for sensitivity. Campolongo's [7] New Morris Method is an extension of the original Morris method extended to identify second order interactions between input parameters.

The software developed by Campolongo [7] allows a Mu (μ) and standard deviation from the Morris Method, as well as a new parameter, Lambda (λ), to be determined for the input factors of the model. Mu (μ) allows the overall influence of the factors to be determined, while the standard deviation identifies factors with possible interactive effects. The new term, lambda, provides a global sensitivity measurement for 2-factor interactions [7]. The software requires the identification of the input factor, and the range of values to be set for these factors (text files), number of sample runs, the discretisation of the parameter space, and the output file (text file)

Input factors were determined as those input parameters, which could be physical changed in an FCCU. Table 1 below lists the 12 parameters and their boundary conditions. In addition to those boundary conditions, a sample run of 10 with a parameter space dicretisation of 0.01 was used for the analysis.

Table 1: Boundary conditions for each parameter for the FCCU model

Factor	Parameter	Lower bound	Upper bound
1	Bed Velocity (m/s)	0.1	1.5
2	300μm size fraction (% mass)	0.001	0.20
3	200μm size fraction (% mass)	0.001	0.40
4	100μm size fraction (% mass)	0.05	0.60
5	80μm size fraction (% mass)	0.1	0.90
6	60μm size fraction (% mass)	0.1	0.90
7	40μm size fraction (% mass)	0.05	0.60
8	20μm size fraction (% mass)	0.001	0.40
9	1μm size fraction (% mass)	0.001	0.20
10	Feed rate (kg/s)	1	350
11	Catalyst density (kg/m^3)	1197	1323
12	Shape factor (perfect sphere = 1)	0.70	1

3. RESULTS

The following results were obtained from the New Morris Method software written by Campolongo [7].

As seen in Fig. 1 there appears to be a a wide spread between all parameters. In general all parameters have a high mu and standard deviation, impling some sensitvity towards the output, with factors 12 and 10 being the most sensitive.

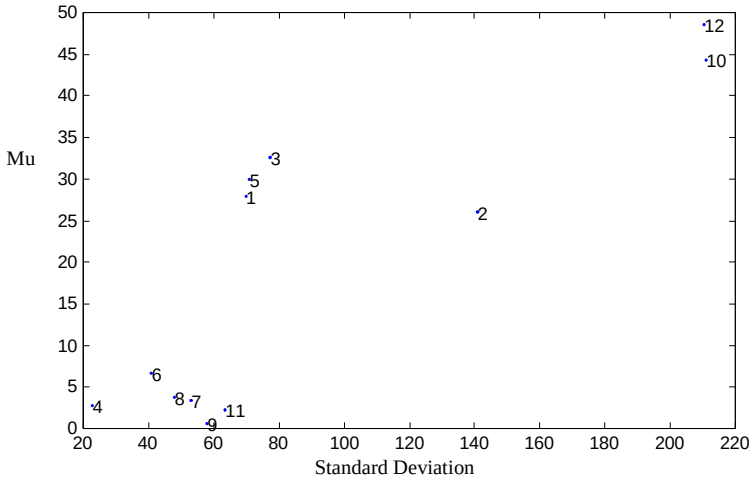

Figure 1: Plot of the Standard Deviation vs mu from using the Morris Method

3.1. New Morris Method

Table 2: Output from the New Morris Method

Pair	lambda	Pair	lambda	Pair	lambda	Pair	lambda	Pair	lambda
1,2	3428	2,6	2508	3,11	**28414**	5,10	**20246**	8,9	6884
1,3	15794	2,7	2841	3,12	9499	5,11	12833	8,10	**20028**
1,4	14366	2,8	**23382**	4,5	4689	5,12	5416	8,11	16037
1,5	1863	2,9	**24240**	4,6	**21862**	6,7	4723	8,12	7820
1,6	16381	2,10	10933	4,7	**22257**	6,8	**23529**	9,10	17066
1,7	8253	2,11	12479	4,8	2676	6,9	**22324**	9,11	12652
1,8	3479	2,12	**31550**	4,9	2991	6,10	3902	9,12	9184
1,9	**28207**	3,4	4981	4,10	**23353**	6,11	4147	10,11	8888
1,10	9222	3,5	2702	4,11	**24453**	6,12	17377	10,12	**31257**
1,11	14631	3,6	2741	4,12	11766	7,8	**21941**	11,12	3452
1,12	12132	3,7	**27127**	5,6	**20570**	7,9	3917		
2,3	13429	3,8	**19996**	5,7	2804	7,10	3971		
2,4	**20545**	3,9	11418	5,8	2855	7,11	**23312**		
2,5	8163	3,10	3725	5,9	**28919**	7,12	12887		

The lambda values seem to be very high for all factor pairs. There are however, several pairs that are much higher than the others, these can be found in bold in Table 2.

4. DISCUSSION

The overall sensitivity analysis (Morris Method) indicates that the shape factor of the particle and feed rate of catalyst into the fluidized bed are the most sensitive parameters for air emissions. Surprisingly, coarse particles (300 and 200μm), which are not very prevalent in catalyst make up, appear to have a relatively high sensitivity, higher than that of the smallest fines. Conventional wisdom states that larger particles do not influence emissions rates, as they are captured by the cyclones and returned to the bed. However, from the sensitivity analysis it appears that coarse particles do influence emission rates dramatically.

Velocity, which is believed to be the most important factor when dealing with air pollution, is not very sensitive. This may be due to the relationship between cyclone removal rates and inlet velocity. As velocity in the bed increases, more particles are carried up into the gas stream, leading to high loading rates in the cyclone and high velocities, which in turn increase the removal efficiencies, causing less emissions to occur [8]. This is supported by the relatively low lambda value for all 2-factor interactions with velocity, except with fine particles, which are not captured by the cyclone due to their size.

The New Morris Method indicates that the coarse particles have several key interactions in the bed. In general, the larger particles interact largely with the finest particle sizes and particle density. The presence of coarse particles may alter the availability of fines, which in turn would alter emission rates. Due to their size, it is reasonable to assume that density would impact on their interactions in the bed, yet how this occurs is unknown. It is possible that using catalyst with a larger percentage of coarse material may help to control emission levels better. Further work is needed to study coarse particle interactions.

The majority of the catalyst particles are in the 100 to 60μm range, therefore interactions in this size range are very important. These size fractions appear to have a generally high value for most 2-factor interactions. In particular, their interactions with the finer fractions, feed rate and density are the most important. These interactions can in part be explained by the sheer volume of this fraction in the bed - a slight change in density of this fraction would lead to an overall shift in the bed composition. Flow patterns and other phenomena will also be changed by a small change in the characteristics of this, the most dominant species in the bed. Interestingly, the fines appear to only interact with the 80 and 60μm size fraction, with very low interactions with the 100 and 40μm fraction. As yet no explanation can be given for this behaviour.

As expected with a fluidized bed, the finer size fractions interact with other parameters, however these interactions are not as prevalent as commonly believed. As expected, velocity and fines interact significantly, but this is due in part to the low removal efficiencies of cyclones for fine particle sizes.

5. CONCLUSION

The common belief that only fines and velocity affect emission rates from FCCUs is not supported by this work. The interactions of other parameters such as catalyst shape and density along with the concentration of large coarse particles are significant. Further work is needed to identify exactly how and why these parameters are so influential. It is hoped that oil refineries can use this information to alter operational conditions in such a way as to lower particle emissions without expensive end of pipe control measures being utilized.

6. ACKNOWLEDGEMENT

The Authors would like to acknowledge the financial support of Caltex Australia's Lytton Refinery.

7. REFERENCES

1. Kunii, D. and O. Levenspiel, *Fluidization Engineering 2ND. ED*. 1991, Butterworth-Heinemann: USA.
2. Johnson, H.J., *The Next Battle Over Clean Air*, in *Rolling Stone*. 2001. p. 48-53.
3. Rucker, J.E. and R.P. Strieter, *The Petroleum Industry*, in *Air Pollution Engineering Manual*, A.J. Buonicore and W.T. Davis, Editors. 1992, Van Nostrand Reinhold: New York. p. 811-834.
4. Lin, T.D.V., *FCCU Advanced Control and Optimization.* Hydrocarbon Processing, 1993. **72**(4): p. 107-114.
5. Geldart, D., *Single Particles, Fixed and Quiescent Beds*, in *Gas Fluidization Technology*, D. Geldart, Editor. 1986, John Wiley & Sons: UK. p. 11-32.
6. Whitcombe, J. and R. Braddock, *Modelling of FCCU Catalyst Emissions.* MODSIM 2001, Paper Submitted for Review
7. Campolongo, F., *Sensitivity Analysis Theory and Application*, in *Environmental Science*. 1998, Griffith University: Brisbane. p. 309.
8. Fassani, F.L. and G. Leonardo Jr, *A study of the Effect of Hight Inlet Solids Loading on a Cyclone Separator Pressure Drop and Collection Efficiency.* Powder Technology, 2000. **107**: p. 60-65.

SENSITIVITY ANALYSIS IN ICTNEO

C. Bielza, S. Ríos-Insua, M. Gómez, J.A. Fernández del Pozo

Artificial Intelligence Department, Technical University of Madrid
Campus de Montegancedo, Boadilla del Monte – 28660 Madrid (Spain)
Email: mcbielza@fi.upm.es; srios@fi.upm.es; mgomez@ujaen.es; jafernandez@fi.upm.es

1. INTRODUCTION

1.1. Neonatal jaundice and IctNeo system

Neonatal jaundice is a common medical problem which arises in a healthy newborn because of the breakdown of excess red blood cells in his system. Bilirubin accumulates when the liver does not excrete it at a normal rate. Pathological jaundice may cause potentially serious central nervous system damages. Current recommendations try to balance out the risks of undertreatment and overtreatment [5], but the current protocol does not delimit clearly when it is best to start each treatment and which treatment to administer. As a consequence of this difficulty among others, the Neonatology Service of Gregorio Marañón Hospital in Madrid suggested the development of a decision support system IctNeo to provide the doctors with an automated problem-solving tool as an aid for improving jaundice management.

The development of the system has been very complex and time consuming, both the structuring of the diagram [2] and the elicitation of probabilities and utilities [4]. IctNeo finds a maximum expected utility treatment strategy based on an influence diagram (ID). Due to the computational intractability of its large ID, IctNeo incorporates some procedures to the standard evaluation algorithm [2]. A user-friendly interface allows for data entry of a patient already treated by the doctor. Then, we can compare the system recommendations and the doctor decisions in order to draw conclusions.

1.2. The need for SA in IctNeo

Once with prototype IctNeo, it is convenient to check the robustness to many elements embedded in it. SA facilitates answers to many questions: influence and importance of each variable and its domain, suitability of probability and utility assignments, whether the hypothesis of the functional form of the utility function is held, etc. It shows the extent to which the model represents the knowledge and where we must intervene to correct inaccurate features.

In this paper we show how IctNeo conducts sensitivity analysis (SA). We start from the situation in which the doctor has provided the most appropriate value for each parameter (both probabilities and utilities), but has imprecision leading to upper and lower values of the parameter. Since we are interested in identifying a treatment strategy, we must distinguish between value sensitivity and decision sensitivity.

1.3. Difficulties of IctNeo ID

The jaundice problem presents a lot of difficulties to conducting usual SAs: too many parameter candidates to be examined due to the size of the ID, many probabilistic dependencies, big domains of the variables, 6 attributes of the multiplicative utility function [1, 4]. The complicated structure of the diagram implies a hard definition of a strategy itself and the existence of many strategies. For those reasons and for explanation purposes, in this paper we reduce our initial ID to have only two decision nodes (see Fig. 1).

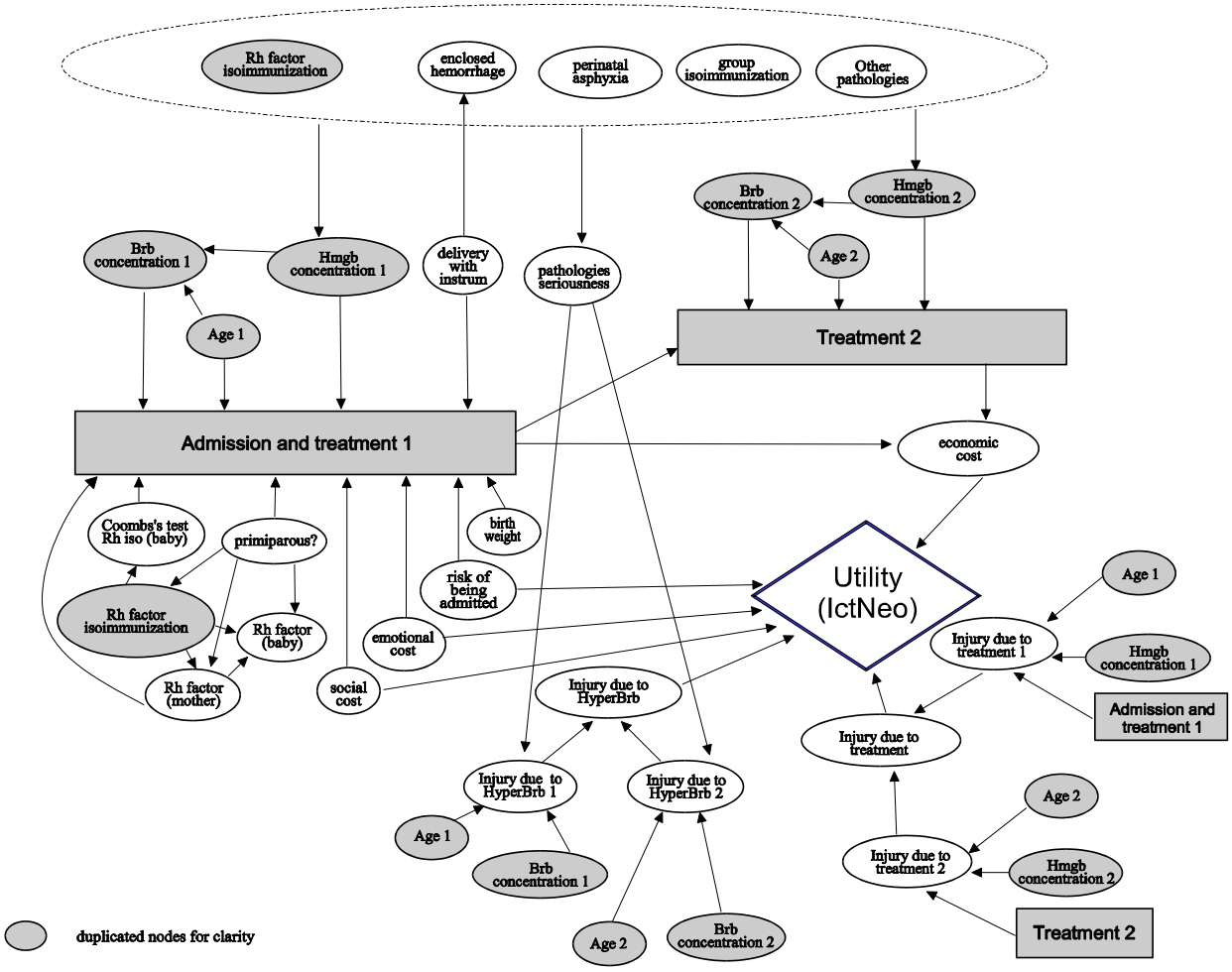

Figure 1.1. ID of the jaundice problem.

2. METHODOLOGY

2.1. Selection of parameters

We interviewed the doctors to find out the most important factors of the jaundice problem and the assignments they felt more uncomfortable with. Basically, they are probabilities of some pathologies, probabilities of the utility function attributes, and some weights of the utility function [1]. Each of these 19 parameters for which the doctors desired to perform SA requires a range along which the parameter will be varied. For probabilities, we take the

interval centred at the baseline value with radius 0.15. For the weights, we take the intervals obtained in [4] where imprecise assignments when providing tradeoffs were allowed as a way of SA. These are narrower, the widest having a length of 0.18.

2.2. Basic sensitivity analyses

First, there is a kind of qualitative SA for every decision-making problem. It refers to the fact of whether we are solving the right problem. The problem identification is essential and for that, we perform SA with respect to the ID structure by careful thought, introspection and many dialogues with the experts.

As far as quantitative SA is concerned, we often find the standard methods but applied in simple IDs, many from the robust Bayesian literature (threshold proximity measures, probability of a threshold crossing, entropy, identifying nondominated alternatives, etc). A detailed SA is difficult in big IDs as ours with a lot of parameters to be examined. In fact, most papers in the literature deal with rather simple problems, with few nodes (especially few decision nodes, leading to almost non-sequential models) and not very complicated utility function structures.

We start with a one-way SA. For that, we solve the problem when one specified parameter is varied from the minimum value of its range to the maximum, with all other parameters held at their baseline values. The results are arranged in a graph called tornado diagram. The results show the sensitivity of the problem especially to parameters related to the risk of being admitted to hospital, social cost, perinatal asphyxia, and all weights of the utility function. All these parameters would need to be considered more closely (see [1] for details).

2.3. Sensitivity based on expected value of perfect information (EVPI)

One-way SA limits us to observe what happens only when one parameter changes at a time. Typically, we will want to explore the impact of several parameters at a time, finding out possible relationships among them. It is not rare, e.g., to find a problem sensitive to its entire parameter set but not to any individual parameter. Moreover, the procedures are focused either on value sensitivity, or on the probability of a decision change (without considering the associated expected utility changes), which can lead to overstate problem sensitivity.

Felli and Hazen [3] introduce a new SA indicator based upon the EVPI that takes simultaneously into account the changes in the optimal value and in the preferred alternative. Also, it allows for studying multiple parameters simultaneously. Methodologically, EVPI represents a natural extension of probabilistic SA and, unlike the measures mentioned above, its calculation is consistent with the maximisation of expected value.

Consider parameter set ξ. The decision maker first solves the problem using ξ_0, the value he feels most likely, obtaining the alternative a_0 that maximises expected utility given that $\xi=\xi_0$. But ξ is uncertain and there is some risk in using only that value to determine the optimal alternative. With others value of ξ, some alternative other than a_0 could yield a higher expected utility. The difference is $\max_a E(V_a|\xi)- E(V_{a0}|\xi)$. Averaging over all possible values of ξ we obtain the EVPI on ξ: $EVPI(\xi)=E_\xi [\max_a E(V_a|\xi)- E(V_{a0}|\xi)]$.

3. RESULTS

This measure is approximated via Monte Carlo simulation generating *N* of ξ and averaging the resulting differences in expected utility [1]. For the 7 most outstanding parameters of the tornado diagram, the results are shown in Table 3.1, with *N*=100. We performed the analyses using a 200-MHz Pentium PC and the C++ random number generator. They were run within our system IctNeo. Expected utilities vary from 0 to 1000. The computation of each row meant 12 hours processing [1]

Table 3.1. EVPI analysis of the jaundice problem.

Parameter ξ	Description	EVPI(ξ)
k_1	Weight for economic cost	0.059
ξ_8	Probability of a low social cost	0.085
k_2	Weight for risk of being admitted	7.725
k_3	Weight for injures due to treatment	8.267
ξ_4	Probability of perinatal asphyxia	32.94
k_4	Weight for injures due to hyperbilir.	67.57
ξ_9	Probability of a low risk of being admitted	139.684
ξ_9, k_3	These parameters jointly	127.529
ξ_8, k_2	These parameters jointly	157.413
ξ_9, ξ_8, ξ_4	These parameters jointly	192.875
k_1, k_2, k_3, k_4	These parameters jointly	347.284
All parameters jointly		392.187

The higher EVPI(ξ), the more sensitivity to ξ, the comparisons of values being made in the same units as the problem payoffs (as opposed to the other measures mentioned above). In our case, the jaundice problem is sensitive to its entire parameter set and to some joint variations of certain parameters, but it is not sensitive to most individual parameters. We might conclude that parameter interactions are important. Also, it may indeed be worthwhile to put considerable effort in modelling the uncertainty related to those parameters.

4. DISCUSSION

We have tried to show how to undertake SA in a big problem by means of several tools. Most decision analysis software packages have built-in SA routines but they are too basic. For that reason we have implemented the SA method described based mainly on the EVPI. Remember that we are accounting for expected utility changes accompanying decision changes. EVPI is easily computed via simulation, being tractable even for large parameter sets.

5. ACKNOWLEDGEMENTS

Research supported by Projects UPM A9902, and CAM 07T/0027/2000.

6. REFERENCES

[1] Bielza C., Gómez M., Ríos-Insua S., Fdz. del Pozo J.A. (2000). Sensitivity analysis in IctNeo. In D. Ríos Insua, F. Ruggeri (eds.), Robust Bayesian Analysis, Lecture Notes in Statistics 152, 317-334, Springer.

[2] Bielza C., Gómez M., Ríos-Insua S., Fdz. del Pozo J.A. (2000). Structural, elicitation and computational issues faced when solving complex decision problems with influence diagrams. *Computers and Operations Research* 27, 7-8, 725-740.

[3] Felli J.C., Hazen G.B. (1998). Sensitivity analysis and the expected value of perfect information. *Medical Decision Making*, 18, 95-109.

[4] Gómez M., Ríos-Insua S., Bielza C., Fdz. del Pozo J.A. (2000). Multiattribute utility analysis in the IctNeo system. In Y.Y. Haimes and R.E. Steuer (eds.), *Research and Practice in Multiple Criteria Decision Making,* LNEMS 487, 81-92, Springer .

[5] Newman T.B., Maisels M.J. (1992). Evaluation and treatment of jaundice in the term infant: a kinder, gentler approach. *Pediatrics*, 89, 5, 809-818.

ASSESSING AND PROPAGATING UNCERTAINTY IN MODEL INPUTS IN CORSIM

G. Molina[1], M.J. Bayarri[2], and J.O. Berger[1]

[1]Institute of Statistics and Decision Sciences
Duke University, Durham,
NC 27708-0251, USA
Email: berger@stat.duke.edu, german@stat.duke.edu

[2]Dept. of Statistics and Operations Research
University of Valencia, Burjassot,
Valencia, 46100, SPAIN
Email: bayarri@uv.es

1. SUMMARY

CORSIM is a large simulator for vehicular traffic, and is being studied with respect to its ability to successfully model and predict behavior of traffic in a 36 block section of Chicago. Inputs to the simulator include information about street configuration, driver behavior, traffic light timing, turning probabilities at each corner and distributions of traffic ingress into the system.

Data is available concerning the turning proportions in the actual neighbourhood, as well as counts as to vehicular input into the system, and internal system counts, during a typical day in May, 2000. Some of the data is accurate (video recordings), but some is quite inaccurate (observer counts of vehicles). The first goal of the research is to incorporate both types of data so as to derive the posterior distribution of turning probabilities and of the parameters of the CORSIM input distribution. These are useful in helping to adjust to situations of missing or incomplete data.

The vehicles passing through an intersection are modelled with a product multinomial distribution, with turning probabilities specific to each intersection. The accurate data is introduced as restrictions on the model, reducing the actual number of latent variables. Analysis requires MCMC sampling, from both the turning probabilities at every intersection and from latent counts of vehicles at different locations. Prior information on turning probabilities is also used, when the data for an intersection is too limited.

This posterior distribution on model inputs will then be used to study sensitivity of the computer model. Studying the uncertainty in model predictions is complicated by the fact that the CORSIM model operates close to feasibility constraints, and these constraints must be built into the uncertainty propagation through the model.

This work is described in more detail in the article “Fast Simulators for Assessment and Propagation of Model Uncertainty,” also in these proceedings. The focus of this conference poster is on the computational aspects of this problem. In particular, we address: (i) the description of the full conditional distributions needed for implementation of the MCMC algorithm and, in particular, how the constraints can be incorporated; (ii) details concerning the run time and convergence of the MCMC algorithm; and (iii) utilisation of the MCMC output for prediction and uncertainty analysis concerning the CORSIM computer model. As this last is the ultimate goal, it is worth emphasising that the incorporation of all uncertainty concerning inputs can significantly affect the model predictions.

APPLICATION OF SENSITIVITY ANALYSIS FOR THE REDUCTION OF A NITROGEN TURNOVER MODEL

M. Ratto[(1)], N. Giglioli[(1)], Å. Forsman[(2)]

[(1)] Joint Research Centre of the European Commission, Institute for Systems, Informatics and Safety, TP 361, 21020 Ispra (VA), Italy
Email: marco.ratto@jrc.it

[(2)] Department of Mathematics, Linkoeping University
SE-581 83 Linkoeping, Sweden

1. INTRODUCTION

Temporal trends and spatial patterns in the state of the environment are often obscured by large year-to-year variation in climate conditions. This makes tools aimed at extracting anthropogenic signals from more or less noisy data highly relevant for environmental assessment and policy making. Aim of this paper is to investigate how sensitivity analysis (SA) methods can be employed to achieve model reductions that facilitate the interpretation of temporal changes in the state of the environment. In addition, it is investigated how sampling frequency and temporal resolution of the mechanistic model influences the analysis. The SA approach is here applied to a mechanistic model of runoff and nitrogen turnover. The SA methods employed include Principal component analysis (PCA) and Regression based SA methods [1].

2. THE MODEL

The present case study considers a nitrogen turnover model (SOIL/SOILN). SOIL/SOILN are a chain of models to be implemented in series. SOIL is a hydrological model, which solves the mass and energy conservation balances at different layers of a soil with given characteristics (clay-sand ratio, soil depth, etc.) [2]. The inputs to the SOIL model are time series of daily meteorological data (precipitation, temperature, cloudiness, wind, etc.), given a geographical region and the soil physico-chemical properties. Outputs are daily time series of water content, water fluxes and temperature in the different layers of the soil. The SOILN model simulates major C and N-flows in agricultural and forest soils and plants [3] and provides, as a main output, the total nitrogen leached. The model is a point-scale model; it has a daily time step and simulates flow and state variables. Input variables are time series of daily meteorological data as in SOIL, management data and variables on soil heat and water conditions simulated by model SOIL.

3. UNCERTAINTY AND SENSITIVITY ANALYSIS

The main objective is the study of the SOILN module. The reference output is the total nitrogen loss averaged in a period of several years. So, from a very huge quantity of input data only a few global output values are of interest. Hence SA is applied to determine the hydrological data requirements with respect to the long-term average of nitrogen losses. This information will be useful for the lumping of SOIL model (the most computationally

expensive). Furthermore, the knowledge of the minimum quantity of data really necessary to implement SOILN model will also allow the use of measured hydrological data, instead of hydrological model simulations, as the input to SOILN.

Input data representation

A sensitivity analysis is performed with a single output variable (the average nitrogen leached) and time series of daily data for many years as the inputs. A total of 20 time series of daily data are fed from SOIL to SOILN: 5 time series respectively for water flow (WF), water content (WC) and temperature; transpiration from soil (transp); water flow in deep percolation (4 series), runoff (2 series), water flow in surface pools. To simplify, the hydrological time series in the different layers have been characterised by a limited set of parameters: firstly only the global averages over the period under consideration were considered. Subsequently, a more detailed representation of water content has been identified. The water content in different soil layers are summarised in frequency tables where the water content (%) is divided in 50 equally large classes and the number of days within each class is counted, with one table for each layer and month.

Sampling methodology

Since the hydrological time series have to fulfil the mass and heat conservation laws, the characteristic parameters of the series cannot be sampled in a purely random way. Instead, the SOIL model has to be applied to sample different replications of the hydrological time series. Such replications can be obtained using artificially generated 30-years meteorological data. Fixed soil conditions (sandy soil) and a fixed class of climate properties (climate of the southern part of Sweden) have been considered. A total of 1000 time series of meteorological data were simulated. Then 96 of them were selected, by choosing sample series that was spread out regarding mean value and coefficient of variation for precipitation. From these, a total of 96 realisations of hydrological time series have been generated with SOIL.

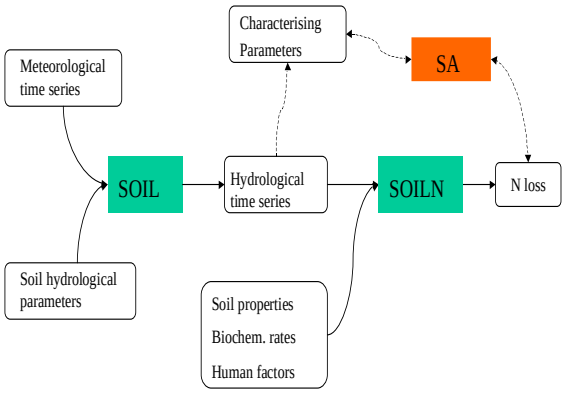

Figure 1: SA scheme for the SOILN model.

SA methodology

Regression/correlation based SA methodologies were used. In Figure 1 the SA scheme is represented by means of a flow sheet. The average nitrogen loss is used as response variable and regression models (stepwise regression analysis) are fitted to the simulation results. This kind of analysis allows studying sensitivity of nitrogen loss with respect to a variation in the properties of the hydrological time series. At the same time, regression models are reduced models mapping the main properties of the hydrological time series to the total average nitrogen loss.

3.1. UA of the average nitrogen leached over 30 years

The total average N-loss from the soil layer has been analysed. The distribution revealed a smooth behaviour [4]. The main statistical properties of the N-loss are shown in Table 1. The standard deviation is about 5% of the mean of the distribution. When the effect of reducing

	Min	Max	Mean	Std.dev
N-loss [g (m^2 day)$^{-1}$]	0.0102	0.0135	1.144E-02	5.230E-04

Table 1. UA of the total average N-loss.

time resolution in the input is analysed, the prediction of the N loss is affected by a systematic error in excess, significant already for the 2 days averaging (see Table 4 in section 3.3). This means that accurate predictions require high time resolution in the input data. On the other hand, the relative error of the N loss prediction with averaged input data is bounded at the 5% even for the 32 days averaging. This may be acceptable remembering that the prediction with coarse time resolution in the input time series is conservative and that the standard deviation of the prediction itself is of the order 5%, too.

3.2. SA of SOILN to the hydrological time series

With the average water flow at the surface AVWFsurf as the only explanatory variable, the regression model explains 68 % of the variation in the response variable. When the average water transpiration AVtrans is added to the model, the R-square increases to 76 % (Table 2). In Table 2 Standardised regression coefficients (SRC) are also shown. A reduced SOIL/SOILN model for the prediction of long term nitrogen leaching is represented by a linear model with SRC as coefficients and where inputs are the factors selected by the stepwise regression procedure.

Next, the water content frequency tables from the *first* layer only were added to the list of explanatory variables. In order to synthesise the analysis, principal component analysis was applied. Principal component transformation has been done separately for each monthly frequency tables. Only components having eigenvalues larger than 1 have been considered. From the initial tables of 50 equally large frequency classes (600 frequencies as a whole), a reduced set of principal variables is obtained consisting of 72 elements. The residual correlation structure is much weaker: correlation coefficients rarely exceed 0.25 and never get over 0.4. On the contrary, in the unmodified input data set correlation coefficients larger than 0.9 were present. Stepwise regression analysis (Table 3) has subsequently been performed for the principal components and the two factors highlighted in Table 2. The R-square is now improved. Regression analysis results, i.e. the significance of the reduced model based on of the SCRs, can also be quite effectively interpreted in light of the mineralisation process occurring in soil. Mineralisation process is responsible of the transformation of N from ammonia (insoluble) to nitrate (soluble). The more effective mineralisation, the higher N-availability is and the higher N-leaching. Mineralisation has an optimal efficiency for water content in the interval 16-23%, and drops to zero for water content smaller than 7% and higher than 80%. Each principal component of the water

#	Entered	R**2	Part. R^2	SRC
1	AVWFSURF	0.685	0.685	0.657
2	AVTRANSP	0.759	0.073	0.32

Table 2: Stepwise regression analysis using the global averages as explanatory variables.

#	Entered	R^2	Part. R^2	SRC	Sound
1	AVWFSURF	0.685	0.685	0.596	Y
2	MAY_PC2	0.795	0.110	0.269	Y
3	AVTRANSP	0.837	0.041	0.273	Y
4	FEB_PC1	0.848	0.012	0.111	N
5	SEP_PC2	0.860	0.012	-0.127	?
6	MAY_PC1	0.872	0.011	-0.106	N
7	JUN_PC6	0.880	0.008	0.091	Y
8	JUN_PC4	0.887	0.007	0.086	N
9	OCT_PC3	0.893	0.005	-0.077	Y

Table 3: Stepwise regression analysis for principal components of WC frequency tables.

content frequency table used for the regression analysis represents particular combinations of water content values, e.g. groups of water content smaller than 10% (small mineralisation), groups in the optimal range for mineralisation, etc. We would expect that principal components representing water content in the optimal range for mineralisation have a positive SRC and vice versa. In the last column of Table 3 the results of this 'soundness' test is shown (more details can be found in [4]). For many elements in the regression this test is positive, implying that mineralisation offers a quite good qualitative interpretation key of the effect of fluctuations in the water content on the N-loss. This also implies that the reduced model provided by SRC can be considered acceptable for the evaluation of long term leaching from soils.

3.3. SA: Effect of time resolution of input data

Model runs have been made by averaging the daily data obtained with the SOIL model at increasing time periods: 2, 4, 8, 16, 32 days averaging. The SA has been performed considering 4 input factors: the first three parameters identified in Table 3 to characterise the climatic-hydrological scenario and an additional parameter (Resol) representing time resolution, having the values: Resol=1, 1/2, 1/4, 1/8, 1/16, 1/32. The runs with averaged input data introduce a systematic error in excess for the prediction of the nitrogen loss (Table 4). In Figure 2 the standardised regression coefficients of the 4 factors are shown for the input/output data obtained by combining daily data runs with runs of increasing averaging. The SA has been performed by considering separately the runs with different averaging, in order to appreciate the increasing importance of averaging in modifying predictions. The SRC for Resol is negative: in fact, as the time resolution increases, the systematic error in excess tends to vanish, implying smaller values for the N-loss. Data averaging begins to be significant at the 4 days averaging and is prevailing starting from 8 days averaging. On the other hand, if the percentage change in the mean and standard deviation is considered, we can see that it does not exceed 5% even for the 32 days averaging. Moreover, the deviation of data is conservative.

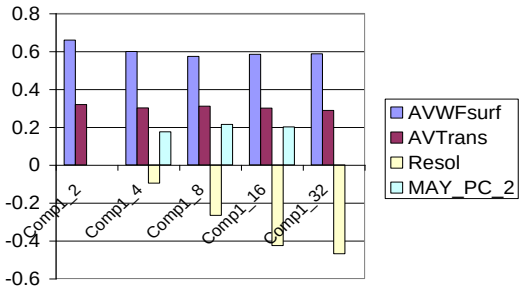

Figure 2. SRC for the runs of daily data combined with increasing averaging.

	Average	St. dev.
Daily data	1.14E-02	5.23E-04
AVE_2	1.15E-02	5.26E-04
AVE_4	1.15E-02	5.31E-04
AVE_8	1.16E-02	5.28E-04
AVE_16	1.17E-02	5.42E-04
AVE_32	1.20E-02	5.49E-04

Table 4: properties of the predicted N-loss.

4. CONCLUSIONS

In the present paper, a SA based approach is applied for the reduction of a nitrogen turnover model. Scope of the analysis was the assessment of hydrological data requirement for the prediction of long term nitrogen leaching from a soil. Starting from hydrological time series of daily data in the input, regression analysis allowed the identification of few synthetic parameters (global averages) allowing an explanation of more than 80% of the total model

output variation. At the same time regression models provided by SRCs can be taken as reduced models for long term nitrogen leaching.

5. ACKNOWLEDGEMENTS

This work has been partially funded by European Commission, General Directorate Information Society, IST Program, through contract IST-1999-11313 (IMPACT project).

6. REFERENCES

[1] Draper, N. R., Smith H., *Applied Regression Analysis*. John Wiley, New York (1981).

[2] Jansson, P-E. & Halldin S., In: Halldin (ed.) *Comparison of forest water and energy exchange models*. Int. Soc. Ecol. Modelling (Copenhagen) pp.145-163 (1979).

[3] Eckersten, H., Jansson, P-E. & Johnsson, H. (1994) SOILN model, User's manual, 2nd ed. Div. of Hydrotech., Commun. 94:4, Dept. of Soil Sciences, Swedish Agricultural University, Uppsala, ISRN SLU-HY-AVDM--94/4--SE. 58 pp.

[4] Ratto M., Tarantola S., Saltelli A. (2000) Deliv. n. 16, SCA-IST-1999-11313.

SOFTWARE DEMONSTRATION

SIMLAB 1.1
SOFTWARE FOR UNCERTAINTY AND SENSITIVITY ANALYSIS

N. Giglioli

Institute for Systems, Informatics and Safety
Joint Research Center of the European Commission
TP. 361 - 21020 Ispra (VA) ITALY
E-mail: nicla.giglioli@jrc.it

ABSTRACT

In many application researchers have to fight against uncertainties that arise from different sources and affect the output results. Among many methods implemented, sensitivity and uncertainty analysis (UA/SA) techniques are useful to address these problems. UA and SA could be performed through SimLab software that works in a Monte Carlo framework and supports the analyst in model output uncertainty assessment.

1. INTRODUCTION

Models are commonly used to analyse the outcome of impossible experiments, to investigate possible consequences of selected courses of action and to optimise choices. Many course of uncertainty affect all those activities and it is crucial for the analyst quantify the level of uncertainty as rigorously as possible. Furthermore, this quantification has to be supported by information on the relevant input factors responsible for a particular fraction of the overall uncertainty in the outcome. This information may be obtained via sensitivity analysis.

Simlab 1.1 (Simulation Laboratory for Uncertainty and Sensitivity Analysis) is a useful tool capable of perform global quantitative analysis. This software is designed for Monte Carlo (MC) analysis and it is based on performing multiple model evaluations with probabilistically selected model input. The results of these evaluations are used to determine both the uncertainty in model predictions and the input variables that drive this uncertainty. It is also highly recommended as part of model validation, even where the models are used for diagnostic purposes, as an element of sound model building. SimLab allows an exploration of the space of possible alternative model assumptions and structure on the prediction of the model, thereby testing both the quality of the model and the robustness of the model based inference (see Giglioli et al. 2001).

This software is an update and user-friendly version of PREP and SPOP implemented at JRC during last years. SimLab is currently used by institutions and research centres in applied business and environmental statistics test cases. This software allows the definition of the input factors distribution and the sample generation according to a specific method (variance-based, regression or screening). This choice (see also Campolongo et al. 2000a) depends on the objectives of the analysis and on the characteristics of the input data. SimLab can execute

an internal model or could be linked to an external application that represents the environment of the model. Finally, it performes uncertainty and sensitivity analysis.

For more information about the methods implemented and the applications examples see Saltelli et al. 2000.

Follows a description of the software and its capabilities.

2. DESCRIPTION OF THE SOFTWARE

SimLab runs under Windows/NT, and the memory required is at least 32 Mb. Its user-friendly menu allows different UA and SA strategies to be selected. An on-line help is also available to the user.

The examples included in SimLab as demo are: a linear model, the Ishigami function, Sobol G function, the Level E model. The first three are simple analytic formulae, while the fourth is a model of medium complexity (solves a system of Partial Differential Equation). For other examples about SimLab applications see SimLab 2000.

SimLab is designed for computing Monte Carlo Analysis that consists of five steps:

1. selection of ranges and distributions for each input factors;
2. generation of a sample from the ranges and distributions according to a specific method (i.e. random, FAST, Morris…)
3. evaluation of the model for each element of the sample; this phase could require high computational cost, depend on the complexity of the model;
4. uncertainty analysis (i.e. confidence bounds, mean, standard error and histograms);
5. sensitivity analysis.

These steps are implemented through three modules: Pre-processor, Model specification and Post-processor modules (see Figure 1) that are analysed in the following sections (see also SimLab 2000).

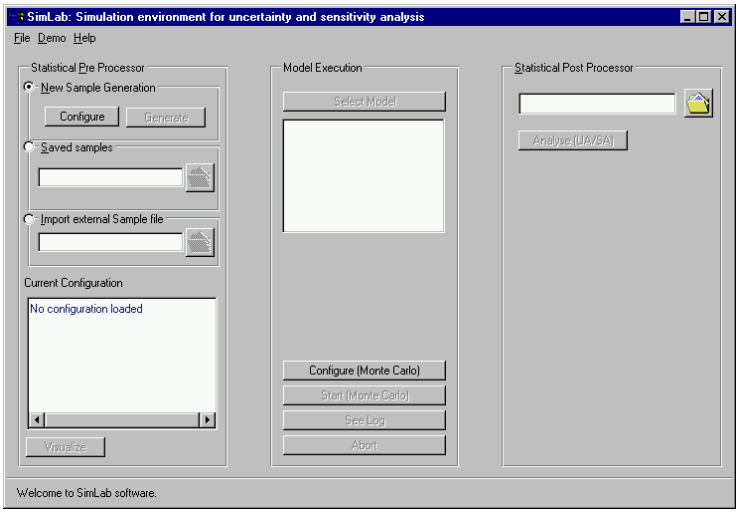

Figure 1***: SimLab. The three vertical panels correspond to the three modules***

2.1. Prep Panel

The Pre-Processor module allows the user to define the list of factors that represents the input of the model, to specify the distribution/parameter assumptions on each factor and the correlation structure (see Figure 2).

A wide range of distributions is available (Normal, Log-normal, piecewise (includes uniform), Log-uniform, Weibull, Exponential, Gamma, Beta, and Triangular) as well two types of correlation structures: rank-correlation based (Iman and Conover (1982)) and "Tree correlation with copula" (Meeuwissen and Cooke (1994)).

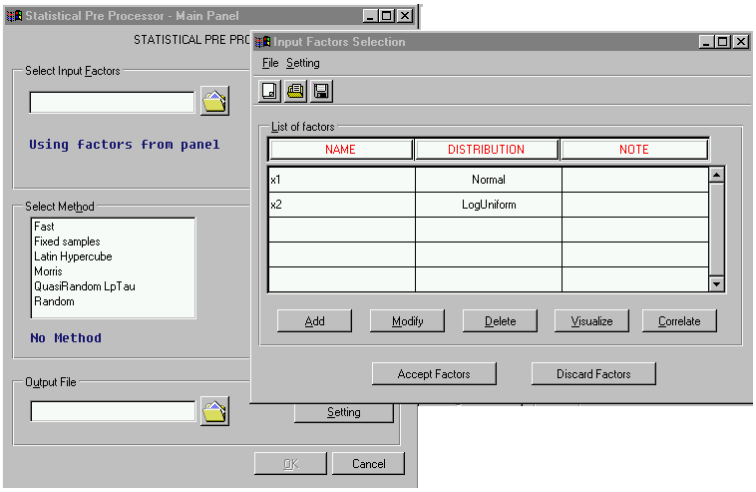

Figure 2: ***Prep-processor module, list of factor and methods***

The next step is the sample generation according to the type of methodology the analyst wants to use. Different choices are available: random sampling, quasi-random LP_τ, Replicated Latin Hypercube, Latin Hypercube, classic and extended FAST (Fourier Amplitude Sensitivity Test), Morris and fixed sample. The last one is useful in the testing phase to run the system with known inputs.

When the sample is generated, for each factor, descriptive statistics and information related to correlation characteristics are estimated. The sampling distribution of each factor and the correlation characteristics amongst the factors can be visualised, by using histograms, cobweb plots (Cooke et al. 2000) or scatter plots respectively.

2.2. Model specification module

This module manages the link between the software and the external program (for example Excel, Matlab or a user built executable) that processes the samples. There are two possibilities of simulation here:

1. the user can link SimLab to his/her external model via executable files or statistical and mathematical packages;
2. the user can define a model within SimLab by using a simple equation editor (formula parser).

When the model is complex the first possibility is clearly the only one available. SimLab strives to facilitate as much as possible the troublesome task of interfacing a given model.

The external model performs model evaluation at each sample point, and yields a set of model outputs.

2.3. Spop Panel

The Post-processor module performs the final steps of the MC analysis, UA (see Figure 3) and SA (see Figure 4).

For the UA, this module provides statistics, confidence bounds, percentiles, histograms and cumulative plots of the model outputs. Non-parametric techniques are also implemented (i.e. Tchebycheff and Kolmogorov confidence bounds).

SA techniques implemented in this section are variance-based (see Chan et al. 2000), regression based (see Helton et al. 2000) or screening based (see Campolongo et al 2000b). For the extended FAST, the Post-processor module also incorporates the computation of sensitivity indices by groups; that is, factors are partitioned into groups according to (known) similar characteristics. When the inputs are correlated special indices are performed (see McKay, 1995 and Bedford, 1998).

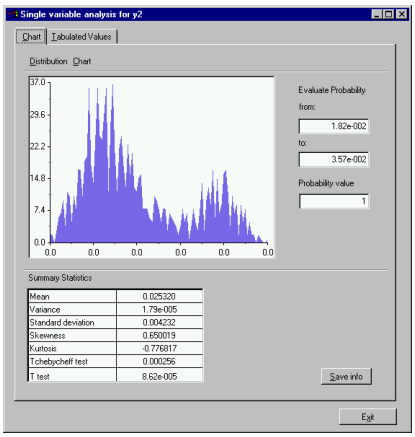

Figure 3: ***Post processor module: an example of UA***

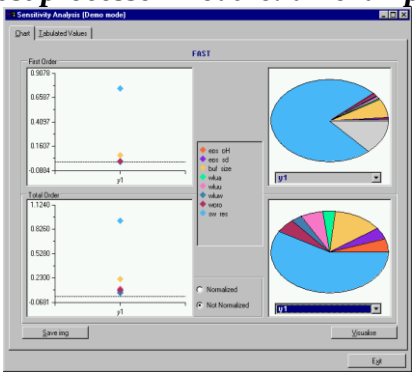

Figure 4: ***Post processor module: an example of SA with FAST method***

3. CONCLUSION

Simlab 1.1 (Simulation Laboratory for Uncertainty and Sensitivity Analysis) is a user friendly and flexible tool capable of performing global quantitative analysis in a Monte Carlo framework. The results obtained from uncertainty and sensitivity analysis are used to determine both the uncertainty in model predictions and the input variables that drive this uncertainty. This methodology is also highly recommended as part of model validation, even where the models are used for diagnostic purposes, as an element of sound model building.

Acknowledgements

SimLab has obtained grants from the European Commission DG XIII-D (SUP COM projects in 1997 and 1998, Validation and Integration, Demonstration and Marketing of a software for Uncertainty & Sensitivity Analysis).

4. REFERENCES

Bedford, T (1998) Sensitivity Indices for (Tree-) Dependent Variables, in Chan, K., S. Tarantola, S., and F. Campolongo F., Eds. Proceedings of the Second International Symposium on Sensitivity Analysis of Model Output (SAMO98), EUR report 17758 EN, Luxembourg, 17-20.

Campolongo F. A. Saltelli, T. Sørensen, S. Tarantola, Hitch hiker's guide to sensitivity analysis, in A. Saltelli, K. Chan, M. Scott (Editors), Sensitivity Analysis, Wiley. 2000a 15-47.

Campolongo F. J. Kleijnen, T. Andres, Screening methods, in A. Saltelli, K. Chan, M. Scott (Editors), Sensitivity Analysis, Wiley. 2000b 65-80.

Chan K. S. Tarantola, A. Saltelli, I. M. Sobol', Variance based methods, in A. Saltelli, K. Chan, M. Scott (Editors), Sensitivity Analysis, Wiley. 2000, 167-197.

Cooke R., Noortwijk J.M., Graphical Methods, in A. Saltelli, K. Chan, M. Scott (Editors), Sensitivity Analysis, Wiley. 2000, 245-264.

Giglioli N, Saltelli A., 2001, SimLab 1.1, Software for Sensitivity and Uncertainty Analysis, tool for sound modelling, submitted to JACM.

Helton, J. C. Sampling-based methods, in A. Saltelli, K. Chan, M. Scott (Editors), Sensitivity Analysis, Wiley. 2000b 101-155.

Hornberger G.M. and R. C. Spear.1981. An approach to the preliminary analysis of environmental systems, in Journal of Environmental management, 12, 7-18.

McKay M.D. (1995) Evaluating Prediction Uncertainty NUREG/CR-6311, LA-12915-MS Los Alamos National Laboratory.

Meeuwissen A.M.H. and R.M. Cooke. 1994. Tree dependent random variables, Report 94-28 TWI, Delft University of Technology.

Saltelli, A., K. Chan, M. Scott. 2000a. Sensitivity analysis. Wiley. New York.

SimLab Software for Uncertainty and Sensitivity Analysis User Manual. 2000. POLIS-JRC/ISIS.

"MAYDAY3.0". A WINDOWS SOFTWARE PACKAGE TO PERFORM UNCERTAINTY AND SENSITIVITY ANALYSIS OF COMPLEX COMPUTER CODE PROBABILISTIC SIMULATIONS

R. Bolado[(1)] and A. Alonso[(2)]

[(1)] Laboratorio de Estadística
E.T.S.I. Industriales, UPM
José Gutiérrez abascal, 2 28006-Madrid. Spain
Email: rbolado@etsii.upm.e

[(2)] Nexus5
Carretera de Canillas, 21, 2ºB
28043 Madrid. Spain.

ABSTRACT

During the last years a software tool has been developed at the Universidad Politécnica de Madrid (CTN-UPM) to perform Uncertainty and Sensitivity Analysis (UA-SA) of complex computer model simulations, in the framework of a probabilistic approach to Performance Assessment of Nuclear Waste Repositories. Nevertheless, this tool is intended to be useful for any kind of computer model that tackles a problem from a probabilistic point of view. MayDay implements the most common and well-known UA and SA techniques in a user-friendly environment. This paper summarises the statistical, computational and graphical tools implemented in the code and their application in the context of a Probabilistic Safety Study.

1. INTRODUCTION

In the past, it was usually complicate and tedious to perform UA and SA since the common tools to perform it were spread over several commercial and non-commercial programs. The intention pursued when developing the first version of MayDay (MayDay1.0) [1] was to collect in a single interactive program a good selection of those tools, in order to help the analyst of probabilistic simulation computer code output to study the results of his code. The evolution of the main software trends during the last years has forced us to move from a UNIX based development platform to a Microsoft WINDOWS development platform. In what follows we will show the main features of the code.

2. MAYDAY AS A WINDOWS PROGRAM

MayDay3.0 [2] is a 32 bit application that inherits, and improves in some cases, the capabilities of MayDay2.0, the previous version of the code developed under Digital UNIX. One of the main tools inherited from the previous versions of the code is the binary file that contains the results of the probabilistic simulations to be studied. The code is totally developed in C++ according to the technology OOP (Object Oriented Programming). It runs under Windows 9X, NT and 2000 platforms.

MayDay3.0 is a multiple document interface application. This feature allows the user to open and analyse simultaneously several data files, and to compare the results of the same statistics when applied to the data in those different files. Additionally, dialog boxes are non-

modal, what allows the user to compute simultaneously different statistics on the data of one or several data files.

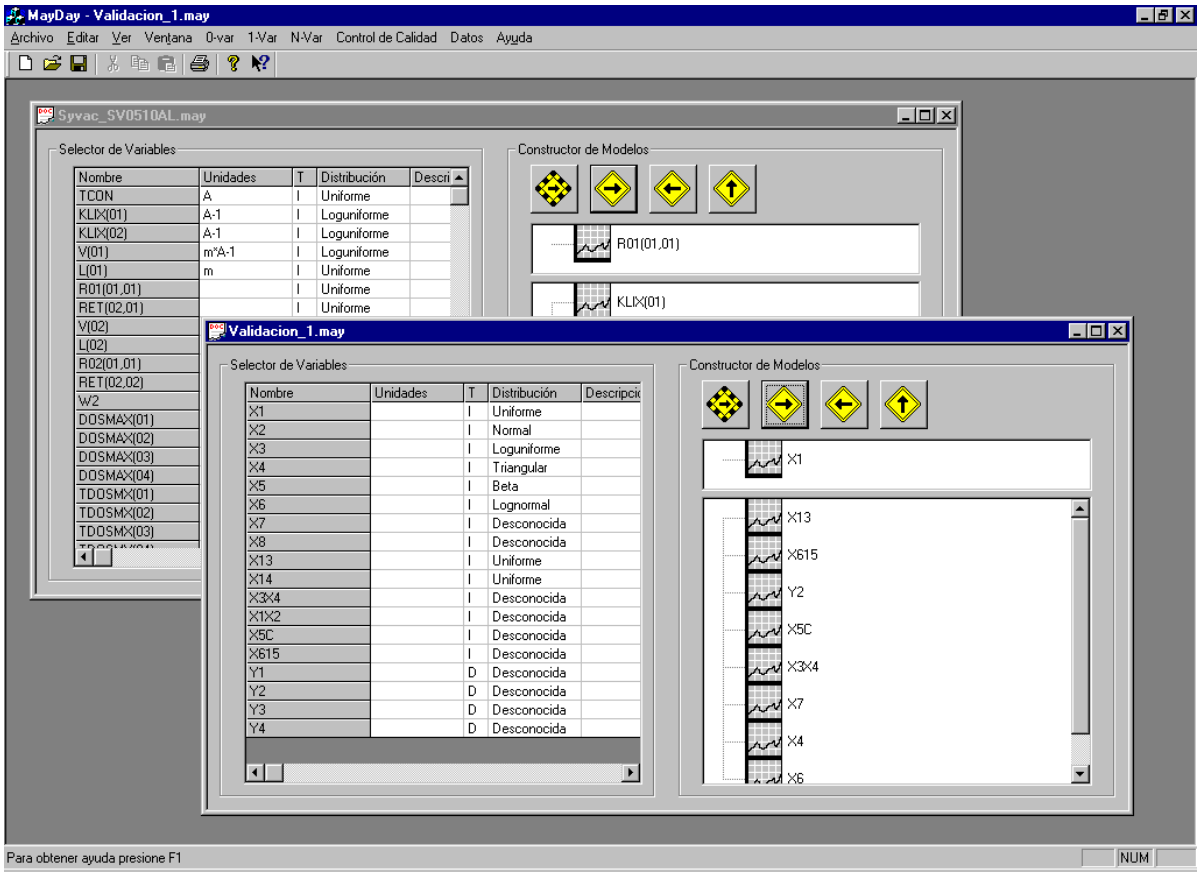

Figure 1.- MayDay´s main window and the variable selector accessing two different data files

3. PERFORMING UNCERTAINTY ANALYSIS WITH MAYDAY

An UA should provide the user the most precise numerical and graphical information about the output variables, conditioned essentially by the sample size. That information will be used to check the compliance of the facility with the safety criteria. So, it is necessary to provide appropriate statistics and graphics to be able to perform that checking. The statistics and graphics implemented in MayDay to perform UA are:

- General or population statistics (the mean, the Tchebychev, Guttman and normal confidence intervals for the mean, the variance, the geometric mean, the skewness coefficient, the kurtosis, the median, the geometric standard deviation,...).
- Order statistics and their 95% confidence intervals.
- The histogram.
- The empirical distribution function, its complementary curve, and their Kolmogorov confidence bands for different confidence levels.

The code lists the values of any input parameter or output variable. Those values may be ordered according to the run number or from the smallest to the largest. All these tools are included in the 0-Var model. In addition to all these tools, the Kolmogorov, Chi-square and Lilliefors goodness of fit tests are also available in the code. The purpose of including these

tests in MayDay is twofold. They may be used to check if input parameters have been properly sampled (the sampled values fit properly their theoretical distributions), and they may be used to check if the output variable samples fit any common distribution (normal, log-normal, exponential,...). The last tool included in the 0-Var model is the Shapiro-Wilk test. this test is used to check the normality of the sample mean in order to decide if the confidence interval under the condition of asymptotic normality of the sample mean may or may not be used.

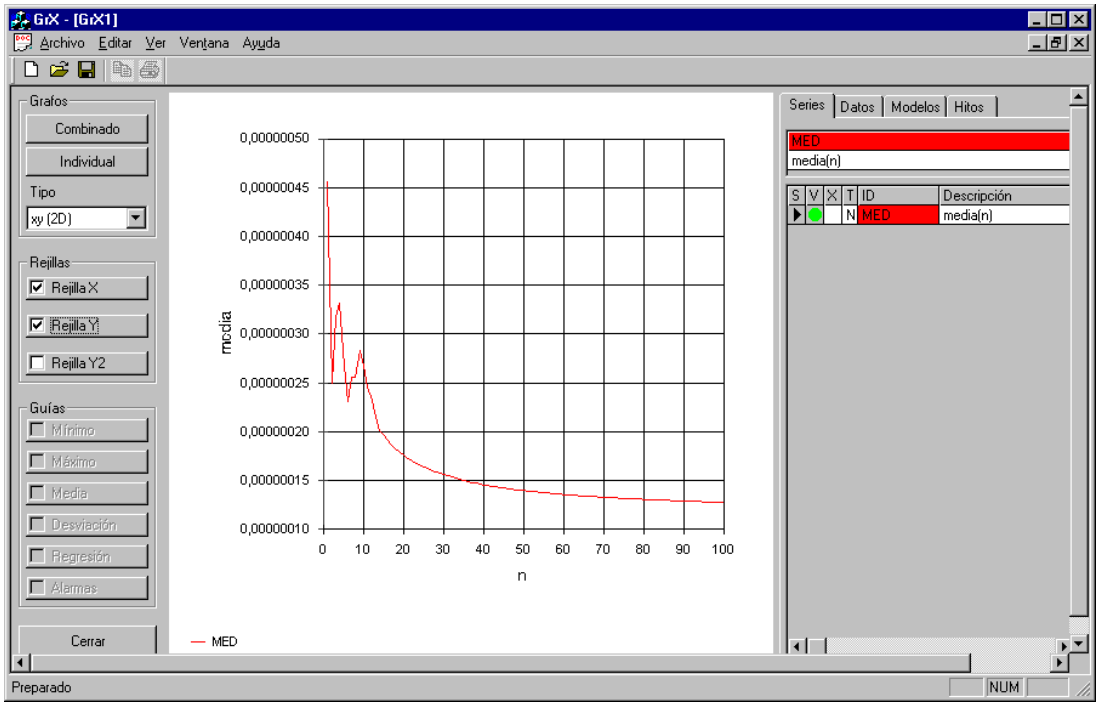

Figure 2.- Plot of the evolution of the mean versus increasing sample size.

Many times, as is the case of the Performance Assessment of a Nuclear Waste Repository, most of the outputs to be studied are dynamic. This fact forces the user to perform the UA on those dynamic variables. MayDay3.0 implements tools to show graphically the evolution of the uncertainty versus time. As an example, the user may plot the evolution versus time of the 95% of a dynamic output variable as much as its 1-α confidence interval, provided that the sample size is large enough to get that information.

4. PERFORMING SENSITIVITY ANALYSIS WITH MAYDAY

An important problem related to the concept '*Sensitivity Analysis*' is its interpretation. There is no unique interpretation of *sensitivity*. Intuitively, *sensitivity* is related to the concept of the partial derivative of an output variable with respect to an input parameter in a specific point, nevertheless this interpretation is not suitable to tackle the problem of *sensitivity* in a probabilistic environment. In what follows there is a series of different interpretations of *sensitivity* and the statistics and additional tools implemented in MayDay to cope with those different interpretations of *sensitivity*.

From a probabilistic point of view the most straightforward interpretation of sensitivity is correlation. Correlation is strongly related to linear regressions and measures the strength of the linear behaviour of one variable vs. another one. MayDay includes the Pearson correlation coefficient to measure correlation (1-Var model). The non-parametric version of correlation

measures the strength of the monotonic behaviour of one variable vs. another one; the Spearman rank correlation coefficient is implemented with that purpose (1-Var model). An extension of this interpretation of sensitivity is the multiple regression model. In this case an output variable is assumed to be explained through a linear combination of several input parameters. The main difference with simple correlations between one input parameter and an output variable is that possible correlations among the input parameters may dramatically affect sensitivity. The Partial Correlation Coefficients (PCC's) and Standardized Regression Coefficients (SRC's) related to Standardized Regressions are implemented in MayDay to tackle this interpretation of uncertainty (N-Var model). The extension to monotonic models is also considered with the Partial Rank Correlation Coefficients (PRCC's) and the Standardized Rank Regression Coefficients (SRRC's) in the N-Var model. A check on the importance of different input parameters is given by appropriate hypothesis tests in the case of the correlation statistics and by the coefficient of determination (R^2) in the case of the statistics related to the Standardized Regressions.

The techniques mentioned in the previous paragraph fail when they are used to analyse non-linear or non-monotonic models. Several parametric and non-parametric statistics are incorporated to the MayDay 1-Var model to measure sensitivity in these cases, some of them are: The Wilcoxon statistic, the two sample Smirnov statistic, the t statistic, the Kruskal-Wallis and Smirnov k-sample statistics and the Cramer-von Mises statistic. These statistics are suitable to identify relationships between specific regions of an input parameter and an output variable, which is not necessarily associated to a linear or monotonic relationship.

An additional interpretation of *sensitivity* is related to the influence of an input parameter on the final variance of an output variable. In this case an input parameter is important if it may be demonstrated that the uncertainty it is affected by is responsible of a large fraction of the output variable variance. The tool implemented in MayDay N-Var model to detect this type of sensitivity is the Fourier Amplitude Sensitivity Test (FAST). The last type of sensitivity considered in the SA that MayDay is able to perform is related to the change in the output variable mean and variance that may be induced by changes in the distribution of the input parameters. The latter interpretation is strongly related to the expected benefits of getting new information about the input parameters. Most of the input parameters involved in a Performance Assessment of a Nuclear Waste Repository are affected by knowledge Uncertainty; they are not random in a classical sense, but there is lack of knowledge about them. Additional research could improve the knowledge about them, so that their associated uncertainty could be reduced. In this case further research should be devoted to parameters that could induce a larger decrease in the output uncertainty or in the overall risk associated to the Repository. The estimators of impact in the mean and in the variance, are included in the MayDay N-Var model to deal with this interpretation of *sensitivity*.

Finally, MayDay implements two graphical ancillary tools to perform sensitivity analysis the scatterplot and the contribution to the mean plot.

4.1. References

1. R. Bolado, A. Alonso and J.A. Moya. '*MayDay. Un código para realizar análisis de incertidumbre y sensibilidad. Manuales*'. Technical Report of ENRESA 7/96. 1996.

2. A. Alonso and R. Bolado. '*MayDay3.0.0 para Microsoft Windows. Notas de versión*'. Technical Report of CTN-UPM. 2000.

CONTENTS

ORAL

POSTER

SOFTWARE DEMONSTRATION